MECHANICAL AND ACOUSTIC BEHAVIOURS OF BIO-MEDIATED RESIDUAL SOIL IN COMPARISON WITH SAND

LIM JUN XIAN

DOCTOR OF PHILOSOPHY (ENGINEERING)

LEE KONG CHIAN FACULTY OF ENGINEERING AND SCIENCE
UNIVERSITI TUNKU ABDUL RAHMAN
MAY 2021

MECHANICAL AND ACOUSTIC BEHAVIOURS OF BIO-MEDIATED RESIDUAL SOIL IN COMPARISON WITH SAND

By

LIM JUN XIAN

A thesis submitted to the Department of Civil Engineering,
Lee Kong Chian Faculty of Engineering and Science,
Universiti Tunku Abdul Rahman,
in partial fulfillment of the requirements for the degree of
Doctor of Philosophy in Engineering
May 2021

ABSTRACT

Mechanical and Acoustic Behaviours of Bio-mediated Residual Soil in comparison with Sand

Lim Jun Xian

Microbial-induced calcite precipitation (MICP) emerged as an innovative and sustainable soil stabilisation technique. The progression of MICP research on soils containing fines is relatively slow compared to clean sands. No study prioritizing microstructural formation and deformation of MICP-treated residual soil was found. There is also no comparative study on the behaviours of MICP-treated residual soil and sand. The aim of this research was to investigate the microstructural formation (e.g. anisotropy and distribution of calcites) and deformation behaviours of MICP-treated residual soil in comparison with sand. In this research, a practical MICP treatment method for residual soil was suggested. Influences of consolidation stress on MICP-treated soils, and the progressive changes in deformation behaviours of MICP-treated soils were also examined through isotropic consolidation and undrained shearing in triaxial tests with mechanical and acoustic emission (AE) measurements. Microscopic and acid washing tests were conducted to examine micro-structural formation of soils. It was found that the deformation behaviour of MICP-treated residual soil was inherently anisotropic but MICP-treated sand behaved as an isotropic material, owing to their different soil fabrics. The consolidation properties of residual soils were markedly improved

by MICP treatment. However, MICP only slightly altered the consolidation properties of sand due to the low cementation level in dense sand ($D_r \approx 82$ %). As the consolidation stress reached 120 kPa (exceeding pre-consolidation pressure), the compressive resistance was contributed by calcite densification. In undrained shearing, MICP-treated residual soils experienced three changes namely: yielding (calcite de-bonding), instability by grains mobilization, and ultimate failure. MICP-treated sand manifested strain hardening with less significant shear strength improvement. This was attributed to the particle arrangement of dense sand which had more dominant effect compared to the weak calcite bonding by MICP. Major mobilizations in sand included the plastic slippage over adjacent particle surfaces and incipient dislocation at the interlocking point contacts.

ACKNOWLEDGEMENTS

I would like to express my deepest gratitude to my research supervisors, Dr. Chong Siaw Yah, Dr. Ong Ying Hui, Prof. Dr. Yasuo Tanaka, and Dr. Lee Min Lee (my main supervisor at the early stage of PhD study). They continuously provided me invaluable advices in every stages of my research. Throughout my study, they monitored my research progress closely and were willing to spend time on having discussions with me. Thankfully, fruitful discussions were still manageable despite of the outbreak of pandemic Covid 19 near the end of my study.

My main supervisor, Dr. Chong Siaw Yah, always trusted on me and I was very much influenced by her cheerfulness. Moreover, I am appreciated to the technical assistantship from Dr. Ong Ying Hui in teaching me the proper ways of culturing bacteria and preparing chemical compounds. Also, I appreciate to the financial support from Dr. Ong for buying an Acoustic Emission transducer from Japan. Notably, I am deeply indebted to the supervision and mentorship from Prof. Dr. Yasuo Tanaka, who often inspires me all rounds. Technically, professor persists to take on a problem by contemplating on the first principle while respecting the rule of nature. He also insisted to invest a great amount of time in making sure the correctness or reasonability of an obtained experimental data. Humanly, he inspired me moving towards a responsible, disciplined, and critical thinker.

Another important mentor lightening me is Dr. Lee Min Lee, who is also an expert in the field of bio-mediated residual soil. Not only is our research collaboration, Dr. Lee is willing to give precious advices on my experiment (especially on the treatment method of bio-mediated residual soil), preparing manuscripts, and thesis writing. Our intrinsic "bonding" is not broken apart despite of his departure to the Nottingham University. In fact, he and Professor Tanaka are the pioneering figures in building and setting up the geotechnical laboratory in UTAR. Without their early contribution, I would not able to carry out my research study and develop myself.

I am deeply indebted to UTAR, which provides adequate facilities, library resources, administrative supports (from IPSR and FGO departments), and the continuous financial support (UTARRF) during my study. The technical support from Mr. Ho (a truly experienced foreman in mechanical workshop) on the fabrication of triaxial cell is also highly rated and acknowledged. In addition, I feel grateful for the assistantships from all final year projects undergraduate students.

Last but not least, I would like to thank the relentless supports from my father, mother, and younger brother throughout my study. They always showed their deepest understanding and encouragement, which are integral in keeping me focused on the research. Their belief is the energy driving me forward from time to time.

APPROVAL SHEET

This thesis entitled "**MECHANICAL AND ACOUSTIC BEHAVIOURS OF BIO-MEDIATED RESIDUAL SOIL IN COMPARISON WITH SAND**" was prepared by LIM JUN XIAN and submitted as partial fulfillment of the requirements for the degree of Doctor of Philosophy in Engineering at Universiti Tunku Abdul Rahman.

Approved by:

(Dr. CHONG SIAW YAH)
Date: 06 May 2021
Supervisor
Department of Civil Engineering
Faculty of Engineering & Science
Universiti Tunku Abdul Rahman

(Dr. ONG YING HUI)
Date: 06 May 2021
Co-supervisor
Department of Chemical Engineering
Faculty of Engineering & Science
Universiti Tunku Abdul Rahman

(Prof. Dr. YASUO TANAKA)
Date: 6th May, 2021
Professor (Co-supervisor)
Department of Civil Engineering
Faculty of Engineering & Science
Universiti Tunku Abdul Rahman

FACULTY OF ENGINEERING & SCIENCE

UNIVERSITI TUNKU ABDUL RAHMAN

Date: 7 May 2021

SUBMISSION OF THESIS

It is hereby certified that **Lim Jun Xian** (ID No: **18UED05300**) has completed this thesis entitled "MECHANICAL AND ACOUSTIC BEHAVIOURS OF BIO-MEDIATED RESIDUAL SOIL IN COMPARISON WITH SAND" under the supervision of Dr. Chong Siaw Yah (Supervisor) from the Department of Civil Engineering, Faculty of Engineering & Science, Dr. Ong Ying Hui (Co-Supervisor) from the Department of Chemical Engineering, Faculty of Engineering & Science, and Prof. Dr. Yasuo Tanaka (Co-supervisor) from the Department of Civil Engineering, Faculty of Engineering & Science.

I understand that University will upload softcopy of my thesis in pdf format into UTAR Institutional Repository, which may be made accessible to UTAR community and public.

Yours truly,

Lim.

(*Lim Jun Xian*)

DECLARATION

I hereby declare that the thesis is based on my original work except for quotations and citations which have been duly acknowledged. I also declare that it has not been previously or concurrently submitted for any other degree at UTAR or other institutions.

Name Lim Jun Xian

Date 7 May 2021

TABLE OF CONTENTS

LIST OF TABLES

LIST OF FIGURES

LIST OF SYMBOLS/ ABBREVIATIONS

Symbol

ρ	Soil density, Mg/m^3
ρ_{min}	Minimum soil density, Mg/m^3
ρ_{max}	Maximum soil density, Mg/m^3
D_r	Relative density, %
q	Deviator stress, kPa
p'	Mean effective pressure/ Stress, kPa
$\Delta p'$	Increment of mean effective pressure, kPa
σ_1	Major principal stress, kPa
σ_3	Minor principal stress, kPa
σ_{in}	Internal air pressure in Bellofram Cylinder, kPa
σ_{out}	External air pressure in Bellofram Cylinder, kPa
$\Delta\sigma_1$	Increment of major principal stress, kPa
$\Delta\sigma_3$	Increment of minor principal stress, kPa
$\Delta\sigma_c$	Increment of cell pressure, kPa
Δu	Increment of pore-water pressure, kPa
K_o	Coefficient of lateral earth pressure at-rest
B	Skempton's pore-water pressure parameter, %
P_y	Yield point
P_Y*	Illuminating yield point
P_I	Instability point
P_U	Ultimate point
e	Void ratio
C_c	Compression index

Cs	Swelling index
ϵ_v	Volumetric strain, %
ϵ_a	Axial strain, %
ϵ_r	Radial strain, %
$\Sigma\epsilon_v$	Cumulative (total) volumetric strain, %
$\Sigma\epsilon_a$	Cumulative (total) axial strain, %
λ	AE incremental rate, counts/ kPa

Abbreviation

MICP	Microbial-Induced Calcite Precipitation
AE	Acoustic Emission
CIUC	Consolidated-Isotropically Undrained Compression
CIUE	Consolidated-Isotropically Undrained Extension
SPT	Standard Penetration Number
SEM	Scanning Electron Microscopy
FFT	Fast-Fourier Transform
LDD	Lowest Dry Density
MDD	Maximum Dry Density
OMC	Optimum Moisture Content
O.D	Optical Density
CFU	Colonies Forming Unit
PVC	Polyvinyl Chloride
EP	Electro-Penumatic
DC	Direct Current
BNC	Bayonet Neill–Concelman

GUI	Graphical User Interface
OCR	Over Consolidation Ratio, defined as the past maximum stress divided by the current effective stress
OC	Over Consolidated
DC	Direct Current

LIST OF APPENDICES

CHAPTER 1

INTRODUCTION

1.1 Background Study

Microbial-induced calcite precipitation (MICP) has emerged as a sustainable soil stabilisation alternative to shed light on issues remained on conventional ground treatment. Through MICP treatment, mechanisms of bio-cementation and bio-clogging can be promoted in the treated soil medium (Dejong et al. 2010; Ivanov and Chu, 2008). The improvements in soil shear strength (Al Qabany and Soga, 2013; Feng and Montoya, 2015; Cui et al., 2017), elastic soil stiffness (Dejong et al., 2010; Lin et al., 2016), liquefaction resistance (Sasaki and Kuwano, 2016; Zamani and Montoya, 2019), one-dimensional compressibility (Lee et al., 2013), and internal erosion resistance (Do et al., 2019) were well reported. Majority of MICP researches (De Jong et al. 2010; Al Qabany and Soga, 2013; Do et al. 2019; Cui et al. 2017; Mujah et al. 2017; Kim et al. 2018; Montoya et al. 2013) were focusing on the poorly-graded sand but limited studies were found on the soil with noticeable amount of fines.

Tropical residual soil is abundantly found in Malaysia (Huat et al., 2004) thus civil engineering projects/ catastrophes on tropical residual soil are unavoidable (Liew, 2004). Naturally, residual soil constitutes a mixture of

coarse and fine grains and is normally classified as sandy silt, silty sand or clayey sand. Heterogeneity of soil characteristics was found to be prevalence in the residual soil deposit (Bolgado et al., 2017). Fabric bonding and anisotropy are usually inherent in the natural residual soil structure. The mechanical behaviours of residual soils were studied by numerous researchers (Meng and Chu, 2011; Rahardjo et al., 2004; Salih and Kassim, 2012; Kumruzzaman and Yin, 2011; Viana da Fonseca, 2003; Taha et al., 1998; Wang and Borden, 1996). However, very few studies on the mechanical behaviours of MICP-treated tropical residual soils (Lee et al. 2013; Ng et al., 2013; Chiet et al., 2016; Henry et al., 2019; Umar et al., 2015) were found. Hence, it is important to investigate the viability and practicability of bio-mediation on residual soil which is widely available in Malaysia.

The MICP-induced soil structure was very much influenced by the confining/ consolidation pressure (Xiao et al., 2020). MICP treated sand would experience breakage of calcite bonding between soil particles while exhibiting strain-softening upon failure state (Cui et al., 2017). Improvement in ultimate shear resistance of MICP treated soil could be attained as a result of the calcite densification effect (Dejong et al., 2010; Montoya, 2012; Cui et al., 2017). Specifically, the stress-deformation behaviour of reported MICP-treated sands were limited to a specific level of consolidation pressure (e.g. below 100 kPa) in order to avoid the demolition of calcite bonding in MICP-induced soil structure (Cui et al. 2017; Xiao et al. 2019b).

Lin et al. (2016) suggested that calcites could be precipitated within the pore space to interconnect the neighbouring soil grains. At microscopic scale, Dejong et al. (2010) observed two calcite fracturing mechanisms in the bio-cemented sand: (a) fracturing of calcite cementation penetrated across the calcite bond, and (b) detachment of calcite bonding at the interfaces between calcite and solid grain. Other microstructural factors influencing the behaviours of MICP-treated soils include overall regularity of soil particles (Xiao et al., 2019b) and relative density of a tested specimen (Xiao et al., 2019a). However, insignificant shear strength improvement is expected for the MICP-treated specimen with significant fines (e.g. residual soil), wherein the calcite crystals might precipitate away from the location where significant structural resistance are contributed (Sasaki and Kuwano, 2017). Lee et al. (2013) observed weak calcite bonding in the MICP-treated residual soil in their study. Zamani and Montoya (2019) further observed that pore-water pressure changes for the MICP-treated soil mixtures (fines contents varied from 0 – 35 %) were different from the untreated soil, with lower pore-water dissipation owing to the precipitated calcites within the pore spaces.

Interestingly, progressive soil changes and breakage of calcite-soil bonding could be detected by shear wave velocity measurement (Dejong et al., 2010). Lin et al. (2016) observed that the continuous structural degradation of bio-cemented sands could be detected by the drastic drops in shear wave velocity. Apart from that, no similar research has been devoted to the examination of MICP soil structural changes through a stress wave monitoring. Acoustic emission (AE) method is regarded as a non-destructive

monitoring technique (Hardy, 2003) which is able to detect the stress waves as generated from the interactions of soil particles (e.g. slippage, rearrangement, fracturing, and crushing). It was previously used to determine the yielding and plastic deformation of soils based on the dissipated acoustic energy (Tanimoto and Tanaka, 1985; Tanimoto and Tanaka, 1986; Tanaka and Shirakawa, 1995). Dilatant behaviours of soils were also able to be characterized by AE rate changes (Tanimoto and Nakamura, 1981; Smith and Dixon, 2019; Lin et al., 2020).

1.2 Problem Statement

Although the studies on MICP-treated sand have been extensively persuaded, the progression of the studies on MICP-treated residual soil is still scarce. Current knowledge on the mechanical behaviours of MICP residual soil is only limited to testing results from the soil specimens without confining pressure and are usually unsaturated in the unconfined compression test. There is limited understanding on the effect of consolidation pressure to the mechanical behaviours of MICP-treated soil.

To present, there is no experimental study prioritizing the formation of microscopic structure and the corresponding stress-deformation behaviour for the MICP-treated residual soil. As the mechanical behaviours of MICP sand have been well reported, it is informative to conduct a parallel examination on MICP-treated sand and residual soil under the identical treatment and testing conditions. From the experimental results, behavioural differences between

these two different types of soils can be directly justified by their physical properties (e.g. gradation, angularity, arrangement, surface texture of particles, and etc.), with the MICP sand served as the benchmark.

Apart from the earlier studies by Dejong et al. (2010) and Lin et al. (2016), no progressive research has been devoted to the examination of MICP soil structural changes through stress wave monitoring. Notably, no research has been focusing on the implementation of AE for the bio-cemented soils, such as MICP-treated residual soil and sand.

1.3 Aim and Objectives

This research aims to investigate the mechanical and deformation behaviours of Microbial-Induced Calcite Precipitated (MICP) residual soil in comparison with sand under monotonic triaxial loading. Three research objectives were designated to accomplish the research aims in this study:

i. To study the effects of MICP on structural formations of soils.
ii. To investigate the influence of consolidation stress on mechanical behaviours of MICP-treated soils in undrained shearing.
iii. To examine the progressive changes in deformation behaviours of MICP-treated soils through mechanical and Acoustic Emission measurements.

1.4 Significance of Study

From the present experimental study, a practical MICP treatment method for residual soil was suggested to facilitate the implementation of MICP on site. The mechanical and microstructural behaviours of MICP-treated residual were also reported; this can help to promote the application of MICP for tropical residual soil in Malaysia. Through the isotropic consolidation experiment, the structural (fabric) anisotropy and resistance (namely, isotropic yield stress and compressibility) of bio-mediated residual soil were examined. The influence of isotropic consolidation pressure towards the undrained shearing behaviours of MICP-treated residual soil was also discussed in this thesis. This can provide some insights on the effect of the consolidation pressure to the performance of MICP-treated soils.

With the implementation of Acoustic Emission (AE) technique in triaxial test, the progressive changes of deformation behaviours in both MICP-treated residual soil and sand can be distinctively determined and corresponded to their respective particles-level interactions.

Other than that, the comparison on the mechanical behaviours of MICP-treated residual soil and sand can serve as a reference for future research on the MICP treatment for soil with fines.

1.5 Scope and Limitations of Study

This research investigated the structural formation and behaviours of MICP-treated soils (i.e., residual soil and sand) by conducting the monotonic triaxial test, which is equipped with AE measurement. Isotropic consolidation and undrained shearing (either triaxial compression or extension) were conducted in the triaxial test. Figure 1.1 illustrates the key components in the scopes of work for the present research. This included the investigation of structural formation of MICP-induced soils (Chapter 4), and the progressive mechanical-AE responses (Chapter 5). The mechanical behaviour of the (MICP-treated) residual soil was compared with a poorly graded sand, in which the sand had been mechanically sieved to a MICP-favourable size range. It was followed by the investigation on the microstructural formation and the behavioural differences between the two mentioned soils. With the implementation of AE, the progressive behavioural changes (i.e., yielding, instability, and ultimate failure) based on the mobilization of soil particles and demolishment of the calcite-cemented structure were further scrutinized.

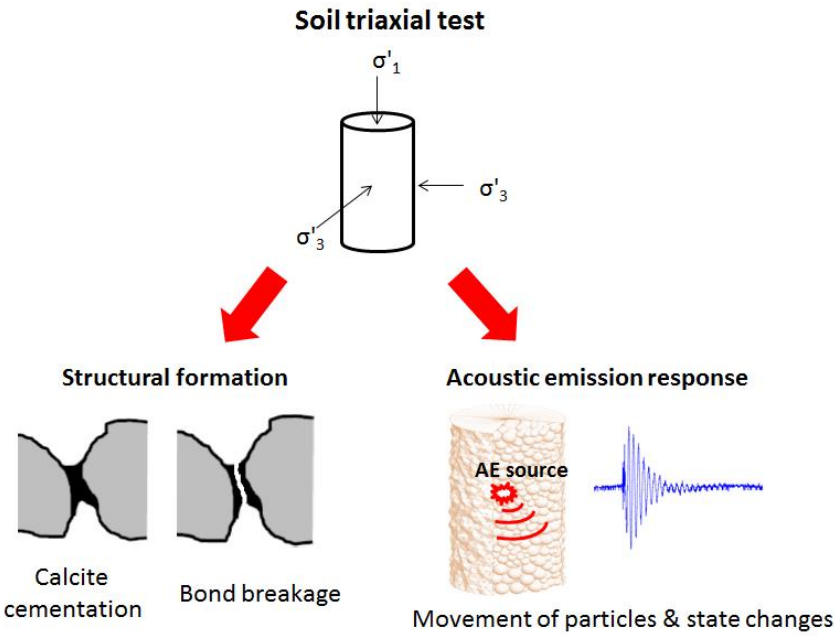

Figure 1.1: Scope of study covering structural formation and responses for MICP-treated soils

Research limitations of present experimental study were listed as followings:

I. Without local strain measurements, the obtained deformation data of soil specimens could be subjected to bedding error, end restraint effect, membrane penetration issue, and etc.

II. The AE response as triggered by grain fragmentation (> 100 kHz) could not be measured by the present AE instrumentation system, which had a resonant frequency of 32 kHz only.

III. The present AE measuring setup was only able to detect stress waves at the bottom of soil specimen and indeed a very simple system. Therefore, the stress waves that propagating to the upper zone and sideway of a soil specimen could be overlooked.

IV. The interval of isotropic consolidation pressures was too wide (i.e. ≥ 40 kPa) in which important behaviours of MICP soils could be undiscovered. Although the anisotropy of MICP-treated residual soil was evidenced, it is still unclear over the exact pressure that the soil anisotropy phenomenon would start to launch.

V. The inter-relationships among percentage of fines, degree of calcite cementation, applied consolidation pressure, yielding resistance, and undrained shear strength were not able to be formed for the MICP residual soil in the present research.

VI. As monotonic stress-controlled (pneumatic) loading was adopted in this research, it is practically difficult to facilitate observing the apparent strain-softening phenomenon during the triaxial shearing. Accurate deformation properties at slow-rate of loading (i.e. <0.001 %/min) were also practically not obtainable.

1.6 Structure of Thesis

This thesis is divided into six main chapters: Introduction (Chapter 1), Literature review (Chapter 2), Research methodology (Chapter 3), Mechanical behaviours of MICP residual soil in comparison with sand (Chapter 4), Acoustic emission and mechanical behaviours of MICP residual soil in comparison with sand (Chapter 5), and Conclusions (Chapter 6). Introductory and closing remarks are also provided in each chapter to outline the important points.

Chapter 1 describes the background of study and the motivations behind the present research. Aim and objectives of research are clearly formulated. Scope and limitations of study are also enveloped to ensure the research objectives can be accomplished effectively.

Chapter 2 provides an extensive review on the mechanical and structural behaviours for MICP-treated soils (i.e. clean sand and soil containing fines). This chapter begins with the review on geological formation, characteristics, and mechanical behaviours of residual soils. Then, the MICP soil treatment and implementation of AE techniques are critically reviewed.

Chapter 3 covers the research framework and physical properties of residual soil and clean sand. The triaxial testing, MICP treatment and AE

measurement procedures in the laboratory are described in detail. Digital processing approaches for the mechanical and AE data are also included.

Chapter 4 discusses the microstructural formation and behavioural differences between MICP-treated residual soil and sand. Void ratio changes and anisotropy behaviours (i.e. relationship between radial and axial strains) were evaluated from the isotropic consolidation results. Consolidation properties, namely isotropic yield stress and compression index, were also evaluated for interpretation. Microscopic observation was further conducted to qualitatively justify the microstructural formation in the MICP-induced soil structure. More importantly, the undrained shearing behaviours of untreated and MICP-treated soils were investigated through the triaxial apparatus. From that, the stress-deformation and pore-water pressure responses were used to justify the observed bio-mediation effect.

Chapter 5 provides an extensive coverage on the deformation and undrained shearing behaviours through AE monitoring. In isotropic consolidation test, the mechanical measurement (as covered in Chapter 4) was correlated with the AE response. Notably, soil compressibility was correlated well to the AE rate under normal consolidation state. Progressive soil changes (namely, yielding instability and ultimate state) were traced in tandem with the mechanical responses when the soil was sheared under triaxial loading. The soil changes as determined from AE measurement was justified by referring to the previous studies and theoretical findings. Lastly, the AE-determined

yielding points were also compared with the yielding data reported by other researchers.

Finally, conclusions and research recommendations for further improvement are presented in Chapter 6 accordingly.

CHAPTER 2

LITERATURE REVIEW

2.1 Introduction

This chapter provides a comprehensive review on the mechanical behaviours and structural aspects for MICP-treated soils (i.e. clean sand and soil containing fines). At first, geological distribution and formation of residual soils in Malaysia are reviewed. The mechanical behaviours of fully saturated residual soils from different countries are further elaborated. Later, MICP method is introduced. The necessary considerations for MICP treatment setup and conditions for different types of soils are critically reviewed. More importantly, the mechanical behaviours MICP soils are discussed in detailed. Microstructural formation and progressive changes of MICP-treated soils are also highlighted. Lastly, Acoustic Emission (AE) technique, which can facilitate the understanding of structural changes in MICP soils, is discussed.

2.2 Residual Soil

2.2.1 Distribution and Formation of Residual Soil

Residual soil is a weathering product which is naturally derived from the parent rock and remained at the original place. It can be found abundantly in many countries, such as Malaysia, Singapore, Hong Kong, Nigeria, South

Africa, Brazil, and United States (Huat et al., 2004). As one of the tropical countries, superficial land area across Malaysia is extensively covered by tropical residual soil. Figure 2.1 shows the geographical distribution of natural soils in Peninsular Malaysia; the natural soil can generally be classified into granitic residual soil, sedimentary residual soil, and alluvium (transported soil distributed along the coastal region).

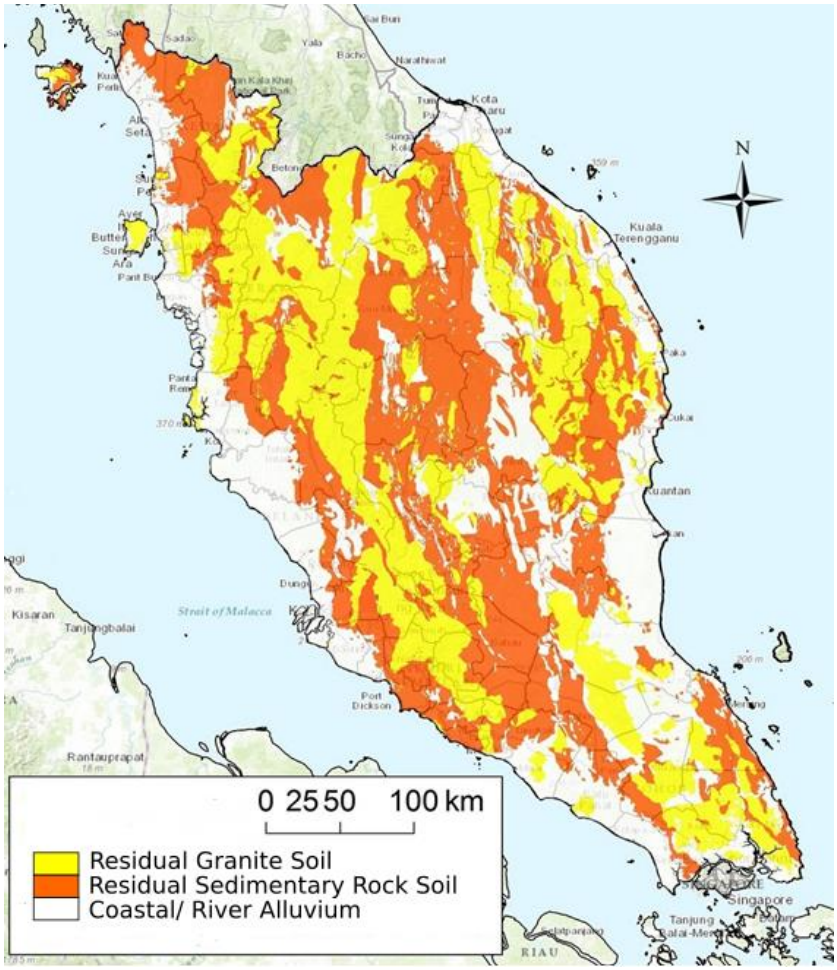

Figure 2.1: Distribution of Tropical Residual Soils in Malaysia (after Ooi, 1982)

Figure 2.2 illustrates the weathering profile across a granitic rock formation, in which the degree of weathering decreased with the depth of soil deposit. To a certain depth, rock fragments would be preserved in the partially weathered layer (i.e. Grade IV onwards) resulting in higher resistance. Mayne (1997) encountered a significant increase in SPT value at the deeper saprolite zone owing to the presence of abundant coarser particles.

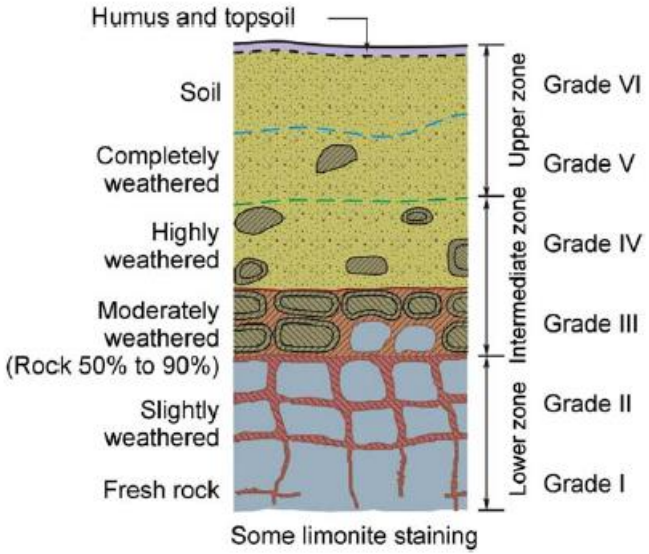

Figure 2.2: Weathering profile in granitic rock formation (after Rahardjo et al., 2004)

The weathering process (i.e. degree and rate of weathering) was very much governed by geographical location, topography, drainage condition, temperature, vegetation condition, stress history, humidity, rainfall intensity, and mineralogy of the rock material (Townsend, 1985). Chemical weathering process is more prevalence under hot and humid condition which can be found in many tropical countries. Decomposition and alteration of mineralogical composition is commonly seen in the chemical weathering process by the

percolation of rainwater (acidic water) to break down the parent rock. The rate of chemical weathering was also greatly depending on the total surface area of the soil fragments or particles. Fine-grained soils, which constituted larger specific surface area of particles, usually experienced faster rate of chemical decomposition to form more stable particles. Occasionally, the weathering process could be expedited by variety forms of physical weathering processes, such as thermal expansion/ contraction, abrasion, wetting/ drying and etc. Through the physical weathering process, the original rock could be physically fragmented into smaller pieces without alteration of its original mineralogy. The degree of weathering was able to be manifested by the pore volume (i.e. initial void ratio) and particle size distribution of weathered residual soils (Rahardjo et al., 2004). The physical indexes and mechanical properties can be correlated to the particle size distribution of the studied residual soil. In addition, it was reported by Huat et al. (2004) that wildly different grain size composition could be found in residual soils originated from a particular type of parent rock (e.g. granite and basalt), depending on the geographical location and degree of weathering.

The residual soils in Malaysia are typically classified as sandy silt, silty sand, or clayey sand. The physical properties of residual soil are greatly dependent on the nature of its parent rock formation (e.g. sedimentary, igneous, and metamorphic rocks). Granitic rock (as originated from the igneous rock) initially constitutes large amount of coarse-sized quartz and minor amount of weathered feldspar. With the progress of time, the feldspar is weathered into clay-sized particles while the quartz remains as the coarser

constituent. As such, the granitic residual soil usually composes the mixture of coarse and fine-grained soil particles. This type of residual soil is widely encountered at construction site underlying the hill terrain (Huat et al., 2004) in Peninsular Malaysia.

Furthermore, Bolgado et al. (2017) found that the geo-mechanical properties (e.g. friction angle, cohesion, and SPT number) and physical characteristics (e.g. Atterberg limit indexes, dry density, and initial void ratio) of selected Argentina residual soils showed in-situ heterogeneity as attributed to the localization effect of the weathering process. Pitts and Kannan (1986) also reported a large variability in particle size distribution for residual soils overlying Jurong Formation bedrock in Singapore. This observation was later reconfirmed by Rahardjo et al. (2004); the residual soil of Jurong formation was formed from different stratified layers of weathered sedimentary rocks, such as sandstone, siltstone, and mudstone. The properties of sedimentary residual soil varied across the depth of soil layer as compared to the other regional residual soil (i.e. Bukit Timah residual soil). The above findings suggest that the behaviours of intact residual soil are very much dictated by the location of sampling and could behave differently from the reconstituted residual soil.

2.2.2 Mechanical Behaviours of Residual Soil

From the literature, various aspects of the mechanical behaviours for undisturbed and reconstituted residual soils were studied extensively (Meng

and Chu, 2011; Rahardjo et al., 2004; Salih and Kassim, 2012; Kumruzzaman and Yin, 2011; Viana da Fonseca, 2003; Taha et al., 1998; Vaughan et al., 1988; Wang and Borden, 1996). The present critical review prioritized the research on stress-strain behaviours of residual soil, with a particular interest on the undrained behaviours. This was underpinned by the fact that residual soil usually constituted noticeable amount of fine contents (silt and clay) and therefore the pore-water pressure response become an important parameter for evaluation. Besides that, the present review concentrated on the mechanics of saturated residual soil despite it was learnt from many cases that in-situ residual soil was usually under partially saturated condition and the effect of matric suction played an important role (Blight and Leong, 2012; Huat et al., 2012). The author believes that investigation of saturated residual soil will undoubtedly carry meaningful implications and can serve as a benchmark understanding since the corresponding studies on mechanical behaviours of saturated residual soil in Malaysia is still very limited.

Meng and Chu (2011) carried out a series of K_o-consolidated undrained triaxial tests on undisturbed Singapore residual soil, which was originated from the Bukit Timah granite. The field-replicated stress condition was committed by conducting one-dimensional consolidation and the intact residual soil was subjected to certain over-consolidation ratio. Figure 2.3 (a) highlights that the effect of over-consolidation was significant in the K_o-consolidated residual soil; the soils distinctively manifested positive dilatancy of stress response under undrained compression. It is obvious that the behaviour of residual soil resembled the one of normal consolidated upon the

pre-consolidation pressure (i.e. 300 kPa) had been reached. The behaviours of normal consolidated residual soil (as highlighted in Figure 2.3 (b)) were influenced by the confining pressure and tended to behave as loose sand by showing high pore-water pressure generation. As illustrated in Figure 2.4, Chu et al. (2015) highlighted that loose sand (when the initial void ratio was far greater than the critical void ratio) would trace down left-hand side to the critical state line and manifested strain-softening under (drained and undrained) compression. On the other hand, the dense sand (when the initial void ratio was far lower than the critical void ratio) would exhibit strain hardening phenomenon (also called non-flow condition) and eventually reached a constant stress ratio asymptote. The above findings inform that the intact residual soil is inherent with structural resistance, which will be diminished once the pre-consolidation pressure is exceeded under a field-replicated anisotropic stress condition. Also, interpretation on stress changes of residual soil under undrained shearing can be underpinned by established knowledges on the behaviours of loose and dense sands.

(a)

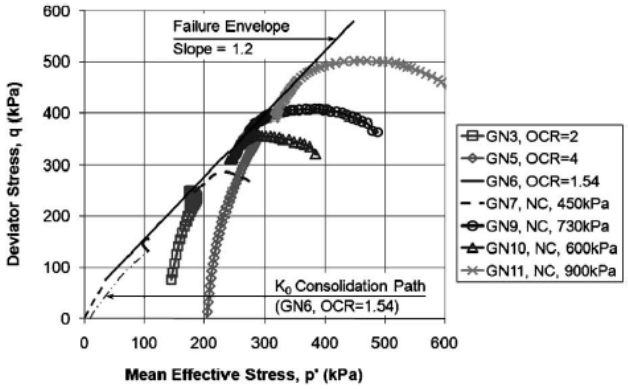

(b)

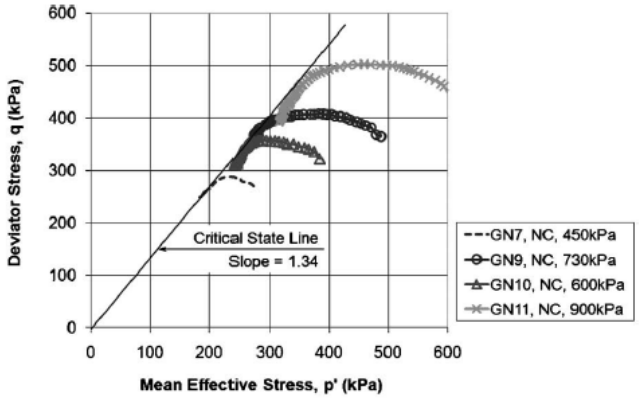

Figure 2.3: Effective stress paths for Singapore residual soil under (a) over-consolidated and (b) normally-consolidated states (Meng and Chu, 2011)

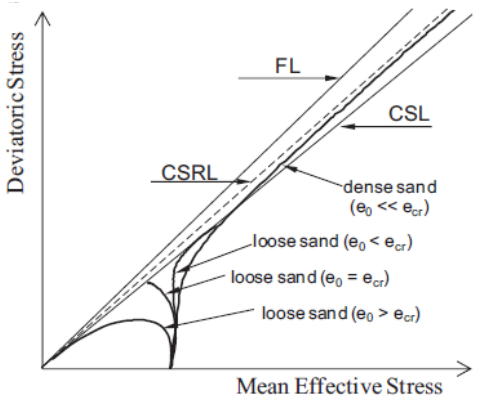

Figure 2.4: Typical behaviours of loose and dense sand in the stress space (Chu et al., 2015)

Similar observations were reported by Kumruzzaman and Yin (2011) for a Hong Kong granitic residual soil. In their study, the mechanical behaviours and shear strength properties were investigated through triaxial compression (i.e. axisymmetric condition) and true triaxial (i.e. plane strain condition) compression tests. The reconstituted/ re-compacted residual soil specimens were compacted and consolidated prior to the undrained compression test. It is apparent from Figure 2.5 that the residual soil specimens started to yield and exhibited plastic deformation at a consolidation pressure as small as 100 kPa only. Beyond 100 kPa, the effective stress paths (consolidated to 200 kPa and 400 kPa) traced down to the critical state line (as obtained from a series of drained tests) owing to the generation of high pore-water pressure. Interestingly, they observed two different failure modes for the soils tested under triaxial (bulging failure) and plane strain (shear banding failure) conditions. The effective frictional angles for the residual soils tested under plane strain condition were also greater than those tested under triaxial compression condition. The comparison between the findings as reported by Kumruzzaman and Yin (2011) and Meng and Chu (2011) suggested that intact residual soil was characterized with apparent structural resistance, which was influenced by level of confining pressure and re-compaction process.

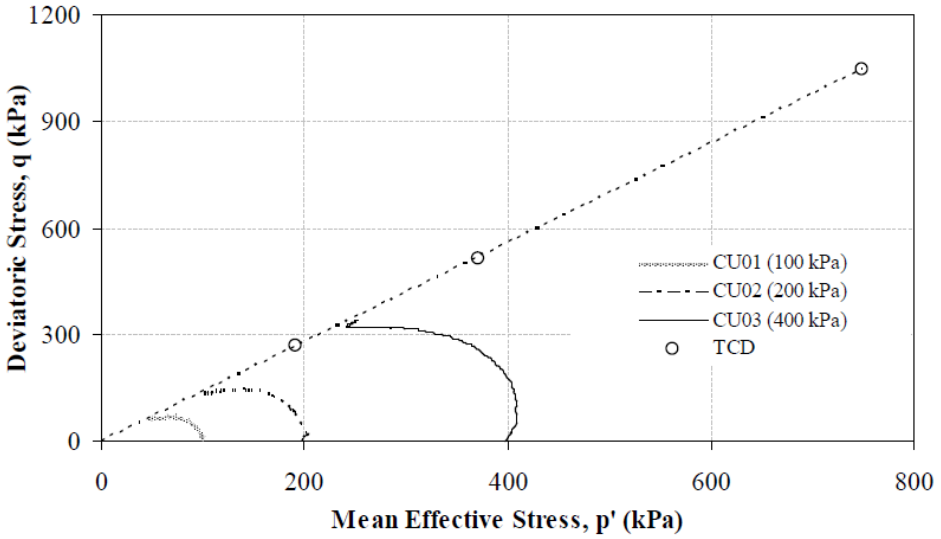

Figure 2.5: Effective stress path for Hong Kong decomposed granitic residual soil (Kumruzzaman and Yin, 2011)

2.2.3 Bonding in Residual Soil

It was learnt from the above-mentioned studies that intact residual soil was inherent with structural resistance, which could be attributed to the structural bonding in the soil structure. This section attempts to highlight the laboratory and in-situ observations to justify the existence of structural bonding in the natural residual soils. Vaughan et al. (1988) justified the existence of structural bonding in residual soil by the zero-stress cohesion intercept along the effective failure envelope and a pragmatic observation on a steep hill being remained stable even after excavation at wet climatic condition (with a high elevation of phreatic surface). It was claimed that such structural bond would be dismantled and irrecoverable after the soil structure was destroyed by loading or straining (i.e. yielded). They further opined that the bonding preserved in a natural residual soil could be somewhat analogous to the sedimentary clay, where the platy particles were held by chemical attractive

actions. Nevertheless, the effect of cementation could also be discovered in the steep natural slope made of sand cemented by calcium carbonate (Clough et al. 1981). Rahardjo et al. (2004) attributed to the fine contents as one of the factors (apart from mineralogy of clay content and in-situ bonding effect) contributing to the bonding effect and significant cementation in the tropical residual soil.

Francisca and Bogado (2019) observed higher shear wave velocity and small-strain stiffness in an undisturbed Argentina residual soil as compared to the re-compacted specimens. This observation was attributed to the partial breakage of particle aggregates and oxides in between the soil particles of undisturbed residual soil. Therefore, the destruction of soil bonding within residual soil could be clearly evidenced from the observed decreasing soil stiffness. Interestingly, Zhang et al. (2017) claimed that soil bonding could be formed by the precipitation of iron oxides in the Leiqiong basaltic residual soil (a residual soil from China). Such bonding, however, was sensitive to the wet-drying cyclic action and would become collapsible after the degree of saturation was increased. From the above review, it is judiciously inferred that bonding preserved in the natural residual soil, arguably attributed to the presence of fine content and mineralogy constituent (e.g. calcium carbonate, and oxides) within the soil structure.

2.2.4 Anisotropy of Residual Soil

Soil anisotropy has been a pivotal research in the realm of soil mechanics for long time. Arthur and Menzies (1972) realized the importance of fabric and stress-induced anisotropies towards the pre-failure and shear strength behaviours of rounded sand as tested in a three-dimensional cubical triaxial apparatus. Li (2011) further found that dynamic behaviours of sand and small-strain elastic properties were governed by the orientation of sand depositing. In addition, Nishimura et al. (2007) investigated the shear strength anisotropy of London clay (over-consolidated clay with fissures) by using the undisturbed specimens subjected to various rotations of principal stress axes in hollow cylinder apparatus. From these precedents, it is clear that (fabric and stress-induced) anisotropy was prevalence in the structured soils (deposited sand and laminated clay) and influential towards soil mechanical behaviours.

In related to the heterogeneity, structural anisotropy was also realized in the residual soil as attributed to the geological formation and subsequent weathering process (Blight and Leong, 2012). The stress-deformation characteristics of a sedimentary residual soil were dictated by the fabric anisotropy and microstructural behaviours. Yet, stress anisotropic was entailed when the direction of applied stress could influence the shearing response of residual soil. Taha et al. (1998) observed the existence of fabric anisotropy in a Malaysian granitic residual soil after conducting a series of direct shear tests using undisturbed specimens (either sampled along the vertical or horizontal direction in reference to the ground surface). In Brazil, Futai et al. (2004)

attributed the existence of fabric anisotropy of a saprolitic soil to the anisotropic characteristic of its mother rock formation. It can be seen from Figure 2.6 that the saprolitic soil (labelled as horizon "C" soil) exhibited anisotropic pattern in which the boundary surface was not centre with respect to the hydrostatic axis (i.e. normalized mean effective pressure axis). Isotropic yielding behaviour could be observed at a much shallower residual soil deposit (i.e. horizon "B" soil) due to the diminishment of anisotropy inherent from the parent rock. In this regard, many researchers also attempted to replicate the in-situ stress state of soil and induce stress anisotropy by conducting K_o-consolidated strength test on residual soils (Meng and Chu, 2011; Guo et al., 2012).

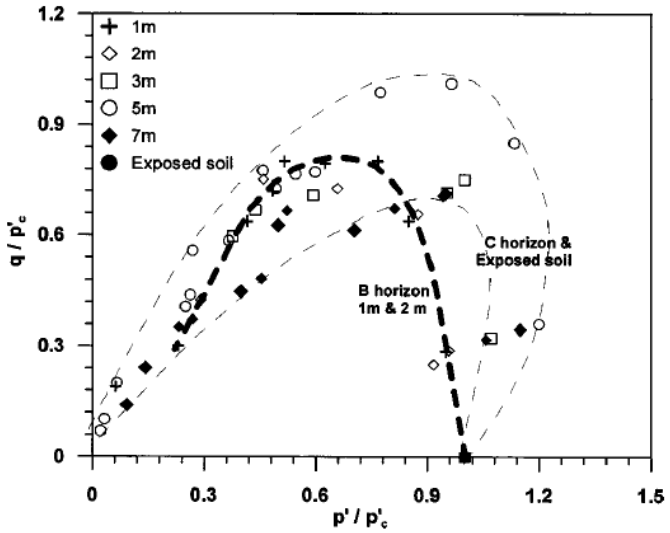

Figure 2.6: Normalized limit state curves (Futai et al., 2004)

From the above critical review, it is apparently shown that natural residual soil can be unique in such a way that structural bond and inherent anisotropy are usually prevalence. The behaviours of an intact residual soil

could be wildly different from that of reconstituted residual soil upon the inherent structure (e.g. natural bonding) had been demolished.

2.2.5 Engineering Relevances of Residual Soil

Numerous cases of slope failure as related to the residual soils, which were derived from different origins of rock formation, had been comprehensively reported in Malaysia (Liew et al., 2004). Undesired ground movement and subsequent progressive failure were found to be governed by the mobilization of shear strength, influence of ground water, and the geometrical considerations of cut slopes. In addition, Gue and Tan (2006) reported that numerous landslide cases had been occurred in residual soil and were largely caused by design error or geological reason. Tan et al. (2004) highlighted the parallel existence of a stiffer residual soil (originated from Kenny Hill formation) zone and a very weak slumped zone (SPT number approximated to zero) overlying the limestone bedrock. Such geological arrangement was tricky in the way that the weak slumped zone was formed underneath the stiffer residual soil deposit; the foundation design could be unsatisfactory if the soil investigation was not adequately committed.

From the above reviews, it is clearly seen that residual soil is widespread in Malaysia and related engineering problems which were encountered from time to time. In view of this matter, a proper geotechnical design and economic implementation of soil stabilization should be persuaded for the residual soil ground. In addition to the traditional mechanical

stabilization technique (e.g. dynamic compaction, soil nailing, reinforcing soil wall, etc.), previous studies showed that chemical stabilization technique was also suitable for improving geotechnical properties of residual soils in superficial layer of ground. Chemical stabilization methods, such as liquid stabilized residual soil (Ali, 2012) and cement-treated residual soil (Basha et al., 2005), had been utilized on residual soils. In spite of furnishing significant strength improvement, conventional chemical stabilization technique (notably, cement grouting) produces higher carbon footprint and the chemical process is toxic in nature. Besides that, a very high grouting pressure (in the scale of MPa) was usually unavoidable for the treatment using cement on account of its high viscosity. Under such high jet grouting pressure, the original ground material would undoubtedly be disturbed to certain extent (Andrus and Chung, 1995).

In recent years, soil bio-mediation (particularly, Microbial-Induced Calcite Precipitation) has emerged as an innovative and sustainable technique for improving engineering properties of different soils (Dejong et al., 2010; Lee et al., 2013; Ivanov et al., 2015). Introduction of the MICP treatment method can shed light on the environmental issues as remained in the conventional ground improvement techniques by using chemical stabilization agent, such as lime, cement, and gypsum grouting (Dejong et al., 2010). Apart from the advantages of being less carbon footprint and non-toxic, the MICP treatment can also offer a wide coverage area from the grouting point attributed to its low viscosity as well as bringing less alterations in ground chemical properties, as compared to the conventional cement grouting.

Therefore, microbial-induced calcite precipitation treatment method was adopted to improve a selected residual soil from Malaysia in the present study.

2.3 Microbial Induced Calcite Precipitation (MICP) as Ground Improvement Method

The term, soil bio-mediation, was generally referred to the geo-bio-chemical process to induce calcite precipitation within soil medium to mediate the soil improvement. Under the umbrella of bio-mediation includes a variety of processes, such as denitrification, microbial-induced calcite precipitation (MICP), iron reduction, and sulphate reduction (Dejong et al., 2010). Those bio-mediation processes promoted a variety conditions (e.g. aerobic/ anaerobic and energy release) for the calcite precipitation.

The typical MICP involves a bio-mineralization process in which the calcite (calcium carbonate, $CaCO_3$) crystals are precipitated through a urea hydrolysis reaction with the engagement of an alkalophilic bacterium (effectively, *Sporosarcina Pasteurrii*). Equations 2.1 and 2.2 show the urea hydrolysis process in which the urea was consumed by the microbe and decomposed into ammonium (NH_4^+) and carbonic acid (CO_3^-) in the presence of water. Calcium carbonate could be precipitated upon the reaction with calcium chloride ($CaCl_2$) in the solution. Favourably, alkaline environment (i.e. pH level > 7) can be induced by the presence of hydroxyl ions (OH^-) from the ammonium to further facilitate the calcite precipitation with available calcium ions (Ca^{2+}). Figure 2.7 illustrates the development of calcite

precipitation through induced urease in the nucleation site as provided by microbes.

$$CO(NH_2)_2 + 2H_2O \rightarrow 2NH_4^+ + CO_3^- \quad (2.1)$$

$$Ca^{2+} + CO_3^+ \rightarrow CaCO_3 \downarrow \quad (2.2)$$

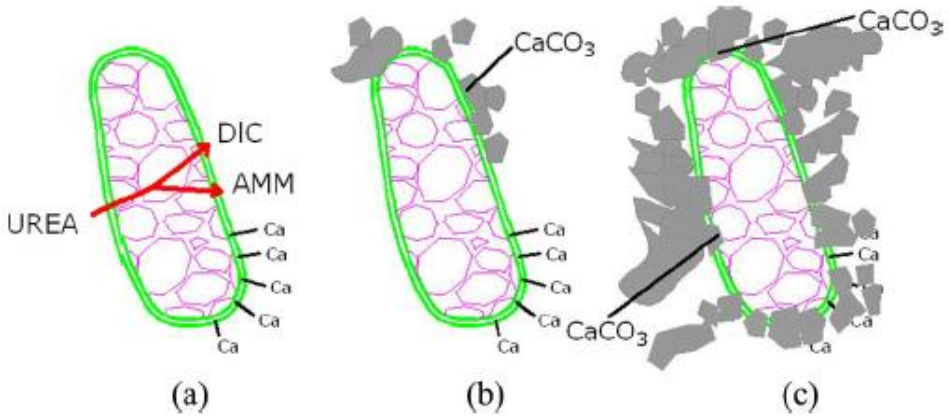

Figure 2.7: Microbes provide nucleation site for the precipitation of calcium carbonates (after Wang et al., 2017)

Through the MICP treatment, abundant amount of calcite crystals could bond two neighbouring soil particles and fill the pore spaces in order to facilitate bio-cementation and bio-clogging mechanisms (Dejong et al. 2010; Ivanov and Chu, 2008). Bio-cementation could fundamentally enhance shear strength and stiffness of soil, whereas bio-clogging could significantly reduce the permeability. From the literature, the improvements in shear strength (Feng and Montoya. 2015; Chou et al., 2011; Cui et al., 2017), initial shear modulus (Dejong et al., 2010), liquefaction resistance (Sasaki and Kuwano, 2016; Zamani and Montoya, 2019), compressibility (Lee et al., 2013), and

erosion resistance (Do et al., 2019) have been investigated extensively. A comprehensive coverage about the recent development of bio-mediated soils can also be found in Terzis and Laloui (2019). To present, most of the bio-mediation research works focused on the laboratory scale of study, whereas only limited contributions was made for the field-scale application (Van Paassen et al. 2010; Gomez et al., 2014; Ghasemi and Montoya, 2020). Figure 2.8(a) and Figure 2.8(b) demonstrates the successfully implementation of MICP treatment in the field scale to increase shear strength for sand and gravel materials, respectively.

(a) (b)

Figure 2.8: Bio-mediation treatment in the field applications: (a) Surface MICP treatment in a desert (Gomez et al., 2014); (b) Stabilization of a bored hole with MICP-treated gravel (Van Paassen et al. 2010)

Numerous research have been devoted to the investigation of the MICP ground improvement technique on coarse-grained materials, i.e. poorly or uniformly-graded sand (Dejong et al. 2010; Al Qabany and Soga, 2013; Do et al. 2019; Cui et al. 2017; Mujah et al. 2017; Kim et al. 2018; Montoya et al.

2013). Unconfined compressive strength of bio-mediated sand could be improved to as high as 2 MPa (Mahawish et al., 2018). Several other studies attempted the MICP technique in improving properties of fine-grained soil (Lee et al. 2013; Sharma and Ramkrishnan, 2016; Li et al. 2016; Chiet et al. 2016; Chen and Kassim, 2015; Henry et al. 2019; Umar et al. 2015). Through bio-encapsulation method, the permeability and shear strength properties of a Singapore soft marine clay were improved by MICP treatment (Ivanov et al., 2015; Li et al., 2016). Besides that, undrained shear strength behaviours (Zamani and Montoya, 2015; Sasaki and Kuwano, 2016) and erosional response (Jiang et al., 2016) for soils containing fines content were investigated.

Most of the studies concluded that the shear strength properties for the coarse-grained materials (i.e. clean sand) could be improved to a greater extent as compared to the soil with noticeable fines content. As a matter of fact, the treatment on the fine-grained materials is less effective than the coarse-grained materials because of the low permeability and small pore size which may obstruct the flowing of cementation reagent and microbes.

2.4 Practical Considerations in MICP Treatment for Soil

2.4.1 Size Compatibility in Soil-Microbe Medium

Transportation of microbes within the soil medium was decided by the size of pore throats, which were greatly depended upon the average grain size of fines particles (i.e. passing aperture size of 63 μm). This was attributed to the fact

that the typical size of a microbe ranged from 0.5 μm to 3 μm (Dejong et al., 2010) and therefore the involvement of finer particles played an important role in affecting the size of pore throat. If the size of a pore throat was undesirably small, the microbes would not be capable to migrate from one to another location thus unable to produce uniform calcite precipitation. The pore size within uniform sand, which was commonly used as a filtering material, was claimed to be governed by the grain size corresponding to 10 % passing (i.e. D_{10}) in a grain size distribution curve (Holtz and Kovacs, 1981; Hazen, 1911). The suggested pore size estimation method was only appropriate for uniform sand and might not be workable for well-graded material (such as residual soil). For this reason, it is also informative to justify the appropriateness of a particular type of soil for practical MICP treatment by other criterion or suggestion from the literature.

From the literature, it was learnt that majority of MICP studies focused on the poorly-graded sand (Dejong et al., 2006; Ivanov and Chu, 2012; Chou et al., 2011; Cui et al., 2017; Feng and Montoya, 2015; Zamani and Montoya, 2019). Taking D_{50} as the mean particle size, the reported particle size of sand used in MICP treatment ranged from 0.12 mm to 0.52 mm. Within this particle size range, significant improvement could be observed in MICP treatment. In addition, Rebata-Landa (2007) suggested that an effective MICP treatment could be achieved within an optimal particle size range of 0.05 mm and 0.4 mm. Even though the prescribed criterion was fulfilled, pre-mixed of bacteria with the residual soil mass was suggested before compaction of a specimen to

avoid the complication due to the issue of geometrical incompatibility between soil and bacteria (Lee et al., 2013; Chiet et al., 2015).

2.4.2 Methods of MICP Treatment in Laboratory

MICP treatment condition was greatly relied upon the soil type, state of field replication, and corresponding state in mechanical testing. This section highlights the methods of MICP treatment for sand and soil constituting fines content in the laboratory, respectively.

2.4.2.1 MICP Treatment Method for Sand

Principally, the MICP treatments of sand (Dejong et al., 2010; Cheng and Cord-Ruwisch, 2012; Feng and Montoya, 2015; Cui et al., 2017) were accomplished in following manners: (a) furnishing a designated volume of microbe-nutrient solution (i.e. corresponding to certain proportion of pore volume in sand) into the sand medium; (b) promoting extensive growth of bacteria with the supplied nutrient in solution; (c) injecting cementation agent (i.e. mixed solution of urea and calcium chloride) to induce calcites through the urea hydrolysis process (as described in Section 2.3). For instance, Cheng and Cord-Ruwisch (2012) implemented the treatment by alternately pouring bacteria solution and cementation agent (1 Mol/L of urea and calcium chloride) into the sand column. Dejong et al. (2006) first injected 400 ml (several times of sand's pore volume) of biological solution (consisting urea, bacteria, and 8 ml of calcium chloride) and repeatedly injected same volume

of cementation reagent (consisting urea and calcium chloride). In addition, Cui et al. (2017) suggested a 60:40 two-phase treatment method for a concrete sand; 40 % pore volume of pure bacteria solution and followed by 60 % pore volume of mixed bacteria solution (mixture of bacteria and calcium chloride) were injected into the sand prior to the introduction of cementation reagent (e.g. urea and calcium chloride). Similarly, the two-phase treatment method had also been implemented in other MICP sand studies (Lin et al., 2016; Zamani and Montoya, 2019). A vast variety of treatment mix proportions was realized from the reported studies while it is crucial to employ the most suitable method of treatment inasmuch as the testing material, practical simplicity, and replicated condition.

On top of the treatment procedures as described above, treatment approaches could also be formulated differently by controlling the degree of saturation (submerged or unsaturated) and the sequence of imposed confining pressure (whether the confining pressure was applied before or after the treatment) throughout the bio-chemical process. Whiffin et al. (2007) adopted a submerged flow treatment method to treat the sand column under a fully submerged condition. Similarly, Dejong et al. (2006) and Feng and Montoya (2015) treated the sand by injecting biological and cementation solutions alternately from the base of a triaxial specimen, within a specific duration. However, it was claimed by Terzis and Laloui (2019) that the most effective calcite precipitation (i.e. at contact between neighbouring particles) could be obtained for the soil treated under partially saturated condition. On the other hand, numerous MICP treatments were carried out under unsaturated

condition, in which the percolated solution was allowed to freely drain at the bottom of specimen (Cheng and Cord-Ruwisch, 2012; Cui et al., 2017). The injection of chemical solution in most MICP treatments were accomplished by using a peristaltic pump whereby the rate of flow could be electronically controlled. Under a special circumstance, Cheng and Cord-Ruwisch (2012) applied surface percolation treatment in which the solution was injected by downward gravity forces only.

Moreover, confining pressure was sometimes applied before the MICP treatment process in an attempt to avoid degradation of calcite cementation as caused by the isotropic consolidation (Feng and Montoya, 2015). The sand specimen was initially set up inside a triaxial cell and later subjected to a series of confining pressures (i.e. 100 kPa, 200 kPa, and 400 kPa), before the MICP treatment process. Under such sequential arrangement, the shearing behaviours of MICP-treated sand subjected to different level of confining pressures (corresponding to different states of compactness) could be investigated. The effect of confining pressure and calcite cementation could comparatively be examined. Quite differently, Cui et al. (2017) treated the sand specimens in an external split mould and transported the specimen into the triaxial cell for mechanical testing (as shown in Figure 2.9). It can be seen that a pair of porous layers was used to provide firm support and reduce the possibility of scouring at the end surfaces of treated specimen. In view of the sand specimen was treated before undergoing consolidation in the triaxial cell, it is arguably that the cemented structure would be influenced by the level of

consolidation pressure. For this reason, the authors conservatively limited the magnitude of confining pressure to 100 kPa throughout their study.

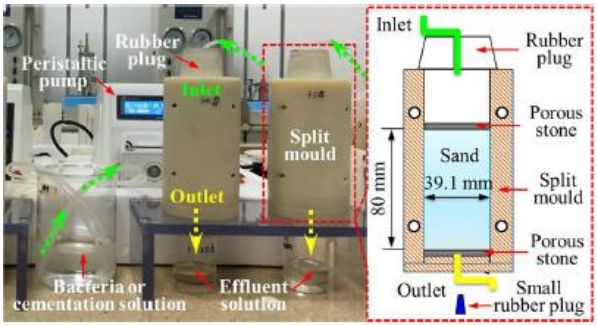

Figure 2.9: MICP treatment split mould (Cui et al., 2017)

2.4.2.2 MICP Treatment Method for Soils Containing Fines

There were several attempts on treating the soils with fine contents (Ng et al., 2013; Ng et al., 2014; Lee et al., 2013; Chiet et al., 2016; Chen and Kassim, 2015; Henry et al., 2019; Umar et al., 2015; Sharma and Ramkrishnan, 2016). However, the MICP treatments on the soils with fines were less effective than those of the coarse-grained materials (i.e. sand and gravel) on account of their low permeability that considerably inhibited the permeation of bacteria/ cementation reagent through the pore spaces of soil medium. Therefore, it is practical to pre-mix the bacteria with dried residual soil mass before it was formed into a specimen to avoid any complication caused by the geometric incompatibility between soil grain and bacteria. As shown in Figure 2.10, tropical residual soil was treated in a cylindrical mould (a nominal height in 120 mm and diameter in 50 mm) and permeated with chemical reagent under a fairly low degree of flow pressure (i.e. differential pressure of 20 kPa, in

excess of atmospheric pressure). The flow pressure of chemical reagent was manually controlled by adjusting the pneumatic pressure inside a pressure tank. The flow pressure of 20 kPa was deemed to be sufficient and effective for the treatment of residual soil inasmuch as the degree of improvements in unconfined compressive strength and hydraulic conductivity (Ng et al., 2013). Lee et al. (2013) found that excessive flow pressure (as high as 200 kPa) would not promote the calcite precipitation within the soil specimen. This was probably linked to the disturbance of original soil arrangement upon the application of high flow pressure of chemical reagent into the specimen. From the above review, it is understood that the flow-pressure treatment setup was applicable and widely adopted for the treatment of less permeable soil (such as residual soil). Since the specimen from flow-pressure setup was mandatory subjected to bio-treatment prior to consolidation, it is necessary to consider of the influence of consolidation pressure towards the MICP-treated residual soil.

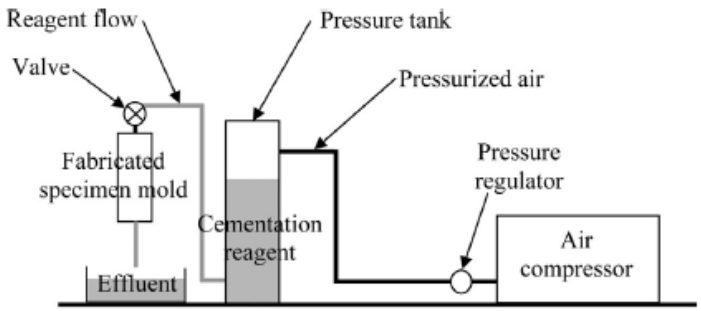

Figure 2.10: Schematic of flow-pressure setup (Lee et al., 2013)

2.4.3 Effect of Chemical Reagent Concentration

From the literature, it was known that concentration of chemical reagent (usually measured in unit of Mol/L) was influential towards the calcite precipitation in soil (Cheng et al., 2016; Al Qabany and Soga, 2014; Chiet et al., 2016). Figure 2.11 illustrates two simplified models of calcite precipitation within the pore space of uniform sand, which were subjected to MICP treatment with low and high chemical concentrations Al Qabany and Soga (2014) concluded that high concentration of reagent (i.e. 1.0 Mol/L) would cause non-uniform calcite formation and therefore produced insignificant soil improvement as attributed to the stress localization effect. When the concentration of reagent reached 1 Mol/L, larger calcite crystals could be formed within the pore space (Cheng et al., 2016) to occupy the pore volume. On the contrary, it was realized that a low concentration of chemical reagent (< 1.0 Mol/L) was sufficient for an efficient strength improvement in the MICP-treated residual soils (Chiet et al., 2016) and uniform distribution of calcite crystal (Mahawish et al., 2018; Al Qabany and Soga, 2014). Coincidentally, Ng et al. (2013) reported that the optimum cementation reagent concentration for MICP treatment for a residual soil in Malaysia was 0.5 Mol/L.

It is also important that adequate level of alkalinity (pH level) in the effluent should be reached to ensure an active urea hydrolysis process. Practically, Feng and Montoya (2015) justified that the pH level needed to ensure the favourable bacterial activity was at least 8.0. Once the pH level was

reduced below the prescribed threshold, supplementary bacteria had to be furnished to facilitate the continuous growth of bacteria.

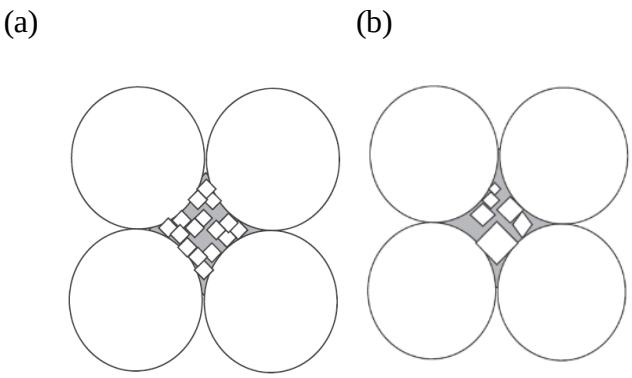

Figure 2.11: Schematic diagrams for pore clogging by calcites: (a) at low chemical concentration; (b) at high chemical concentration (Qabany and Soga, 2014)

2.4.4 Effect of Temperature during Treatment

The formation of calcites could be affected by the temperature as related to the activeness of enzyme process. Cheng et al. (2016) investigated the effect of treatment temperature on the shear strength properties of clean sands by simulating the subsurface soil temperature under cold (i.e. 4 °C), tropical (i.e. 25 °C), and hot (i.e. 50 °C) conditions. At a same amount of calcite content, the highest shear strength was obtained for sample treated under the temperature of 25 °C. Besides that, Henry et al. (2019) found that the MICP treated residual soil showed the highest shear strength when the treatment temperature reached 55 °C. Under a room temperature ranging from 25 °C to 30 °C, Lee at al. (2013) also managed to obtain a significant shear strength improvement on the MICP-treated residual soil. Therefore, it can be inferred that the formation of calcites in MICP-treated soil was affected by

temperature. Nevertheless, the MICP treatment under atmospheric temperature was sufficient to improve the soil properties.

2.5 Mechanical Behaviours of MICP-treated Soils

2.5.1 MICP-treated Sand

In general, the mechanical behaviours of MICP-treated soils can be understood from the aspects of consolidation (namely, isotropic, or one-dimensional consolidation) and shearing behaviours. Feng and Montoya (2014) conducted a series of Oedometer experiments to investigate the one-dimensional consolidation behaviours of untreated and MICP treated sands. It can be seen from Figure 2.12 that the initial void ratio of the MICP-treated sand was much lower than that of untreated sand; both lightly (i.e. calcite content of 0.2 % only) and highly cemented (i.e. calcite content of 2.2 %) sands experienced gradual change in void ratio while the untreated sand started to deform abruptly from the commencement of loading. The difference in compressibility (reaching normal consolidation state) between both untreated and bio-treated sands was not concluded in their study. The results suggested that the MICP-treated sands possessed certain degree of structural resistance (yield strength) as compared to that of untreated sand. Recently, Xiao et al. (2020) further confirmed that the sand specimens with higher calcite content would exhibit less compressibility under one-dimensional consolidation. In the one-dimensional consolidation test, the lateral deformation was constraint by rigid wall and radial strain was not measured. Therefore, it is informative to investigate the directional movements

(vertically and laterally) of soil grains with MICP-treated structure by simultaneously monitoring on the vertical and radial strains in an isotropic consolidation test in which the lateral movement was not restraint whatsoever.

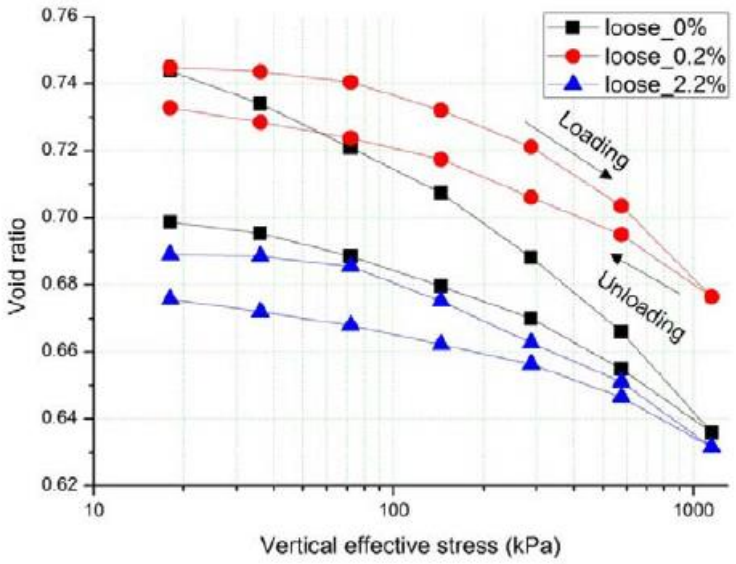

Figure 2.12: Void ratio changes for loose sand at various cementation levels (Feng and Montoya, 2014)

During the shearing stage, strain-softening response was apparently observed for heavily treated MICP sands under undrained and drained shearing. It was analogous to the mechanical behaviour of dense sand whose failure was in brittle manner (Lade and Trads, 2014). Figure 2.13 depicts a typical stress-strain response for untreated and MICP-treated sands as reported by Dejong et al. (2010). The mechanical responses were also correlated to the shear wave velocity measurement throughout the undrained compression experiment. From the stress-strain response, it was obvious that the shear strength of MICP-treated sand was mobilized at a peak deviator stress ratio before experiencing strain-softening and progressed to the ultimate critical

state. The peak shearing stress ratio for the MICP-treated sand specimen (stress ratio of 1.7) was greater than untreated sand specimen (stress ratio of 1.2).

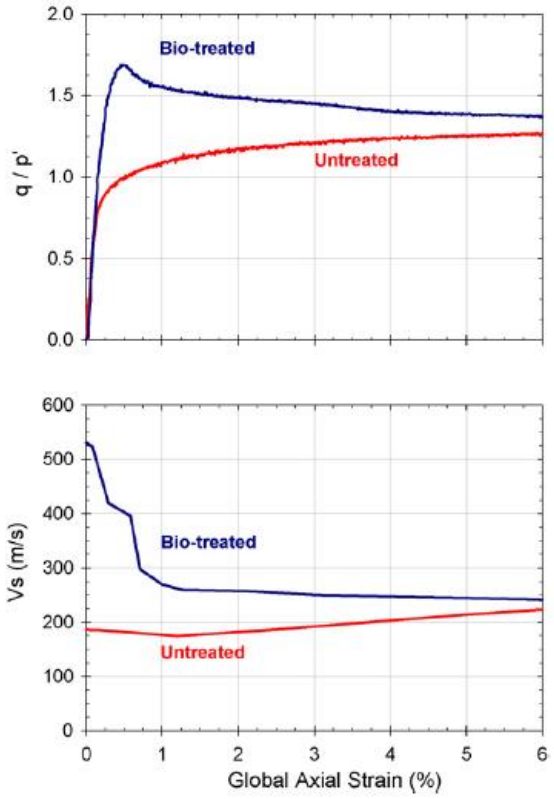

Figure 2.13: Stress-strain and shear wave velocity responses for MICP-treated sand under undrained triaxial shearing experiment (Dejong et al., 2010)

The significant improvement in shear strength parameters for MICP-treated sand was also observed by Cui et al. (2017). It was confirmed that the effective friction angle increased linearly with the cementation level, whereas the cohesion parameter increased exponentially with the cementation level. Cui et al. (2017) observed that the brittleness of MICP-treated soils increased with respect to the cementation level (as illustrated in Figure 2.14). Appreciably high cementation level (at least 10% net calcite content of dry

soil mass) is necessary for MICP-treated sand to display strain-softening and brittle behaviours under shearing, The brittle failure pattern of a heavily cemented sand, which was physically accompanied by a slip surface, is shown in Figure 2.15.

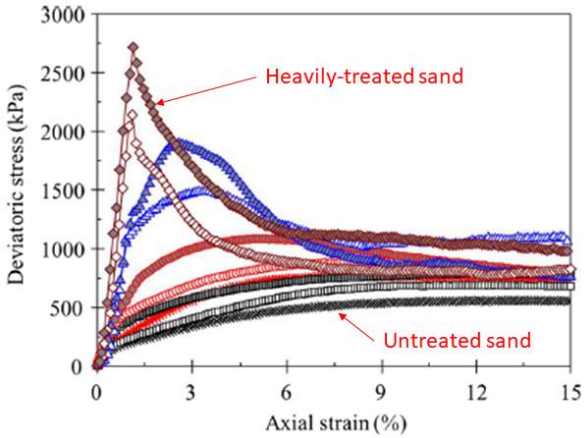

Figure 2.14: Influence of cementation level on stress-strain responses under undrained triaxial shearing experiment (Cui et al., 2017)

Figure 2.15: Failure patterns for heavily treated sand in undrained compression test (Cui et al., 2017)

Similar shearing behaviour was also reported by Feng and Montoya (2015) after conducting a series of triaxial drained test (as depicted in Figure 2.16). The phenomenon of strain-softening was not observable for the sand specimen with a calcite content as low as 1.5 %. Once the average calcite content reached 3.5 %, it was deemed to be a heavily treated sand and the prescribed brittle failure prevailed. From the above studies, it is inferred that strain-softening was a trait of heavily cemented MICP sand under drained and undrained triaxial shear tests. However, such trait would not be apparently spotted in MICP-treated sand, which is either formed with a dense or lightly cemented structure.

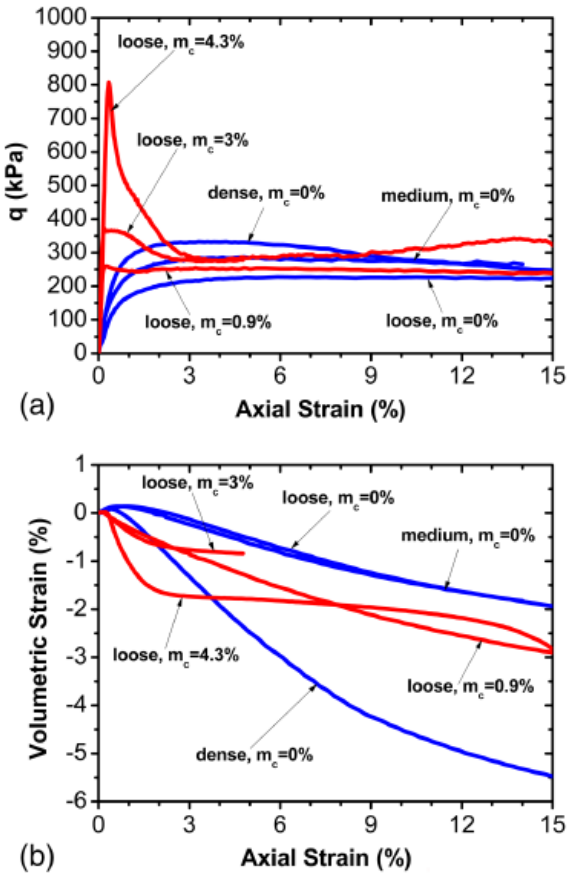

Figure 2.16: Stress-strain and volumetric responses of sand with varying cementation levels under 100 kPa of effective confining pressure in triaxial drained experiment (Feng and Montoya, 2015)

2.5.2 MICP-treated Soil with Fines

Lee et al. (2013) conducted a series of one-dimensional consolidation tests on untreated and MICP-treated residual soil, comprising 62 % of fines content. From Figure 2.17, it was observed that the MICP-treated residual soil would deform less as compared to the untreated residual soil, under a same vertical consolidation pressure. They also reported that the pre-consolidation stress and compression index were not appreciably altered. The recompression index of the bio-mediated soil, however, decreased and resembled the deformation behaviour of those naturally aged clays as reported by others. The insignificant improvement in deformation properties of the described residual soil was arguably linked to the high percentage of fines content that inhibiting the calcite cementation. This is based on the fact that MICP-treated sand was characterized with apparent improvement in yield stress, as previously discussed.

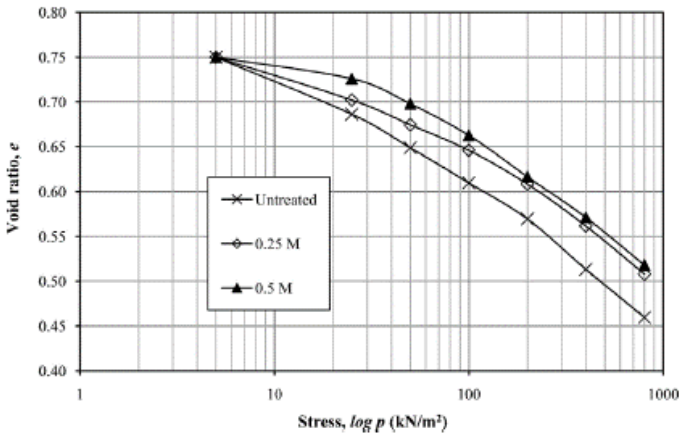

Figure 2.17: Void ratio changes at various concentration of cementation reagent (Lee et al., 2013)

Extensive efforts have been placed on the shearing behaviours of MICP-treated residual soils through unconfined compression test (Ng et al., 2013; Ng et al., 2014; Chiet et al., 2016). Typical stress-strain curves for MICP-treated residual soils is presented in Figure 2.18. Significant shear strength improvement was observed for the MICP-treated residual soils which comprise considerable amount of fine contents. Henry (2019) and Umar (2015) observed that the unconfined compressive strength and cementation level of the MICP-treated residual soil could be correlated to the curing duration and temperature. It is worth mentioning that calcite contents of the above-mentioned MICP treated residual soils (generally below 3 %) were lower than the cementation level required for reaching soil brittleness (i.e. 7.26 %) for sand, as described earlier. This comparison further implied that calcite crystals could easily precipitated within the coarser particles as compared to the soils containing fine contents. This is probably attributed to the fact that bacteria and chemical reagent could transport through the coarser medium of clean sand smoothly. In addition, the MICP-treated residual soil could probably not manifest strain-softening and apparent brittleness during undrained shear test.

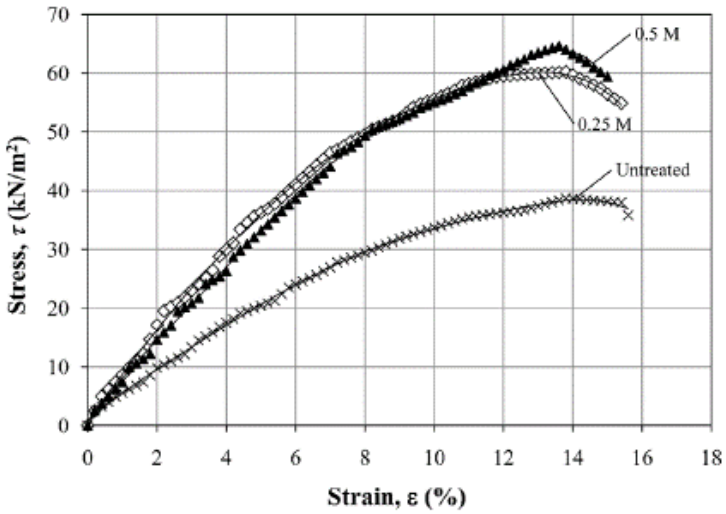

Figure 2.18: Stress-strain curves at various concentration of cementation reagent (Lee et al., 2013)

Current knowledge on the mechanical behaviours of bio-mediated residual soil has largely been limited to the unconfined compression test in which the soil specimens were usually unsaturated. It is necessary to investigate the stress-deformation behaviours of saturated MICP-treated residual soil subjected to field-replicated stress conditions and surrounded by certain degree of confining stress beneath the ground surface.

In undrained cyclic triaxial tests, Sasaki and Kuwano (2016) concluded that the presence of fine contents would impair the liquefaction resistance of MICP-treated sand containing different amount of fines (ranging from 0 – 30 %) due to the calcite being precipitated at the location where no structural resistance was contributed to the soil specimen. Zamani and Montoya (2018) found that bio-cemented silt aggregates (i.e. silt-sized particles being cemented by calcium carbonate) played a dominant role in framing the force chain and providing undrained shearing resistance in a MICP-treated silty

sand, which constituted fines content of nearly 35 %. It was also observed that the altered structural formation promoted a metastable soil arrangement while reducing the tendency in generation of excess pore-water pressure. From the above findings, it is anticipated that the mechanical behaviour for MICP-treated residual soil under monotonic undrained shearing would very much be dictated by the fines content and particle size distribution in the original residual soil. Yet, the cemented assemblages from fines (silt and clay particles) could form a unique load-bearing force chain in addition to the particle contact mechanism as manifested by sand particles.

2.6 Microstructural Formations of MICP-treated Soils

At microscopic scale, it is widely agreed that the soil behaviours of MICP-structured soil were fundamentally governed by calcite cementation and calcite densification mechanisms. Calcite cementation was crudely regarded as the calcite binding effect bridging or interconnecting neighbouring soil grains, although detailed microscopic studies recognized other different mechanisms in the formation of MICP soil. It follows that, macroscopic observations were extensively explained on the basis of those two calcite-induced mechanisms (Dejong et al., 2010; Ivanov and Chu, 2012; Lin et al., 2016). In subsequent sections, these two fundamental mechanisms are elaborated and justified by macroscopic laboratory observations.

2.6.1 Calcite Cementation

Figure 2.20 illustrates simplified calcite binding models for a MICP-treated sand, as reported by Dejong et al. (2010). The MICP structure was also justified by microscopic observations, such as SEM and X-ray analyses. It was reported that a thin layer of calcite distribution was still preserved on the surface of sand grains, after the bonding at particle contact had been fallen apart by shearing. The actual calcite cementation between two neighbouring soil particles was arguably formed by the surface-adsorbed calcite crystals and precipitation at point of contact (as shown in the "actual" configuration in Figure 2.19). Similar mechanism of calcite cementation was also reported by Cui et al. (2017) in their investigated MICP-treated sand structure, as illustrated in Figure 2.20.

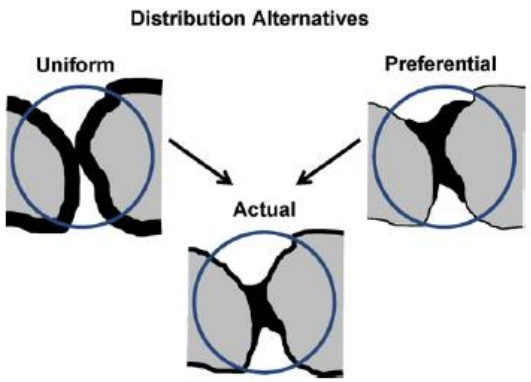

Figure 2.19: Simplified models of calcite binding (Dejong et al., 2010)

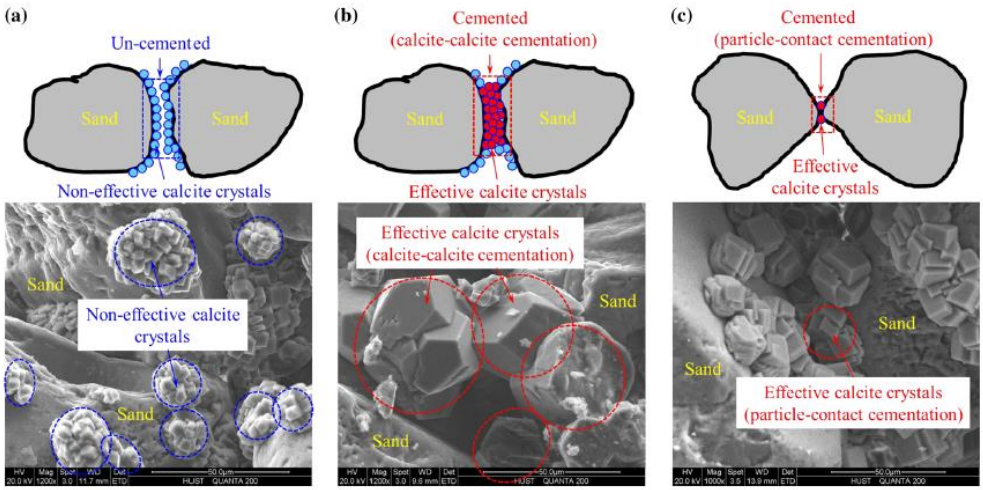

Figure 2.20: Microscopic configurations of calcite cementation of sands (Cui et al., 2017)

Terzis and Laloui (2018) examined the configuration and interaction effect between the precipitated calcites and adjacent sand grains. From their microscopic study (Figure 2.21), active calcite bond was observed in bridging two neighbouring soil grains, whereas inactive calcite crystals adsorbed onto the surface of individual soil grain. Besides that, Cheng et al. (2016) claimed that treatment of fine sand (i.e. average grain size of 0.15 mm) could promote uniform and abundant calcite bonding between soil particles, as compared to the coarser sand grain.

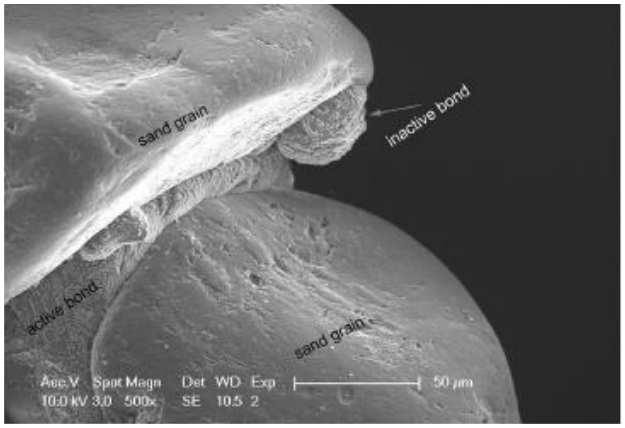

Figure 2.21: Active and inactive calcite bonds (Terzis and Laloui, 2018)

Based on the previous calcite cementation model, Lin et al. (2016) further reported three simplified calcite formations (as illustrated in Figure 2.22) within the soil matrix. Apart from the described calcite cementation mechanism, particle-to-particle calcite bridging, and matrix-supporting structure were observed. The newly introduced matrix supporting mechanism was pertinent to the inter-connection of solid particles through the extensive growth of calcite crystals within the pore space of sand structure. Unlike the calcite bonding, matrix supporting system was simply a load-bearing structure.

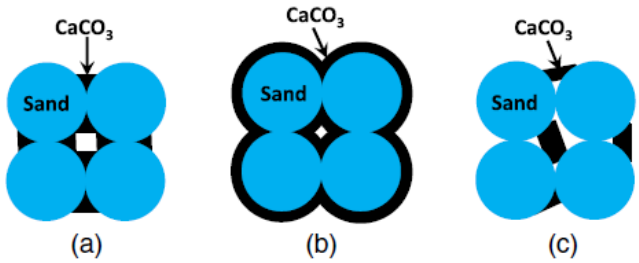

Figure 2.22: Ideal calcite precipitation models: (a) contact cementing, (b) calcite coating, and (c) matrix supporting (Lin et al., 2016)

The calcite cementation effect was observed to be influential towards the macroscopic behaviours of the treated soils. The calcite bonding would not only promote the increase of initial small-strain stiffness of treated sand, but also favourably improve the shearing resistance (e.g. peak strength and ultimate shearing resistances) of sand. This was attributed to the calcite bonding at contact point of soil particles and the inducement of force chain of load transfer within the treated soil specimen. It can be understood that the shearing stress was transmitted uniformly along the force chain system in lightly treated sand, whereas obvious stress localization could be expected in the heavily treated sand (Lin, et al., 2015).

However, the presence of fines (silt and clay-sized particles) within the residual soil could complicate the formation of effective calcite precipitation. The calcite precipitation could occur at the location where no significant structural resistance being contributed (Sasaki and Kuwano, 2017). Apart from the fines content, it is believed that other soil physical properties such as soil gradation, grain size, surface texture and shape of grain may also greatly influence the structural configuration of the MICP-treated soil. Xiao et al. (2019b) observed that more effective calcite cementations could be formed in soil particles of less overall regularity. The liquefaction failure mechanism and the corresponding pore-water pressure response were also found to be governed by the relative density of sand (Xiao et al., 2019a). Hence, it can be expected that the fabric of the MICP-treated residual soil and its failure mechanism could be wildly different from those of the MICP-treated sand. To present, there is no experimental study prioritizing on examining the formation

of microscopic structure and the corresponding structural behaviour for the MICP-treated residual soil. A direct way of assessing the differences in formation and mechanism of MICP treatment between residual soil and sand is through conducting experimental tests on both of the materials (namely, clean sand and residual soil) under the same testing condition.

2.6.2 Calcite Densification

Calcite densification mechanism is a phenomenon concerning void filling of pore volume by the calcite crystals precipitated in the MICP treatment. It was universally agreed by many that such void filling effect could promote the decrease in permeability for a variety of soils (Ivanov and Chu, 2012; Ng et al., 2014; Zamani et al., 2016; Hataf and Baharifard, 2019). In fact, such mechanism could also be seen in traditional soil stabilization technique, such as cement stabilization method. Li et al. (2015) observed the effect of densification in cement-treated sand, whereby the cement powder content significantly altered unconfined compressive strength and hydraulic conductivity of soils. The alteration in soil matrix as attributed to the calcite precipitation (through MICP) within the pore space would also influence the mechanical behaviours of tested soil. Upon the breakage of calcite bonding, calcite densification was claimed to be playing a dominant role to furnish higher degree of ultimate shearing resistance (normally presented in terms of q / p' ratio) as compared to the untreated counterpart. The precipitated calcite could clog the voids leading to fewer tendencies of pore water dissipation and less movement of soil grains being triggered (Canakci et al. 2015). Zamani

and Montoya (2018) further concluded that calcite precipitation in silty sands could result in the formation of calcite-silt aggregates acting like a single soil grain. This phenomenon could lead to less particle movement and reduction of excess pore-water pressure when the MICP soil structure was subjected to external loading.

Mahawish et al. (2018) concluded that the calcite assemblage (i.e. agglomeration of calcite crystals) as trapped inside the pore space could contribute to the compressive strength of soil. Cheng et al. (2016) explicitly concluded that larger agglomeration of calcite crystals within the pore space and gaps of soil medium could contribute to the compressive strength. The formation of calcite crystals could be correlated to the increase of shear wave velocity, reflecting a more rigid structure (Lin et al., 2020). It is also anticipated that the soil can become more and more compressible as the calcite assemblage would be continuously fractured into smaller pieces with the increase of consolidation stress.

2.6.3 Distribution of Precipitated Calcites

It was learnt from the above-mentioned review that MICP-treated soil structure could be formed at particle-level through the mechanisms of calcite cementation and calcite densification within the pore space. However, the formation of calcites would probably be heterogeneous and non-uniform throughout the volume of soil specimen. Do et al. (2019) observed that the uniformity of calcite crystals was affected by the numbers of treatment cycle,

spatial distribution of bacteria, and direction of chemical reagent flow. It was realized that the non-uniformity distribution of calcite crystals was increased with respect to the treatment cycle and cementation level. For example, the treated specimen showed a fairly uniform calcite distribution profile when it was lightly treated but showed the trend of heterogeneous when it was heavily treated

The calcite content would accumulate near the injection point and tended to reduce with distance away from the injection point of solution (Feng and Montoya, 2015; Lin et al., 2016; Do et al., 2019). During the bio-mediation treatment process, Lin et al. (2016) further found that the calcite distribution was not influenced by the confining pressures as small as 100 kPa only. Furthermore, Jiang et al. (2016) realized that the distribution of calcite was largely affected by the flow direction and hydraulic pressure of chemical reagent. Two extreme findings were reported: (a) calcites greatly accumulated near the top part of injection point for a sand-Kaolin clay mixture with the least stable grain arrangement (they defined stability of grain arrangement based on gap ratio, i.e. ratio between the minimum grain size among coarse particles and maximum grain size among fine-grained particles); (b) oppositely, calcites were found to be accumulated further away from the injection point in a sand-clay mixture with less porosity and greater stability. The above discrepancy was attributed to the fact that precipitated calcites in the top part of soil was subjected to less degree of downward pressure on account of its higher porosity.

Moreover, Van Paasssen (2011) observed the segregation of finer particles from coarser grains and heterogeneous distribution of calcite precipitation in the sand-gravel mixture, as illustrated in Figure 2.23. It is anticipated from the above studies that the stress-deformation behaviour of well-graded soils with the presence of fines (for instance, residual soil) would be governed by the uniformity of calcite distribution and the structural heterogeneity, as induced by the bio-mediation treatment. The aspects of non-uniformity and heterogeneity in MICP-structured soils were arguably pertinent to the anisotropic deformation response that can perhaps be examined in the isotropic consolidation test, as discussed in Section 2.5.1.

Figure 2.23: Heterogeneous calcite distribution (Van Paassen, 2011)

2.7 Structural Changes of MICP-treated Soils

MICP-treated soil was said to experience several distinctive stages of structural/ behavioural change when it was subjected to an external stress (i.e.

isotropic confining pressure or deviator stress during shear test). This includes initial yielding, progressive degradation of calcite cementation, dilatancy behaviour, and ultimate state. On top of the conventional stress-strain-time measurement, these changes could be detected by real-time wave propagation monitoring, popularly through shear wave velocity measurement (Dejong et al., 2010; Lin et al., 2016; Do et al., 2019). It is learnt that structural degradation of MICP-treated soils could be determined through shear wave propagation monitoring, which were based on active wave propagation technique (also called bender element test). The bender element test required triggering of an active shear wave from a piezo-electrical transmitter and received by another receiving transducer at the far end within a tested soil specimen.

Dejong et al. (2010) investigated the progressive structural changes in MICP-cemented sand through triaxial test instrumented with shear wave velocity measurement. The shear wave velocity was continuously monitored from the commencement of biological treatment to undrained shearing stage. Theoretically, shear modulus is a multiplying product from dry density of soil and square of shear wave velocity within linear elastic regime. As such, higher magnitude of measured shear wave velocity indicates a soil structure of greater rigidity. It can be observed from Figure 2.24 that the studied MICP sand initially reached elasto-plastic yielding, which was regarded as onset soil de-bonding, and ultimately progressed to critical state (attaining a constant q/p' ratio). Throughout the process of shearing, progressive breakage of calcite cementation was corresponded by the abrupt decrease of measured shear wave

velocity. At the critical state, MICP-treated sand possessed much greater q/p' stress ratio and coincidentally in line with the increase of shear wave velocity. The mechanism of calcite de-bonding could perhaps be grasped from the behaviour of soil being cemented by Portland cement (Rotta et al., 2003). The breakage of bonding in cemented-treated soil was found to be corresponding to the onset of yielding of soil specimens, as depicted in Figure 2.25.

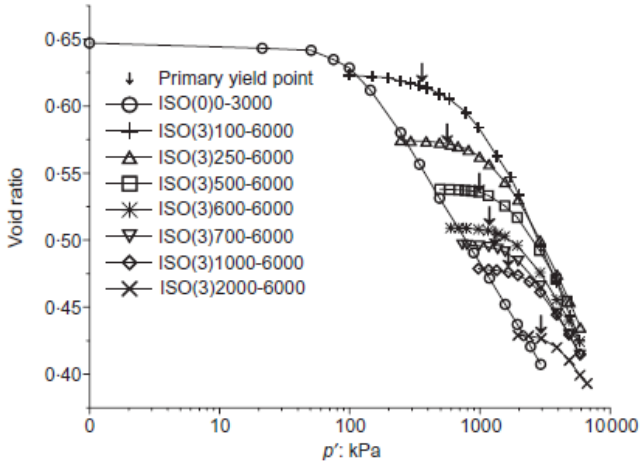

Figure 2.24: Gradual breakage of cement bond as corresponded to primary yield point under isotropic consolidation test (Rotta et al., 2003)

As shown in Figure 2.25, Lin et al. (2016) also distinguished the behaviour of MICP-treated sand from the untreated sand based on the shear wave velocity measurement. The shear wave velocity for MICP-treated sands were incipient to drop at axial strain of about 0.1 ~ 0.2 %, hinting the onset of mobilization of soil grains and yielding. The marked changes in shear wave velocity, however, were not observable in the untreated sand under three different levels of effective confining stress (i.e. 25 kPa, 50 kPa, and 100 kPa). This finding is reasonable on account of the initial low density (i.e. Relative density ≈ 40%) was adopted. Without any form of pre-stressing or

cementation, it is conceivable that untreated and loosely-packed sand would possess little or negligible degree of yield resistance. With the increase of axial strain amplitude, the MICP-treated sands continued to experience structural degradation and manifested localized failure by a slip plane. At strain amplitude of nearly 10 %, the measured shear wave velocity increased with the calcite content of sand while the untreated sand showed the lowest shear wave velocity. This observation was attributed to the preservation of non-fractured calcite bonding away from the location of slip surface.

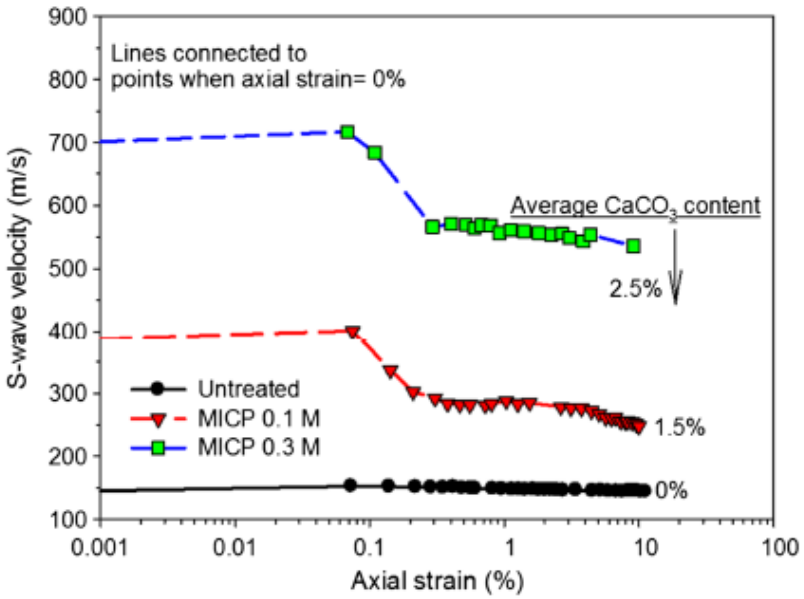

Figure 2.25: Shear wave velocity change as determined by shear wave velocity change during drained shear test (Lin et al., 2016)

Despite of the brilliantness of the above-mentioned shear wave monitoring method, it is usually preferable to investigate the wave propagation behaviours of soil under the most native manner without disturbing the specimen. Practical uncertainties can also be avoided inasmuch as the bender element test was influenced by a number of factors, such as size and type of

piezo-electrical transducer, frequency of triggered signal, electromagnetic coupling effect, and method in determination of arrival time of signal (Leong et al., 2009; Chan, 2010). For these reasons, an alternative approach of stress wave or energy dissipation monitoring instrumentation has to be persuaded in order to investigate the structural changes of soil.

2.8 Acoustic Emission Monitoring on Soils

Acoustic emission (AE) technique can detect onset energy dissipation of stored strain energy in a stressed soil material as a result of grains movement, particle slippage, fracturing, and other pertinent phenomena (Hardy, 2003). This kind of non-destructive wave measuring method has widely been used in laboratory element tests (Tanimoto and Tanaka, 1986; Tanaka and Shirakawa, 1995; Mao and Towhata, 2015; Lin et al., 2020) to investigate a variety of soil characteristics, while some contributions were also made for the large-scaled model test (Dixon et al., 2002; Deng et al., 2014) and in-situ monitoring (Koerner and Lord, 1972; Tanimoto et al., 1978).

Configuration of a typical AE signal was illustrated by Figure 2.26. It can be clearly seen that an event hit comprised of numerous AE spikes (peak and trough points), which were distributed beyond a prescribed noise threshold level. AE counts rate (traditionally called the ring-down count) was defined as the total AE spikes within a specified duration of quantification, normally counting at every 10 s (Tanimoto and Tanaka, 1986) or even 5 s (Lin et al., 2020). Similarly, AE event rate was defined as the total number of event

hit occurred within a specified duration (Hardy, 2003). These two parameters (namely, AE hit and counts rate) were universally used to quantify the energy dissipation in stressed soils by researchers. In a more specified way, the dissipation of acoustic energy can principally be represented by the area under the envelope of a transient AE wave (as shown by the shaded area in Figure 2.26). In addition, the dominant frequency of acquired AE signal can be determined by carrying out Fast-Fourier transform (FFT) analysis.

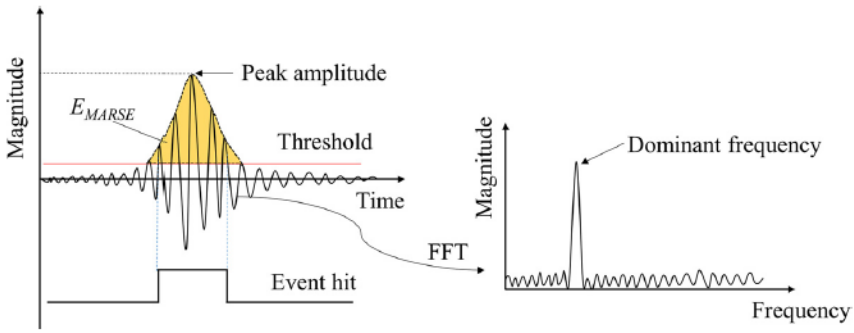

Figure 2.26: Illustration of an acoustic signal and related parameters (Mao et al., 2018)

In laboratory, Koerner et al. (1972) observed that the stress-strain response of soil could be correlated to the AE measurement using the cumulative counts rate, acting as analogous to the shear strain parameter. Incipient occurrence of soil yielding and onset of plastic deformation could also be determined from the energy dissipation through AE monitoring (Tanimoto and Tanaka, 1985; Tanimoto and Tanaka, 1986; Tanaka and Shirakawa, 1995). A classic example of yield point determination was demonstrated in Figure 2.27. The occurrence of elastic-plastic yield point was clearly manifested by the onset of acoustic emission count rate during the

triaxial shearing stage. Such distinctive state change was not able to be identified by the external measurement of stress-strain response alone, since the small strain responses of soil could not be investigated. Moreover, Lin et al. (2020) defined the yield point as the intersection point between AE hit rate curve and the initial tangent line, as depicted in Figure 2.28. Although the yield point (labelled as Y_{AE} in Figure 2.28) as determined from AE measurement was very close to that from mechanical measurement (labelled as Y_s in Figure 2.28), there might be a possibility of having an earlier "yield" point since the axial strain amplitude was not plotted to a much smaller level (e.g. below 1 %). Nevertheless, the reported findings suggested that AE technique can become an alternative in the determination of soil yielding.

(a) Global strain range

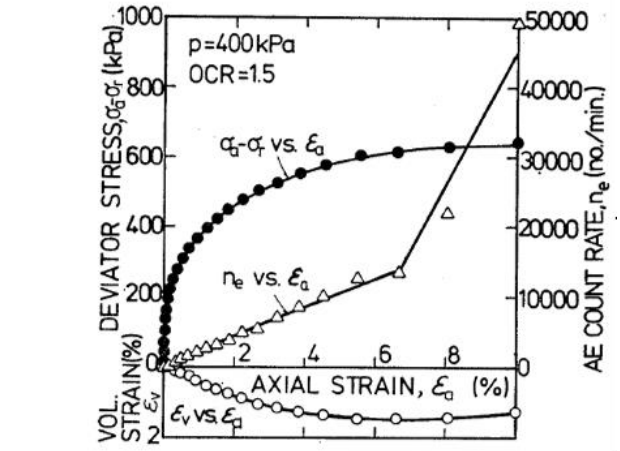

(b) Small strain range

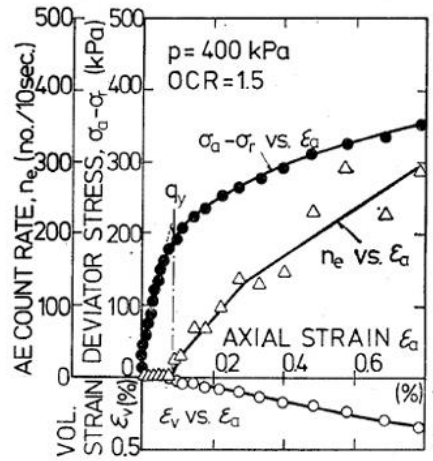

Figure 2.27: Determination of yield point by acoustic emission: (a) small-strain range; (b) global strain range (Tanimoto and Tanaka, 1986)

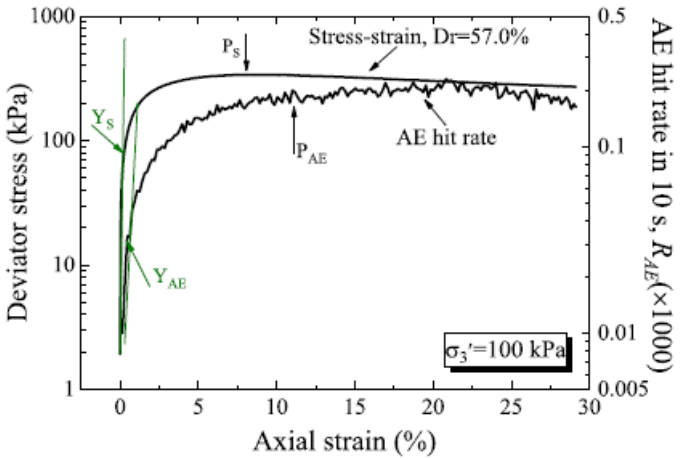

Figure 2.28: Yield point as determined by stress-strain and acoustic emission measurements (Lin et al., 2020)

Moreover, dilatant behaviours of soils could also be characterized by AE rate changes (Tanimoto and Nakamura, 1981; Smith and Dixon, 2019). Recently, Lin et al. (2020) managed to trace occurrence of yielding and peak strength for dense sands through AE responses from multiple points of measurement. Figure 2.29 shows that AE hit rate could continuously correspond to the stress-strain measurement of soil. The peak strength can also be determined from the measurement of mechanical (labelled as P_s in Figure 2.29) and AE (labelled as P_{AE} in Figure 2.29). Specifically, it was realized that higher AE hit rate was obtained for the sand failed in uniform bulging as attributed to the mobilization from majority of soil grains. However, it was found that occurrence of shear band could prohibit the propagation of acoustic waves as the movement of soil grains were limited to the zone of strain localization only.

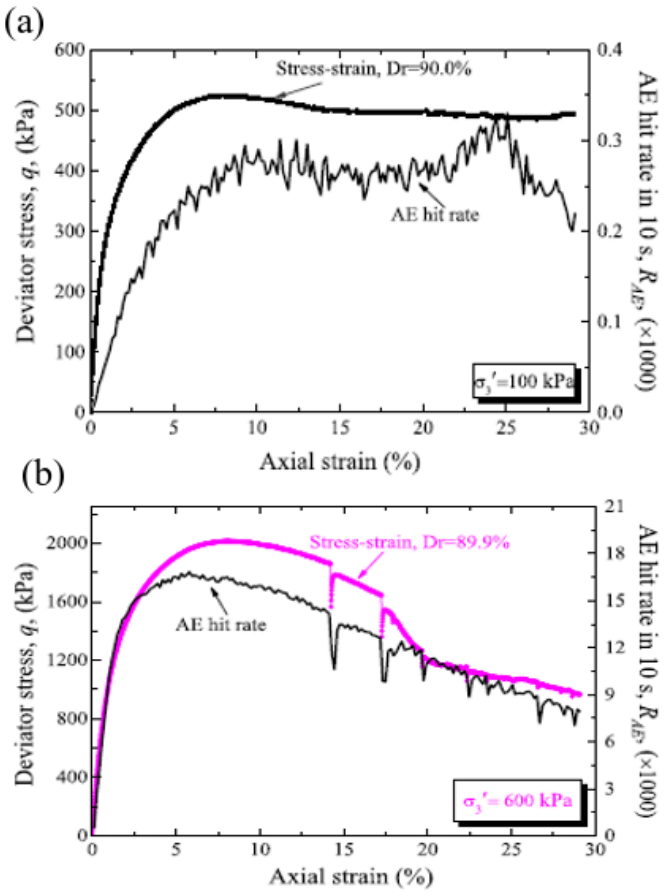

Figure 2.29: Evolution of AE hit rate and stress-strain relationships for a dense sand under triaxial drained shearing: (a) failure by bulging; (b) failure by shear banding (Lin et al., 2020)

Apart from the AE research concerning the mobilization of soil grains and major change in the soil structure, Mao and Towhata (2015) investigated the phenomenon of single-particle fragmentation by using a very sensitive AE transducer, which could be operated under very high frequency measuring range. Their research focused on high-frequency measuring response (>100 kHz), as different from the typical frequency range (<20 kHz) being observed in numerous soil element tests (Koerner et al., 1981; Smith and Dixon, 2019; Tanimoto and Nakamura, 1982; Tanimoto and Tanaka, 1986; Naderi-Boldaji et al., 2017). In addition, Mao et al. (2018) claimed that the frequency content of acoustic energy as generated from the abrasion or sliding between two solid

particles was depended upon the confining stress level. Smith and Dixon (2019) further proved that AE rate of shearing increased with respect to the rate of straining and level of confining stress.

To the author's knowledge, there is no research has yet been devoted towards the structural changes through the passive stress wave measurement (i.e. to monitor the generated stress wave from the soil spontaneously) in cemented and MICP-treated soil. Therefore, the authors believe that the implementation of AE measurement on MICP-treated soil can contribute to the basic apprehension on real-time structural changes of MICP-treated soil structure through the mechanism of wave propagation.

2.9 Concluding Remarks

Several implicative statements can be drawn from the present critical review:

<u>On MICP experiment and treatment</u>

1. Most MICP research has been devoted to the experimental investigation on clean sand, whereas little attention has been placed on the MICP residual soil. Therefore, more efforts are deserved for the investigation of mechanical behaviours of MICP-treated residual soil.

2. The flow pressure treatment setup can be used for the soil with significant amount of fine contents, such as tropical residual soil. A reasonably low concentration of chemical reagent (i.e. 0.5 Mol/ L) under a low level of flow pressure (i.e. <1 bar) was judiciously

suggested to promote effective calcite precipitation. It is also preferable to pre-mix the bacteria into the residual soil mass prior to MICP treatment in order to avoid the complications as caused by the percolation of bacteria in the residual soil.

On deformation and shearing behaviours of MICP soils

1. It is worthwhile conducting isotropic consolidation experiments for both MICP-treated sand and residual soil in order to comprehend the deformation behaviours of MICP-structured soils concerning the directional movement of soil grains.

2. Under shearing, strain-softening effect and brittleness were apparently observed for the heavily treated sands owing to the stress localization in the vicinity of shear band. A direct way of assessing the differences in structural formation between residual soil and sand is perhaps through experimental tests conducted on both of the materials (clean sand and residual soil) under a same testing condition.

3. Current available understanding on MICP-treated residual soil was only focusing on the unconfined compression test without imposing confining stress to replicate the actual stress state underneath the ground. For this reason, triaxial stress experiment has to be implemented to investigate the stress-deformation behaviours of MICP-treated residual soils. It is also realized the

importance of examining the effect of consolidation pressure towards the MICP-treated soil.

On MICP structural formation and changes

1. Alterations of properties in the MICP soils are attributed to the mechanisms of calcite cementation and densification. Calcite cementation was formed by the bonding between two neighbouring soil particles, and calcite densification was directed to the void filling mechanism of precipitated calcites. Yielding of cemented soil was dictated by the breakage of soil bonding and calcite densification played a dominant role after yielded.

2. The presence of fines (silt and clay-sized particles) within the residual soil could complicate the formation of effective calcite precipitation. The calcite precipitation could occur at the location where no significant structural resistance being contributed.

3. Acoustic emission technique appeared to be a suitable alternative in facilitating the investigation of structural changes as related to the mobilization of soil particles in MICP-treated soils. It follows that the behavioural differences between original and MICP-treated soils can be clearly distinguished.

CHAPTER 3

RESEARCH METHODOLOGY

3.1 Introduction

This chapter presents the research framework, physical properties of tested materials (i.e. residual soil and sand), procedures of MICP treatment, triaxial testing (instrumented with mechanical and acoustic emission measurements) and physical assessment (i.e. acid washing and microscopic tests) on the MICP-cemented specimens. Finally, the data processing for the mechanical and acoustic emission measurement are elaborated.

3.2 Research Framework

The aim of this research was to investigate the mechanical and deformation behaviours of Microbial-Induced Calcite Precipitated (MICP) residual soil in comparison with sand under monotonic triaxial loading. Figure 3.1 illustrates the research framework, highlighting the four major stages (i.e. exploration, preparation, experiment, and data analysis) in the research.

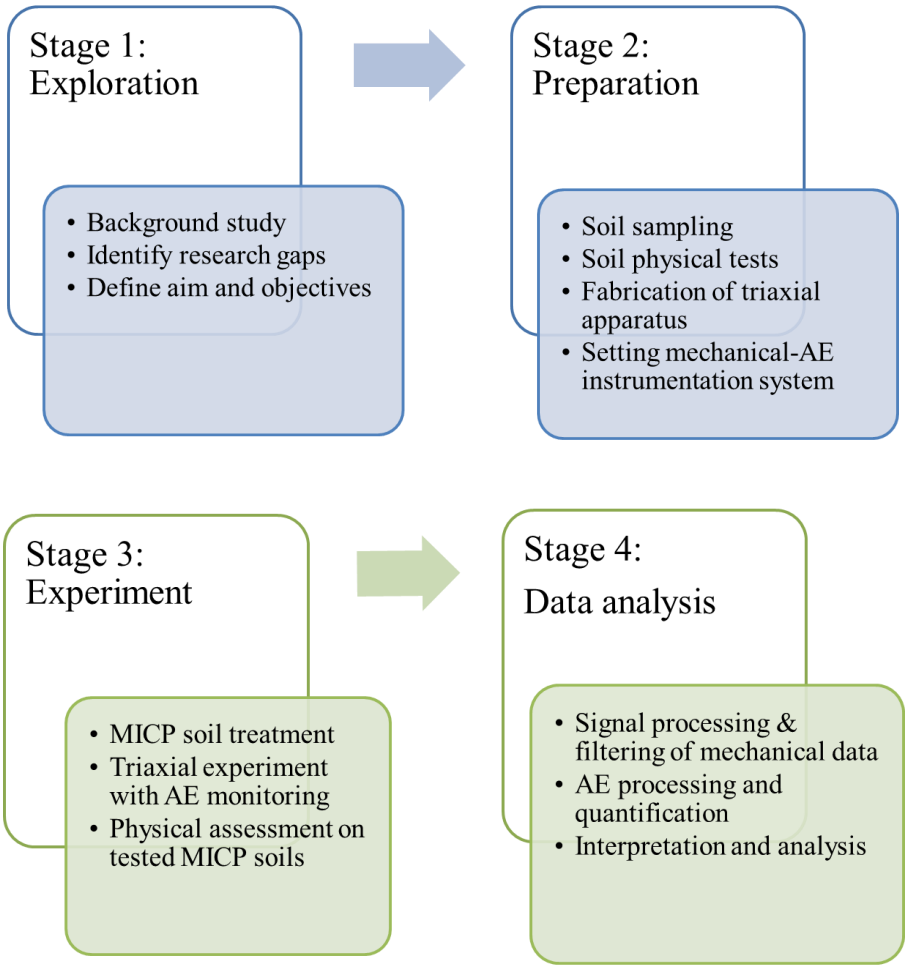

Figure 3.1: Research framework

At the early stage of this research, a state-of-the-art review was conducted on the mechanical behaviours of microbial-induced calcite precipitation (MICP) soils to identify research gaps. Based on the identified research gaps, research topic and the objectives were formulated accordingly. To accomplish that, it is also required to commit brainstorming for research ideas and consultation with the experts in related fields of research (i.e. realms of MICP and AE).

Next, it was followed by the preparation stage, including sample collection, soil physical properties determination, triaxial cell fabrication and setting up of triaxial testing apparatus with AE measurement. Tropical residual soil was sampled from a construction site in Malaysia. Clean sand was mechanically sieved to the MICP-favourable size range to permit a direct comparison between MICP-treated residual soil and sand. The selected soils were classified based on their physical properties. Meanwhile, a monotonic (static loading) triaxial apparatus was designated and fabricated in the workshop to facilitate the subsequent mechanical investigation. The triaxial testing system is equipped with both mechanical and AE measurements.

For the main experiment, triaxial testing was adopted to replicate the typical field stress condition under the laboratory condition. The residual soil and sand were first subjected to MICP treatment process prior to the triaxial testing, including isotropic consolidation and undrained shearing (i.e. compression and extension). After the triaxial test, calcite content measurement was carried out to justify the presence of calcite precipitation within the pore space of MICP-treated soils. In addition, a series of scanning electron microscopic (SEM) tests were conducted to examine the microscopic structure of MICP-treated soils.

After completing the experiments, the acquired mechanical and AE data were digitally filtered to remove the noise by using Python program. It was followed by data analysis and interpretation on the behaviours of MICP-treated soils. Finally, literature review, research methodology, experimental

findings, discussions, and conclusions were systematically compiled into present dissertation.

3.3 Testing Materials

3.3.1 Physical Properties of Residual Soil

Tropical residual soil was collected from a construction site situated at Bandar Sungai Long, Selangor, Malaysia; geographical coordinate of the site was located at 3.045050, 101.806062. A highly weathered tropical residual soil was sampled at superficial layer (i.e. 1-2 m deep) of a granitic deposit, which was originated from the Permian-Jurassic igneous rock formation (Foo, 1983). The residual soil, which constituted numerous fragmented soil agglomerations, was first air dried and disaggregated into individual particles by using a rubber mallet before it was sieved through a sieve with aperture size of 20 mm to remove the gravel-sized particles.

Table 3.1 shows the physical properties of the residual soil obtained from laboratory testing. The residual soil constituted nearly 32 % of fines (passing sieve size of 63 μm) and it was classified as Very Clayey Sand in accordance with British Standard, BS 1377: Part 2 (BSI, 1990). The outcome of present classification showed reasonable agreement with the common understanding on granitic residual soil. Huat et al. (2004) also reported that granitic residual soil was predominantly formed with coarse-grained soils (i.e. quartz) and certain amount of fine-grained particles (i.e. weathered feldspar).

Table 3.1: Physical properties of residual soil

Properties	Value	Unit
Original Residual Soil		
Composition		
Gravel	16.7	%
Sand	51.7	%
Silt	24.0	%
Clay	7.6	%
D_{10}	0.006	mm
D_{50}	0.568	mm
Liquid Limit	55.1	%
Plastic Limit	29.4	%
Plasticity Index	25.7	%
Compacted Residual Soil (passing 4.75 mm sieve)		
Lowest Dry Density (LDD)	1.198	Mg/m^3
Maximum Dry Density (MDD)	1.799	Mg/m^3
Optimum Moisture Content (OMC)	15.6	%

Figure 3.2 shows the experimental results of standard Proctor compaction test for the studied residual soil, which had been mechanically sieved through 4.75 mm of aperture size. From the compaction curve, the maximum dry density (MDD) was 1799 kg/m^3, corresponding to optimum moisture content (OMC) of 15.6 %. The lowest dry density (LDD) as listed in Table 3.1 was obtained by freely depositing dry mass of residual soil (also passing 4.75 mm sieve) into a rigid steel mould (i.e. the nominal diameter is 50 mm and nominal height is 100) under loose state. Determinations of MDD and LDD by using the compaction test would help to quantify the densities of two types of soils in relative manner. This could later facilitate the direct comparison between residual soil and sand at a specified relative density.

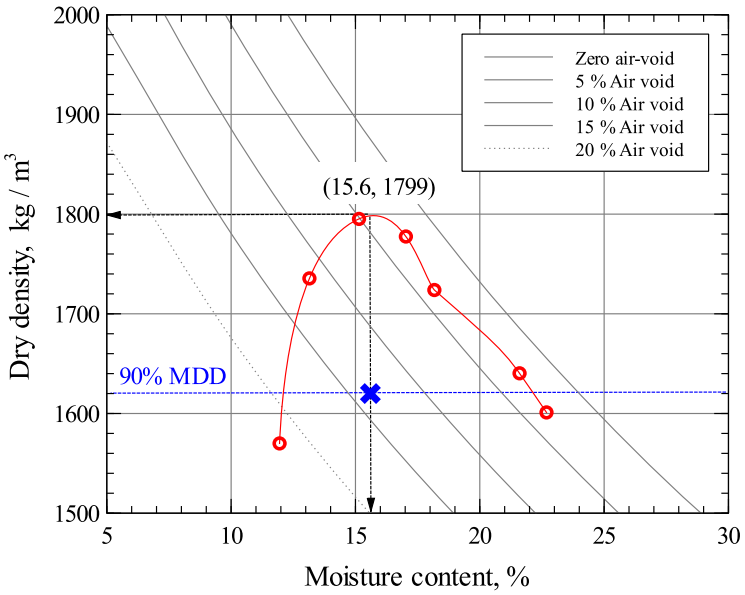

Figure 3.2: Compaction curve for the studied residual soil

3.3.2 Physical Properties of Sand

Table 3.2 shows physical properties of the selected sand, which was a quartz sand and originally used for concrete mixing. The sand was classified as Poorly-graded Clean Sand, with the medium-sized sand particles being dominant. The sand was later sieved to a specified size range (i.e. 0.15 mm to 0.6 mm). Figure 3.3 presents the tools required for determining the maximum and minimum densities of sand in laboratory. The maximum dry density was determined according to the procedure as stipulated in JGS (2000); whereas the lowest dry density was obtained by depositing the loose sand into a steel mould with the nominal diameter of 50 mm and nominal height of 100 mm. For determining the maximum dry density according to JGS (2000), the dry sand was first poured into steel mould in ten layers. After each layer of sand was poured, a mini hammer was used to hit the side wall of steel mould for 100 times while the mould was slowly rotated to facilitate uniform

densification. It can also be noted that the diameter of presently adopted mould was similar to the one stipulated in the standard (i.e. nominal diameter of 60 mm), although a much smaller height (i.e. 40 mm) was suggested in the standard.

Table 3.2: Physical properties of Sand

Properties	Value	Unit
Original Sand		
Composition		
Gravel	1.8	%
Sand	95.8	%
Fines	2.4	%
D_{10}	0.136	mm
D_{30}	0.283	mm
D_{50}	0.418	mm
D_{60}	0.496	mm
C_u	3.65	-
C_c	1.19	-
Dry-tamped Sand (size range between 0.15 mm to 0.6 mm)		
Lowest Dry Density (LDD)	1.176	Mg/m^3
Maximum Dry Density (MDD)	1.422	Mg/m^3
Moisture Content (OMC)	-	%

Figure 3.3: Apparatus required for determination of sand density

3.4 MICP Treatment

3.4.1 Bacteria Preparation for Soil Treatment

Among numerous types of urease-based bacterium for calcite precipitation, the *Sporosarcina pasteurii* produced the highest urea hydrolysis rate (Fujita et al., 2000). *Sporosarcina pasteurii* (DSM-33), which was an alkalophilic and urealytic bacterium, was used in the present study for MICP treatment. Figure 3.4 shows the entire process of preparing the microbes for the subsequent soil treatment and preparation.

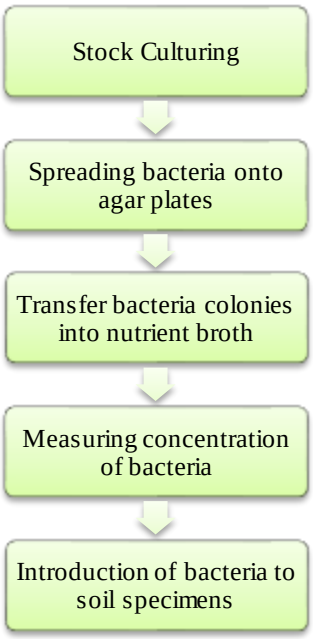

Figure 3.4: Process of preparing bacteria solution

The stock culture was prepared based on procedures suggested by (Ng, 2013) and stored in several centrifuge tubes in a freezer at a temperature of -20 °C. This stage of preparation was regarded as stock culturing of bacteria in which the microbial source can be kept at the most favourable conditions. The

cultured bacteria are therefore free from ambient contamination and undesired growth of bacteria. The prepared stock of bacteria was subsequently extracted for cell suspension preparation stage.

Next, the extracted bacteria were spread onto agar plates by using a sterile wire loop and this step is called as streak plate technique. The microbes were transferred onto the surface of stiffened nutrient agar by looping (functionally speaking, the bacteria were diluted on the agar surface). The streak agar plate was later cultured in an incubator at the temperature of 37 °C for 24 hours to allow the growth of bacteria.

After the bacteria preparation, bacterial colonies were transferred from the cultured agar plates into several conical flasks filled with nutrient broth solution (1 g of soluble nutrient broth powder into 100 ml of distilled water) and cultured in a shaking incubator with 150 r.p.m at the temperature of 37 °C for 24 hours (as systematically shown in Figure 3.5).

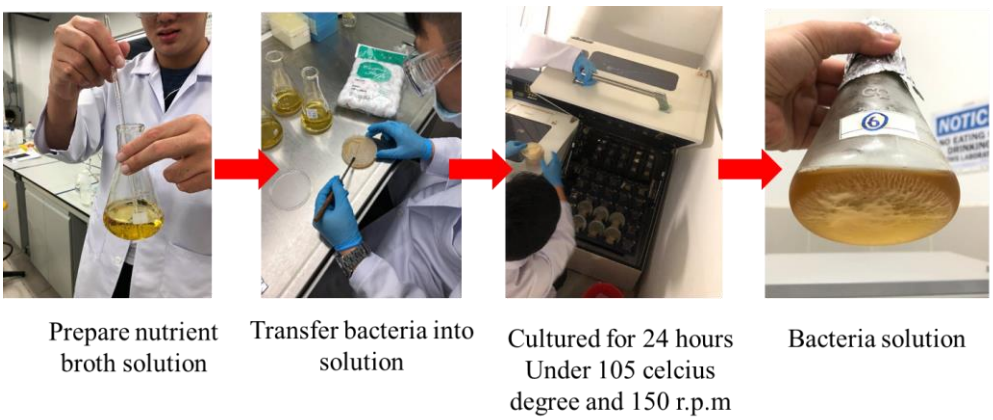

Figure 3.5: Preparation of microbial solution

Subsequently, the concentration of cultured bacteria was evaluated prior to the application in soil. The gross concentration of bacteria solution was determined using a spectrophotometer device, as shown in Figure 3.6. The concentration was measured in terms of optical density at a wavelength of 600 nm (i.e. $O.D_{600}$). From the calibration tests, a correlation between colonies forming unit (cfu) and $O.D_{600}$ was established, and the multiplier factor was found to be 4×10^7. The optical density of the cultured bacteria was herein designated to reach an approximate value of 1.6 in order to furnish sufficient amount of bacteria. This corresponded to a microbial density of 6.4×10^7 colonies forming unit (cfu) per ml upon multiplying with the calibration factor. Then, the bacteria solution was ready to be applied into the soil.

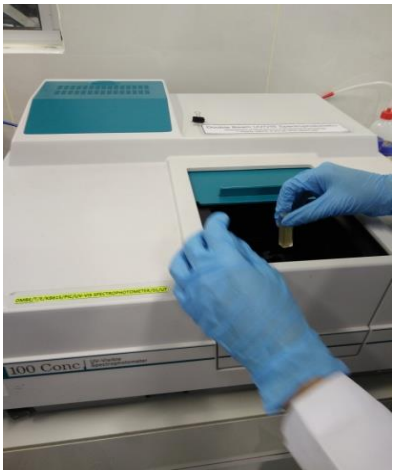

Figure 3.6: Determination of gross concentration for microbial solution in Spectrophotometer machine

3.4.2 Preparation of MICP-treated Soil Specimens

Figure 3.7 shows the grain size distribution curves for the original residual soil and sand. The sand was sieved to a particle size ranging from 0.15 mm to 0.6

mm to be compatible with the MICP-favourable size range as suggested by previous studies (Cui et al., 2017; Ivanov and Chu, 2008), whereas the residual soil was sieved through an aperture size of 4.75 mm.

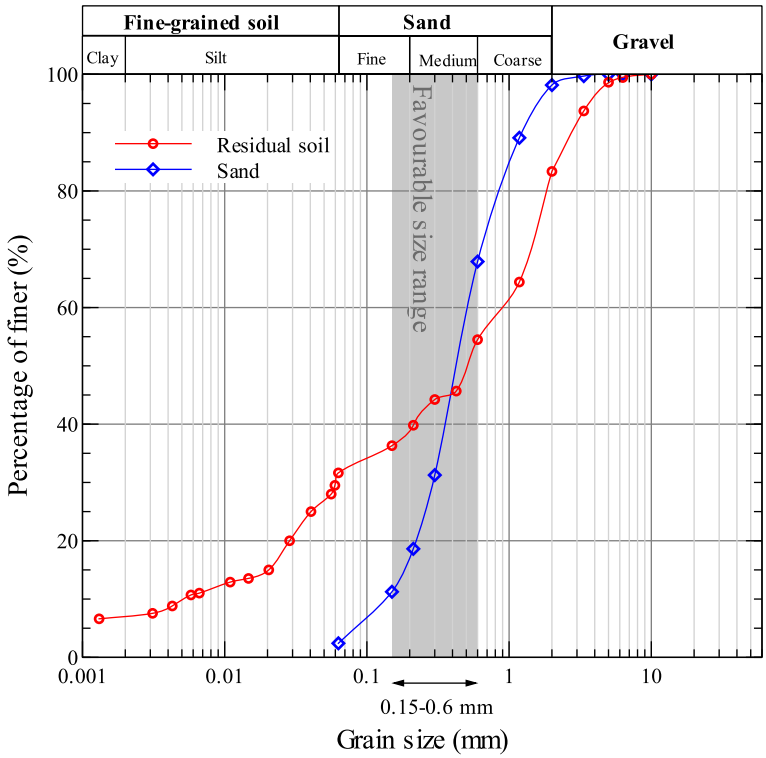

Figure 3.7: Grain size distribution curves for residual soil and sand

Triaxial soil specimen, which had a nominal diameter of 50 mm and nominal height of 100 mm, was prepared by dynamic compaction on the residual soil. Table 3.3 summarizes the densities of the prepared residual soil and sand specimens. In the present experiment, the residual soil specimen was compacted to 90 % of its maximum dry density (MDD) and the corresponding optimum moisture content. The bacteria solution with the equivalent gravimetric mass of water needed for certain moisture content (i.e. optimum moisture content), was pre-mixed into the dry residual soil before compaction

in order to avoid the complication due to the geometric incompatibility between bacteria and soil grains. Based on the compaction procedures as presented in Section 3.3.1, the relative density (denoted as D_r) of compacted residual soil specimen was estimated to be approximately 78 %. On the other hand, the triaxial sand specimen with a diameter of 50 mm and height of 100 mm, was prepared by tamping the dry sand to achieve a relative density of nearly 82 %. The formula for computing the relative density is presented in Equation 3.1.

Table 3.3: Densities of prepared soil specimens

Properties	Value	Unit
Residual Soil Specimen		
Density of specimen	1.620	Mg/m^3
Relative Density (D_r) of specimen	≈ 78	%
Sand Specimen		
Density of specimen	1.370	Mg/m^3
Relative Density (D_r) of specimen	≈ 82	%

$$D_r = \left(\frac{\rho_{max}}{\rho}\right)\left(\frac{\rho-\rho_{min}}{\rho_{max}-\rho_{min}}\right) \quad (3.1)$$

where
D_r = Relative density, %
ρ = Soil density, Mg/m^3
ρ_{max} = Maximum soil density, Mg/m^3
ρ_{min} = Minimum soil density, Mg/m^3

It is, however, recognized that the procedure used for determining the relative density of residual soil may not be completely compatible to that of determining the relative density of clean sand. The relative density of residual soil that includes large fines content may be affected by various factors such

as different gradations (e.g. fines content), mineralogy, and grain properties (e.g. particle breakage, surface texture and shape) and there is no standardized testing procedure for the MDD and LDD tests. Terzaghi and Peck (1996) adopted relative density to distinguish degree of denseness for granular materials (e.g. "free-drained" sand and gravel without fines) and also realized the importance of mica content in affecting the soil structure. Relative density is very useful in quantifying the denseness of a particular type of soil, but it is not desirable to define the states of two different soils by only using relative density as the soil behaviours are affected by other factors such as gradation, mineralogy, and grain properties.

Despite that, it is reasonable to compare the behaviours of residual soil and sand in the present study by keeping them under a nearly same degree of compaction (i.e. their relative densities were more or less 80 %). Similar approach was adopted by Tanaka (1999), the relative densities of decomposed granitic soil and crushed mudstone (soils constituted fine-grained particles) were computed based on the compaction test results for a correlation of the soil liquefaction strength and relative densities. The liquefaction strengths of two different soils were successfully comprehended by referring to their relative densities.

Hence, it is important to ensure that the degrees of compaction for both sand and residual soil in present study are relatively similar (in the dense state). By keeping the degree of compaction for two soils at a relatively same state, a

more reasonable assessment on the mechanical behaviours of the original and MICP-treated soils can be done.

3.4.3 MICP Treatment for Residual Soil

Figure 3.8 illustrates the schematic of flow-pressure MICP treatment setup for the residual soil specimen and Figure 3.9 shows the photograph of MICP-treated specimens in the PVC moulds. The MICP treatment process was carried out by percolating the chemical solution (namely, nutrient solution and chemical reagent) from the top end of the soil specimen. Pair of PVC caps was provided at both ends of the sampling tube to ensure no water leakage during the MICP treatment process. A head difference of 2 m (≈ 20 kPa of flow pressure) was maintained in the percolating system to facilitate a close-to-uniform flow throughout the specimen. The applied flow pressure was deemed to be sufficient and effective for the treatment of residual soil following the recommendations by Ng et al (2013).

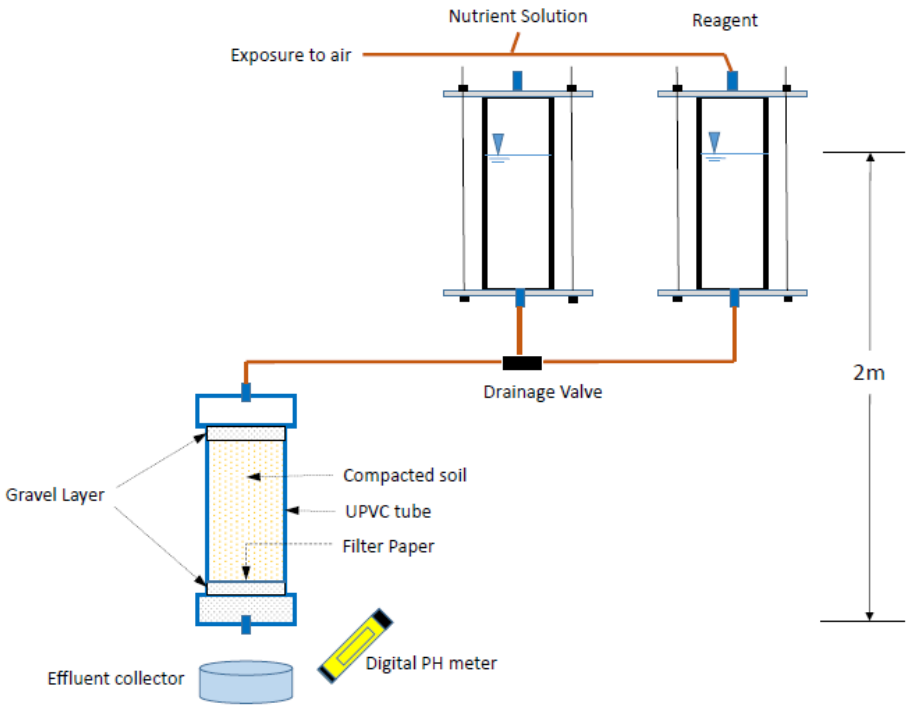

Figure 3.8: Flow-pressure setup for MICP treatment of residual soil

Figure 3.9: Photograph of MICP-treated residual soil specimens

Figure 3.10 outlines the modified two-phase MICP treatment procedures adopted in this study. It involved three primary phases: (a) injection of nutrient solution (consisting of nutrient broth and bacteria); (b) injection of chemical reagent (e.g. urea and calcium chloride); followed by (c) recirculation of the effluent solution into the soil specimen to facilitate a complete urea hydrolysis process. After the nutrient solution was introduced, a retention period of 4 to 6 hours was allocated so that the pre-mixed microbes have sufficient time to grow and adsorb onto the soil particles. This intuitive approach was also recognized in many other studies (Dejong et al. 2010; Ng et al. 2013; Ng et al. 2014). It is worth emphasizing that the dominant part of urea hydrolysis involved the pre-mixed bacteria which were introduced during the specimen preparation stage, while the supplementary microbes as suspended in the nutrient solution were only provided for further growth of bacteria. The modified two-phase treatment processes as described above were repeated for three cycles to promote sufficient degree of cementation. Throughout the treatment process, the pH level of the effluent was periodically checked to ensure that it was greater than 8.0 (active urease hydrolysis), being consistent with the procedures reported by Feng and Montoya (2015).

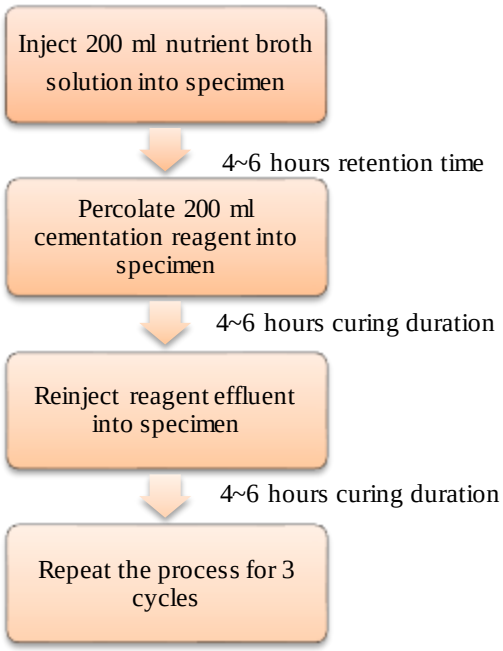

Figure 3.10: Modified two-phase MICP treatment for residual soil

The chemical reagent, comprising of urea and calcium chloride, was designated to constitute a concentration of 0.5 Mol/ L. Specifically, 30.3 g of urea and 55.6 g of calcium chloride were mixed into 2 L distilled water to form the chemical reagent solution. Al Qabany and Soga (2013) claimed that a high concentration of chemical reagent (i.e. 1 Mol/L) would cause inhomogeneous and localized calcite precipitation within the pore space of soil, and eventually lead to an overall lower stiffness and shear strength of the treated sample. As such, an intermediate level of concentration (e.g. 0.5 Mol / L) was essential to promote more uniform calcite precipitation. Besides that, the nutrient solution was formed by mixing 50 ml of microbial solution (as described in Section 3.4.1) into a urea-nutrient broth mixture, which constituted 30.3 g of urea and 8 g of nutrient broth powder in 1 L of distilled water.

Prior to soil demoulding, the treated soil specimens were permitted to rest in the laboratory for a day to allow the discharge of excessive chemical reagent that entrapped inside the soil specimen. The photograph of a demoulded MICP residual soil specimen is also shown in Figure 3.11. The soil specimen was extruded from the PVC tube by using a hydraulic soil extruder machine. After demoulding, (white) calcite crystals could be observed on the surfaces of treated soil specimen as shown in Figure 3.11. Calcite sediment was also observed in the effluent collector base. The gravel-like particles from filter layer were also found to be greatly cemented and were strong enough to withstand the force by hand remoulding.

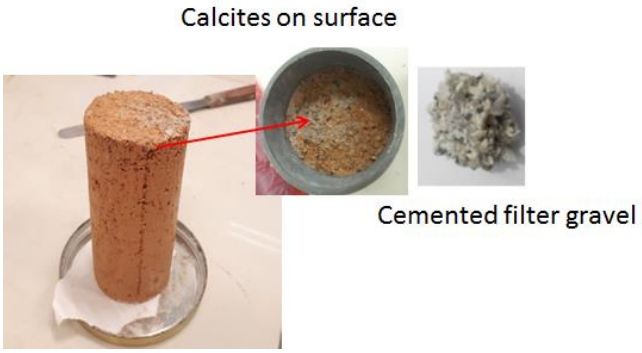

Figure 3.11: MICP-treated residual soil specimen

3.4.4 MICP Treatment for Sand

The treatment procedure for sand was physically different from the residual soil as chemical reagent could easily percolate through the sand specimen due to the larger pore spaces in sand. The MICP treatment setup configuration for the sand specimen is shown in Figure 3.12 whereas an actual photograph is

shown in Figure 3.13. The dry-tamped sand specimen was first permeated with two pore volume of bacteria solution to allow the adsorption of bacteria onto the soil grains. Chemical reagent was then injected from the top of specimen by using a mini water pump, which could easily be operated at a low voltage (i.e. 5 V – 12 V). The bottom of the PVC tube was adhered to a porous wooden plate and the effluent could be collected by using a container. The effluent was recirculated continuously for one hour and a retention period of three hours was allowed. The treatment process for the sand specimen was repeated for nine cycles in order to obtain a cementation level (i.e. net calcite content) similar to that of the MICP-treated residual soil.

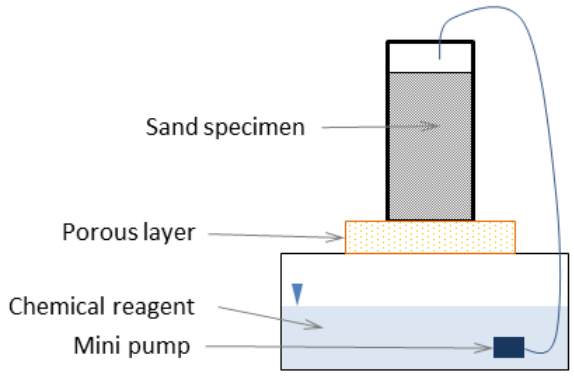

Figure 3.12: Schematic MICP setup for sand

Figure 3.13: Photograph of MICP treatment setup for sand

Figure 3.14 shows the post-treatment configuration of MICP-treated sand specimen. The process of demoulding sand specimen was like the procedure of demoulding the MICP-treated residual soil specimen as mentioned in Section 3.4.3. After demoulding, the treated sand was able to stand firmly by itself; it was exposed to atmospheric drying before the commencement of triaxial testing.

Figure 3.14: Photograph of MICP-treated sands after demoulded

3.5 Triaxial Testing Setup

The mechanical behaviours of saturated (untreated and MICP-treated) soils were investigated in a stress-controlled triaxial apparatus. Figure 3.15 illustrates the overall configuration of the triaxial apparatus system as developed in the laboratory. By controlling pneumatic air pressures, the internal/ external pressure of soil specimen (i.e. cell and back pressure) and

axial loading (through a loading piston) could be applied independently in the course of triaxial experiment.

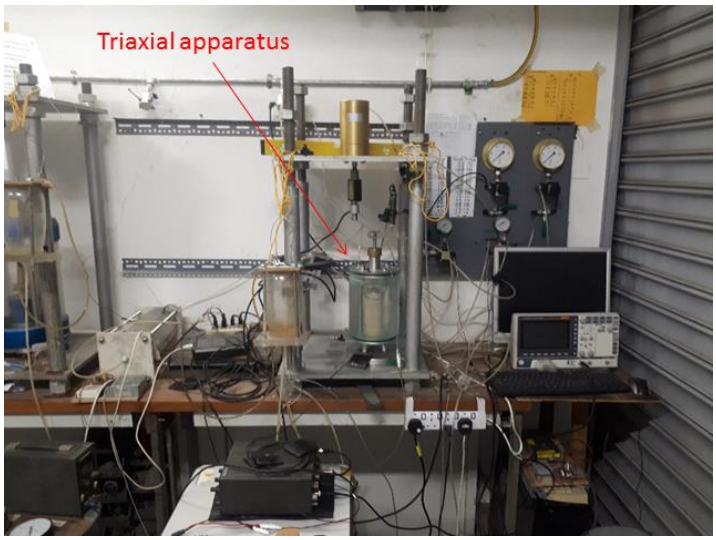

Figure 3.15: Configuration of the triaxial testing system

As shown in Figure 3.16, two Electro-pneumatic (E/P) transducers were used in controlling positive/ negative (i.e. vacuuming pressure) inside and outside of a soil specimen, meanwhile a pair of pressure regulators were used to facilitate manual controlling of the pneumatic pressures for the axial loading system. Application of pressure through E/P transducer was accomplished by sending analogue input signals (ranging from 0-10 V) to a Fujikura RT-series E/P transducer from a desktop computer continuously, in which a National Instrument PCI-6024E multi-function card was installed. Through the electro-magnetic principle, magnitude of pneumatic pressure could be electronically adjusted to facilitate the testing. A vacuum generator (PISCO VH-series type) was mounted onto the outlet port of an E/P transducer to enable the application of vacuuming pressure during the double-vacuuming

saturation stage. The vacuum generator could produce a maximum suction pressure of 93 kPa, with the highest supplied pressure of 5 bar (i.e. 500 kPa) to the triaxial cell.

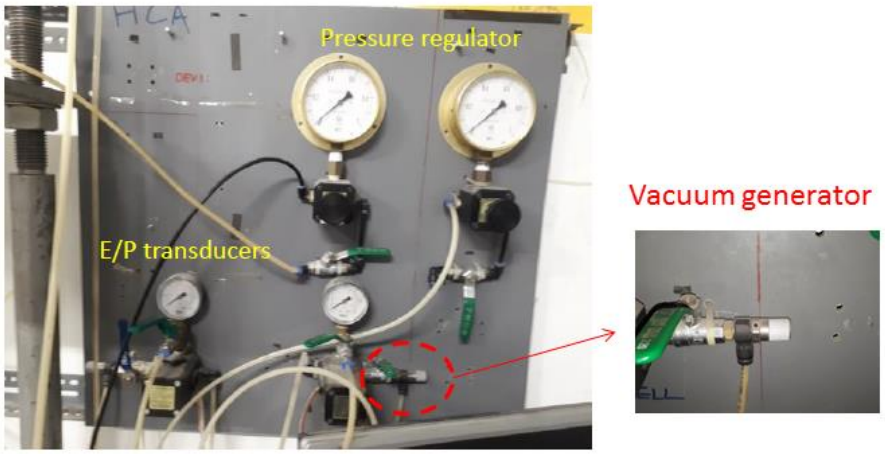

Figure 3.16: Pressure control panel

3.5.1 Triaxial Cell Apparatus

Figure 3.17 shows the key components equipped in a triaxial cell apparatus. The triaxial cell apparatus, which the top and base plates were primary made of aluminium, was underpinned by a pair of vertical rods. The diameter of base aluminium plate (i.e. 155 mm) was marginally greater than the top plate (i.e. 150 mm). The acrylic wall had a nominal thickness of 15 mm and was used to accommodate the cell water. Pair of O-rings was put onto the trenches of the top and base aluminium plates to prevent water leakage under the application of high water pressure. As the base pedestal involved installation of acoustic emission transducer, the designation details were elaborated in Section 3.6.

(a) Components in the triaxial cell apparatus

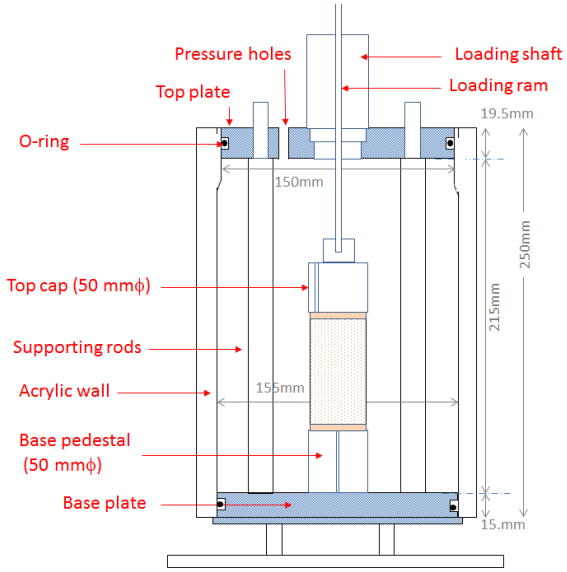

(b) Photoraph of triaxial cell apparatus

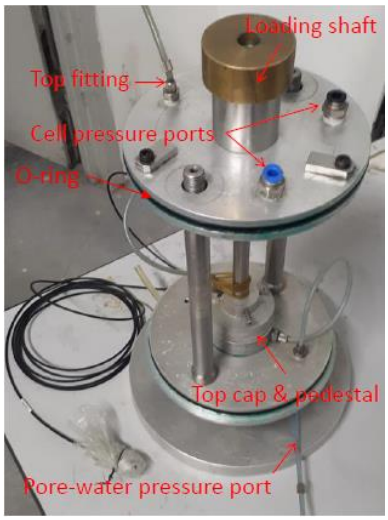

Figure 3.17: Configuration of the triaxial cell apparatus

Drainage holes with internal diameter of 2 mm were provided at the top cap and base pedestal to facilitate the double-vacuuming saturation process and measurement of internal soil responses (e.g. volumetric and pore-water pressure changes). It is worth mentioning that the diameter of drainage hole was designated to be sufficiently small to guarantee precise pore-water pressure measurement and to accomplish the system compliance (Bishop and

Henkel, 1962). In the present study, compatible-sized PISCO fittings were used for all connections for polyurethane tubes. The inner diameter and external diameter of polyurethane tube was 2 mm and 4 mm, respectively. The advantage of using this type of fitting connection was the flexible assemblage between pressure transducers and fitting system to measure the soil responses.

Figure 3.18 further illustrates the fabrication details of the loading shaft, which is crucial in providing a smooth loading and non-leaking condition during the triaxial test. Pairs of linear-motion bearings and brass rings were used to align the stainless steel loading ram with a nominal diameter of 12 mm. Smaller O-rings (inner ring diameter of 16 mm, labelled as P16) were provided on the brass rings and a larger O-ring (inner ring diameter of 30 mm, labelled as P30) was put onto the lower end of loading shaft, which was later screwed at the top plate of triaxial apparatus. It could also be seen that a base cap ring was attached onto one end of loading shaft in order to prevent the sliding out of linear-motion bearings and brass rings. The triaxial apparatus was proven to be capable in withstanding water pressure up to 500 kPa (5 bar) without experiencing any leakage problem. Application of grease on the surface of O-ring was essential to reduce the leakage (especially during vacuuming) by filling the space in the trench (a recess to accommodate O-ring). It was also important to ensure that the surfaces of O-ring and trench were totally free from dust/ grain to guarantee proper sealing.

(a) Photo of loading shaft

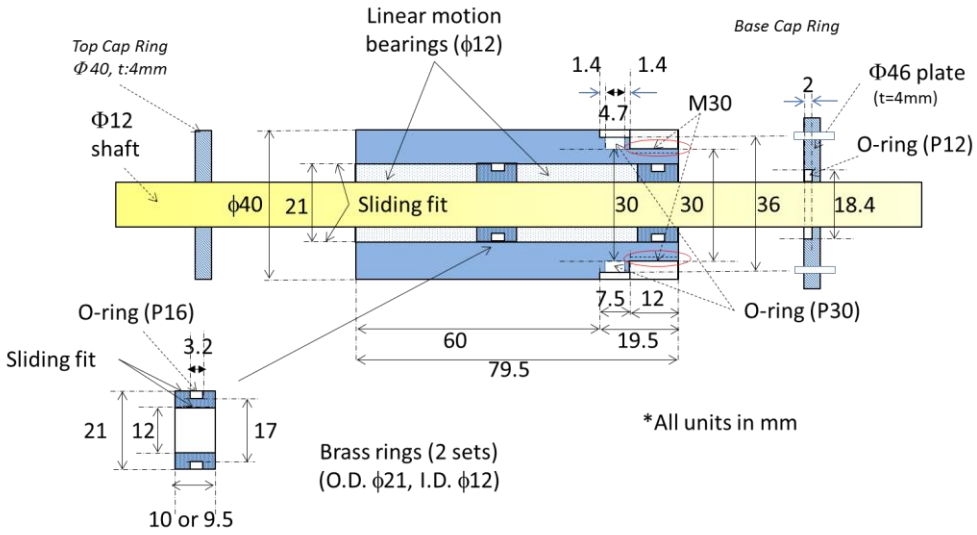

(b) Detailed layout of loading shaft

Figure 3.18: Cross-sectional view of loading shaft

3.5.2 Instrumentation and Data Acquisition Systems for Mechanical Responses

Figure 3.19 shows the instrumentation system for the triaxial setup. The triaxial apparatus was equipped with several strain-gauge type of transducers to monitor volumetric change, fluid pressure change (TML PWF-PB Flush diaphragm type Pressure Transducer), axial displacement (TML CDP-25

displacement transducer), and loading responses (TML TCLZ-500NA load cell). Cell water and pore-water pressures were synchronically monitored by using two pressure transducers, which were labelled as "cell" and "pore-water" pressure transducers throughout the thesis. Particularly, the fabricated volume change device was operated by a full Wheatstone bridge circuit involving four pieces of TML F-series strain gauges. As shown in Figure 3.18, the strain gauges were adhered onto an aluminium bar in the volume change device. The strain-gauged system was enclosed in an acrylic pressure chamber to permit the application of pneumatic back pressure during the B bar check. The volume change of soil specimen was obtained by measuring the amount of dissipated pore water when the specimen was gradually stressed.

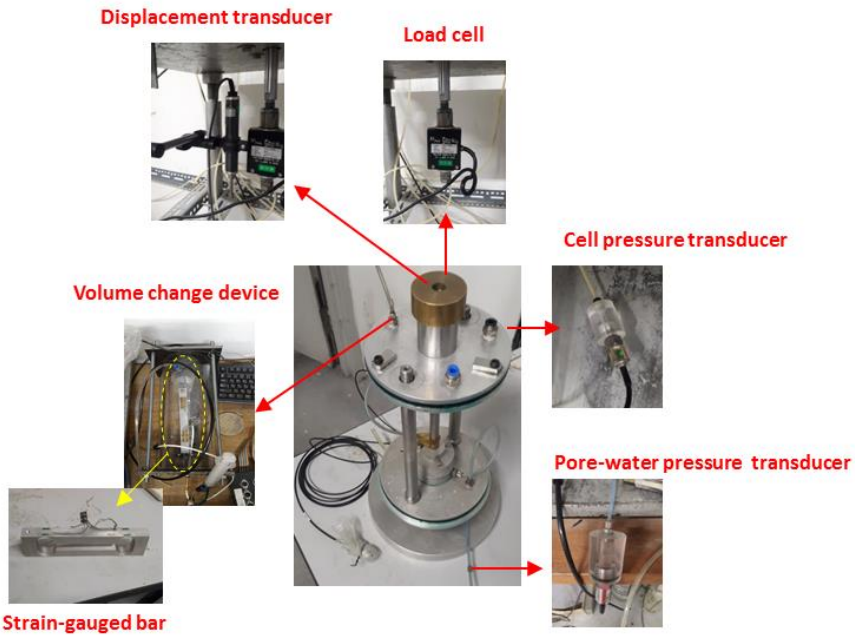

Figure 3.19: Instrumentation system for soil responses monitoring

Moreover, Figure 3.20 presents the data acquisition system for collection of mechanical properties data during the triaxial testing. All transducers were connected to a centralized bridge box, which was powered by a DC voltage of 5.0 V. All signal wires were soldered onto DIN–type pin connection to transmit the analogue voltage signal, which was sent into a sensitive data logger (Graphtec midi data logger GL220) for data monitoring and acquisition. The analogue data was digitized and transmitted to a laptop through a USB cable. The multi-channel data logger had a built-in analogue-to-digital converter, with a resolution of 16 bits. The smallest sampling time interval could reach 10 ms when limited channels were used. For the triaxial experiment, the sampling time interval adopted was 125 ms.

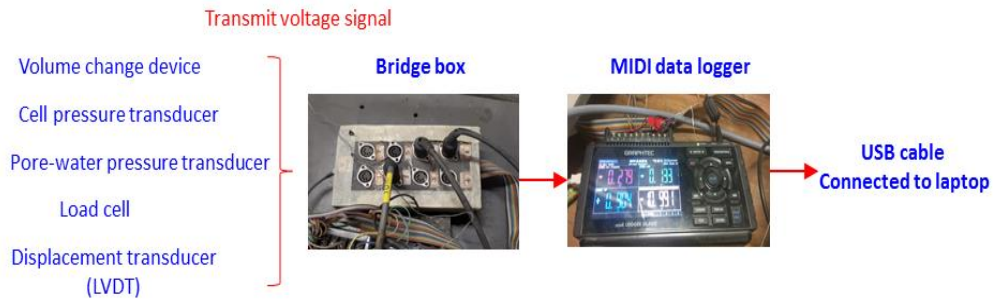

Figure 3.20: Data acquisition system for mechanical measurement

Table 3.4 lists the measurement accuracies and sensitivities of transducers selected for the triaxial experiment. Under ambient monitoring, actual accuracy of a particular response could be obtained. In addition to the accuracy of a manufactured transducer, the effects of ambient and electrical noises were considered pragmatically. The calibration diagram of volume change device is also depicted in Figure 3.21. Amount of expelled pore water

(corresponding to volumetric change of a saturated soil specimen) could be obtained by multiplying the linear gradient with change of voltage output (along the abscissa). The incremental changes of other soil responses (namely, linear displacement, vertical stress, pore-water pressure, and cell pressure) could also be obtained in same manner.

Table 3.4: Specifications of transducers

Transducer	Accuracy	Sensitivity
Volume change device	±0.1ml	10.9 ml/mV
Displacement transducer	±0.01 mm	0.90 mm/mV
Cell Pressure transducer	±1.0 kPa	187 kPa/mV
Pore-water pressure transducer	±1.0 kPa	202 kPa/mV
Load cell transducer	±0.001 kN	0.515 kN/mV

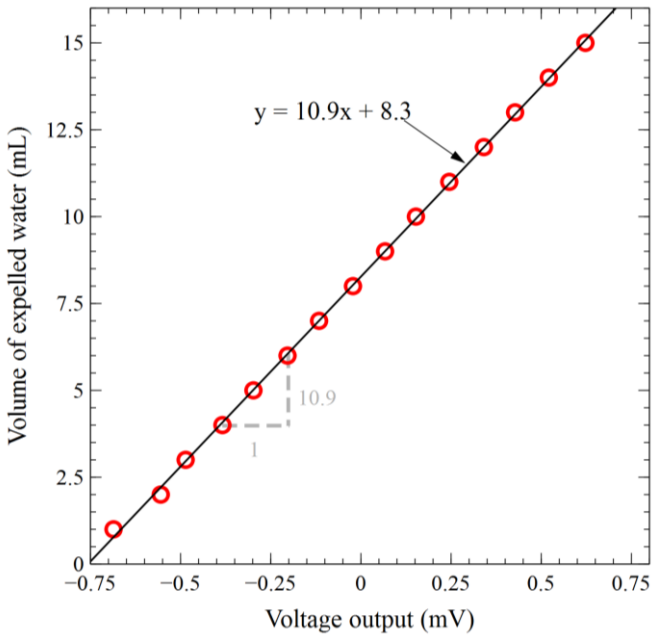

Figure 3.21: Relationship between volume of expelled pore water and output voltage

3.5.3 Double-Vacuuming Saturation Method

Figure 3.22 shows the soil specimen setup in the triaxial apparatus. The soil specimen was enclosed by a rubber membrane (with a nominal thickness of 0.3 mm), which was tightened by several rubber bands on the top cap and base pedestal. Once the soil specimen had been set up properly, the triaxial cell was properly enclosed by the cylindrical acrylic cell before water was filled into triaxial cell. Pair of completely dried porous stones (with a nominal thickness of 6 mm) was placed on the top and bottom ends of triaxial specimen to provide a solid support at both ends of specimen and drainage path for pore water. Filter papers were also provided on the interface between soil and porous stone to prevent the losing of fine particles (i.e. passing 63 μm) from the residual soil specimen and the clogging of porous stones.

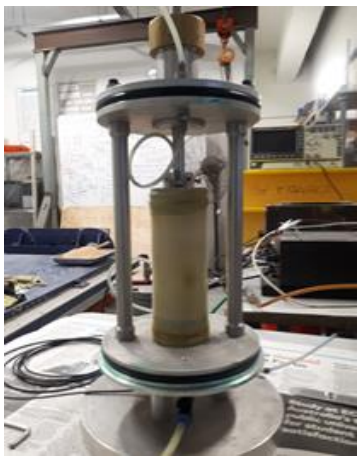

Figure 3.22: Setting up of a triaxial soil specimen

Double-vacuuming saturation method (Tanaka and Lee, 2016; Lim et al., 2019) was implemented in the present experiment to facilitate an effective saturation process for the studied residual soil. The residual soil composed of

substantial amount of fines content. The saturation process of residual soil is always problematic due to the lower permeability. Tanaka and Lee (2016) proposed the implementation of double-vacuuming saturation method on residual soil by using a pneumatic system equipped with E/P transducer and vacuum generator. The vacuuming saturation method, which was first proposed by Rad and Clough (1984), was used to saturate a clayey sand-type of residual soil with a low back pressure. This method is also called as dry setting method in ASTM D4767 and is very popular in the Japanese geotechnical practice (e.g. Ampadu and Tatsuoka, 1993). One of the advantages of the vacuuming saturation method includes the application of a low back pressure (e.g. 100~200 kPa) for achieving a satisfactory saturation as compared to the standard saturation method adopted in current Malaysia practices where a very high back pressure such as 400 to 800 kPa was always required (Tanaka and Lee, 2016). When a much lower back pressure was adopted, a greater range of effective pressures (i.e. difference between pneumatic cell pressure and back pressure) can be attained since the industrialised pneumatic pressure is typically limited to 700 to 800 kPa only. It follows that the soil responses at greater depth below ground surface can be replicated as the soil was subjected to a lower back pressure.

Figure 3.23 shows a schematic diagram for the double-vacuuming saturation method. The saturation process was achieved by controlling pressures through a pair of E/P transducers incorporated with vacuum generators, which had already been described in the beginning part of Section 3.5. The cell pressure transducer and a PISCO VUS11-series vacuum sensor

(as shown in Figure 3.24), were used to monitor the differential suction changes during the vacuuming saturation stage. Principally, the vacuuming saturation process was achieved by the removal of air from the top of soil specimen. It was followed by the permeation of de-aired water from the bottom of soil specimen slowly to saturate the specimen. The difference between internal and external suctions of the soil specimen was maintained at 20 kPa throughout the double-vacuuming saturation process.

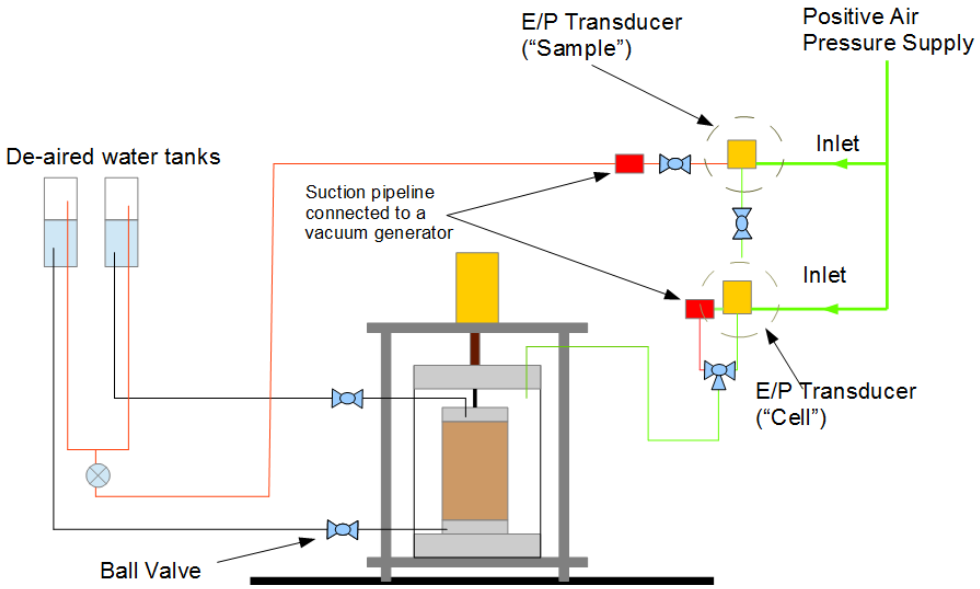

Figure 3.23: Schematic diagram for double-vacuuming saturation

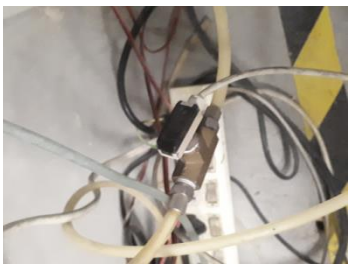

Figure 3.24: Vacuum sensor

The procedures of double-vacuuming saturation are listed as follows:

(a) Increase the suction pressure in the de-aired water tank and open the drainage valve connected to the top-end of soil specimen gradually. As summarized in Table 3.5, the suction pressure (from "sample" E/P transducer) was increased from 20 kPa, 40 kPa, 60 kPa, 80 kPa, to 90 kPa. On the course of increasing vacuuming pressure in the soil specimen, corresponding cell suction pressure (from "cell" E/P transducer) was applied to ensure the difference between internal and external soil suction pressures was maintained at 20 kPa. This process should be maintained for at least one hour until no air bubble was observed in the water tank.

(c) The bottom drainage valve was slowly opened to allow the equalization of vacuuming pressure throughout the height of soil specimen. It should be noted that the elevations of the two water tanks were remained same until this step.

(d) After equalization period for about 30 minutes, the de-aired water tank connected to the bottom of specimen was slowly elevated to a higher position to create a hydraulic gradient (about 2 m). The de-aired water could slowly permeate from the bottom segment of soil specimen and slowly pushed the air bubble out from the soil specimen.

(e) After two hours, the void in the soil specimen would be fully filled with water throughout its entire height as evidenced by a continuous outflow of water droplet from the tube connecting to the de-aired water tank. Lastly, the vacuuming pressures for soil specimen and cell water were decreased simultaneously in steps (reversed sequence in Table 3.4) to reach the original state (i.e., -20 kPa for the specimen and 0 kPa for the cell pressures).

Table 3.5: Application of suction during saturation

Step	Internal suction (kPa)	Cell suction (kPa)
1	20	0
2	40	20
3	60	40
4	80	60
5	90	70

3.5.4 B bar Check

After the completion of double-vacuuming saturation process, the cell pressure was switched back to positive pressure of 20 kPa and the inner pressure of soil was kept at 0 kPa (atmospheric pressure). Then, B bar test was conducted to check whether a satisfactory degree of saturation was achieved for the soil specimen. Figure 3.25 shows the schematic diagram of triaxial testing system equipped with B bar check, isotropic consolidation, and undrained shearing tests. The top part of soil specimen was connected to a volume change device and the base of specimen was connected to a pore-water pressure transducer. Back-pressure was applied onto the soil specimen through a tube fully filled

with de-aired water. The magnitude of back-pressure could be manually controlled by the pressure regulator.

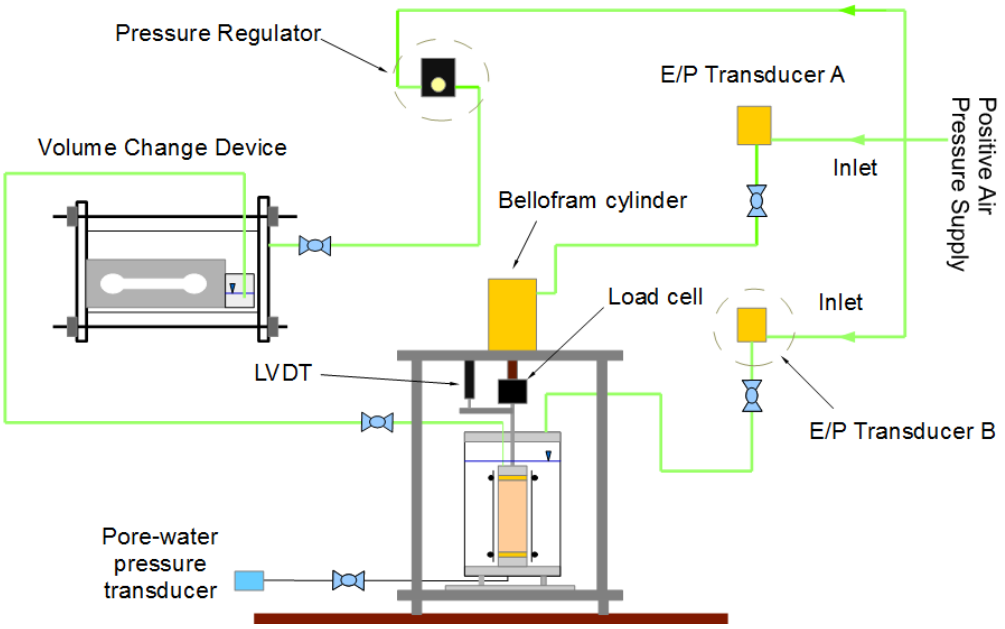

Figure 3.25: Schematic for monotonic triaxial apparatus after vacuuming saturation stage

In present study, a back-pressure of 100 kPa was consistently used to dissolve the tiny air bubble remained in the pore volume of soil specimen. Figure 3.26 demonstrates the changes of pore-water pressure during the B bar check. By using the same triaxial system, Tanaka and Lee (2016) observed that the pore-water pressure increased spontaneously with respect to the cell pressure. The double-vacuuming saturation method was capable to saturate residual soil under low back pressure.

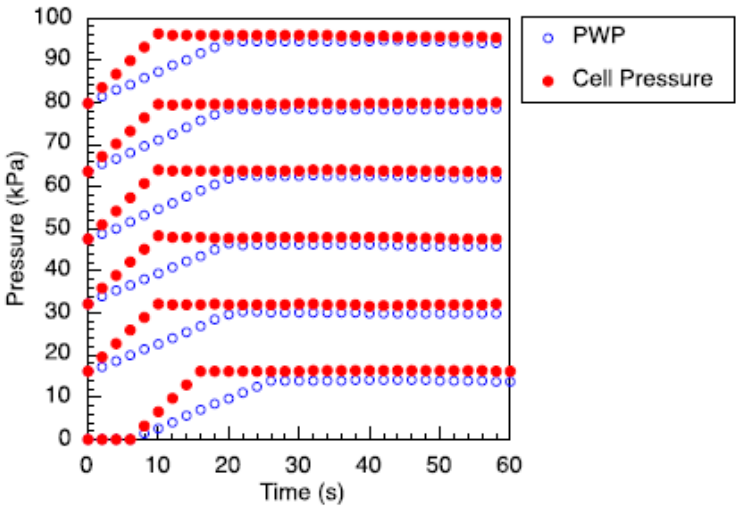

Figure 3.26: Pore-water pressure responses during B bar check (Tanaka and Lee, 2016)

The B bar check was conducted by applying cell pressure (i.e. total stress) to the soil specimen when the drainage valve was remained closed. The incremental change of pore-water pressure was compared with the applied cell pressure to yield the Skempton's *B* value (as defined in Equation 3.2). If the *B* value was not satisfactory (i.e. less than 95 %), the back pressure was slightly increased and the process was repeated until a satisfactory degree of saturation could be accomplished. Normally, the entire double-vacuuming saturation and B-bar check processes can be completed within 3-4 hours.

Pore-water pressure equation by Skempton (1954):

$$B = \frac{\Delta u}{\Delta \sigma_c} \tag{3. 2}$$

where
B = Skempton's pore-water pressure parameter
Δu = increment of pore-water pressure, kPa
$\Delta \sigma_c$ = *i*ncrement of cell pressure, kPa

3.5.5 Isotropic Consolidation Test

The saturated soil specimens were subjected to isotropic consolidation in the triaxial cell. During the isotropic consolidation test, all-round confining pressures (as illustrated in Figure 3.27) were exerted on the soil specimen. Under such stress condition, an isotropic material would experience an equal degree of deformation in all directions. It was practically accomplished by applying a certain increment of confining pressure to the soil specimen before the drainage valve was opened. After cell pressure stabilization, the drainage valve was opened slowly to permit the dissipation of water from the pore space. Unlike the conventional British triaxial cell (Bishop and Henkel, 1962), the loading ram in present triaxial apparatus was rigidly connected to the top cap and therefore isotropic pressure could not be applied by merely pressurizing the cell water. It should be noted that a supplementary vertical stress was required to be applied onto the loading ram in the present triaxial cell to achieve an isotropic stress condition.

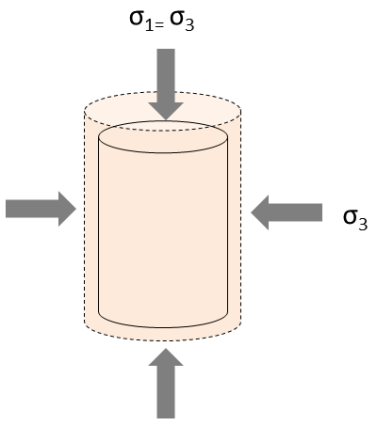

Figure 3.27: Isotropic stress condition

3.5.6 Undrained Shearing Test

In continuation to the isotropic consolidation test, undrained shearing (either triaxial compression or extension test) was commenced by first closing the drainage valve and then applying the vertical loading continuously onto the soil specimen. Figure 3.28 illustrates the stress state of a soil specimen under the triaxial compression and extension loading. On top of the constant confining pressure (i.e. minor principal stress, as denoted by σ_3), incremental vertical stress (i.e. major principal stress, as denoted by $\Delta\sigma_1$) was also applied continuously to induce the shearing of the soil specimen.

In principle, triaxial compression loading was exerted when the stress increment was compressive (i.e. greater than zero), whereas the triaxial extension condition was triggered once the stress increment became extensive (i.e. less than zero). During the triaxial extension test, the vertical stress was slowly reduced by moving up the loading ram, while the radial stress (i.e. cell water pressure) was remained constant. It is worth mentioning that the minimum (total) principal stress was practically zero during the triaxial extension test to prevent the detaching of top cap from the top surface of specimen. Stress-controlled loading system was herein adopted to reduce the mechanical noise generated by the stepper motor, which was used to operate for the constant strain-rate loading. Tanimoto and Tanaka (1986) also used similar loading system to investigate acoustic behaviour of soil by applying a slow constant rate of loading, under stress-controlled manner. Herein, the motivation of using the stress-controlled system was driven by the fact that

acoustic emission monitoring was carried out in the present research and it was therefore crucial to reduce the machinery noise.

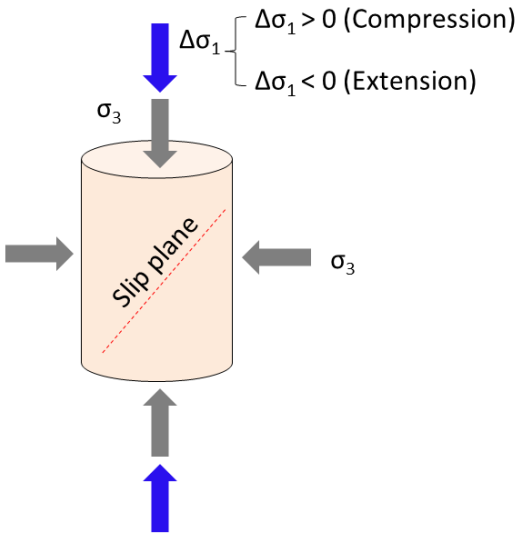

Figure 3.28: Shearing stress condition

The present triaxial apparatus was equipped with a Bellofram cylinder (SC type Fujikura Air Bellofram cylinder, model of BF-DA-80-62) to facilitate stress-controlled loading condition. Figure 3.29 shows the photograph of a Bellofrom cylinder loading system. Continuous small increment of vertical stress was applied through the pressure regulator and E/P transducer until the soil specimen was sheared to failure at large strain amplitude. To further ensure a frictionless movement, the surface of the stainless-steel loading ram with specially treated so as to reduce the mechanical noise caused by the friction between loading ram and linear bearing in the loading shaft.

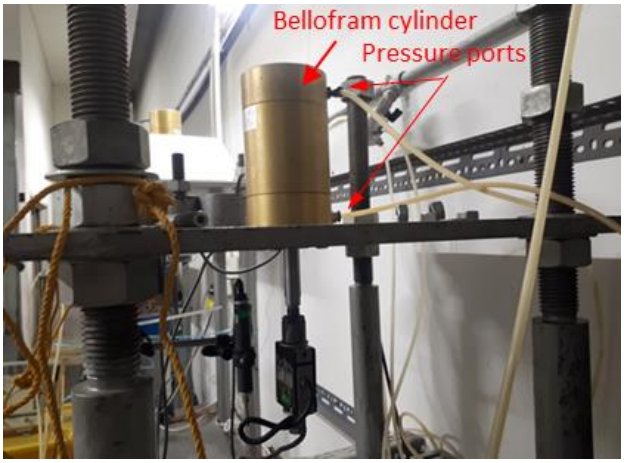

Figure 3.29: Bellofram cylinder

The working principle of an air Bellofram cylinder was also illustrated in Figure 3.30. Specifically, the movement of loading ram was controlled by the air pressure difference (i.e. σ_{in} and σ_{out}) between the top and bottom diaphragm rubber inside the Bellofram cylinder. Slow rate of stress-controlled loading was adopted by ensuring that the actual loading rate was lower than a threshold value (i.e. 0.3 kPa / s). The threshold loading rate was correspondingly determined from the elastic range in a monotonic strain-rate loading experiment (with 0.1 % / min). The slow-rate loading was accomplished by consistently supplying pneumatic pressure at a rate of 1 kPa at every 20 s in the present experiment.

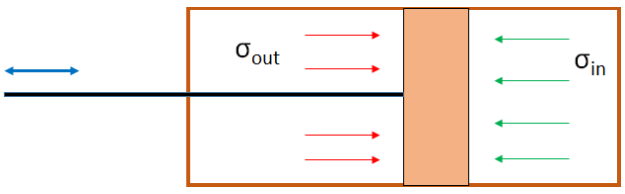

Figure 3.30: Schematic on the working principle of Bellofram cylinder

In addition, a screwing-type coupling was fabricated for pulling action as required in the triaxial extension test. As shown in Figure 3.31 (a), the extension coupling was rigidly connected to the loading ram and load cell. The base of triaxial cell was firmly clamped to counter react with the pulling force to guarantee that tensile force was able to be transferred to the soil specimen along the vertical direction. Figure 3.31 (b) also shows the design schematic of the triaxial extension coupling. Pair of cylindrical nuts was screwed tightly in order to avoid the extension coupling from loosening when it was vertically pulled up.

(a)

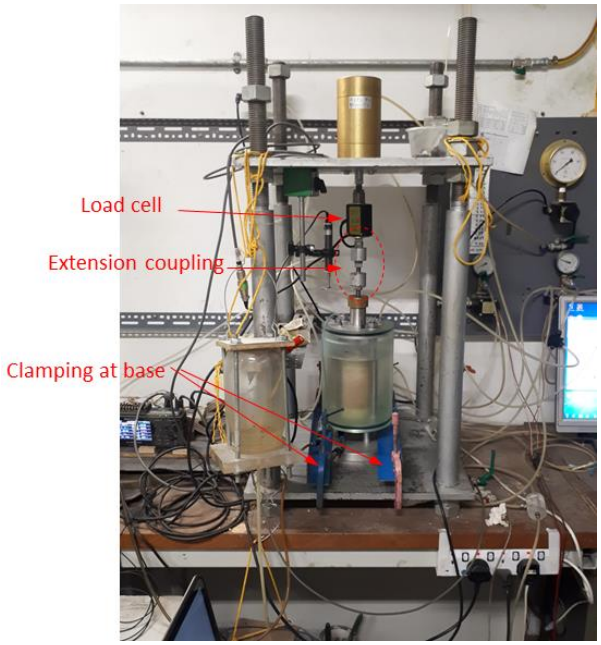

(b)

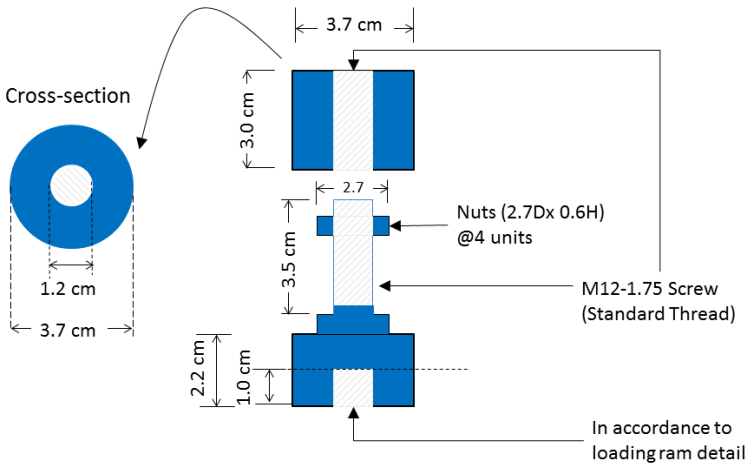

Figure 3.31: Screw connection for triaxial extension test: (a) photograph and (b) schematic diagram

3.6 Acoustic Emission (AE) Monitoring

3.6.1 Triaxial Apparatus Instrumented with AE Measurement

Figure 3.32 shows the experimental setup of a triaxial testing apparatus, which was specially devised to accommodate an AE transducer in the base pedestal.

As the key components of triaxial apparatus had been elaborated in the section 3.5.1, the AE instrumentation and data acquisition system are focused in this section.

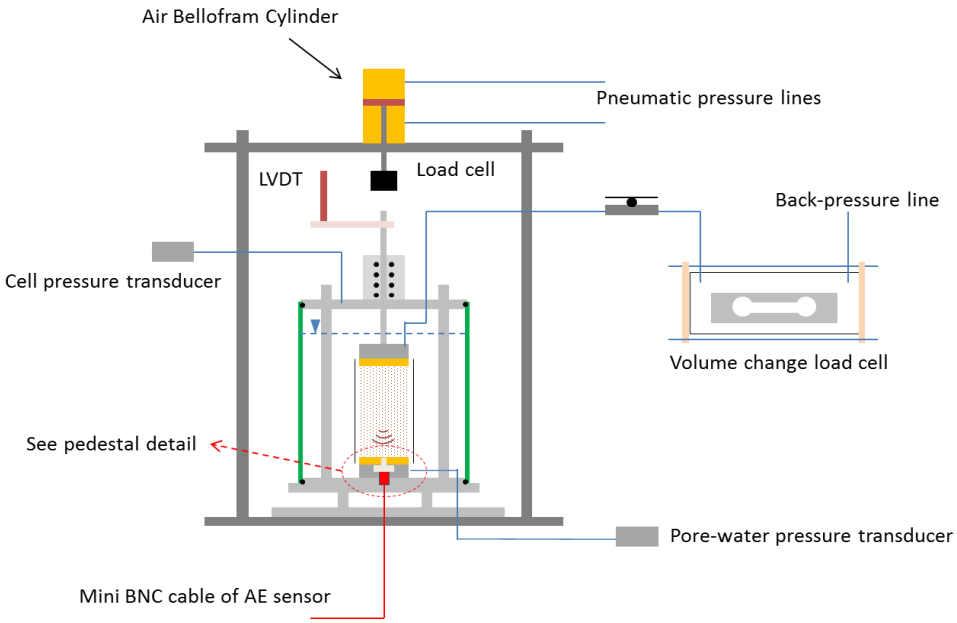

Figure 3.32: Schematic of triaxial apparatus instrumented with AE measurement

3.6.2 Fabrication Details of AE Base Pedestal

Figure 3.33 shows the detailed configuration of the base pedestal with an AE transducer. The selected AE transducer was known as a voltage-output type of piezoelectric accelerometer that had a built-in preamplifier in the transducer casing. Specifically, the accelerometer belongs to a model of PA 12C manufactured by Fuji Ceramics Corporation. From Figure 3.33, it can be seen that the nominal height of transducer was 25 mm while the edge-to-edge diameter of the top hexagon surface was 12 mm. In principle, the sensor can sensitively detect the micro-level vibration and then translate the physical

vibration into electrical form along the longitudinal direction of the transducer. This was made possible by the piezo-electrical mechanism acting on the piezo-ceramic disc in the transducer. The resonant frequency of measurement for this sensor was central at 32 kHz and responsive over a wide range of frequency (between 100 Hz and 100 kHz). It was speculated that stress waves as generated by the soil movement can propagate through soil grains structure and pore water when a saturated soil was compressed or sheared. For this reason, higher extent of AE signal can be detected in saturated soil specimen, as compared to the partially saturated soil. As the frequency of reported AE signal generated by soil mobilization was normally below 20 kHz (Koerner et al., 1981; Tanimoto and Tanaka, 1986; Smith and Dixon, 2019), the selected AE transducer is considered suitable and can be used for the investigation of soil in this study.

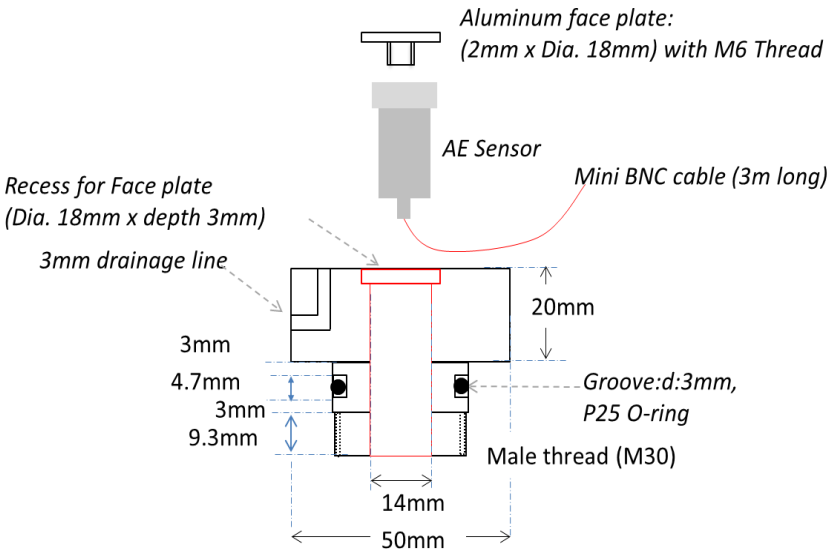

Figure 3.33: Design details for the base pedestal with AE transducer

Aluminium was used for the fabrication of AE base pedestal as it was understood that acoustic wave can propagate sufficiently fast in aluminium (typically 6300 m/s) among most engineering materials and capable to stay away from being rusty. As can be seen from the design configuration, a centre hole having a nominal diameter of 14 mm was allowed for the housing of AE transducer. An aluminium face plate, which was screwed onto the top surface of AE sensor, was devised to be in touch with a porous stone in order to facilitate direct capturing of acoustic waves. The face plate was adhered to a shallow recess (with a depth of 3 mm) by using high strength flex glue, which can provide a rubberized, waterproofing, and durable sealing contact. Similar application of this kind of adhesive material could also be found in strain-gauge type of load cell where a flexible sealing could facilitate electrical resistance change in each strain gauge element. After a curing duration of one-week, waterproofing ability of the AE base pedestal was examined by pressurization with cell water. It was positively confirmed that the base pedestal assemblage was water-resisting up to a water pressure as high as 5 bar (i.e. 500 kPa).

On top of that, a 3 mm drainage hole was drilled to a depth of 15 mm below the contact surface of base pedestal to facilitate precise pore-water pressure measurement. The outlet of drainage hole was allocated at the side of base pedestal because the bottom side of pedestal had been used to attach with the AE transducer. A threaded PICSO tube fitting was used to connect the drainage hole and the polyurethane tube (outer diameter of 2 mm and inner diameter of 1 mm). It should be noted that the location of the tube fitting must

be approximately 15 mm below the top surface of base pedestal to allow a space for tightening of rubber bands on a sleeve of rubber membrane during setting up of soil specimen.

Figure 3.34 shows the installation procedure of the AE transducer onto the aluminium base pedestal. Firstly, a mini BNC cable (i.e. 3m long) was screwed into female threaded side of the AE transducer. The transducer was later connected to the male thread of aluminium face plate to form a solid assemblage.

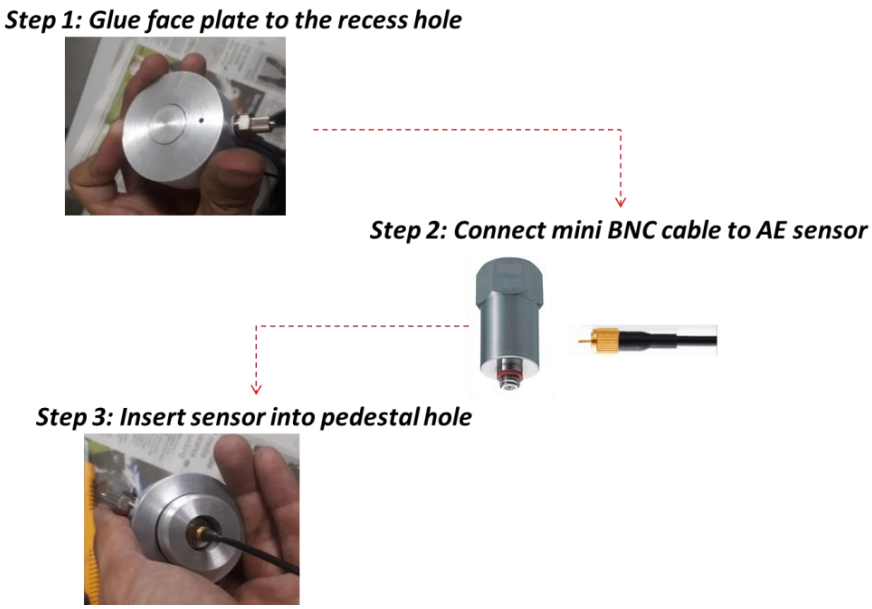

Figure 3.34: Procedure of installing AE transducer into base pedestal

Since the base of soil specimen was placed on top of a porous layer to allow the drainage of pore water, it is crucial to devise a base pedestal that can sensitively collect the true AE signal generated from the soil specimen. Tanimoto and Tanaka (1986) used a more expensive metallic porous layer (also known as sintered porous metal filter) to facilitate the receiving of AE

signal. Lord and Koerner (1972) suggested two approaches to facilitate direct AE signal measurement, including protrusion of a metallic waveguide into the soil specimen or embedding the AE transducer into the centre part of a larger soil specimen. In the present study, it was decided to adopt a composite porous filter considering of the cost-effectiveness and unfavourable disturbance on the soil body. To facilitate a more direct AE measurement, the centre hole of a porous stone was fitted with an aluminium plate (18 mm diameter and 5 mm thickness). Figure 3.35 shows the pictures of the composite porous stone that was formed by press fitting a thin aluminium plate into the centre hole of a porous stone. From the preliminary test, it was found that the metallic-porous stone composite was more effective in detecting the movement of soil grains, as compared to the one with porous stone only.

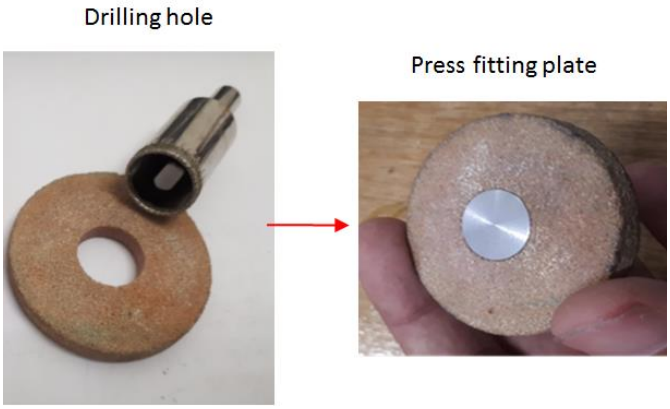

Figure 3.35: Composite porous stone

3.6.3 Instrumentation and Data Acquisition Systems for AE monitoring

Figure 3.36 depicts a data acquisition system to measure the AE as well as mechanical responses of soil. Since the acquired AE signal was very weak (in

millivolts), a voltage amplifier (with a model name of TEAC SA16) was required to magnify and filter the signal. The amplifier was supplied by a voltage of 12 V through a DC power supply, which could guarantee a stable voltage supply throughout the experiment. Photograph for the power supply and pre-amplifier were shown in Figure 3.37. It should be noted with care that a step-down transformer was also required for the DC power supply device as the device was only capable to withstand voltage up to 100 V.

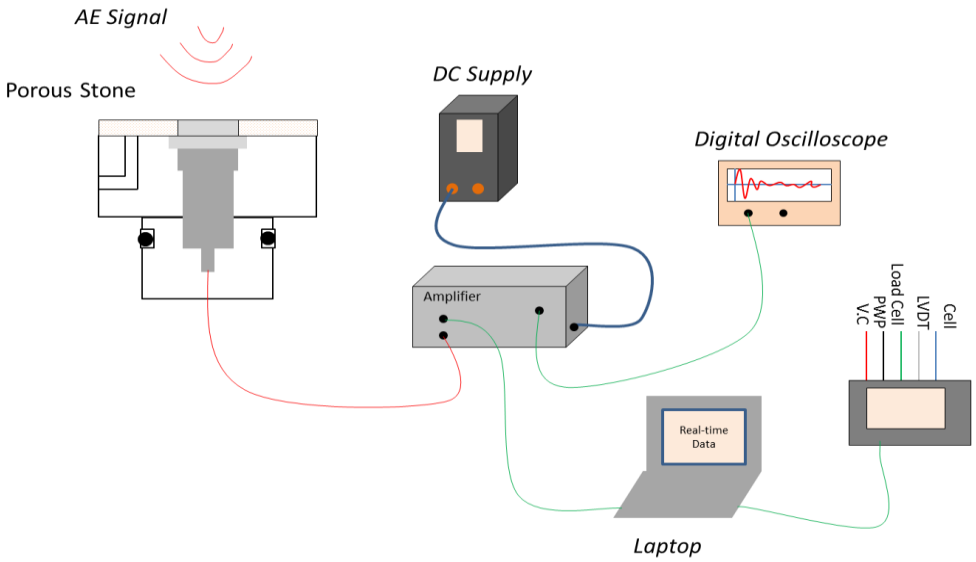

Figure 3.36: Schematic of data acquisition setup for present AE study

Figure 3.37: Power supply and pre-amplifier

Through the signal amplifier, the voltage of analogue signal could be increased with a gain factor of 500 before it was transmitted to an analogue-to-digital converter. With the present setup (as shown in Figure 3.36), an output line was used for the real-time monitoring in a digital Oscilloscope (as shown in Figure 3.38) while another output line was assigned for the connection to a laptop for data recording purpose. The digital Oscilloscope (GWinstek GDS-1000B series) was characterized with a vertical resolution of 8 bit/ per division and a precise time resolution of 1 ns per division. The in-built analogue-to-digital converter within the Oscilloscope was able to convert the obtained analogue signal into digital data.

Figure 3.38: Digital Oscilloscope

Since the true AE signal for granular material was reported to be audible and usually characterized with frequency content below 20 kHz only, the mentioned digital Oscilloscope could be used to capture the continuous signal. According to the well-known Nyquist theorem, the acquisition frequency of device shall be at least two times higher than the maximum frequency of measured signal. Herein, the maximum measuring frequency of the Oscilloscope was 1 GHz and absolutely satisfied the requirement of sampling frequency (i.e. 40 kHz). A coaxial-type of Bayonet Neill–Concelman (BNC) shielding cable was used to transmit the digital signal from the amplifier device into the digital Oscilloscope. This could minimize the effect of electromagnetic inference on the transmitted signal in cable. In the second output line, the amplified signal was transmitted to a laptop through a BNC-audio jack cable. The amplified analogue signal was later digitized and deposited to a laptop through a sound card, which was specified with a sampling frequency of 48 kHz. It is worth highlighting that the present developed AE system only demanded a sound card with low sampling frequency that was cheaply available in the market. The appropriateness of

using the sound card was also justified by the monitoring of true AE signals in digital Oscilloscope, which was specified with a higher sampling frequency (i.e. 1 GHz) as compared to the frequency of measured signal. The present AE system provided a low-cost alternative to facilitate the study of acoustic behaviours of soil in the laboratory.

3.7 Physical Assessment on MICP-treated Soils

After the triaxial experiment of MICP-treated soil specimens, qualitative (microscopic observation) and quantitative (calcite content measurement) assessments were carried out to justify the presence of precipitated calcites within the MICP-treated soil.

3.7.1 Acid Washing Test

Gravimetric analysis by acid washing was performed to determine the amount of calcium carbonate precipitated in the soil mass. Figure 3.39 shows the sampled soil mass experimental setup for the acid washing test. A portion of soil mass was extracted from the treated specimen for carrying out the acid washing test. Approximately 20 grams of soil mass was first sampled from the oven-dried MICP-treated soil in which the tested specimen had been disaggregated and mixed uniformly. The sampled soil mass was later washed with 1 Molar of hydrochloric acid for several cycles to dissolve the calcium carbonate in the soil completely. The acid-washed soil was then oven-dried for

24 hours at a temperature of 105 °C. Lastly, the mass difference between the original and the acid-washed soils yielded the amount of calcite precipitation.

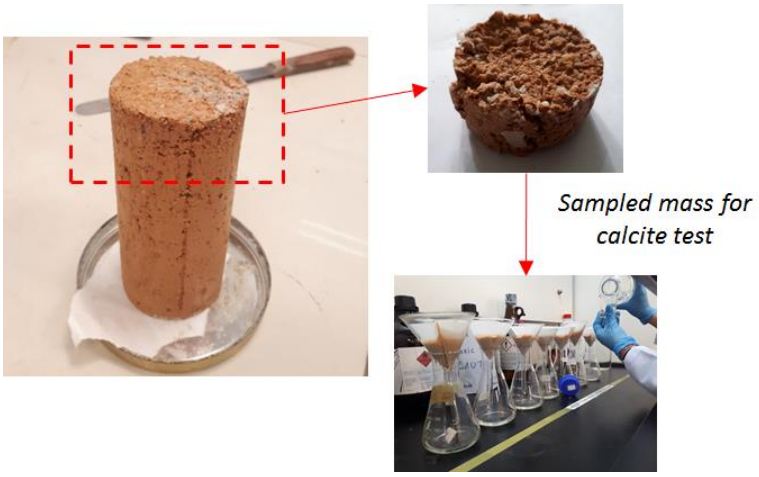

Figure 3.39: Determination of calcite content through acid washing test

3.7.2 Scanning Electron Microscopic (SEM) Test

Microstructures of soils (both untreated and MICP-treated soils) were examined qualitatively through a high-resolution scanning electron microscope (SEM) machine (as shown in Figure 3.40). At first, small amount of dried mass was sampled from a representative material (e.g. triaxial soil specimen) and transferred to a sample stub on the platform of SEM machine. Before the microscopic assessment, the sampled soil mass was subjected to vacuuming coating treatment to protect the electron source from being contaminated and facilitate high-resolution images. The procedures of preparing sample and carrying out the SEM test had also been reported by Velasco (2013) and stipulated in laboratory standard (ISO 13322-1). The micro-structural configurations of soils could be observed closely, and it was

useful in relating the mechanical responses of the soil as obtained from the triaxial testing.

Figure 3.40: Scanning electron microscope (SEM) machine

3.8 Data Processing

Two different types of experimental data could be obtained from the data logging system in triaxial tests, namely mechanical and AE data. The mechanical data consisted of axial displacement, axial stress, cell pressure, and pore-water pressure measurements. All these physical measurements were corresponded to the mechanical responses of tested soil specimens. This section highlights the methodology of manipulating and processing the mechanical data using Python. In addition, the digitized AE signal was numerically processed, and its intensity was quantified. It follows that mechanical behaviour of soil could be interpreted with the AE stress wave measurement, after the two types of processed data were synchronized.

3.8.1 Processing of Mechanical Data

The acquired mechanical measurements were spontaneously subjected to fluctuation as caused by the ambient vibration and electrical noise. Therefore, data smoothening was performed to moderate the mechanical signals. Firstly, the original mechanical data was processed through 5^{th}-order Butterworth low-pass filtering stage to reduce the noise fluctuation. The numerical filtering was carried out through Python, which is a general-purposed and high-level interpreted programming language. Python script for processing the mechanical data was compiled in Appendix B for reference. The processed data was checked in parallel with the original data to avoid the possible affection on nature of measurement; in such a way that the original and processed data should show similar baseline. The comparison between original and processed axial strain data is illustrated in Figure 3.41. Secondly, the amount of filtered data was cut down by taking average at every 2.5 s to reduce the data storage memory. The data averaging can be carried out in MS Excel program, in which the data could easily be manipulated in array form.

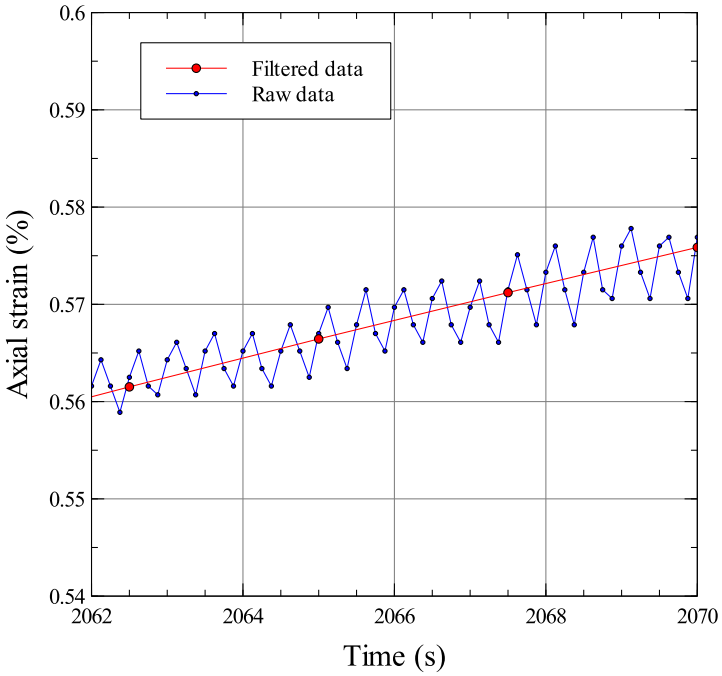

Figure 3.41: Typical profile of digital filtering on axial strain data

3.8.2 Processing of AE data

Before the commencement of triaxial experiments, background noise was monitored to understand the characteristics of vibration noise in the laboratory. Figure 3.42 shows a typical record consisting of a true AE signal and the ambient noise. It can be seen from the recording that the noise profile was not only affected by the baseline drift because of low-frequency content, but also contaminated with higher-frequency component. A periodic air-compressor noise was also found to be devastated and able to mask the true AE signal. In spite of that, the air-compressor noise could still be filtered in the post-processing stage as it occurred under a predictable fashion. It was realized that the air compressor machine would exhale and produced noise at nearly every

ten minutes. A thorough understanding of noise pattern can be very beneficial for the subsequent stage of AE analysis.

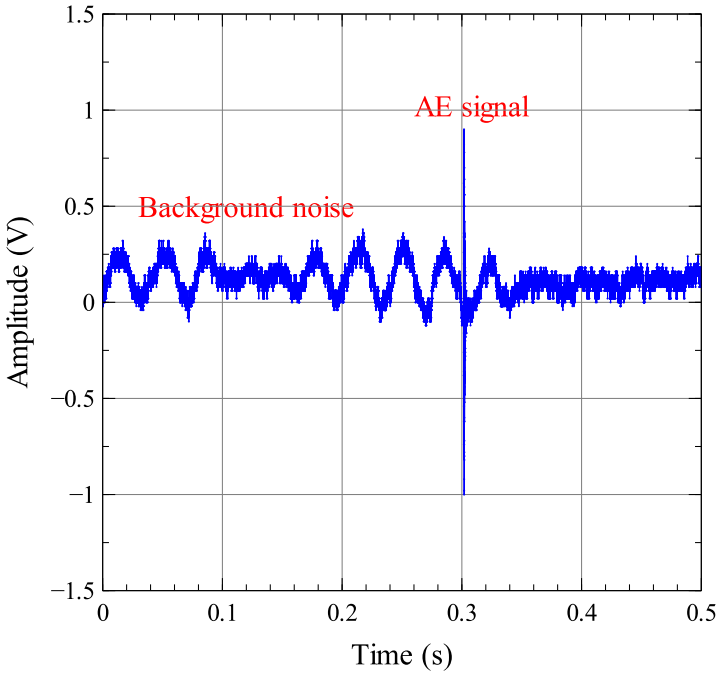

Figure 3.42: Recorded AE signal and ambient noise

Computer programs were utilized to process the acquired AE data and compute the AE counts rate to quantify the soil response. A graphical user interface (GUI) software, called Audacity, was used in the present study to record, acquire, and filtering the real-time acoustic emission data. This open-source software allows real-time digitizing, recording, and playing back quality audio data. The original audio data, which could be either in the form of WAV or MP3 format, was later digitized into process able 'TXT' or 'CSV' format for detailed analysis. After obtaining the data-type file (for instance, csv format), a series of signal analysis could be accomplished through another open-source computer program, namely Python. Mathematical analysis, such as fast-Fourier transform, bandpass filtering, waveform peak detection, and

threshold counting, could be carried out accordingly. Figure 3.43 depicts a detailed configuration of a true AE signal as distinguished by noise threshold, which was defined marginally greater than the background noise. It could also be observed that the AE signal manifested trend of attenuation. The dominant frequency of captured AE signal was found to be in the range of 3000 to 6000 Hz. Therefore, the raw data was subjected to bandpass filtering with a bandpass frequency ranging from 100 Hz to 20 kHz to eliminate the noise. The Python scripts for counting the peak data points (AE spikes), wherein the prescribed noise threshold level was exceeded, were also provided in Appendix C and D. Finally, the AE counts rate (at every 5 s) and cumulative counts rate could be computed to quantify representative AE response for respective soil specimens.

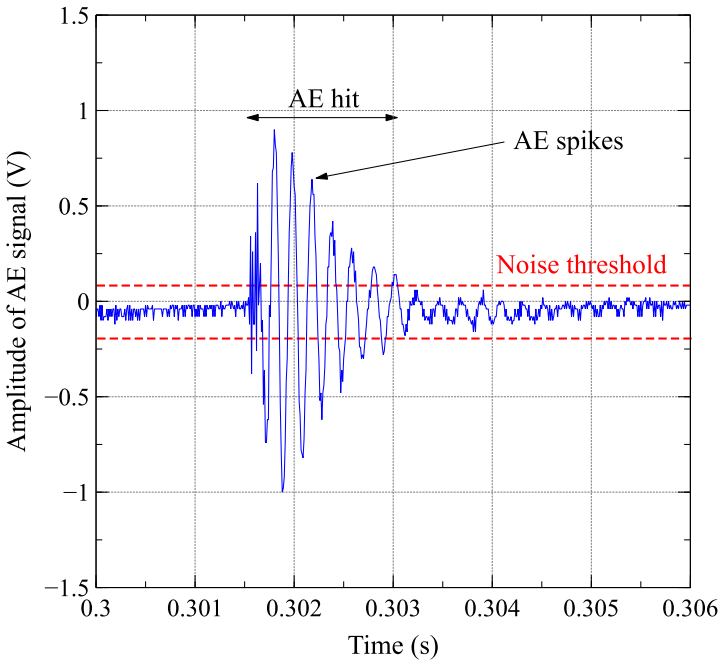

Figure 3.43: Configuration of an AE signal and noise threshold

3.9 Testing Program

Table 3.6 shows the test program for the triaxial experiment in the present study. Structural formation and corresponding stress-deformation behaviours for the (MICP-treated) residual soil and sand were investigated in Chapter 4. Three different levels of consolidation pressure (namely, 40 kPa, 120 kPa, and 220 kPa) were designated for the experiment to facilitate the comparative investigation between (MICP) residual soil and sand. Testing on the (MICP) residual soils consolidated to 80 kPa were additionally conducted for comprehending the soil yielding behaviour; the relevant results will only be provided in Section 5.3.3.2 and Appendix I-J for reference. It should be mentioned that a supplementary set of triaxial extension tests were also carried out for the (MICP) residual soils to validate the anisotropic deformation behaviour observed during the isotropic consolidation stage, as covered in Chapter 4. Triaxial extension test was not carried out for the sand specimens because (MICP-treated) sands behaved as an isotropic material.

Further interpretations could be made upon the implementation of acoustic emission monitoring on the soil structural changes and the experimental results were covered in Chapter 5. Moreover, additional testings on four isotropic hardening soils (namely UR-OCR5.0-C, UR-OCR2.5-C, BR-OCR5.0-C, and BR-OCR2.5-C) were carried out. This was motivated by the fact that state changes (namely, yielding and dilation) had been reported by Tanimoto and Tanaka (1986) in the mechanically hardened sands (soils being

subjected to certain degree of over-consolidation ratio) and the approach of determination state changes can serve as a benchmark for the present study.

Table 3.6: Test program

Soil label	MICP treatment	Stress condition	Consolidation Stress [#] (kPa)	Measurement	
				Mechanical	AE
Sand					
US-40-C	No	CIUC	40	Yes	Yes
US-120-C	No	CIUC	120	Yes	Yes
US-220-C	No	CIUC	220	Yes	Yes
MICP Sand					
BS-40-C	Yes	CIUC	40	Yes	Yes
BS-120-C	Yes	CIUC	120	Yes	Yes
BS-220-C	Yes	CIUC	220	Yes	Yes
Residual soil					
UR-40-C	No	CIUC	40	Yes	Yes
UR-80-C*	No	CIUC	80	Yes	Yes
UR-120-C	No	CIUC	120	Yes	Yes
UR-220-C	No	CIUC	220	Yes	Yes
UR-OCR5.0-C	No	CIUC	55	Yes	Yes
UR-OCR2.5-C[b]	No	CIUC	88	Yes	Yes
UR-40-E	No	CIUE	40	Yes	Yes
UR-80-E*	No	CIUE	80	Yes	Yes
UR-120-E	No	CIUE	120	Yes	Yes
UR-220-E	No	CIUE	220	Yes	Yes
MICP residual soil					
BR-40-C	Yes	CIUC	40	Yes	Yes
BR-80-C*	Yes	CIUC	80	Yes	Yes
BR-120-C	Yes	CIUC	120	Yes	Yes
BR-220-C	Yes	CIUC	220	Yes	Yes
BR-OCR5.0-C	Yes	CIUC	55	Yes	Yes
BR-OCR2.5-C[c]	Yes	CIUC	88	Yes	No
BR-40-E	Yes	CIUE	40	Yes	Yes
BR-80-E*	Yes	CIUE	80	Yes	Yes
BR-120-E	Yes	CIUE	120	Yes	Yes
BR-220-E	Yes	CIUE	220	Yes	Yes

Notes
[a] The consolidation stress was defined as (nominal) isotropic consolidation stress.
[b] Load-unload-reloading test was carried out to investigate the yielding and Kaiser's effect.
[c] AE data was not obtainable in this particular soil due to device malfunction.
Isotropic consolidation pressure prior to undrained shearing.
MICP referred to Microbial-induced calcite precipitation.
CIUC referred to Isotropic-consolidated undrained compression test.
CIUE referred to Isotropic-consolidated undrained extension test.
OCR referred to over-consolidation ratio.

3.10 Summary

This chapter first presents the physical properties of studied residual soil and sand. The tropical residual soil was classified to be a very Clayey Sand whereas the sand was classified as clean Poorly-graded Sand. The clean sand was sieved to MICP-favourable particle size range to serve as a benchmark relative to the MICP-treated residual soil. In view of different permeability between the residual soil and sand, different treatment setup was used for the residual soil and sand, respectively. A consistent mix proportion of chemical reagent (e.g. urea and calcium chloride) was adopted for the two studied soils to promote calcite precipitation in the soil specimen.

Next, design and fabrication of monotonic triaxial apparatus and its instrumentation system are described in detail. The triaxial apparatus was equipped with cell pressure, pore-water pressure, axial stress, and axial displacement measurements. Stress-controlled loading system was adopted in present study to avoid mechanical noise caused by the stepper-motor loading device. In addition, the procedures of double-vacuuming saturation, B bar check, isotropic consolidation, and undrained shearing were mentioned accordingly.

Subsequently, the development of Acoustic Emission system (e.g. experimental and data acquisition systems) was mentioned explicitly. The data processing for mechanical and AE data were also covered. Finally, the testing program for this study was systematically tabulated.

CHAPTER 4

MECHANICAL BEHAVIOURS OF MICP RESIDUAL SOIL IN COMPARISON WITH SAND

4.1 Introduction

This chapter discusses the mechanical behaviours (obtained from the isotropic consolidation and undrained shearing tests) and microstructural formation of the MICP-treated residual soil and sand, respectively. First of all, the time-series deformation data were presented. Next, void ratio changes and anisotropic deformation (i.e. changes of radial against vertical strains) were used to evaluate the isotropic consolidation responses. Furthermore, undrained shearing tests were conducted to investigate stress-strain and pore-water pressure responses of the (MICP) soils. The microstructural formation of MICP soils was predicted from the mechanical responses and reinforced by the microscopic observation through Scanning Electron Microscope (SEM). Based on the experimental observations, differences in MICP formation and mechanical behaviours between residual soil and sand were examined.

4.2 Basic Characteristics of Investigated Soils

Table 4.1 shows the characteristics of residual soil and sand specimens as tested in this study, including initial dry density, initial void ratio, final void ratio at the end of isotropic consolidation, and net calcite content. The initial void ratio (dry density) of the MICP-treated soil specimen was computed by considering the dry mass of soil and calcite content. The MICP-treated soils can be regarded as lightly treated soils as the net calcite content was considerably low as compared to the implicative threshold level, namely 10 % as reported by Cui et al. (2017). It should be highlighted that the experimental results for residual soils consolidated at 80 kPa were not used for main discussion/ interpretation throughout this thesis, since the experimental data of (MICP-treated) sands at the same pressure were absent. However, the results for (MICP-treated) residual soils consolidated at 80 kPa were used for the interpretation of yielding behaviour in Chapter 5 and supplemented in Appendix I and J for future reference.

Table 4.1: Basic characteristics of tested soils

Soil label	Stress condition	Initial dry density (Mg/m^3)	Initial void ratio	Final void ratio #	Consolidation Stress (kPa)	Net calcite content (%)
Sand						
US-40-C	CIUC	1.37	0.930	0.929	40	-
US-120-C	CIUC	1.37	0.930	0.922	120	-
US-220-C	CIUC	1.37	0.930	0.905	220	-
MICP Sand						
BS-40-C	CIUC	1.43 [a]	0.859	0.859	40	3.8
BS-120-C	CIUC	1.43	0.859	0.843	120	3.8
BS-220-C	CIUC	1.42	0.863	0.843	220	3.6
Residual soil						
UR-40-C	CIUC	1.62	0.635	0.635	40	-
UR-80-C	CIUC	1.62	0.635	0.634	80	-
UR-120-C	CIUC	1.62	0.635	0.596	120	-
UR-220-C	CIUC	1.62	0.635	0.560	220	-
UR-OCR5.0-C	CIUC	1.62	0.635	0.571	55	-
UR-OCR2.5-C[b]	CIUC	1.62	0.635	0.562	88	-
UR-40-E	CIUE	1.62	0.635	0.634	40	-
UR-80-E	CIUE	1.62	0.635	0.631	80	-
UR-120-E	CIUE	1.62	0.635	0.611	120	-
UR-220-E	CIUE	1.62	0.635	0.588	220	-
MICP residual soil						
BR-40-C	CIUC	1.68	0.580	0.580	40	3.5
BR-80-C	CIUC	1.67	0.585	0.583	80	3.2
BR-120-C	CIUC	1.66	0.595	0.571	120	2.5
BR-220-C	CIUC	1.66	0.592	0.566	220	2.7
BR-OCR5.0-C	CIUC	1.64	0.616	0.583	55	1.2
BR-OCR2.5-C[c]	CIUC	1.64	0.619	0.598	88	1.0
BR-40-E	CIUE	1.66	0.599	0.597	40	2.3
BR-80-E	CIUE	1.66	0.597	0.592	80	2.4
BR-120-E	CIUE	1.66	0.600	0.585	120	2.2
BR-220-E	CIUE	1.65	0.606	0.555	220	1.8

Notes:
[a] Dry density as computed based on the measured calcite content after the triaxial test.
[b] Load-unload-reloading test was carried out to validate the Kaiser's effect.
[c] AE data was not obtainable for this particular soil specimen due to device malfunction.
Void ratio obtained after isotropic consolidation test, prior to the undrained shearing stage.

4.3 Mechanical Behaviour of MICP-treated Residual Soil

This section elaborates the experimental results for isotropic consolidation to undrained compression and extension (CIUC and CIUE) tests. Undrained shearing was adopted in the present experiment in light of the fact that the studied residual soil constituted significant fines (≈ 32 %) and therefore the pore-water pressure effect was important in undrained condition. The triaxial

extension test was carried out to validate the structural anisotropy in the MICP residual soil, which will be discussed in depth in the subsequent section.

4.3.1 Isotropic Consolidation Behaviour of MICP-treated Residual Soil

4.3.1.1 Time-series Consolidation Responses of Tested Residual Soils

Figure 4.1 shows the isotropic consolidation responses (i.e. cumulative volumetric strain-stress-time change) of representative residual soil specimens. The participated soil specimens were UR-120-C, BR-120-C, UR-220-C, and BR-220-C. The isotropic consolidation results of other soil specimens, such as UR-120-E, UR-220-E, BR-120-E, BR-220-E, US-120-C, US-220-C, BS-120-C, and BS-220-C, were also provided in Appendix E-H for reference. This experimental result fundamentally served as a steppingstone for subsequent deformation analysis of all tested soils. In later sections (from Section 4.3.1.2 onwards), states corresponding to the completion of primary consolidation (i.e. when > 95 % dissipation of pore-water pressure and steady-state of volumetric change) were selected at the end of consecutive consolidation increments. It follows that the deformation behaviours of soils can be analysed reliably and consistently. It can be observed from Figure 4.1 that the MICP-treated residual soils (i.e. BR-120-C and BR-220-C) were stiffer than the untreated residual soils inasmuch as the lower magnitude of soil deformations.

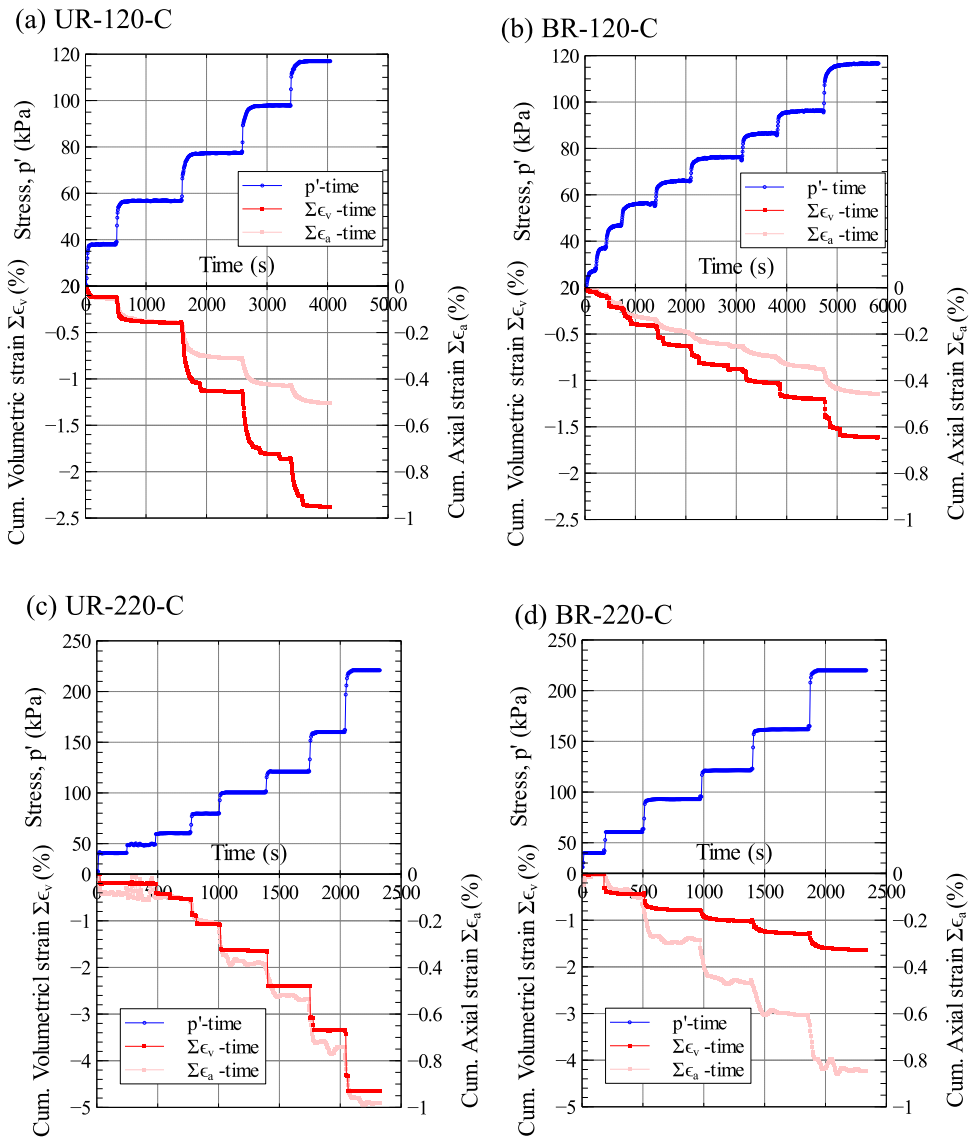

Figure 4.1: Isotropic consolidation time-series responses of representative soil specimens

4.3.1.2 Void Ratio Changes of MICP-treated Residual Soil

Figure 4.2 shows the isotropic consolidation curves for the MICP-treated residual soil specimens. A lower void ratio was obtained for the MICP-treated residual soil specimens as compared to its untreated counterpart owing to the calcite precipitation. The reduction in void ratio as a result of calcite precipitation was also reported in other experimental investigations (DeJong et

al., 2010; Lin et al., 2016). The magnitudes of the initial void ratio among the untreated specimens were found to be more consistent than the MICP-treated specimens. These findings could be due to spatial non-uniformity in the distribution of the precipitated calcite crystals within the pore space of soil. The issue of non-uniformity in calcite distribution, which had been highlighted in Section 2.6.3, was also observed in a recent experimental investigation on the same type of residual soil under different moisture content and density (Lim et al., 2020).

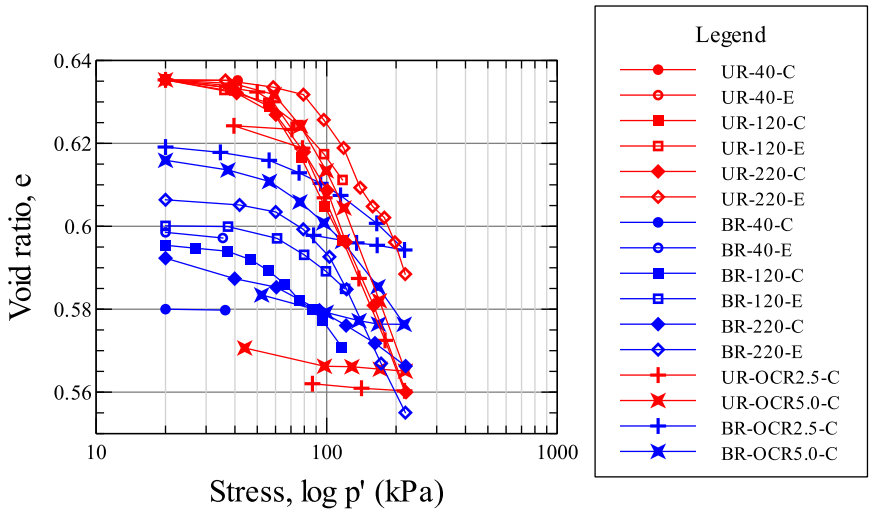

Figure 4.2: e-log p' for the untreated and MICP-treated residual soil specimens

Both untreated and MICP-treated residual soils showed a consolidation curve with an apparent curvature change point, as similar to different types of reported geo-materials (Terzaghi et al., 1996; Taylor, 1948). This point refers to the first structural degradation of tested soils corresponded to the incipient occurrence of isotropic yielding and can be determined using classical approach such as Casagrande's method (Taylor, 1948). Table 4.2 summarizes the results of isotropic yield stress and compression index for the residual soil

specimens. It is worth mentioning that the consolidation properties of the tested soil specimens were only evaluated for specimens being consolidated to 220 kPa (e.g. UR-220-C, UR-220-E, UR-OCR2.5-C, UR-OCR-5.0-C, BR-220-C, BR-220-E, BR-OCR2.5-C, BR-OCR5.0-C), inasmuch as the fact that those soil specimens had become normally consolidated. The compression index (denoted as C_c) was determined at the final stress increment along the normal consolidation line. In addition, the swelling indexes were obtained from the (MICP-treated) residual soils, which had been subjected to an OCR ratio of 5.

Table 4.2: Deformation characteristics for tested residual soil specimens

Soil specimen	Compression index C_c	Swelling index C_s	Isotropic yield stress (kPa)	Net calcite content (%)
Residual soil				
UR-220-C	0.149	-	81.6	-
UR-OCR5.0-C	0.150	0.008	87.3	-
UR-OCR2.5-C	0.144	-	71.2	-
UR-220-E	0.172	-	89.6	-
MICP residual soil				
BR-40-C				3.5
BR-120-C				2.5
BR-220-C	0.042		97.9	2.7
BR-40-E				2.3
BR-120-E				2.2
BR-220-E	0.112		97.6	1.8
BR-OCR5.0-C	0.080	0.014	99.7	1.2
BR-OCR2.5-C	0.053	-	97.3	1.0

Note:
-The isotropic yield stress and compression indexes were determined from the soil specimens being consolidated to 220 kPa only.
-Swelling index was not determined for the soils being consolidated to OCR = 2.5 only, since the soils had not been experienced heavily over-consolidated state.

It was evidenced that the isotropic yield stress for the residual soils had been enhanced after the bio-mediation process. The average isotropic yield stress of MICP-treated residual soil was increased by 15.7 kPa (based on the

Casagrande's method). The isotropic yield stress of UR-220-C specimen was increased by 16.3 kPa, while the UR-220-E specimen was merely increased by 8 kPa. The lower increase in the yield stress of the extension test specimens could be explained by the fact that a lower degree of cementation (i.e. calcite content) was obtained in the BR-220-E specimen than the BR-220-C specimen. As different from BR-220-E specimen, the BR-220-C specimen did not manifest apparent curvature change along the isotropic consolidation curve, arguably attributed to its stiffer soil structure. The obtained yield stress could probably be much greater than the present value if the soil would deform abruptly at a higher consolidation stress level (beyond 220 kPa). It is clear from Table 4.2 that the BR-220-C specimen had the highest level of calcite content (i.e. 2.7 %) among all other MICP-treated soil specimens which were consolidated to stress levels > 120 kPa (i.e. BR-120-C, BR-120-E, BR-220-E, and BR-OCR5.0-C). The specimen was coincidentally characterized with the stiffest MICP-induced structure.

The marked increase in yield stress can physically be linked to the increase in the inter-particle resistance by the formation of calcite cementation, which could be attributed to the calcite bonding at particle-to-particle contact or binding of adjacent particles by an extensive calcite cementation (DeJong et al., 2010; Cui et al., 2017). The cementation was perhaps analogous to those of natural bonded clays (Terzaghi et al. 1996) and artificial cemented soils (Rotta et al. 2003). Cemented soil usually experienced de-bonding at the onset of first yielding (Rotta et al., 2003; Malandraki and Toll, 2001; Rios and Baudet, 2014). Beyond the yield point, calcite bonds

would be diminished and accompanied by apparent movement of soil particles. It is further anticipated that the microstructural resistance of MICP-treated residual soil would be greatly dictated by the fines (i.e. silt and clay particles). On top of the calcite cementation bridging two adjacent solid particles, aggregation of calcites-to-fines could also be formed. It follows that the load was not only transferred along the force chain of coarser grains, but also through the cemented fines aggregation (Zamani and Montoya, 2018).

After the calcite bonding was broken, the fractured calcites could still provide stiffness to the soil structure through calcite densification mechanism (DeJong et al. 2010; Montoya, 2012; Canakci et al. 2015; Cheng et al., 2016). The precipitated calcites could clog the pore space leading to fewer tendencies of pore-water dissipation and less movement of soil grains being triggered (Canakci et al. 2015; Zamani and Montoya, 2019). It is anticipated that the structural resistance of MICP-induced soil specimen would become weaker as the calcite assemblage was continuously fractured into smaller pieces with the increase of isotropic consolidation stress. As presented in Table 4.2, the average compression index for the untreated and MICP-treated residual soils was 0.154 and 0.072 (i.e. decrease by 0.082), respectively. Therefore, it is confirmed that the present MICP-treated residual soil was characterized with a more resistant structure on account of the effect of calcite densification in post-yielding stage.

4.3.1.3 Anisotropic Deformation of MICP-treated Residual Soil

Figures 4.3 (a) – (c) depict a series of relationships correlating deformations of (MICP) residual soils and consolidation stress. In these figures, the cumulative volumetric, axial, and radial strains were correlated to the isotropic consolidation stress respectively for all tested residual soil specimens. It can be observed from Figure 4.3 (c) that the untreated residual soil specimens deformed to greater magnitudes in horizontal direction, as compared to the MICP-treated specimens. This could be related to the increase in horizontal rigidity in the MICP-treated residual soil, as discussed in Section 4.3.1.2. The axial strains for both untreated and MICP residual soils were within similar range. In the followings, inter-relationship between incremental axial and radial strain components will be examined to comprehend the anisotropic deformation behaviour.

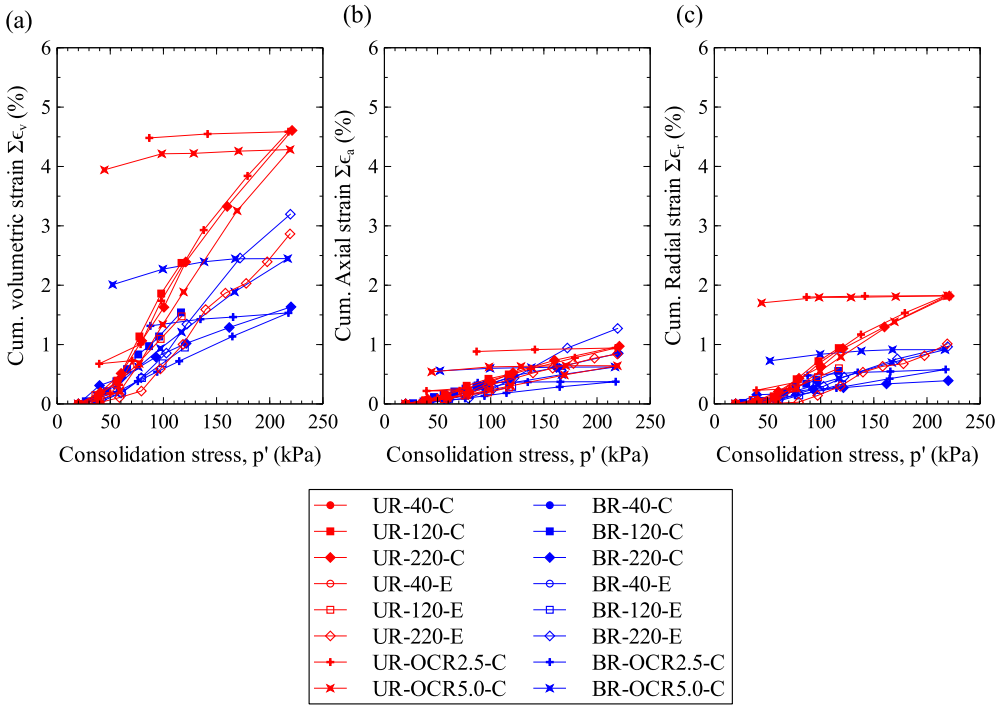

Figure 4.3: Relationships between deformations of (MICP) residual soils and consolidation stress: (a) Cumulative volumetric strain vs consolidation stress; (b) Cumulative axial strain vs consolidation stress; (c) Cumulative radial strain vs consolidation stress

Figure 4.4 shows the relationship between radial strain (ϵ_r) and axial strain (ϵ_a) for the untreated and MICP-treated residual soils. An isotropic line, along which the magnitude of axial strain equals to the radial strain, was plotted to show the degree of anisotropy among the soils. It was found that the MICP-treated residual soils (e.g. BR-220-C and BR-220-E) experienced greater axial deformations whereas the untreated residual soils tended to deform along the radial direction. It follows that the MICP-treated residual soil had a greater radial resistance whereas the untreated residual soil showed a greater resistance along vertical direction.

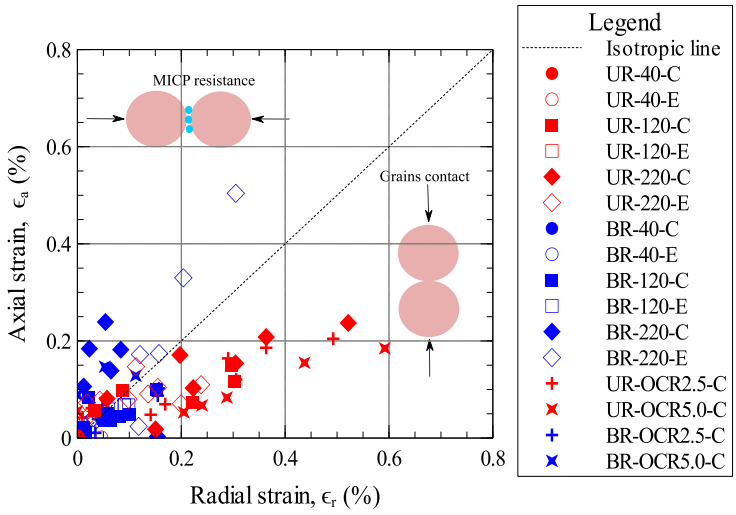

Figure 4.4: Anisotropic deformation for (MICP-treated) residual soil

It has been well understood that sedimentary clay (e.g. London clay) exhibits nature of anisotropy as attributed to the arrangement and orientation of platy soil grains (Atkinson, 1975; Terzaghi et al., 1996). The mechanical behaviour (e.g. undrained shear strength, stiffness, and anisotropy) of sedimentary clay would be dictated by its microstructural formation and particles' arrangement. From the isotropic triaxial compression test on fissured London clay, Atkinson (1975) found that anisotropic deformation was profound when the direction of principal stress oriented in reference to the direction of soil fabric. However, mechanism of anisotropy in the present MICP-treated residual soil was more complicated due to the interactive involvement of soil compaction and bio-mediation mechanisms. When the specimen was vertically compacted, soil grains were constrained against the rigid wall of the mould and this would facilitate a greater resistance along the vertical direction. In related to the matter, Aiban and Aurifullah (2007) claimed that a higher vertical resistance could be promoted by the confinement

effect of the mould. Upon MICP treatment, it is anticipated that the formation of calcite precipitation was favourable along the flow path of chemical reagent (Do et al., 2019). This would subsequently promote calcite bonding and confinement to the vertical chains of the soil grains side-by-side.

To further justify the above anticipation, triaxial extension tests were carried out on the (MICP-treated) residual soils to understand the stress-deformation behaviour of this unique soil structure under a more complete set of triaxial stress condition. The deformation behaviour (i.e. isotropic compression and unloading) of OC residual soils (namely, UR-OCR5.0-C and BR-OCR5.0-C), in which the MICP-treated residual soil also exhibited structural anisotropy over the untreated counterpart, will explicitly be discussed in subsequent Section 4.2.1.4. It should be noted that the lightly OC residual soils (i.e. with OCR = 2.5) were not included for the analysis in Section 4.2.1.4 since the soils had not been experienced apparent over-consolidation effect.

4.3.1.4 Unloading Behaviour of Untreated and MICP-treated Over-consolidated Residual Soils

From Table 4.2, it was found that the swelling indexes for MICP-treated residual soils were greater than that of original residual soils. The tendency in swelling could be linked to the rebound of lateral strain by the recovery movement of precipitated calcites within the anisotropic structure of MICP-treated residual soil. This finding also indicated that the dislocated soil grains (in the original residual soil structure) experienced plastic deformation, in

which only a limited degree of deformation (both axial and radial strains) was recoverable.

This phenomenon can be better comprehended by referring to Figure 4.5, which directly compares the unloading deformations between untreated and MICP-treated OCR residual soils under isotropic consolidation. It should be noted that only the results of heavily over-consolidated residual soils (i.e. UR-OCR5.0-C and BR-OCR5.0-C) were used in this comparison, whereas the results of lightly over-consolidated soils were omitted inasmuch as the limited unloading data points. Figure 4.5 clearly shows that the untreated soil manifested isotropic deformation upon unloading, since the gradient of fitted unloading line of soil was close to the slope of an ideal isotropic material. On the contrary, the gradient of rebound fitting line for the MICP-treated soil was much higher than the gradient of an ideal isotropic line; the bio-mediated structure tended to rebound laterally.

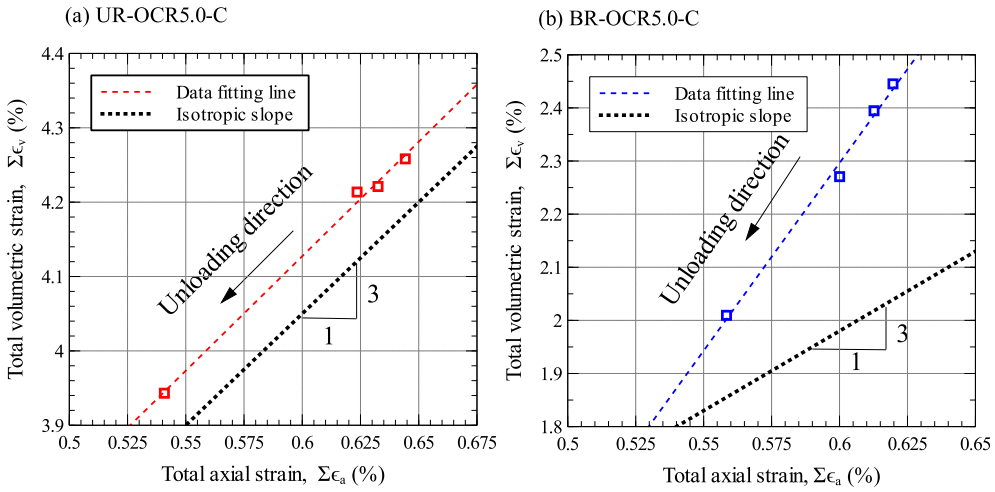

Figure 4.5: Comparison of axial and volumetric strains under isotropic unloading stage among over-consolidated residual soils: (a) Untreated; (b) MICP-treated

When the MICP-treated residual soil specimen was isotropically loaded, the axial deformation was greater and less deformation was observed along the radial direction. With the progress of isotropic compression, soil grains would be relocated downward to contact with other grains while the cemented calcites would become fracturing progressively. Although this finding had been realized in previous section, the treated overconsolidated (abbreviated as OC) soil somewhat exhibited less tendency to deform vertically than the other normally consolidated residual soils (as evidenced in Figure 4.6). This was caused by the low degree of calcite cementation (i.e. only 1.2 % of net calcite content) in the investigated BR-OCR5.0-C specimen. Nevertheless, the overconsolidated MICP-treated residual soil was still characterized with anisotropic arrangement, since the gradient of MICP fitting line (the blue-colour fitting line in Figure 4.6) was much steeper than the untreated soil. Once the soil was unloaded, the mobilized grains were found reluctant moving back to the original positions and therefore only a slight recovering deformation could be observed in the original residual soil structure. The calcite formation, which favoured along the lateral direction of adjacent soil grains, was capable to restore noticeable degree of strain energy along the radial direction. Despite of the light cementation, the characteristic of anisotropy can still be observed when the overconsolidated soil specimen was subjected to isotropic loading (Figure 4.6) and unloading (Figure 4.5). Figure 4.7 shows a simplified spherical model to illustrate the anticipated phenomena and interaction of soil grains in the bio-mediated OC structure, as discussed above.

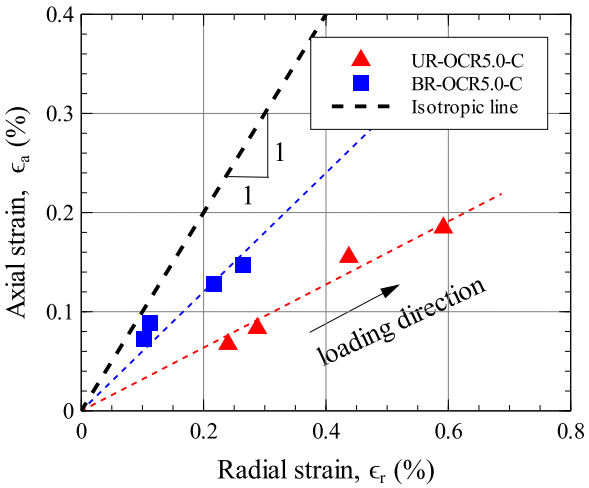

Figure 4.6: Relationship of incremental radial and axial strains between untreated and MICP-treated OC residual soils at higher consolidation stress levels (from 100 kPa to 220 kPa)

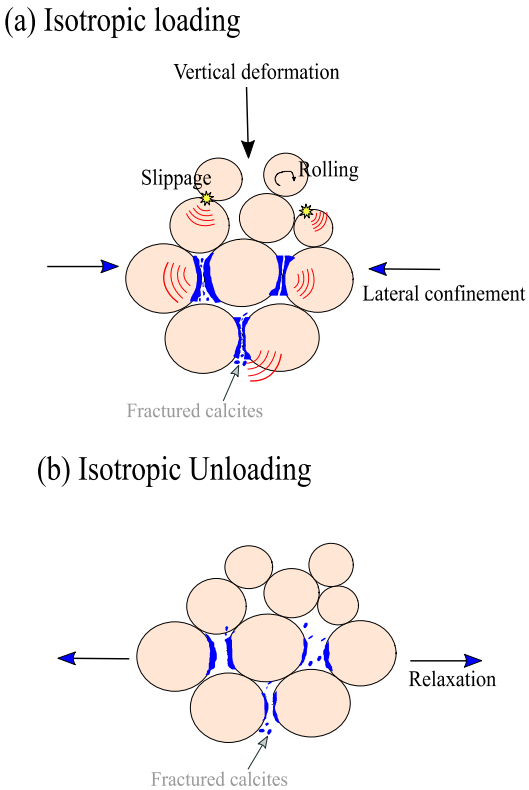

Figure 4.7: Simplified illustration for interaction of particles under isotropic consolidation of MICP-treated OC residual soil

Despite of the above observations in soil anisotropy, the global strain measurements (i.e. axial and volumetric strains) could be subjected to bedding error at the end restrains (i.e. top cap and base pedestal) and membrane penetration error. In future, it is suggested carrying out the local strain(s) measurement, precise membrane penetration calibration, and anisotropic small-strain stiffness measurements for the triaxial soil specimens in order to further validate the present experimental findings.

4.3.2 Undrained Compression Behaviour of MICP-treated Residual Soil

Figure 4.8 presents the stress-strain responses under undrained compression for the MICP-treated residual soils, which were subjected to isotropic consolidation pressures of 40, 120, and 220 kPa. As similar to the untreated residual soil, MICP-treated residual soil specimens failed in bulging manner since only a low cementation degree was entailed. At consolidation pressure of 40 kPa (Figure 4.8 (a)), the effect of soil compaction preserved in the untreated residual soil as evidenced from the strain-softening behaviour. Beyond the curvature change points along the stress-strain curves, all MICP-treated residual soils apparently showed a much greater shearing resistance than the untreated counterpart. The global strength improvement can probably be attributed to the calcite densification effect as presence in the pore spaces (DeJong et al., 2010). Being one of the limitations in conventional undrained testing, the determination of yield point was practically impossible due to the fact that only global stress-strain measurement was instrumented. For this reason, triaxial testing with AE measurement was also conducted to

investigate the yielding, soil mobilization, and particle-level interaction of soils. Related findings of the implementation of AE on MICP soils will be presented in Chapter 5 of this thesis.

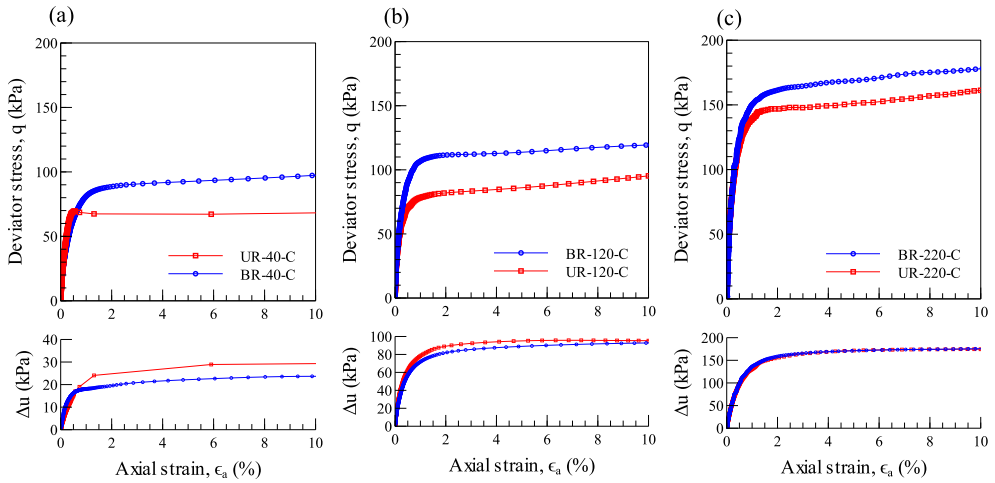

Figure 4.8: Mechanical responses of triaxial compression tests for untreated and MICP-treated residual soils after subjected to different consolidation pressures

Strength improvements were still observable in the soils that have been consolidated to 120 kPa and 220 kPa. With the increase of consolidation pressure, skeleton of (MICP-treated) residual soils progressively degraded and accompanied by increase of excess pore-water pressure. Lim et al. (2020) also observed that the effect of MICP on undrained shear resistance for a tropical residual soil was completely diminished as the consolidation pressure reached 150 kPa. Calcite clusters within the pore space could be fractured into smaller fragments, with the increase of consolidation pressure and axial strain amplitude. This phenomenon can be explained by the less improvement in ultimate shearing strength as the consolidation pressure increased from 120 kPa to 220 kPa. It can also be observed that the excess pore-water pressure of BR-120-C was slightly lower than the untreated counterpart, implying that the

fractured calcite clusters could still provide marginal shearing resistance. At the consolidation pressure of 220 kPa, the excess pore-water pressure of the MICP-treated residual soil resembled that of untreated soil. A marginal ultimate strength increase could still be observed in the BR-220-C specimen and therefore it was deduced that calcite densification effect remained in the soil structure. The increase in ultimate shear strength was probably associated with the effect of densification and confinement from the laterally-bonded soil structure (as mentioned in Figure 4.4 and Figure 4.7), since the BR-220-C specimen still managed to show anisotropic behaviour at 220 kPa. This implied that the laterally-precipitated calcite was still capable of providing shearing resistance with an anisotropic MICP-treated soil structure. Similarly, Xiao et al. (2020) found that calcite precipitation could still furnish resistances to the skeleton of sands even subjected to a high level of confining stress.

4.3.3 Undrained Extension Behaviour of MICP-treated Residual Soil

The particular anisotropic structure of MICP-treated residual soil was herein examined under triaxial extension tests and the results were presented in Figure 4.9. All triaxial extension specimens were failed by necking near the central part of the specimens. It is apparent that the strength improvement of the MICP-treated residual soil under triaxial extension test can only be realized for soil sample with an initial consolidation pressure of 40 kPa. Behaviour of dilation was also observed in the BR-40-E specimen by exhibiting a decrease in the excess pore-water pressure. Although the calcite content of BR-40-E was marginally lower than that of BR-40-C, the bio-

mediation effect was still evidenced in the structural resistance under the triaxial extension condition. Once the consolidation pressure exceeded 40 kPa, the mechanical and pore-water pressure responses of MICP-treated residual soils resembled the one of untreated residual soils. Opposing to the triaxial compression test, the CIUE MICP-treated residual soils were characterized with lower shearing resistance and only showed strength improvement for sample consolidated under pressure of 40 kPa. This finding justified the observed structural anisotropy in the deformation of MICP-treated residual soil. In the formation of MICP-treated residual soil, the calcite precipitation would not contribute much cementation along the vertical plane and resulted in less improvement of tensile strength among the CIUE specimens.

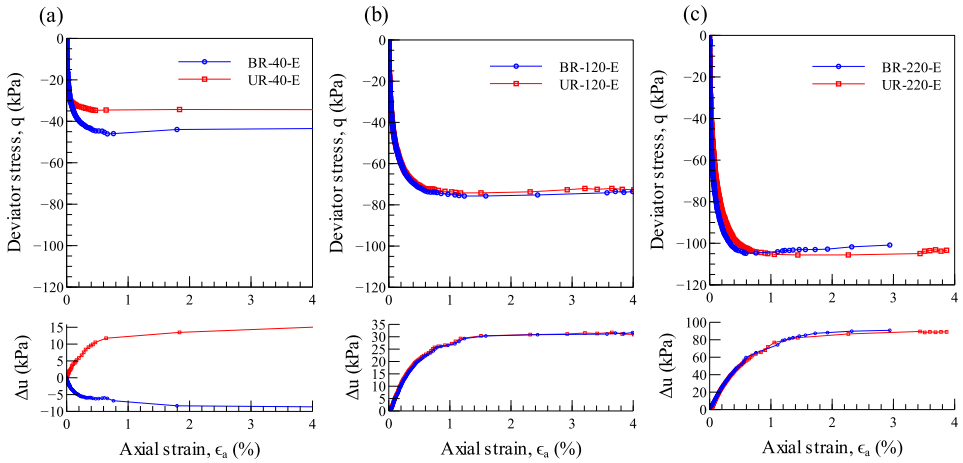

Figure 4.9: Mechanical responses of triaxial extension tests for untreated and MICP-treated residual soils after subjected to different consolidation pressures

4.3.4 Microscopic Assessment on MICP-treated Residual Soil

This section discusses the microscopic configurations of the untreated and MICP-treated residual soils. At first, the microstructural configuration of pure

calcites was assessed in order to differentiate calcite crystals from the original soil particles. Figure 4.10 illustrates the microscopic structures of the fine contents (passing an aperture sieve size of 63μm) from the original residual soil as well as the precipitated calcite crystal. Silt and clay-sized particles were distributed within the sampled residual soil, and the clay-sized particles were observed to be platy (Figure 4.10 (b)). It can be seen from Figure 4.10 (c) - (d) that the calcite assemblage was formed by numerous block-like calcite crystals.

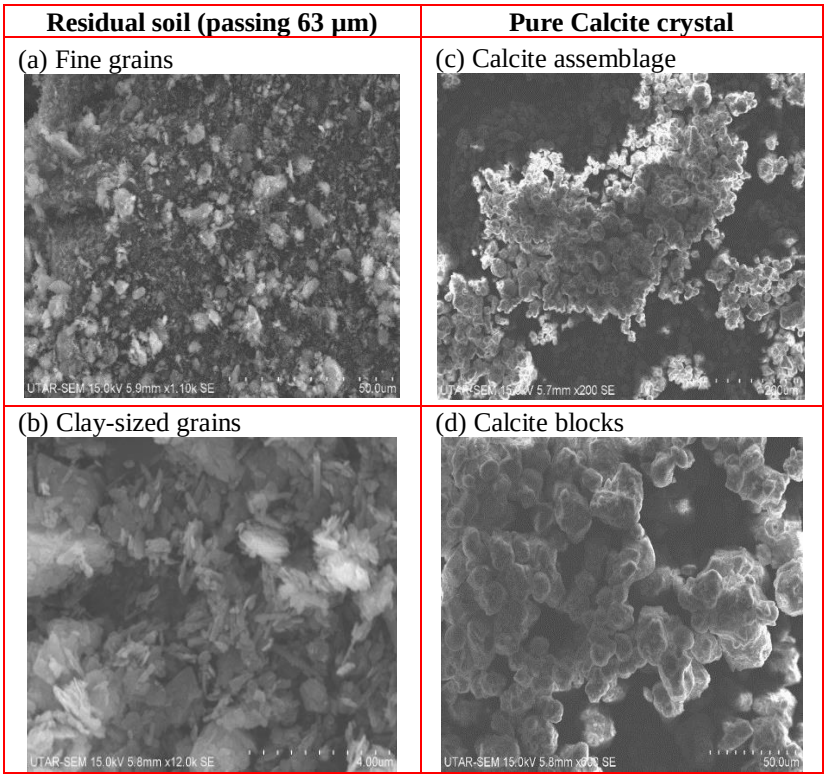

Figure 4.10: Microscopic images for pure calcite crystal and fine particles of residual soil

As shown in Figure 4.11 (a), a wide range of particle sizes was found in the untreated residual soil. Sub-angular grains were observed in the sand-sized grains of residual soil. From Figure 4.11 (b) – (c), agglomerations of fine

grains were found to be adhering on the surface of coarser grains. They were formed in sheeted structure and were possibly susceptible to fragmentation. It is anticipated that the presence of fine-grained clusters would hinder the direct formation of calcite bonding in between two neighbouring soil particles, as similarly claimed by Sasaki and Kuwano (2016). Moreover, different kinds of calcite precipitated structures were observed in the MICP-treated residual soil samples. These include a wide coverage of calcite precipitation (Figure 4.11(d)), presence of calcite crystals on the surface of soil grains (Figure 4.11(e)), and calcite bonding between the solid grains (Figure 4.11(f)). The present microscopic observations can be used to qualitatively validate the mechanisms of calcite formation (namely, calcite cementation and densification) in the studied residual soil.

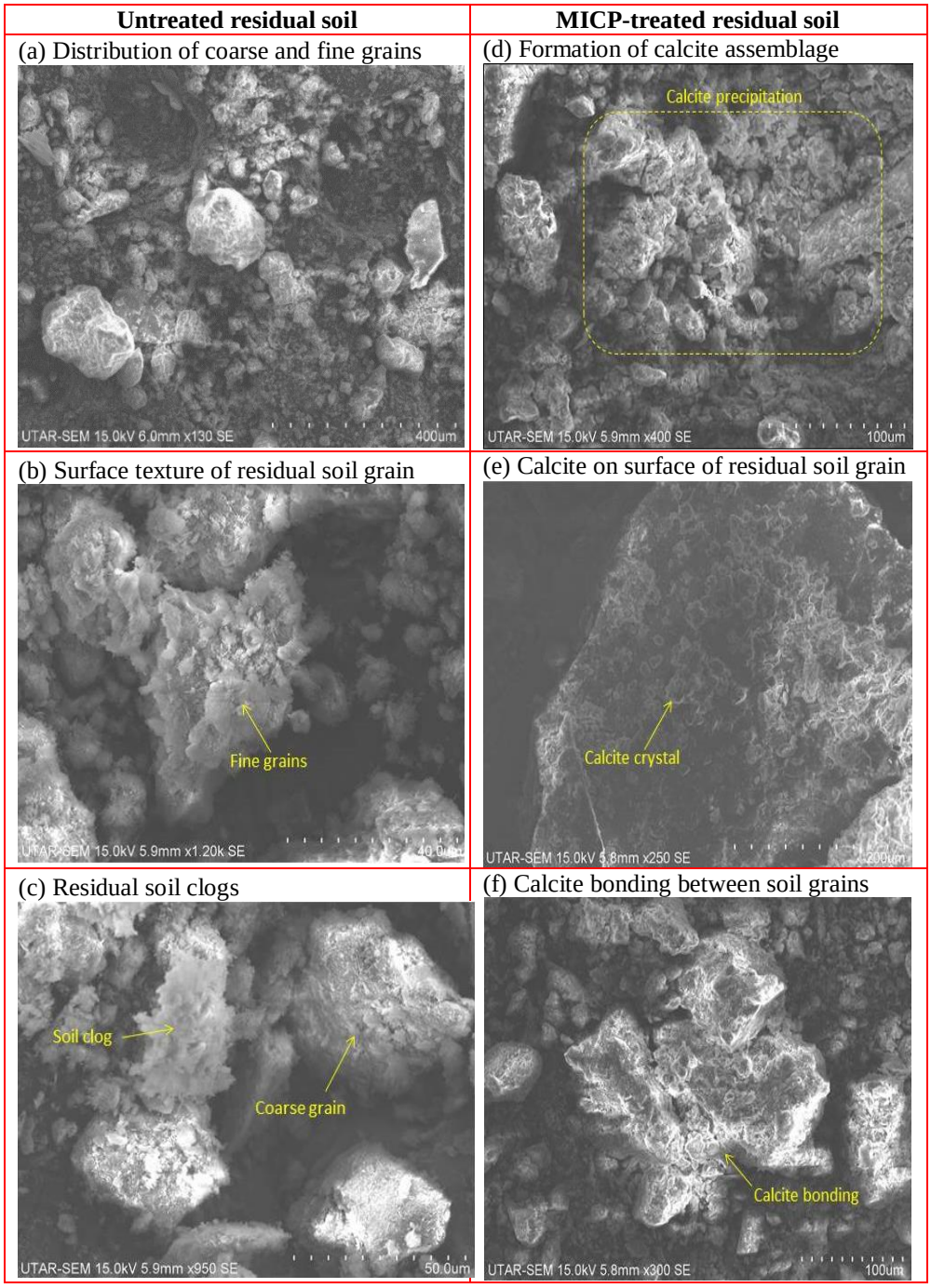

Figure 4.11: Microscopic images for untreated and MICP-treated residual soils

4.4 Mechanical Behaviour of MICP-treated Sand

This section elaborates the experimental results of isotropic consolidation and undrained compression (CIUC) tests for untreated and MICP-treated sands.

Unlike the (MICP) residual soil, triaxial extension test was not conducted for the (MICP) sand as the deformation behaviour was found to be isotropic.

4.4.1 Isotropic Consolidation Behaviour of MICP-treated Sand

4.4.1.1 Void Ratio Changes of MICP-treated Sand

According to Figure 4.12, the MICP-treated sands showed more consistent initial dry densities as compared to the MICP-treated residual soils (as depicted in Figure 4.2). This observation suggested that the formation of calcites throughout the residual soil specimen was arguably less uniform as compared to the MICP-treated sand specimens. The MICP-treated sand has been known to have a uniform calcite distribution profile (Feng and Montoya, 2015), while non-uniformity of calcite distribution had been reported in specimens made of sand-clay mixture (Jiang et al., 2016).

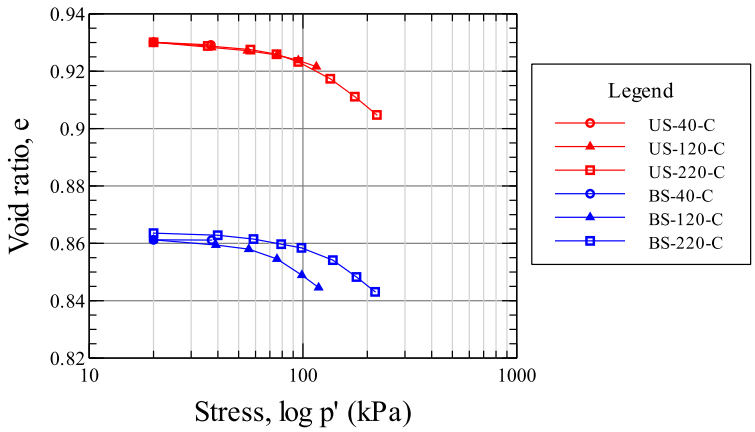

Figure 4.12: e-log p' for the untreated and MICP-treated sand specimens

The consolidation properties of MICP-treated sand, which were obtained in same manner as the MICP-treated residual soil, were also summarized in Table 4.3. It is obvious that the untreated and MICP-treated sands showed only a marginal alteration in the isotropic yield stress and compressibility. This finding indicated that a weak calcite cementation was formed in the MICP-treated sand. Similarly, Feng and Montoya (2014) observed slight alterations in the deformation properties of lightly-cemented sand during the K_o consolidation test.

In addition, the soil specimen "BS-120-C" started to exhibit significant deformation change as compared to the untreated counterpart, implying that the structure of the MICP-treated sand could be different from the original sand despite a similar consolidation change had been realized in between US-220-C and BS-220-C specimens. This observation indicated that original sand structure could occasionally be disturbed by the flow of chemical reagent and the precipitated calcite crystals might not contribute much to the stiffness of MICP-treated sands. A similar finding was also observed in a repeated test for the BS-120-C specimen from the same batch of sand treatment. As particle breakage is prevalence for granular material at higher consolidation pressures (Hardin, 1985; Shipton and Coop, 2012), it is essential to determine the crushability of original and MICP-treated soil grains (for residual soil and sand, respectively). At high confinement, it is interesting to know the role of calcite clusters relative to the individual soil grains and whether noticeable structural resistance could still be furnished.

Table 4.3: Deformation characteristics for tested sands

Soil specimen	Isotropic yield stress (kPa)	Compression index C_c	Net calcite content (%)
Sand			
US-220-C	119.1	0.062	-
MICP Sand			
BS-40-C	-	-	3.8
BS-120-C	-	-	3.8
BS-220-C	121.0	0.059	3.6

4.4.1.2 Anisotropic Deformation of MICP-treated Sand

Figure 4.13 shows a series of relationships correlating deformations of (MICP) sands and consolidation stress. The UR-220-C specimen (residual soil) showed a total volumetric deformation of 4.6 % (Figure 4.3 (a)), while the US-220-C sand specimen showed a total volumetric deformation of 1.31 % (Figure 4.13 (a)) only. This can be explained by the poorly-graded grains arrangement in the studied sand as well as having a dense initial structure (D_r *= 82 %*). In assessing the mechanical effect of Kaolin content within a carbonate sand, Shipton and Coop (2012) also observed that the deformation of pure sand was smaller as compared to the sand which was mixed with a high amount of Kaolin. Their Kaolin-sand mixture showed a greater compressibility and a lower isotropic yield stress as compared to the clean sand. The reported results showed a good agreement with the present findings on deformation behaviours of residual soil and sand. Besides that, the magnitudes of axial strain component for (MICP) sands were similar to those of radial strains.

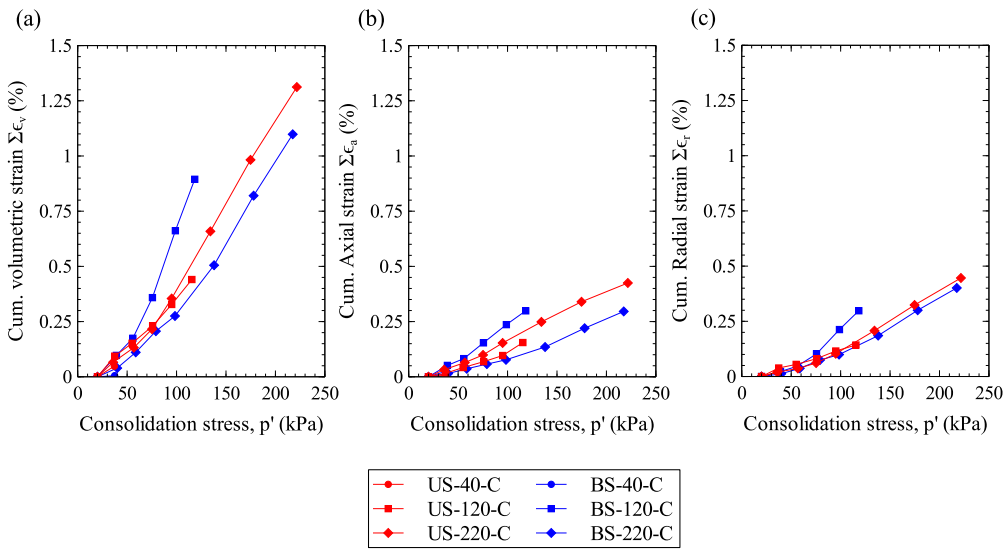

Figure 4.13: Relationships between deformations of (MICP) sands and consolidation stress: (a) Cumulative volumetric strain vs consolidation stress; (b) Cumulative axial strain vs consolidation stress; (c) Cumulative radial strain vs consolidation stress

According to Figure 4.13 (b) – (c) and Figure 4.14, the deformations of both untreated and MICP-treated sands almost resembled an isotropic material since the data points located in proximity to the isotropic line. The isotropic behaviour was probably caused by the process of dry tamping in alteration of the original anisotropy from air-pluviation process, which had been recognized in previous studies (El-Sohby, 1969; Ladd et al., 1977). Anisotropic structural arrangement would be produced when the dry (elongated) sand was freely placed into a mould (Oda, 1972), but the unique soil fabric would be diminished by mechanical tamping effect. It was reported that the mechanical behaviour (modulus, strength, and dilatancy rate) of soil was very much governed by the initial soil fabric (e.g. microstructural arrangement and shape of soil grain) as well as the method of specimen preparation.

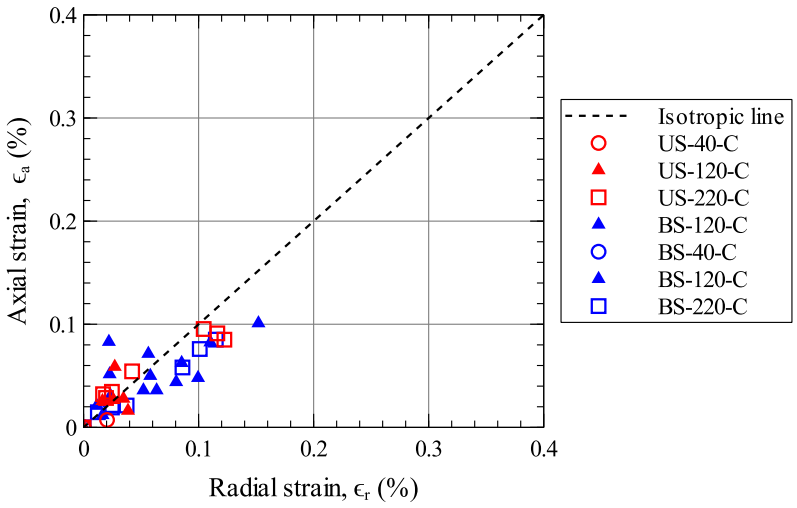

Figure 4.14: Anisotropic deformation for (MICP-treated) sand

4.4.2 Undrained Shearing Behaviour of MICP-treated Sand

Figures 4.15 (a) - (c) show the stress-strain and pore-water pressure responses of the (MICP) sand specimens which were consolidated to 40 kPa - 220 kPa. Dilation was apparently observed in both untreated and MICP-treated sands (e.g. 40 kPa and 120 kPa) as the excess pore-water pressure continued to decrease with axial strain amplitude. Similar behaviour of dilation was also reported in over-consolidated silty sand and sandy silt under undrained shearing (Khin et al., 2009). In addition, strain hardening effect could also be observed from the continuous increase of deviator stress along the stress-strain curves. At the consolidation pressure of 40 kPa, the untreated sand could preserve the structural effect of dry-tamping by showing a continuous pore-water pressure decrease. Through bio-mediation process, there was only a marginal increase in the shearing resistance. This was caused by the light calcite cementation within the sand structure of high density (D_r = 82 %). The densely-packed sand particles were surrounded by an all-round distribution of

calcite crystals that could not form effective bonding between the sand grains with a low degree of cementation (i.e. calcite contents = 3.6 ~ 3.8 %).

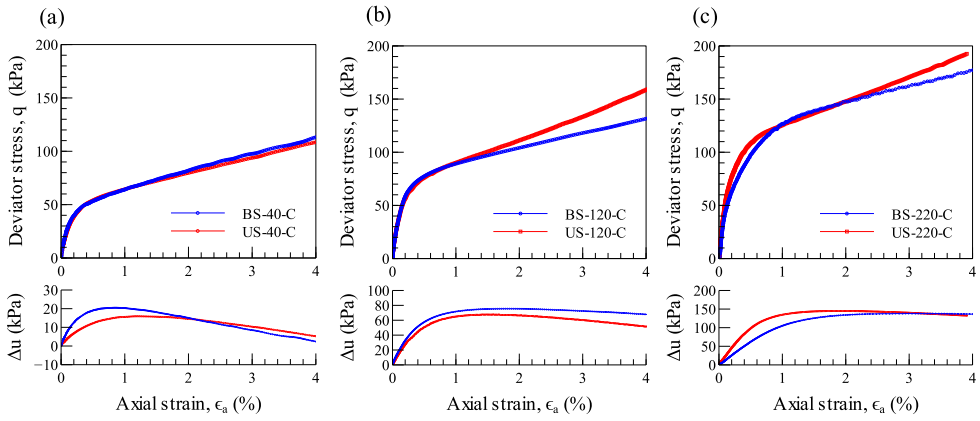

Figure 4.15: Stress-strain and excess pore-water pressure responses for untreated and MICP-treated sands after subjected to different consolidation pressures

At the consolidation pressure of 120 kPa, the untreated sands have a greater deviator stress increase as dilation was more significant compared to the MICP-treated sands. Once the sand had been consolidated to 220 kPa, the dilation of the untreated sand was diminished and only a marginal increase in deviator stress was observed. This finding leads to two thoughts: (a) the structural effect of original dense sand was required to be overcome by consolidating the sand to a minimum pressure of 220 kPa; (b) the bio-treatment process could alter the soil arrangement by the reagent permeation and formation of calcite structure along the flow path. Besides that, no significant effect of calcite densification was observed in the MICP-treated sand. This can be explained by the larger pore size in the sand structure than that of residual soil and a low degree of cementation was produced in the sand specimens.

4.4.3 Microscopic Assessment on MICP-treated Sand

The studied sand constituted sub-angular soil grains, as illustrated in Figure 4.16 (a) - (b). The resistance of sand could probably be contributed by the interlocking of soil particles. After the bio-mediation treatment, calcite crystals could be observed sticking on the surface of cross-sectional side across the sand particles (Figure 4.16 (c)). The sectional side had a rough surface texture whereas the longitudinal surface was too smooth for the calcite crystals to adhere on. Xiao et al. (2019b) also observed an effective bonding between the sides of angular particles and adsorption of surface calcites in the heavily-cemented soil. In addition, a weak and unstable calcite bonding was observed in the MICP-treated sand as the area of bonding point was far too small relative to the dimension of sand grains (Figure 4.16 (d)). These microscopic observations on sand provided supporting evidences to explain why the isotropic yield stress for MICP-treated sand was not significantly improved.

Untreated sand	MICP-treated sand
(a) Sand grains 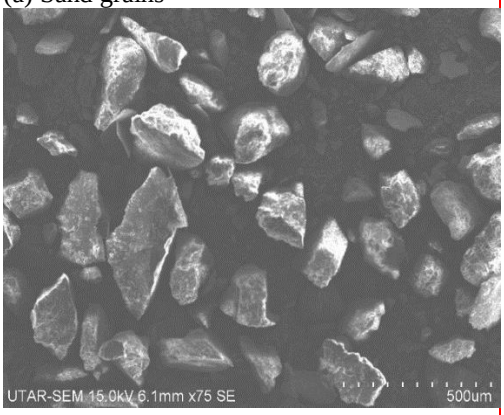	(c) Precipitation of calcite on sand grain 
(b) Surface texture of sand grain 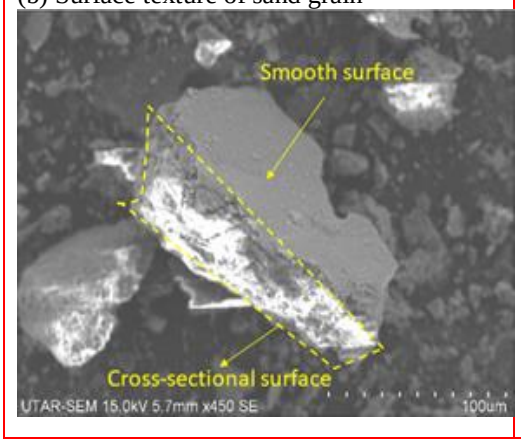	(d) Calcite bonding between sand grains 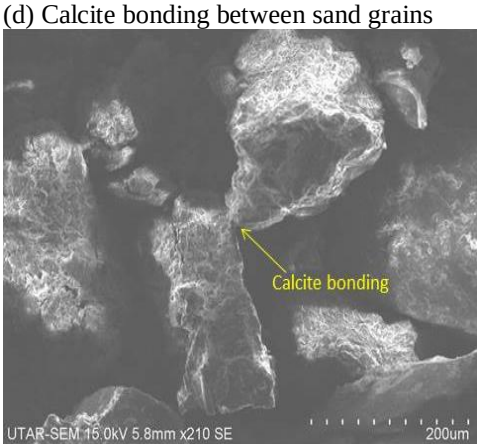

Figure 4.16: Microscopic images for untreated and MICP-treated sands

4.5 Comparison between MICP-treated Residual Soil and Sand

4.5.1 Anisotropic Structures in MICP Soils

Fabric anisotropy was evidenced in the MICP-treated residual soil when it was subjected to isotropic consolidation stresses and shearing forces. In the former scenario, the MICP-treated residual soil tended to deform along vertical plane of the specimen, whereas the untreated counterpart behaved oppositely. In undrained shearing, the MICP-treated residual soil was observed to be directional-dependent by showing a less effect of bio-mediation under the triaxial extension test.

Residual soil, which constituted a mixture of coarse and fine-grained particles, could be featured with a wide range of pore throat sizes and the finer particles could adhere on the surface of coarse grains (as evidenced in Figures 4.11(b) - (c)). Therefore, calcites would preferably be precipitated along the chemical reagent flow path and deposited away from the locations of accumulated fine grains. The calcite bonds were tendentiously formed side-by-side between solid grains and furnished a significant resistance along lateral direction of a specimen. On top of that, calcite cementation can be expected in the bonding between soil grains (Figure 4.11(f)), in which the adhered fine particles could hinder the formation of an effective binding, at which the calcite cementation could not be formed directly between two neighbouring particles. It is also inferred that the calcite precipitation within the residual soil was highly dependent on the initial grain arrangement of the soil specimen. This was evidenced by the relatively large variations in the initial void ratios of treated residual soil specimens as compared with those of sand specimens (as distinguishable from Figure 4.2 and Figure 4.12).

Both untreated and MICP-treated sands manifested nature of isotropic deformation, as attributed to the effect of dry tamping and less significance of calcite cementation in the dense sand. In contrast to the MICP-treated residual soil, the bio-mediation treatment provided fairly uniform calcite distribution throughout the MICP-treated sand specimen.

The present microscopic findings (soil formation and anisotropy) are insightful for establishing constitutive relationship and numerical modelling of the MICP-treated residual soil and sand under the prescribed treatment conditions. It is informed from this study that characteristic of anisotropic deformation should be considered for contact model/ mechanism between adjacent soil particles when simulated using the discrete element modelling (DEM).

4.5.2 Structural Behaviours of MICP-treated Soils

It is informed from the isotropic consolidation test that calcite densification played a significant role as a greater compression index was obtained in the MICP-treated residual soil. The MICP-treated residual soil was also inherent with a fairly weak calcite bonding, as evidenced by the insignificant improvement in yielding resistance. It is anticipated that the ineffective calcite bonding was possibly caused by the presence of fine grains being adhered on the surface of the coarse-grained particles. Upon yielding, the breakage of calcite bonding was triggered and the effect of calcite densification becomes dominant in the MICP-treated residual soil structure. During the undrained shearing, the aggregations of calcite crystal contributed shearing resistance and were gradually fractured with the increase of axial strain amplitude. The laterally-formed calcite structures could also facilitate shearing resistance through confinement towards the chains of load-bearing soil grains. Such resistance, however, was not observed in the triaxial extension test which further reinforced the finding on unique structural anisotropy in residual soil.

There is no noticeable improvement observed in the stress-deformation behaviours of the MICP-treated sand as attributed to the low calcite level within the dense sand. The minor improvement in mechanical behaviour could only be preserved at a low consolidation pressure (i.e. 40 kPa) owing to the weak calcite cementation. It was attributed to the different grain size distribution, dense sand structure, and surface texture of soil grains, as physically evidenced from the microscopic observations (Figure 4.16). Unlike the widely-reported loose sand (typically with $D_r \approx 30$ - 40 %), insignificant improvement was obtained in the present dense sand ($D_r \approx 82$ %) as the initial effect of physical grains' contact concealed the bio-mediation effect. Throughout the undrained compression, the MICP-treated sands experienced strain hardening. As different from the MICP-treated residual soil, calcite densification was not obvious in the MICP-treated sand as calcite clusters could not favourably be precipitated to occupy the larger pore space in sand structure. Nevertheless, the present finding highlighted that bio-mediation effect contributed little to the dense sand (with angular and sub-angular particles) under low cementation level, whereas studied residual soil is more suitable for MICP treatment.

4.5.3 Effective Stress Path

Figures 4.17 (a) and (b) compare the stress changes for the (MICP-treated) residual soils and sands, respectively. The soils tended to trace down to the left of effective stress paths and exhibited plastic deformation from low to high consolidation pressures. At the lowest consolidation pressure (i.e. 40 kPa), the

MICP-treated residual soils (BR-40-C & BR-40-E) and sands (BS-40-C) preserved the original soil structure (i.e. compaction or MICP-induced). It is distinguishable that the effective stress path under consolidation pressure of 40 kPa tended to progress vertically and geometrically similar to typical over-consolidated soils (Atkinson and Bransby, 1978) by showing apparent elasticity. The effective stress paths of the present MICP-treated soils were also in line with the trend as reported by Zamani and Montoya (2018), primarily attributed to the less tendency of excess pore-water pressure generation in the MICP-induced structure. In consistent with Lim et al. (2020), the effect of soil bio-mediation was slowly diminished with the increase of consolidation pressure. In addition, the effect of bio-mediation was insignificant in governing the shearing behaviours of CIUE-series residual soil owing to the observed fabric anisotropy (described in Section 4.3.3). The present understanding of consolidation effect on changes in deformation behaviour can be informative in engineering practice as related to MICP residual soil ground. After the in-situ ground has been treated, it is desirable to know the threshold consolidation pressure (i.e. surcharge loading) whereupon the MICP structural effect would be degraded.

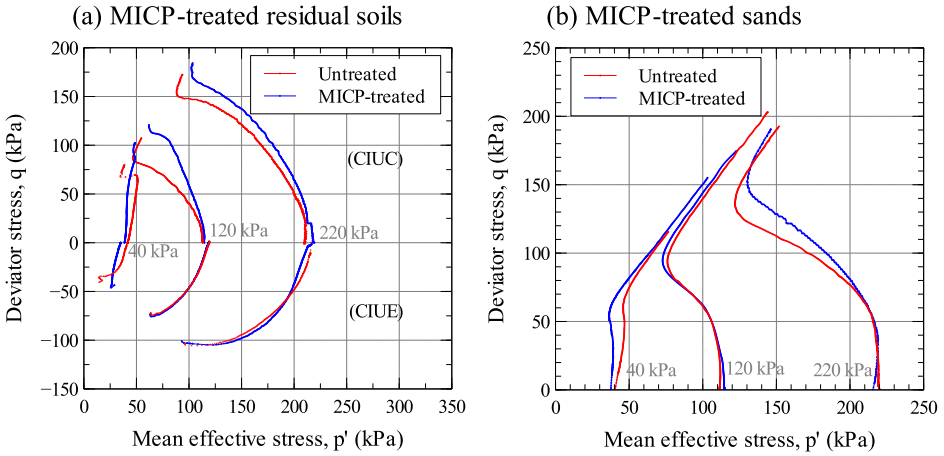

Note: The shown values were referred to the initial consolidation pressures prior to undrained shearing for all tested soil specimens, namely 40 kPa, 120 kPa, and 220 kPa.

Figure 4.17: Effective stress paths for tested soils: (a) Residual soils; (b) Sands

The studied sands exhibited strain hardening throughout the undrained shearing. Dilation was clearly seen in the untreated sands being consolidated to 40 kPa and 120 kPa. After the untreated sand was consolidated to 220 kPa, the effect of dilation was diminished and there was an obvious change in the pattern of stress path (Figure 4.17(b)). Both untreated and MICP-treated sands appeared to progress towards a constant stress ratio at different levels of consolidation pressure, suggesting that the calcite densification effect was not as pronounced as the treated residual soil. It is worth emphasizing that failure envelope and the corresponding shear strength properties (e.g. effective frictional angle and cohesion parameter) were not determined in this chapter for the investigated soils for following reasons: (i) Prior to shearing, MICP-induced structure would be demolished by consolidation pressure of 120 kPa and 220 kPa, therefore the failure state might not be representative; (ii) Sands continuously manifested strain hardening at larger strain level.

4.6 Concluding Remarks

Based on the present experimental study, following conclusive statements can be drawn in understanding of the structural formation and behaviour for MICP-treated soils:

(a) The MICP-treated residual soil was inherent with structural anisotropy leading to the soil to have a tendency of deforming along vertical plane of the specimen. Owing to this particular soil structure, the MICP-treated residual soil was also featured with directional-dependency by exhibiting less bio-mediation effect in triaxial extension test as compared to the compression test.

(b) The isotropic yield stress and compressibility were markedly improved in residual soil upon the bio-mediation. This was fundamentally contributed by the calcite bonding (yield) and densification (compressibility). It is justified that a well-graded residual soil arrangement favoured the calcite formations by densification mechanism but at the expense of producing a less uniform calcite structure. It is further confirmed that calcite densification played a significant role in providing the shearing resistance in compression. The densified calcite aggregates were progressively fractured with increase of consolidation pressure and shear strain amplitude.

(c) During isotropic unloading, the MICP-treated residual soils tended to deform in lateral direction whereas the original residual soils manifested

isotropic behaviour on account of anisotropic deformation in the bio-mediated residual soil.

(d) The MICP-treated sand constituted a more uniform calcareous structure and manifested an isotropic deformation pattern with a stiffer structure as compared to the MICP-treated residual soil. Insignificant improvement was realized in the MICP-treated sand, as a result of weak bonding and unnoticeable calcite densification. The initial dense structure of sand overshadowed the effect of bio-mediation (i.e. marginal cementation and alteration in initial sand arrangement) and therefore the behaviours of the sands were governed predominantly by dilation only.

(e) Bio-mediation effect was more profound in the well-graded soil (i.e. residual soil) than the present studied sand (dense, poorly-graded, and angular grains). Low cementation level of the present studied sand did not facilitate favourable bio-mediation effect.

In the present experimental study, the mechanical behaviours and structural formations of MICP-treated soils (e.g. residual soil and sand) were investigated in detail. However, soil behaviours at smaller strain range (e.g. yielding) could not be examined through the conventional triaxial shear test, which could only be used to investigate larger-strain response and ultimate shearing behaviours. For this reason, Acoustic Emission (AE) measurement was further instrumented in the present triaxial setup and related experimental results will be discussed in Chapter 5.

CHAPTER 5

ACOUSTIC EMISSION AND MECHANICAL BEHAVIOURS OF MICP RESIDUAL SOIL IN COMPARISON WITH SAND

5.1 Introduction

The mechanical behaviour of MICP-treated residual soil and sand had been discussed in Chapter 4, in which only ultimate strength behaviours (in global strain range) were discussed. It was realized that the details of deformation behaviours such as yielding behaviour (in smaller strain range, i.e. below 1 %) and progressive changes in deformation behaviours cannot be fully examined by analysing the conventional stress-strain measurement alone. For this reason, Acoustic Emission (AE) measurement is herein used to analyse the experimental results in terms of micro-structural view points and their results are presented in this chapter. Essentially, this chapter serves as an extension to Chapter 4 and elaborates mechanical behaviours of (MICP) residual soil and sand through AE analysis. The isotropic consolidation and undrained shearing tests were carried out with the AE instrumentation on residual soil and sand (both untreated and MICP-treated) as listed in Table 4.1. In addition, (MICP) over-consolidated residual soils were conducted to justify the approach in determination of yielding and to investigate the effect of over-consolidation on bio-mediated residual soil.

5.2 Isotropic Consolidation Behaviours of Residual Soils and Sands as Investigated by Acoustic Emission

In Chapter 4, it is understood that poorly-graded sands could facilitate a more uniform calcite distribution structure than the residual soils. The MICP treatment could marginally improve the isotropic yield stress and compressibility of the residual soils. Upon yielding, calcite bonds would be diminished and the subsequent deformation behaviours of the MICP-treated soils were governed by the calcite densification. Besides that, MICP treatment would induce the residual soil an anisotropic soil structure while the MICP-treatment on sands inducing an isotropic response. These findings were investigated in greater depths through AE monitoring in this section.

5.2.1 AE Rate-Time Monitoring

Similar to Figure 4.1 (Chapter 4), the volumetric and axial strain responses were herein correlated to the AE rate (counts rate at every 5 s) for selected MICP-treated and untreated residual soils in Figure 5.1 (b) & (d) and Figure 5.1 (a) & (c), respectively.

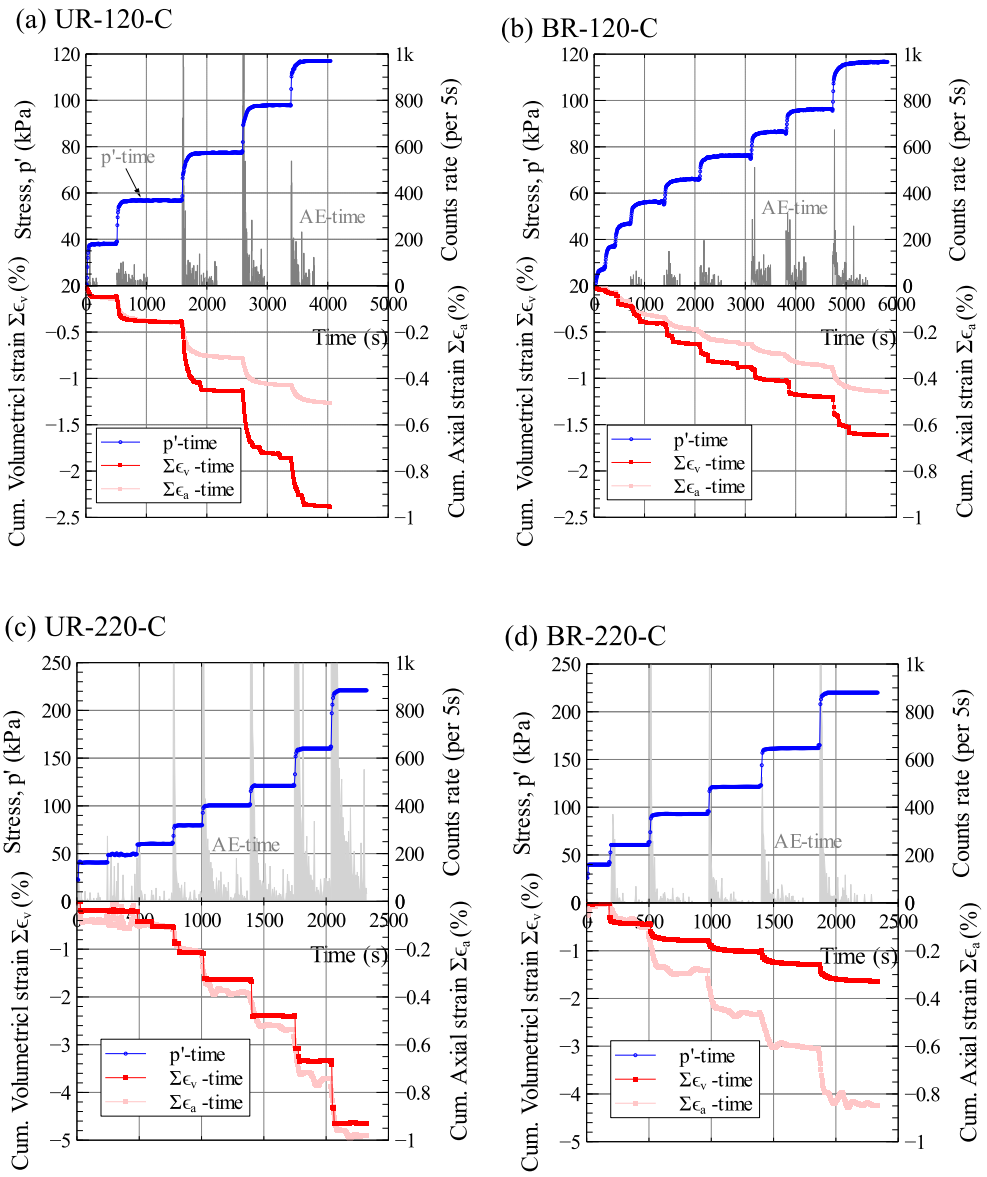

Figure 5.1: Consolidation responses of tested residual soils as monitored by AE: (a) UR-120-C, (b) BR-120-C, (c) UR-220-C, and (d) BR-220-C

It is apparent from Figure 5.1 that the AE counts rate increased abruptly upon the start of each isotropic consolidation step. The rate of acoustic emissions gradually attenuated with time progress under a constant applied isotropic stress Firstly, all tested residual soils showed continuous AE bursts from a consolidation stress of about 60 kPa - 100 kPa onwards that indicates the stress state of soils falling into a normally consolidated state.

Further analysis of this is shown in Section 5.2.2 by using the cumulative AE counts. Secondly, the bio-mediated residual soils emitted lower level of AE compared with the untreated residual soils. Next, the volumetric and axial strain responses of untreated and MICP-treated sands in comparison with the AE count rate were presented in Figures 5.2 (a) & (c) and (b) & (d), respectively.

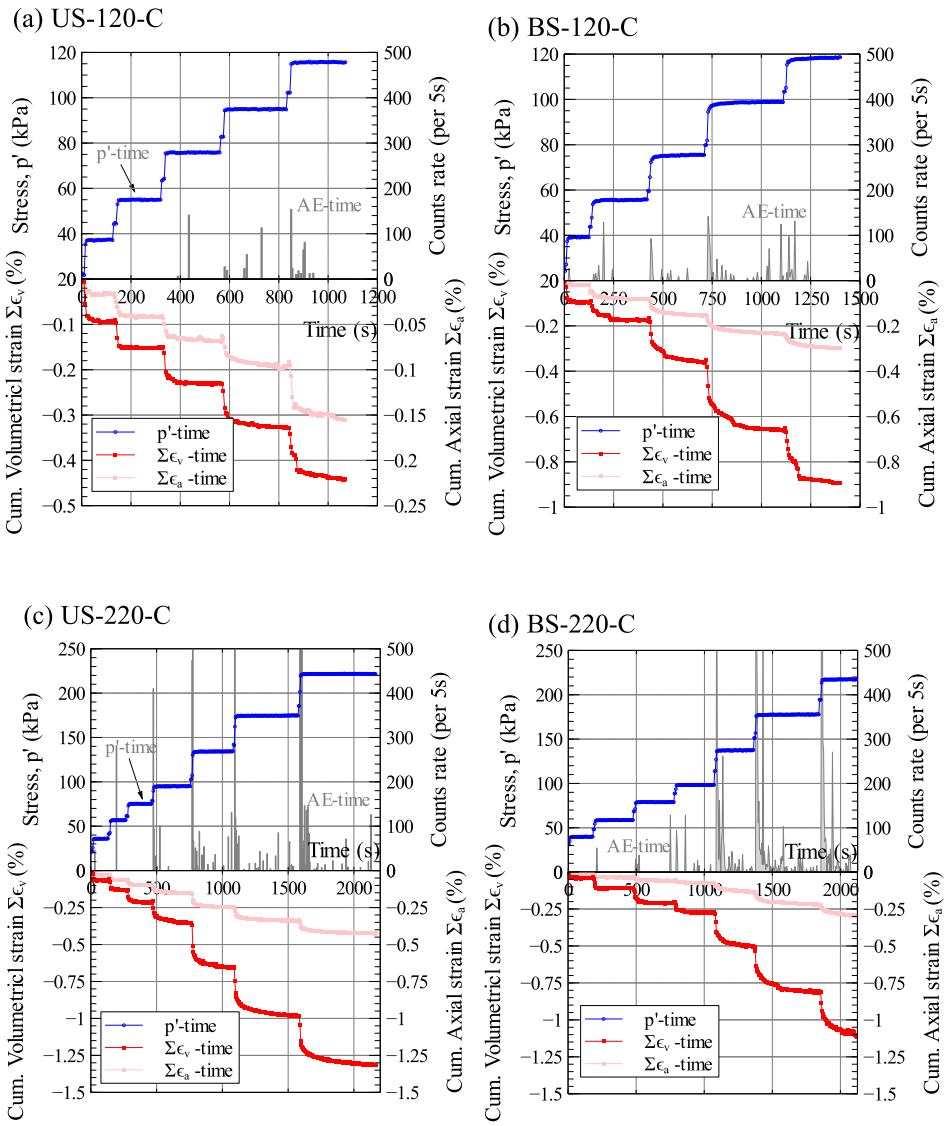

Figure 5.2: Monitoring consolidation-AE responses for untreated and MICP-treated sands: (a) US-120-C, (b) BS-120-C, (c) US-220-C, and (d) BS-220-C

It should be noted that the scale of AE counts rate was herein enlarged to 500 (counts per 5s) as the magnitude of AE response for (MICP) sands was much less. As will be discussed in Section 5.2.2 below, untreated and MICP-treated sands deformed to a less extent than the (MICP) residual soil. This corresponds to the lesser intensity of AE rate in the sands than the residual soil. Similar to the residual soil, the sands showed larger AE bursts after being consolidated above around 100 kPa and this was observed in conjunction with the increasing soil deformations.

5.2.2 Correlation between Void Ratios and Acoustic Emission Changes

Figure 5.3 depicts the deformation curves for the tested residual soils, in which AE measurements were interpreted in parallel with the void ratio changes.

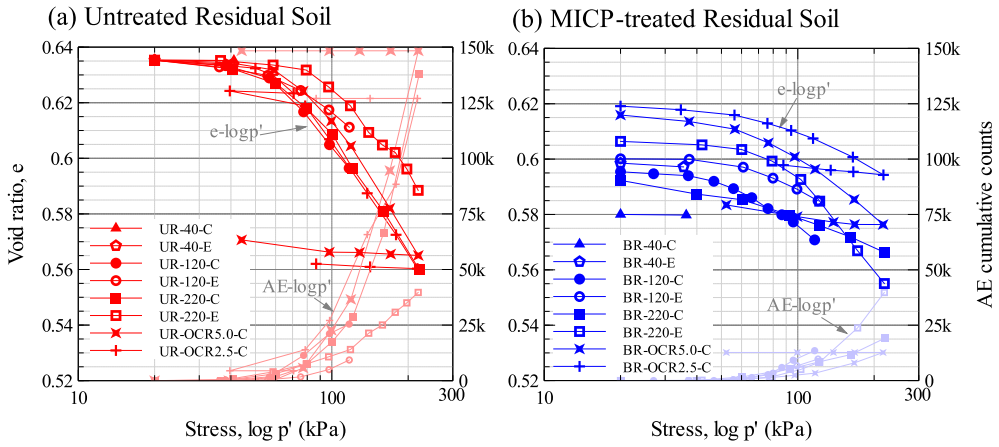

Figure 5.3: Deformation characteristics for untreated and MICP-treated residual soil specimens

The configuration of cumulative AE change is somewhat analogous to the void ratio curve. The void ratio (i.e. volumetric deformation) and cumulative AE counts increased with respect to the isotropic consolidation stress. Similar observation was reported by Tanimoto and Tanaka (1986) for a decomposed granite soil, where the pre-consolidation stress could be identified from the AE change. Smith and Dixon (2019) also observed that cumulative AE counts rate and volumetric strain were proportional to the level of confining pressure in a poorly-graded sand. It is obvious that the MICP-treated residual soils were stiffer than the untreated residual soil, in view of the less deformation changes and low level of AE. As discussed in Chapter 4, diminishment of major soil structural arrangement (e.g. breakage of calcite bonding) in MICP-treated soils would be triggered upon reaching the isotropic yield stress. Subsequent resistance of deformation would be dominantly taken up by calcite densification.

Figures 5.4 (a) and (b) present the deformation curves for untreated and MICP-treated sands, respectively.

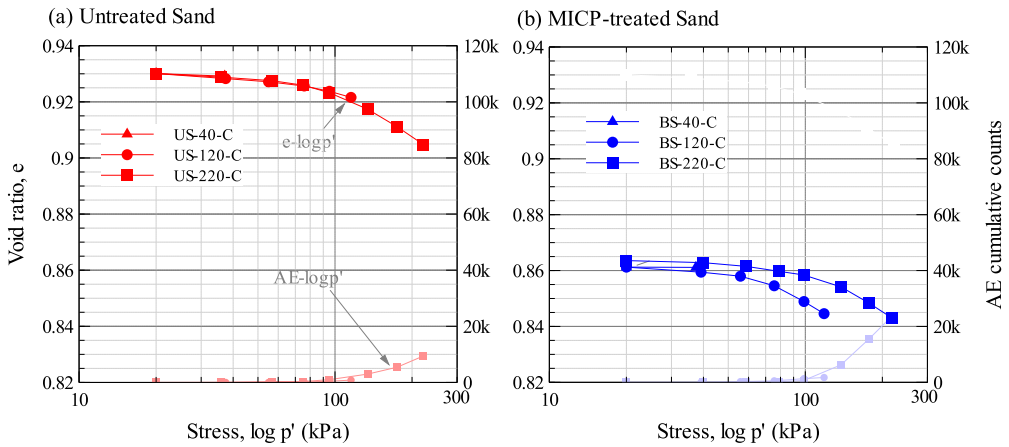

Figure 5.4: Deformation characteristics for untreated and MICP-treated sand specimens

The void ratios of MICP-treated sands (approximate to 0.86) were much lower than those of untreated sands (approximate to 0.93). This variation was attributed to the effects of calcite densification on the two different types of soils. It is also obvious that the highest magnitude of cumulative AE counts as obtained from the tested residual soils (nearly 1.5 x 10^5 counts) were far greater than that of sands (nearly 2.4 x 10^4 counts). Plotting scale of the highest AE count was also set to be 1.2 x 10^5 (more or less the scale for residual soils, i.e. 1.5 x 10^5) for all sands in order to facilitate consistent interpretation. The BS-220-C specimen showed a much higher extent in total AE counts at its final stress increment as compared to the untreated sand specimen. This was probably caused by the energy dissipation of calcite fracturing in the MICP-treated sand, although the obtained compressibility from the BS-220-C specimen was still lower than the untreated specimen.

5.2.3 Determination of Isotropic Yield Points through AE Measurements

In this section, the soil deformation behaviours were examined closely with the AE measurements. Figure 5.5 and Figure 5.6 present the correlations between consolidation stress, cumulative AE counts, axial strain, and volumetric strain for (MICP-treated) and OC residual soils, respectively.

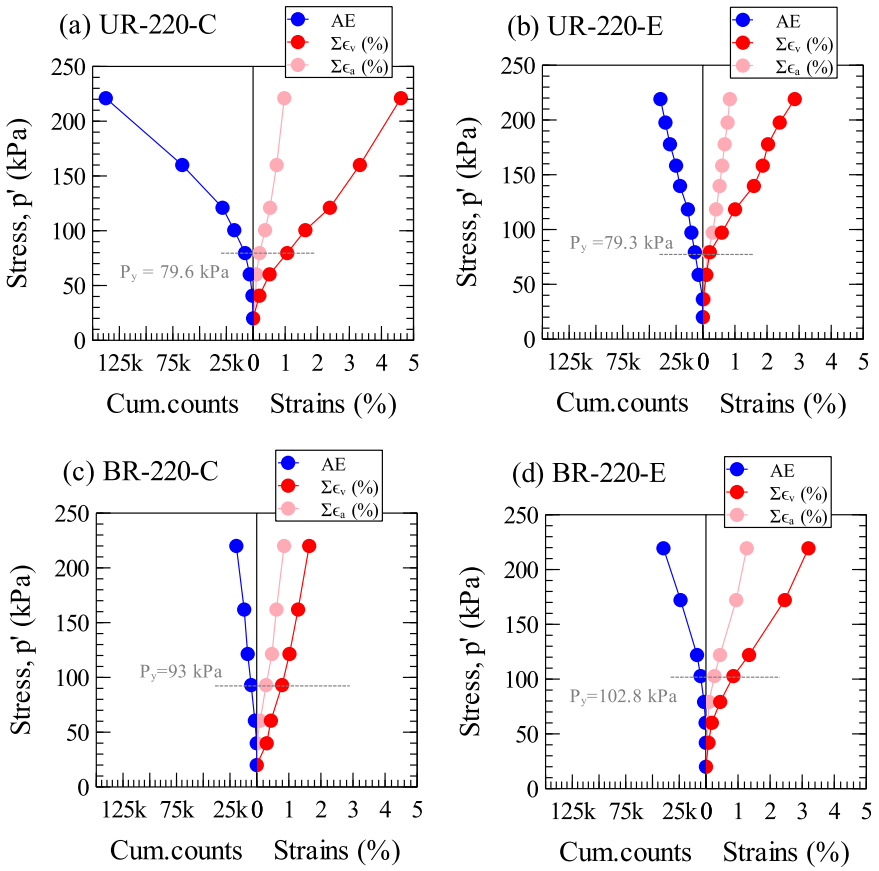

Figure 5.5: Evaluation of isotropic yield stress from AE measurements for all tested residual soils

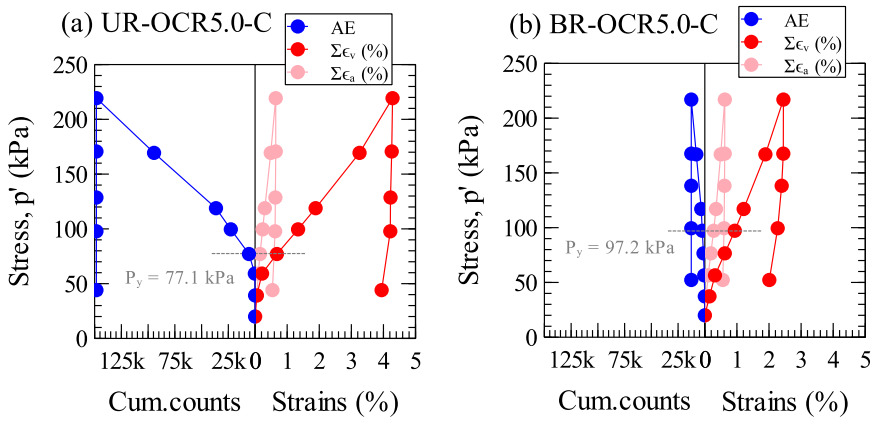

Figure 5.6: Evaluation of isotropic yield stress from AE measurements for OCR residual soils

The onset of increasing cumulative AE counts (denoted as P_y) was herein defined as the isotropic yield point in the consolidation test. The plotting scale of maximum AE count was consistently limited to 1.5 x 10^5 so as to facilitate the AE interpretation of (MICP-treated) residual soils. This approach of determination is fundamental in the sense that the incipient increase of AE can be well corresponded to the changes in axial and volumetric strains. From the figures, it is noticed that the isotropic yield stresses of MICP-treated residual soils (i.e. from 93 kPa – 102.8 kPa) were greater than the untreated counterparts (i.e. from 77.1 kPa – 79.6 kPa). The present AE yield point is perhaps conservative in view of the fact that an established finding suggested pre-consolidation pressure would correspond to the intersection of initial and normal consolidation line, along the strain energy curves (Becker et al., 1987). Surprisingly, some extent of initial soil mobilization was observed in the earlier volumetric strains (except in Figure 5.5 (b) and Figure 5.6 (a)) increase prior to the AE yield point. It is obvious to note that the UR-OCR5.0-C specimen deformed more abruptly in terms of AE and volumetric strain, as compared to the BR-OCR5.0-C specimen. It is

strange that the BR-OCR5.0-C specimen showed the least amount of AE among all other tested residual soils, since the level of volumetric strain was quite similar to the other OC residual soils.

As similar to the interpretation for (MICP) residual soils, the observations of strains and AE measurements for (MICP) sands were shown in Figure 5.7, through which the AE yield point could be determined. Both untreated and MICP-treated sands yielded at a similar level of stress, and their strain responses were also resembled to each other.

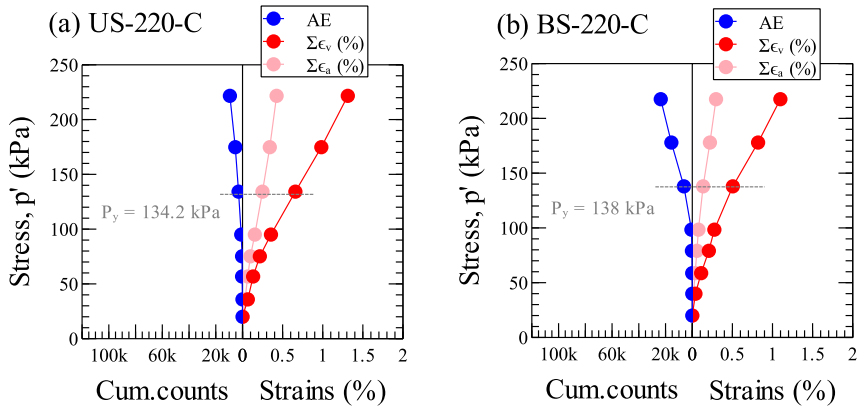

Figure 5.7: Evaluation of isotropic yield stress from AE measurements for all tested sands

5.2.4 Isotropic Consolidation Properties of Tested Soils

The deformation and AE properties for (MICP-treated) residual soils are summarized in Table 5.1. The specimens BR-OCR5.0 and BR-OCR2.5-C were only treated to low calcite contents of 1.2 % and 1.0 %, respectively. On top of the classical Casagrande's method (as discussed in Chapter 4), AE yield

point was also tabulated for interpretation. It can be noticed that the isotropic yield stresses as determined from the AE interpretation were overall less than that of the one using Casagrande's approach, except for the UR-OCR5.0-C and BR-220-E specimens. This discrepancy can be anticipated as the lagging effect between the dissipation of pore water and the subsequent movement of soil grains, owing to different kinds of measurement. Similar finding was also reported in soils with increasing degree of saturation (Naderi-Boldaji et al., 2017).

Table 5.1: Deformation characteristics for tested residual soil specimens with AE measurements

Soil specimen	Compression index C_c	Swelling index C_s	Isotropic yield stress (kPa)		λ (counts / kPa)
			AE	Casagrande's	
Residual soil					
UR-220-C	0.149	-	79.6	81.6	509359
UR-OCR5.0-C	0.150	0.008	77.1	87.3	481292
UR-OCR2.5-C	0.144	-	70.7*	71.2	457219
UR-220-E	0.172	-	79.3	89.6	105082
MICP residual soil					
BR-220-C	0.042	-	93.0	97.9	55190
BR-OCR5.0-C	0.080	0.014	97.2	99.7	41350
BR-OCR2.5-C[a]	0.053	-	-	97.3	-
BR-220-E	0.112	-	102.8	97.6	151703

* The isotropic yield stress was determined from the load-unloading test, as will be covered in Section 5.2.5.

[a] The BR-OCR2.5-C specimen was not tested with AE measurement due to the device malfunction.

For consistency, the isotropic yielding was obtained from the AE interpretation throughout the present study. It is found that the average isotropic yield stress of MICP-treated residual soil was increased by 21 kPa, while the average compression index was decreased by 0.082. This finding informed that calcite bonding and densification were distinctly formed in the well graded residual soil structure. Coincidentally, both approaches showed

that the isotropic yield stresses of the MICP-treated residual soil specimens had been fairly increased. It should be highlighted that the obtained isotropic yield stress and compression index were merely a crude indication as it is believed that fragmentation of calcites/ residual soil agglomeration could progressively occur at a much higher consolidation stress (i.e. beyond 220 kPa).

Table 5.2 summarizes the isotropic consolidation properties of (MICP-treated) sands as determined by strains and AE measurements.

Table 5.2: Deformation characteristics for tested sand specimens with AE measurement

Soil specimen	Compression index C_c	Swelling index C_s	Isotropic yield stress (kPa)		λ (counts / kPa)
			AE	Casagrande's	
Sand					
US-220-C	0.062	-	134.2	119.1	39003
MICP Sand					
BS-220-C	0.059	-	138.0	121.0	36726

The isotropic yield stress of (MICP) sands obtained from the AE measurement was greater than that predicted theoretically by the Casagrande's method. Through AE interpretation, the isotropic yield stress of MICP-treated sand (i.e. 138 kPa) was greater than that of untreated sand (i.e. 134.2 kPa). The untreated and MICP-treated sands showed lower compression index (average compression index of 0.061) and higher AE yield stress (average yield stress of 136.1 kPa) as compared to the (MICP-treated) residual soils. However, the increase of yield stress from untreated specimen for MICP-treated sand was merely 3.8 kPa, whereas the increase of improvement for MICP-treated

residual soil was 21 kPa. In light of lower decrease of compressibility (by 0.003 only), calcite densification effect was less profound in the MICP-treated sand due to the larger pore volumes hindering the calcite filling. It is concluded that only marginal strengthening on inter-particular resistance was formed by the weak calcite cementation at the cross-sectional side surfaces of sub-angular sand particles, which was observed in the microscopic structure of sand (referred to Section 4.4.3 in the Chapter 4).

Figure 5.8 shows the correlation between compression index and AE incremental rate. The AE incremental rate (denoted as λ) was defined as the incremental cumulative AE counts divided by the logarithm of consolidation pressure difference along the normal consolidation line. This variable is essentially comparable to the compression index by demonstrating the nature of compressibility and mobilization of soil grains at normal consolidation state. A shaded zone was included to distinguish the soils with weaker structural resistance from the stiffer soils. It is worth noticing that the AE incremental rate for BR-OCR2.5-C specimen was not listed as the AE measurement was missing due to the malfunction of AE instrumentation device.

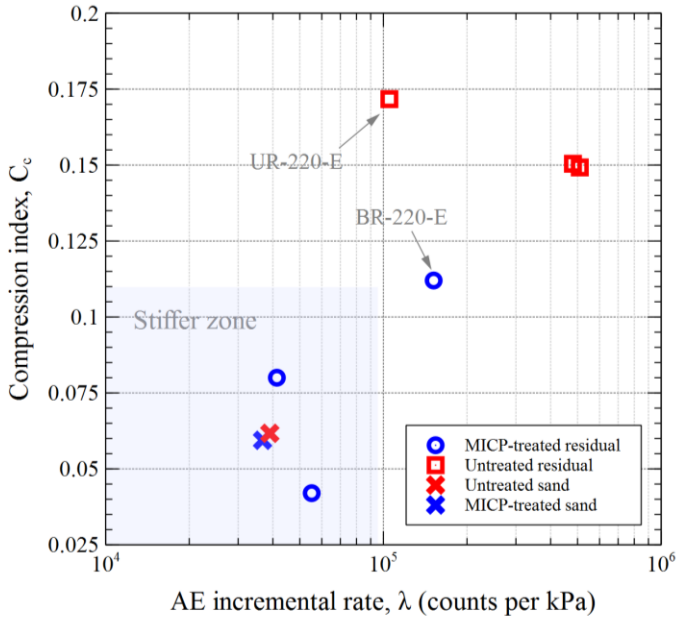

Figure 5.8: Relationship between compression index and AE incremental rate for untreated and MICP-treated residual soil specimens

It is observed that the compression index increased with the AE incremental rate as the soil structures were becoming weaker. Even more, it is possible to differentiate the MICP-treated and original residual soils by their compressibility and AE incremental rate. The MICP-treated residual soils showed lower magnitudes in compressibility (as enveloped in the anticipated shaded zone in Figure 5.8) and AE incremental rate than the untreated residual soil. It should be noted that the BR-220-E specimen was behaviourally similar to the untreated residual soil since the particular specimen had the lowest calcite content (i.e. 1.8 % only) among all presented MICP-treated residual soils. In addition, the (MICP) sands were considerably stiffer than the residual soils (except for BR-220-C specimen) on account of the dense structure. Naderi-Boldaji et al. (2017) reported that the compression index linearly increased with the total AE hit numbers for a series of partially-saturated soils.

The effect of matric suction probably contributed to the cementation of unsaturated soils and the corresponding linear correlation. It is arguable that the AE characteristics of bio-cemented and compacted residual soils were different from the unsaturated soil, as the trend of Figure 5.8 was not in agreement with the finding reported by Naderi-Boldaji et al. (2017).

5.2.5 Validation of Kaiser's Effect in Unloading-Reloading Test

Isotropic yielding of soil was further examined in an unloading-reloading test for the UR-OCR 2.5-C specimen in order to validate the existence of Kaiser's effect on the tested materials. The experimental results were depicted in Figure 5.9. Upon reaching a designated consolidation stress of 70.7 kPa, the soil specimen was unloaded to 40 kPa so as to impose an over-consolidation effect to the soil specimen. Once the reloading stress went beyond a consolidation stress level of 70.7 kPa, AE signals were strikingly observable in tandem with apparent volumetric deformation. It follows that, the Kaiser's effect (Hardy Jr., 2003) was evidenced in the present experiment, with a sensitivity of stress being 7.8 kPa. This finding confirmed that mechanically-induced soil structure (i.e. structure subjected to certain level of OCR) could furnish a well-defined yield point that can be determined by AE monitoring.

Note: Kaiser's effect (Hardy, 2003) was referred to the phenomenon in which acoustic emission was absent when the applied stress was not exceeding the past maximum applied stress, and vice versa.

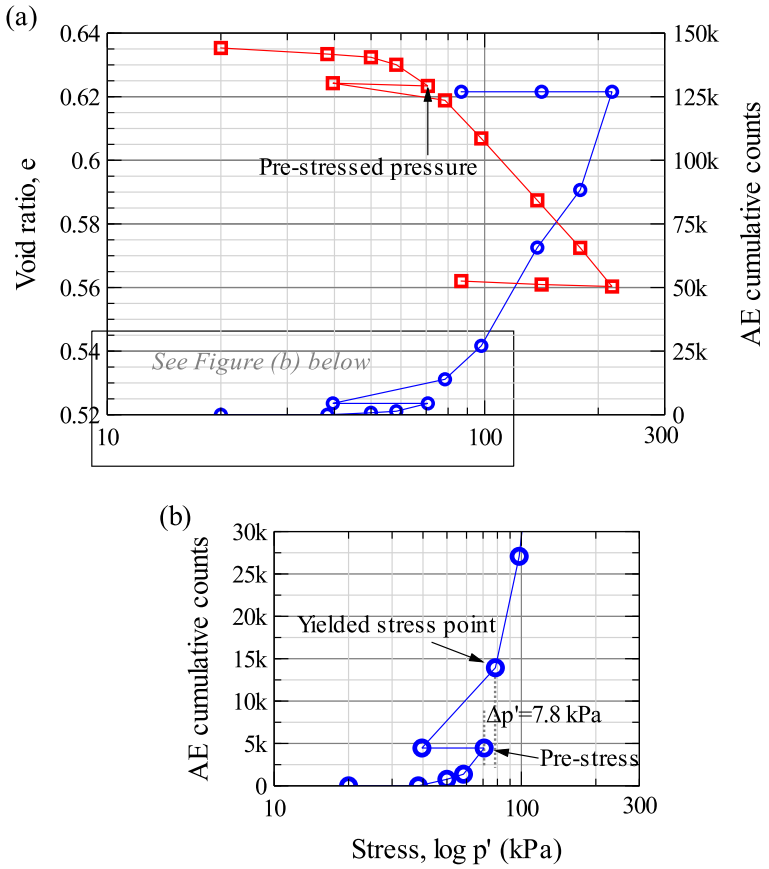

Figure 5.9: Isotropic yielding and Kaiser's effect: (a) relationship among void ratio, consolidation stress, and cumulative AE counts; (b) relationship between cumulative AE counts and consolidation stress at yielding range

5.3 Progressive Changes of Deformation Behaviour in Undrained Shearing through Acoustic Emission Measurement

This section discusses on how the deformation behaviour of tested soils in shearing can be analysed by AE measurement through the AE time-series monitoring. The author perceived that interpretation of AE changes under time space is advantageous when the axial load was increased monotonically with time as used in this study. This approach is rather spontaneous from the first principle (everything progresses with time) and it is able to observe the soil

responses, such as strain and pore-water pressure under monotonically increasing shear stress and to correlate them to AE change.

As noted earlier, the present triaxial test was conducted by applying a constant stress-rate of loading onto the soil specimens, as shown in Figure 5.10. This figure presents a typical example of the deviator stress (q) and AE rate changes in the time frame for the UR-OCR5.0-C specimen (i.e. untreated residual soil subjected to an OCR of 5). When the specimen was sheared by monotonic loading, pore-water pressure, axial strain, and AE counts rate also increased at different rates with respect to time. The rates of the increase in pore-water pressure and axial strain were distinctively different against the shear stress increase, and their changes may be corresponded to the different phases of AE rate changes over initial, intermediate, and global strain ranges. Therefore, in the following three progressive changes of AE rate (namely, yielding point P_Y, instability point P_I, and ultimate point P_U) could be defined from the correlation between mechanical responses and instantaneous AE rate change.

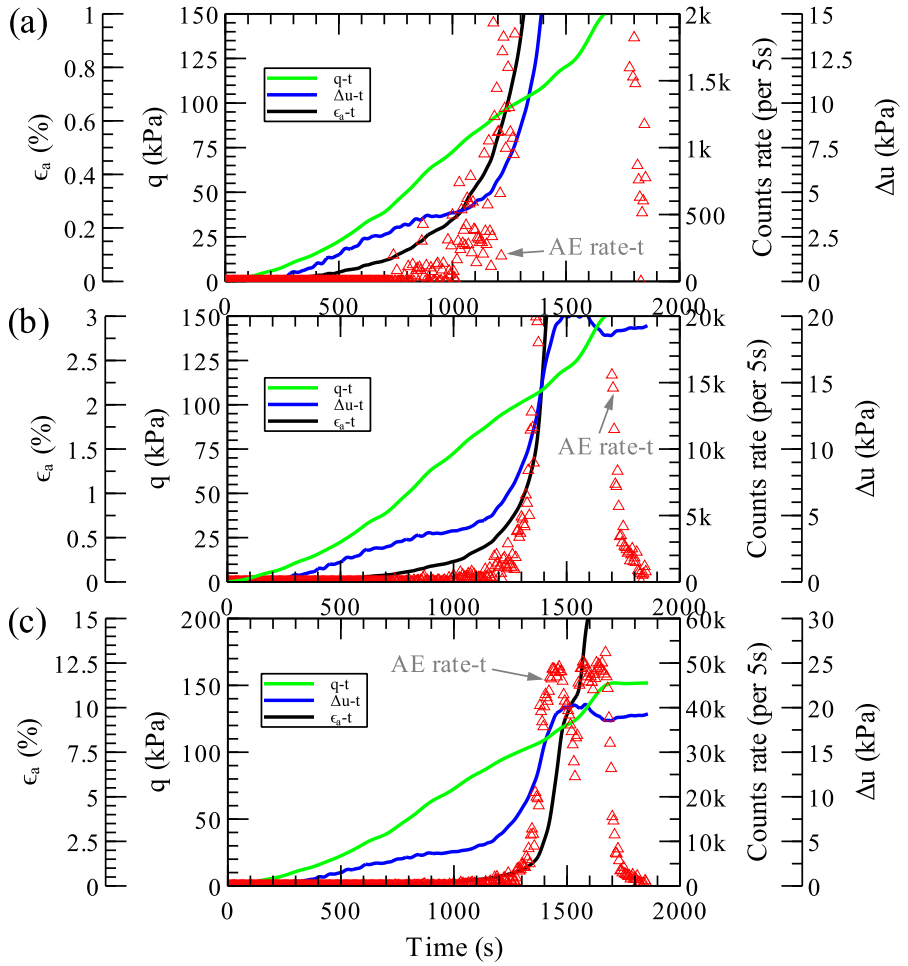

Figure 5.10: Correlation between mechanical responses and instantaneous AE rate change for UR-OCR5.0-C specimen covering different strain ranges: (a) initial, (b) intermediate, and (c) global

It should be noted that the UR-OCR5.0-C specimen was served as a benchmark and leading example throughout the subsequent sections of time-series interpretation since most reported studies (Tanimoto and Tanaka, 1985; Tanimoto and Tanaka, 1986; Tanaka and Shirakawa, 1995) have been focused on the soils subjected to a certain OCR. The observed deformation behaviour and AE rate changes can therefore be comprehended with respect to the reported findings. Other types of tested soils, such as compacted and MICP-treated residual soils and sands, were followed suit and will be discussed in

later sections. The above progressive changes of deformation behaviour were also found in soils formed with bio-mediated and compacted structures.

5.3.1 Determination of the AE Yielding Point (P_Y) in Deformation Behaviour

Tanimoto and Tanaka (1986) defined the first yielding point for over-consolidated sand by the onset of AE starting, as a boundary from elastic to plastic behaviour. The acoustic emission is corresponded to the irrecoverable movement of soil particles and the deformation behaviour is arguably plastic in nature. Figure 5.11 (a) illustrates the approach of determining yield point in which acoustic energy was incipient to release upon exhibiting plastic deformation. Similarly, the yield point was able to be determined by the onset of AE in the studied OC residual soil. It is realized from the present study that the onset of AE counts rate coincided with the intersection point between initial gradient and slope of first rising curvature in the cumulative AE count curve. This particular intersection point was regarded as yield point (denoted as P_Y) and corresponds to the classical elastic-plastic distinction point. Upon yielding, the rate of axial strain and pore-water pressure would noticeably be increased as shown in Figure 5.11 (b). The above-mentioned approach of identifying the yield point was implemented for all other tested soils (e.g. MICP-treated and compacted soils) in the present study to facilitate a consistent interpretation of soil deformation behaviours.

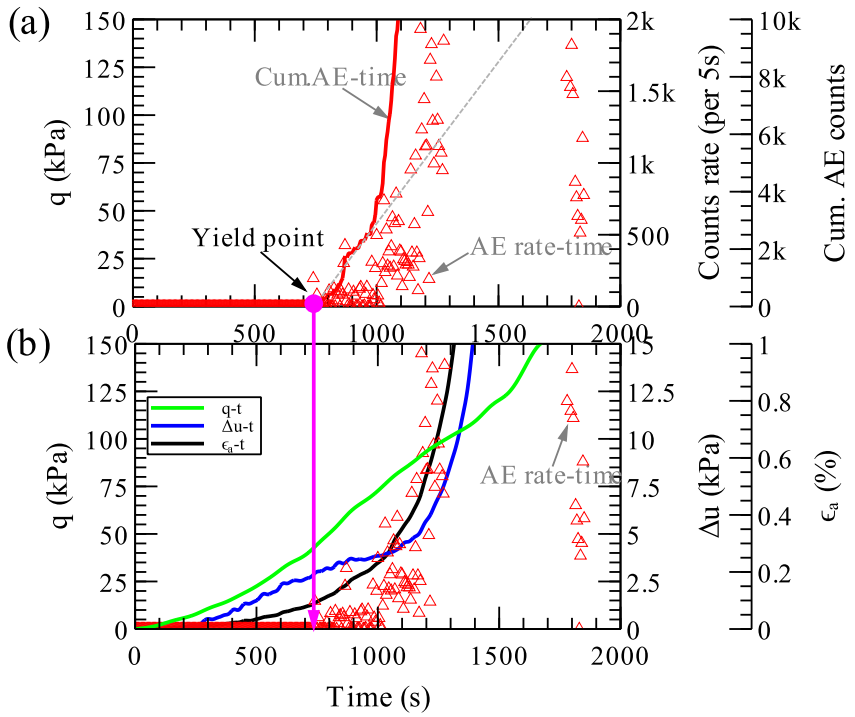

Figure 5.11: Yielding point of UR-OCR5.0-C specimen as determined AE interpretation: (a) AE interpretation for yielding; (b) Pore-water pressure and axial strain responses within yielding range

Figure 5.12 shows the interpretation results for determining AE yield points among over-consolidated, untreated, and MICP-treated residual soils. Two OC residual soil specimens (namely, BR-OCR5.0-C and UR-OCR2.5-C), which manifested similar yielding behaviour as the UR-OCR5.0-C specimen, were also shown in Figure 5.12 (a) and (b) to further validate the finding on OC residual soil. The yield point was able to be determined by distinctive AE rate changes. There were some early AE spikes being detected at the beginning of shearing in the BR-OCR5.0-C specimen, probably owing to the calcite fracturing phenomenon. The calcite fracturing phenomenon could also be observed in the bio-mediated residual soil and sand as discussed subsequently.

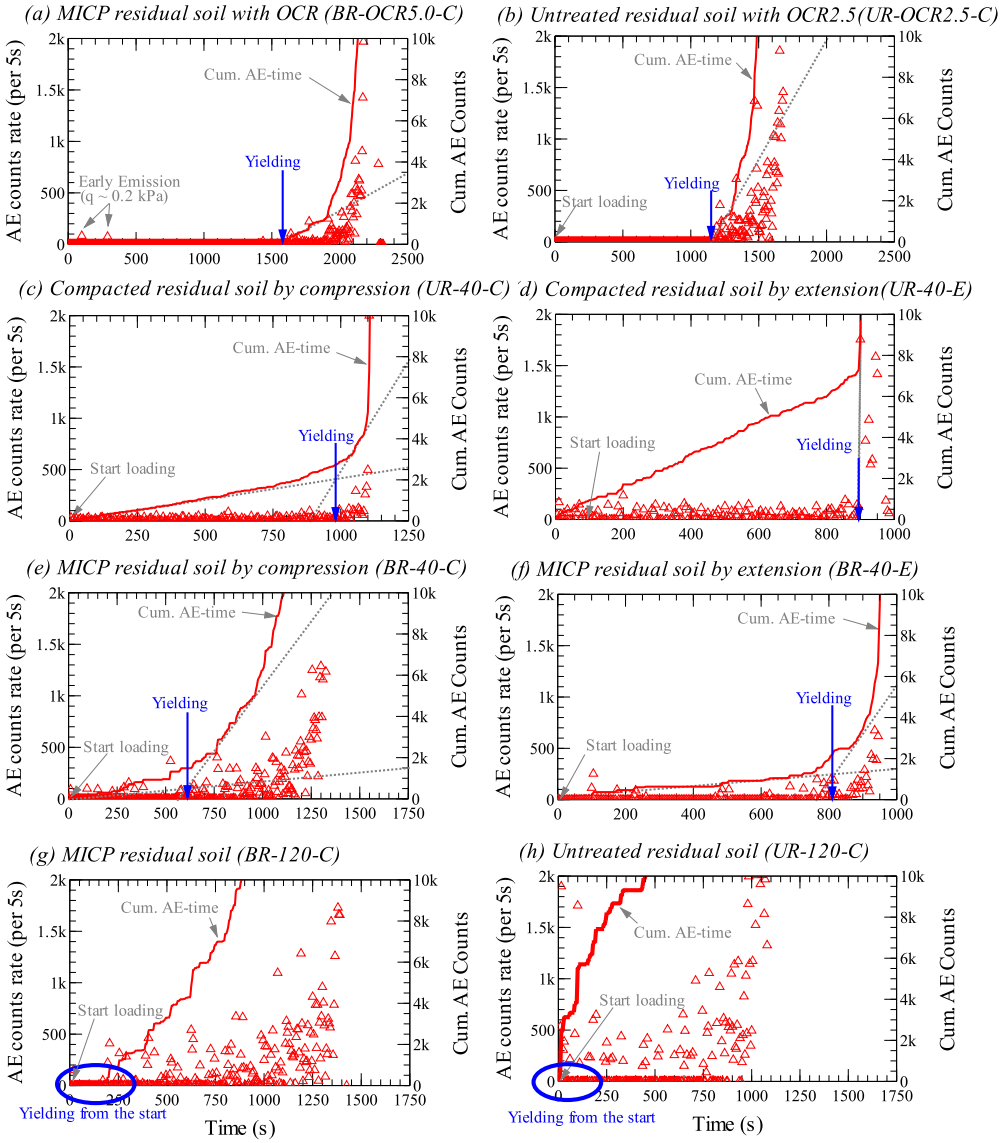

Figure 5.12: Yielding points of different types of tested residual soils as determined by AE interpretation: (a) BR-OCR5.0-C; (b) UR-OCR2.5-C; (c) UR-40-C; (d) UR-40-E; (e) BR-40-C; (f) BR-40-E; (g) BR-120-C; (h) UR-120-C

It is also obvious that the effect of initial compaction was preserved in the untreated residual soil specimens (namely, UR-40-EC and UR-40-E) being consolidated to a low pressure (i.e. 40 kPa) by manifesting distinctive yield points. The compacted residual soils manifested uniformly low AE before reaching the yield points, which were also determined in accordance to the

described method for OC residual soils. Figure 5.12 (e) - (f) further shows that the bio-mediated residual soils (consolidated to 40 kPa) yielded much earlier than the untreated residual soils; while some early spikes were able to be detected. The early AE signals were arguably linked to the localized fragmentation of calcites or residual soil clogs in the (MICP-treated) residual soil before a major structural degradation was triggered (i.e. yielded). When the consolidation pressure reached 120 kPa (Figure 5.12 (g) - (h)), both untreated and MICP-treated residual soils yielded from the commencement of undrained shearing as the soils became normally consolidated.

In addition, the responses of excess pore-water pressure and axial strain were examined in parallel with the AE rate change in Figure 5.13. The axial deformation was able to be corresponded to the instantaneous AE rate change when the soil was continuously sheared. This observation suggested that the AE and strain energy were instinctively correlated to each other, when the particles movement was triggered. Two obvious observations can be obtained from the figure: (a) Some degrees of pore-water pressure and axial deformation had been developed at slower rate prior to yielding; (b) when the soils became normally consolidated (i.e. BR-120-C and UR-120-C), there was a significant generation of pore-water pressure from the start of undrained shearing.

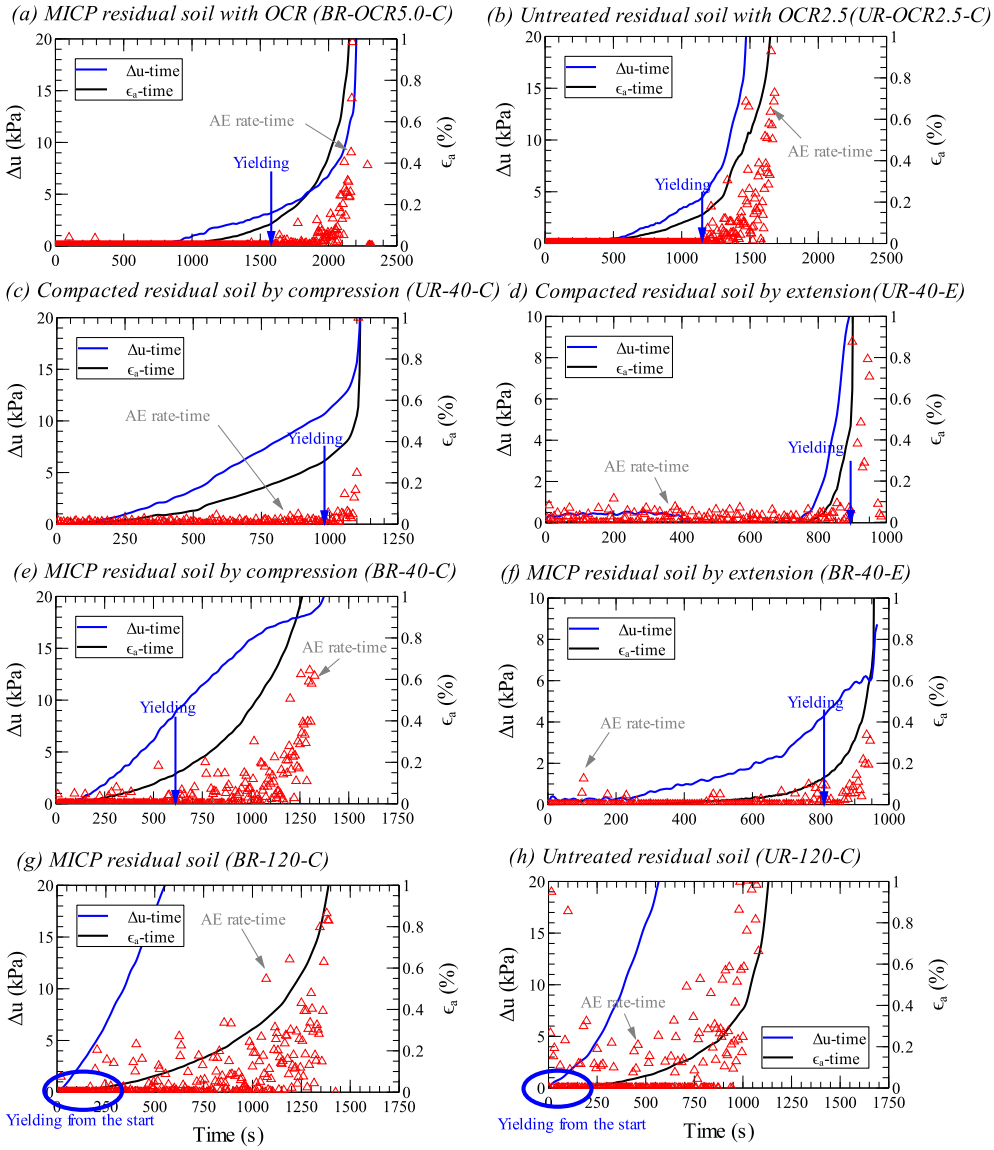

Figure 5.13: Correlation between mechanical and AE responses of tested residual soils at yielding strain range: (a) BR-OCR5.0-C; (b) UR-OCR2.5-C; (c) UR-40-C; (d) UR-40-E; (e) BR-40-C; (f) BR-40-E; (g) BR-120-C; (h) UR-120-C

Figure 5.14 shows the yield points as determined for the untreated and MICP-treated sands, following the method as described previously. The distribution of AE signals was apparently more scattered and numerous AE spikes could still be observed before the AE rate started to increase abruptly. For this reason, the yield points of (MICP) sands were not only obtained from

the intersection of two cumulative AE lines (i.e. initial and the first rising slope), but also conservatively justified by the onset rise in AE counts rate. It should be noted that the BS-120-C specimen (as shown in Figure 5.14 (c)) showed some early AE bursts, probably due to the frictional effect from the triaxial loading system. Thus, the first few AE data points were omitted in the re-computation of cumulative AE counts to determine the AE yield point.

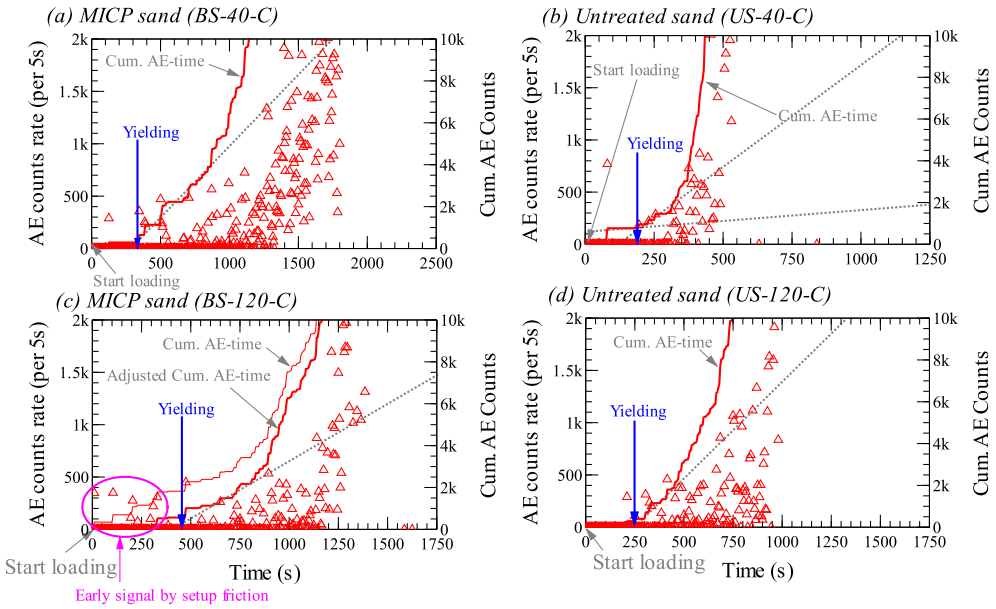

Figure 5.14: Yielding points of untreated and MICP-treated sands as determined by AE interpretation: (a) BS-40-C; (b) US-40-C; (c) BS-120-C; (d) US-120-C

The corresponding pore-water pressure and axial strain responses were presented in Figure 5.15. It is interesting to note that the excess pore-water pressure of BS-40-C specimen decreased (sign of dilatancy) immediately after yielding, whereas the US-40-C specimen still exhibited pore-water pressure increase (compressible behaviour of the soil skeleton) after the respective specimen yielded.

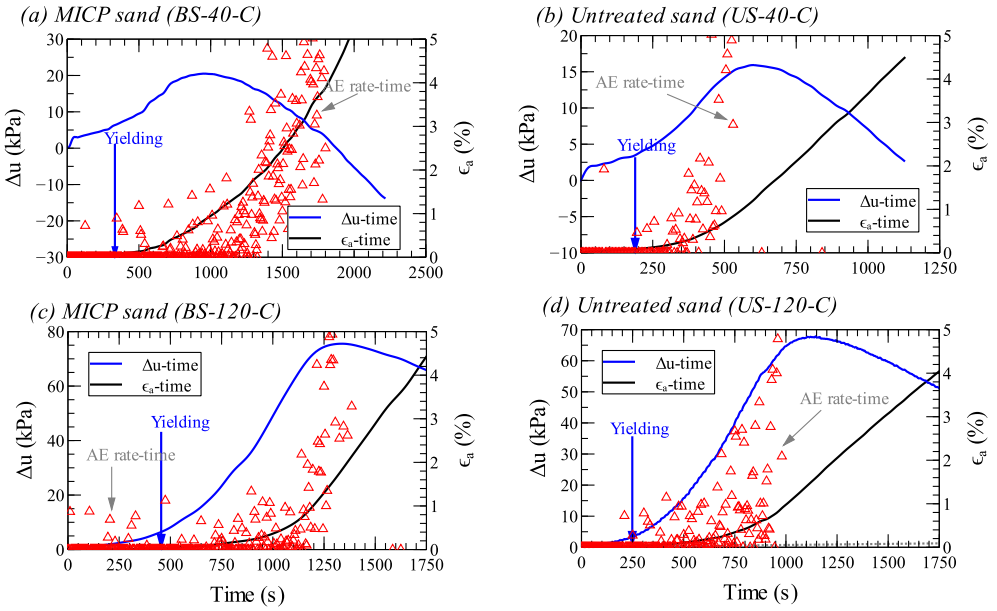

Figure 5.15: Correlation between mechanical and AE responses of tested sands at yielding strain range: (a) BS-40-C; (b) US-40-C; (c) BS-120-C; (d) US-120-C

Based on the above discussions, it can be inferred that the OC residual soils were characterized with a distinctive AE yield point; no AE spikes were detected prior to the occurrence of yield point. The yielding resistances were still preserved in the compacted and bio-mediated soils, which were consolidated to a low pressure (i.e. 40 kPa). The yielding resistances would be diminished upon the soils were consolidated to at least 120 kPa. Unlike the OC residual soils, noticeable extent of continuous AE spikes were observed from the beginning of shear in the untreated and bio-mediated residual soils and sands. These findings altogether eventuated two classes of yielding determination, should AE interpretation was used.

If numerous early AE signals existed, the initial gradient line would become steeper (rather than horizontal) and we defined the intersection point as illuminating yield point (denoted as P_Y*). This illuminating yield point was

neither prescriptive nor truly corresponding to the classical yield point as determined for those OC soils, but it was regarded as the first structural degradation state of the tested soil. In other words, classical yield point will only be defined for soils without early acoustic emission and showing horizontal initial gradient, whereas the rest will be conservatively defined as illuminating yield point. Figure 5.16 clearly demonstrates the difference between classical and illuminating yield points as adopted in the present study. The motivation for defining such point was that less intensive AE (not continuously) in the early stage of loading could be caused by the localized movement of soil grains only, without major structural changes (yielding). Thus, the illuminating yield point should not be unconsciously overlooked. In the overall context, both terms were adopted to simply denote the first structural changes (i.e. calcite de-bonding or degradation of major structural resistance) of soil specimen in undrained shearing.

(a) Classical yield point

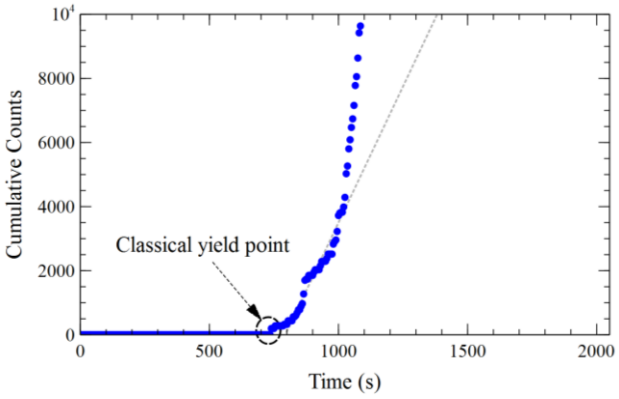

(b) Illuminating yield point

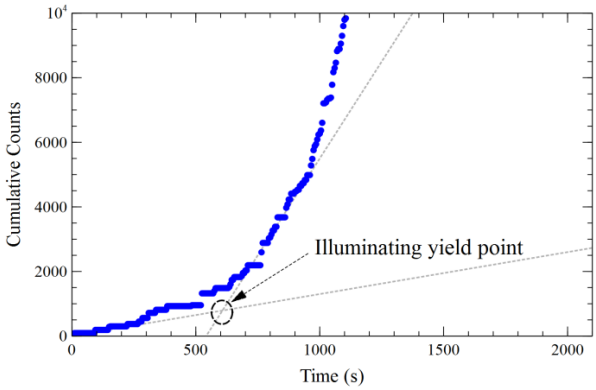

Figure 5.16: Demonstrating difference between classical and illuminating yield points

5.3.2 Determination of AE Mobilization and Ultimate Points (P_I and P_U) in Deformation Behaviour

When the AE counts approached a more intensive level (as shown in Figure 5.17), an abrupt jump of AE rate could be observed easily. The intersection point between initial and rising slope of cumulative counts rate curve was named as instability point (denoted as P_I). This state point was corresponded to abrupt rise of pore-water pressure and strain responses; it was also related to the significant mobilization of soil particles.

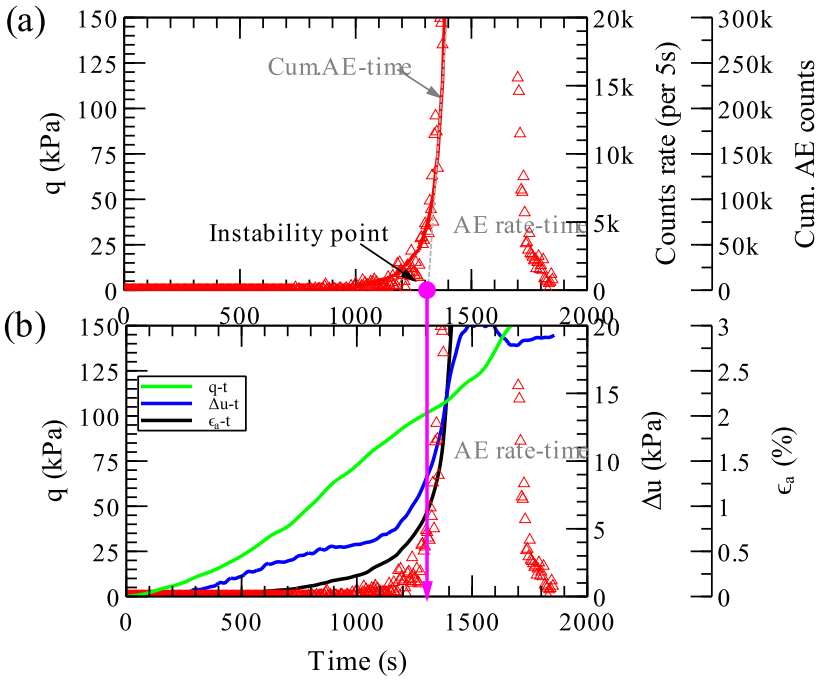

Figure 5.17: Instability point of UR-OCR5.0-C specimen as determined AE interpretation: (a) AE interpretation within intermediate strain range; (b) Pore-water pressure and axial strain responses within intermediate strain range

In addition, the instability points for all other tested residual soils and sands were provided in Figure 5.18 and Figure 5.19, respectively. It can be seen that the instability points could be consistently determined among all tested residual soils and sands as very active movement of soil grains were experienced.

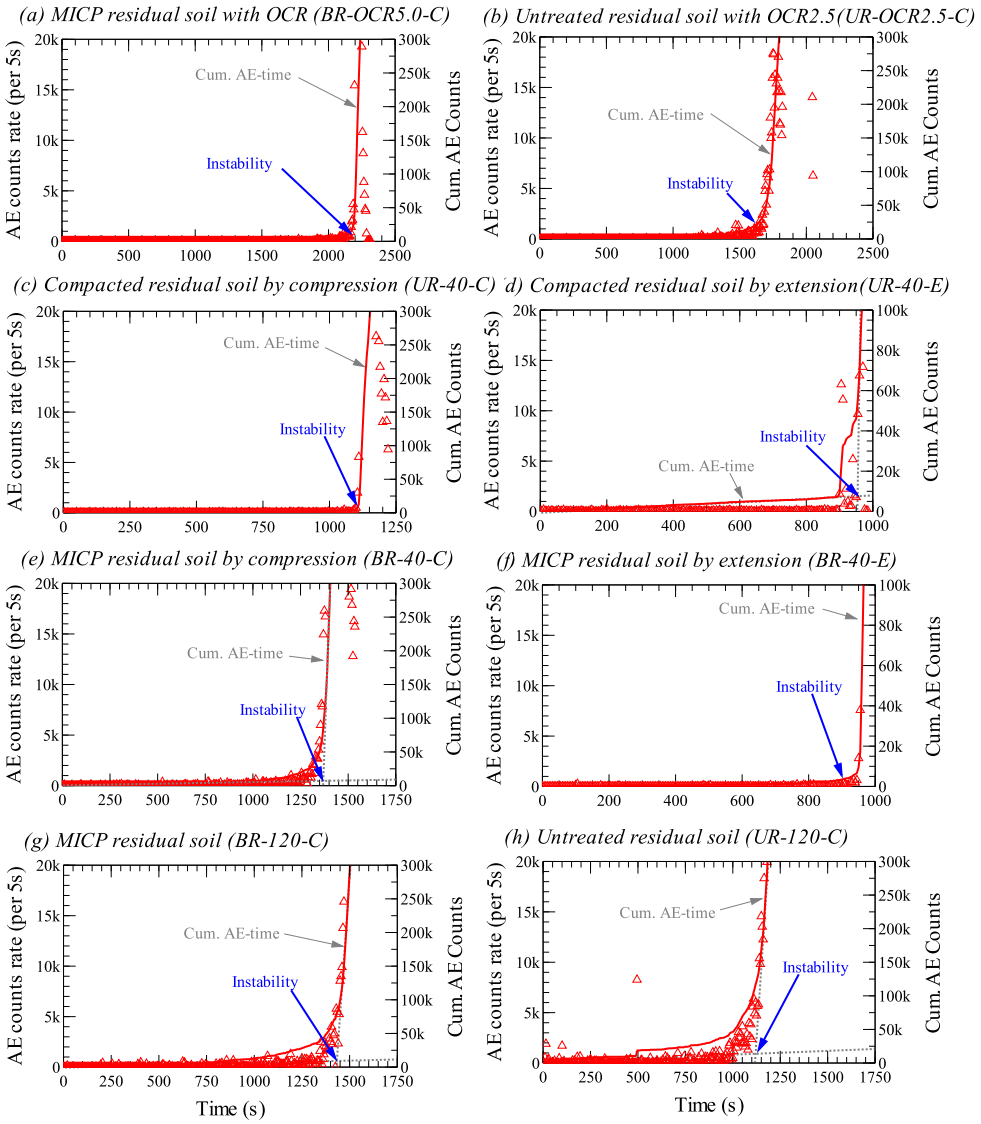

Figure 5.18: Instability point of different types of residual soils as determined AE interpretation: (a) BR-OCR5.0-C; (b) UR-OCR2.5-C; (c) UR-40-C; (d) UR-40-E; (e) BR-40-C; (f) BR-40-E; (g) BR-120-C; (h) UR-120-C

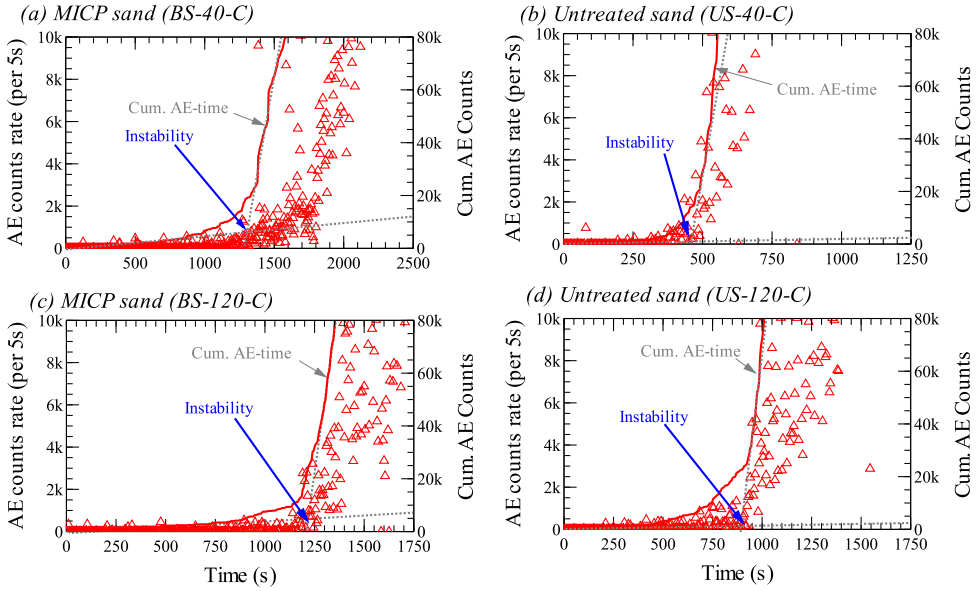

Figure 5.19: Instability point of untreated and MICP-treated sands as determined AE interpretation: (a) BS-40-C; (b) US-40-C; (c) BS-120-C; (d) US-120-C

The pore-water pressure and strain responses were interpreted with respect to the determined instability points in Figure 5.20 – 5.21. It is apparent from Figure 5.20 that the axial strain and pore-water pressure increased abruptly upon all tested residual soils arrived at the instability point. This finding implied that the residual soils experienced significant grains mobilization (i.e. increasing AE rate) and structural degradation, on account of the sudden deformation change (i.e. increasing axial strain) and compressible soil skeleton (i.e. increasing pore-water pressure). Appendix K further showed that the rate of strain as linked to the particles movement was correlated to the instantaneous AE rate change. Figure 5.21 shows that grains mobilization of (MICP) sands was related to the dilatancy as the instability points were in proximity of the strain range whereupon the excess pore-water pressure was incipient to drop.

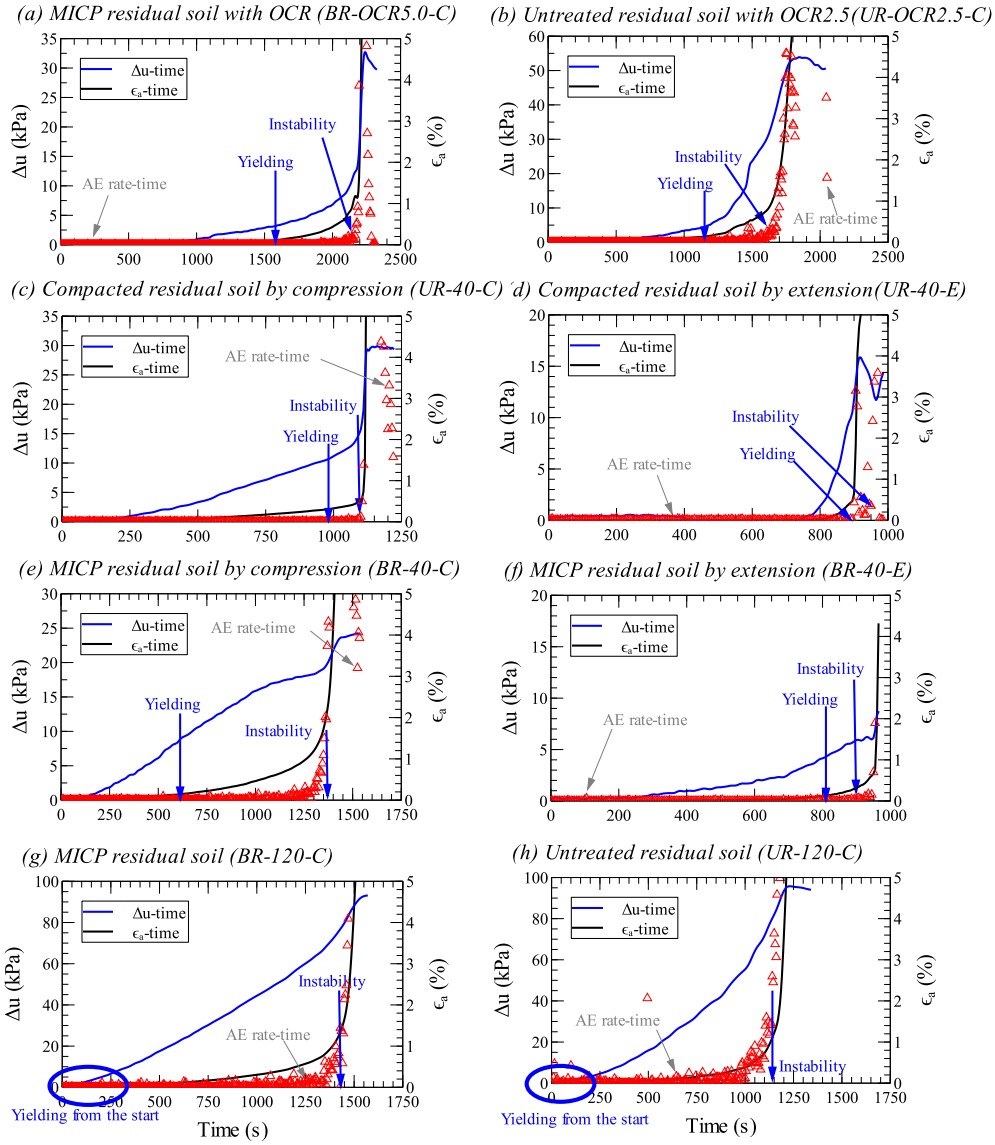

Figure 5.20: Correlation between mechanical and AE responses of tested residual soils at intermediate strain range: (a) BR-OCR5.0-C; (b) UR-OCR2.5-C; (c) UR-40-C; (d) UR-40-E; (e) BR-40-C; (f) BR-40-E; (g) BR-120-C; (h) UR-120-C

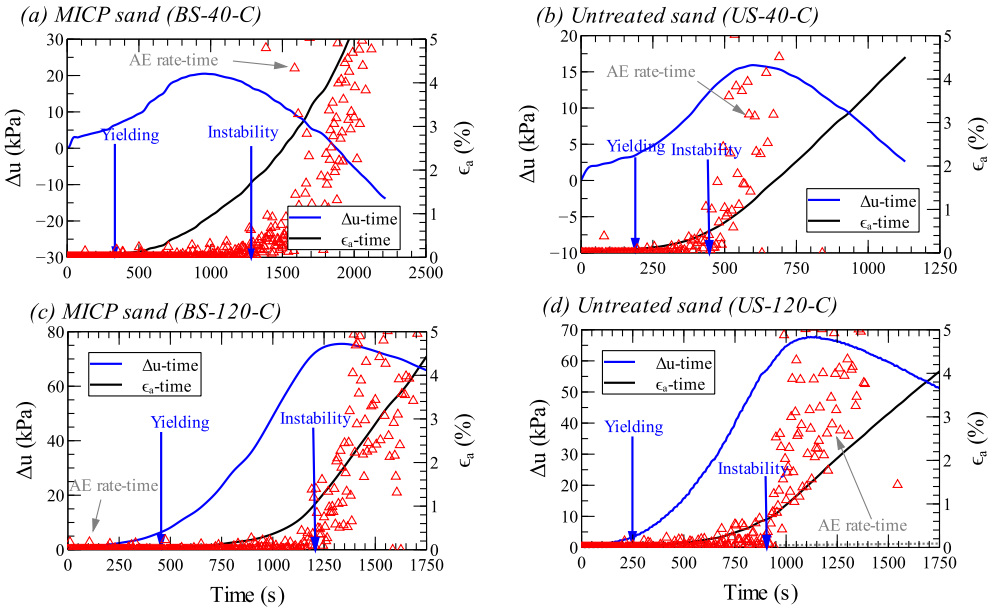

Figure 5.21: Correlation between mechanical and AE responses of tested sands at intermediate strain range

As can be seen in Figure 5.22, the AE counts rate started to reach steady rate near the end of testing and an ultimate point was defined as P_U. It was observed that the strain was still increasing despite the AE rate was decreased at the ultimate state.

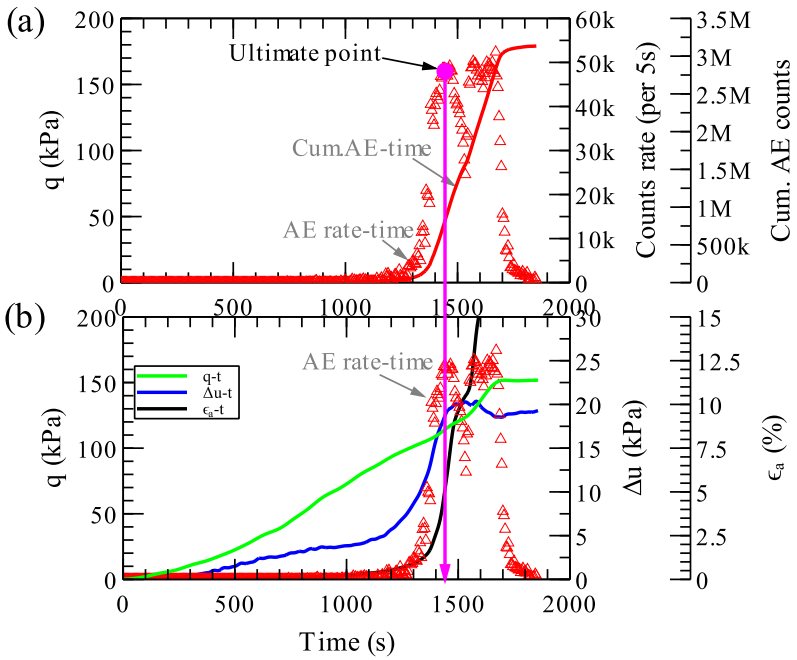

Figure 5.22: Ultimate point of UR-OCR5.0-C specimen as determined AE interpretation

Similarly, the ultimate points for all other types of residual soils are shown in Figure 5.23. The obtained three progressive points can be summarized in Figure 5.24 and corresponded to the excess pore-water pressure and axial deformation changes. The pore-water pressure change started to become steady upon reaching the ultimate point. It is worth mentioning that the AE rate retarded as the axial strain continuously increased. This could be caused by the soil bulging in which radial movement of soil

particles were more dominant and the measurement beyond this state became mechanically unreliable.

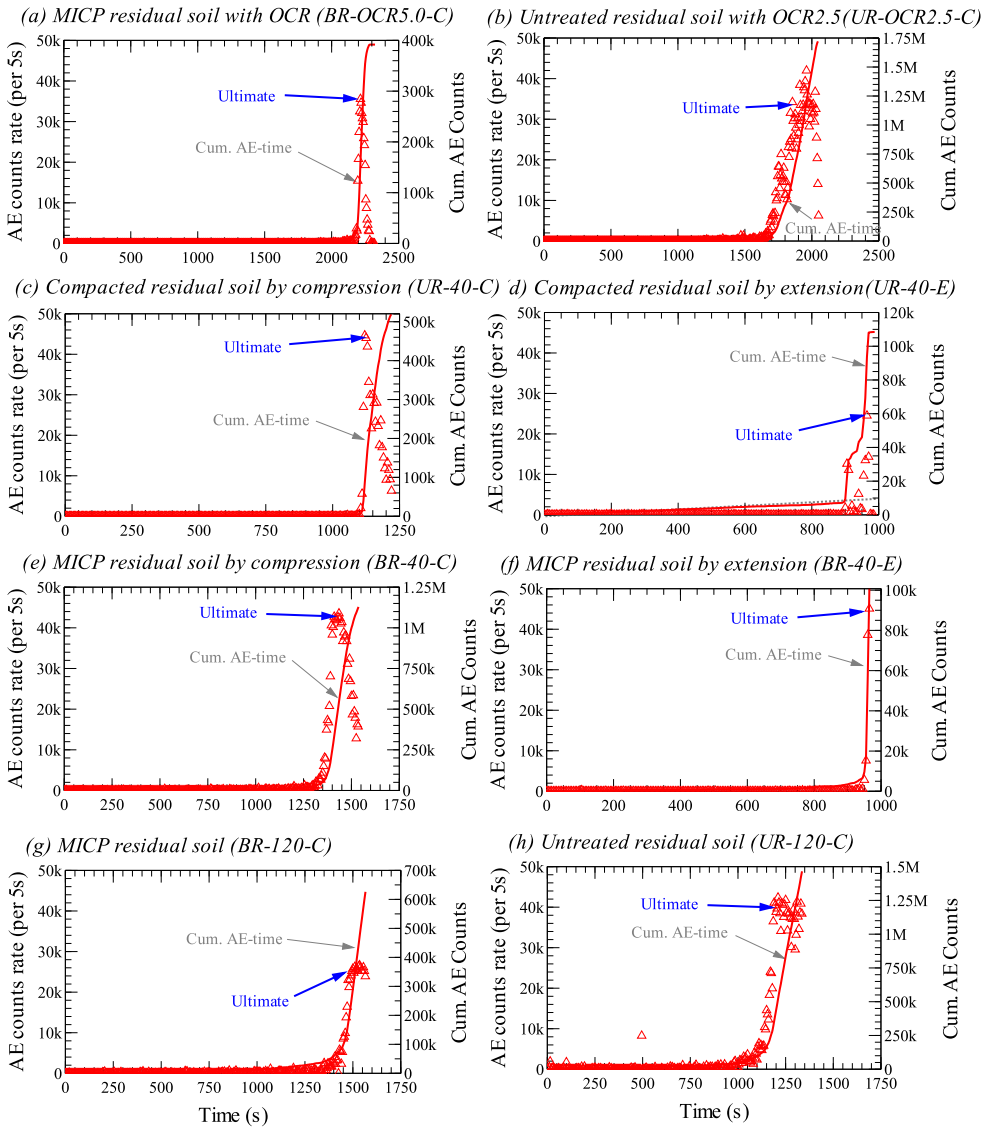

Figure 5.23: Ultimate point of all other types of residual soils as determined AE interpretation: (a) BR-OCR5.0-C; (b) UR-OCR2.5-C; (c) UR-40-C; (d) UR-40-E; (e) BR-40-C; (f) BR-40-E; (g) BR-120-C; (h) UR-120-C

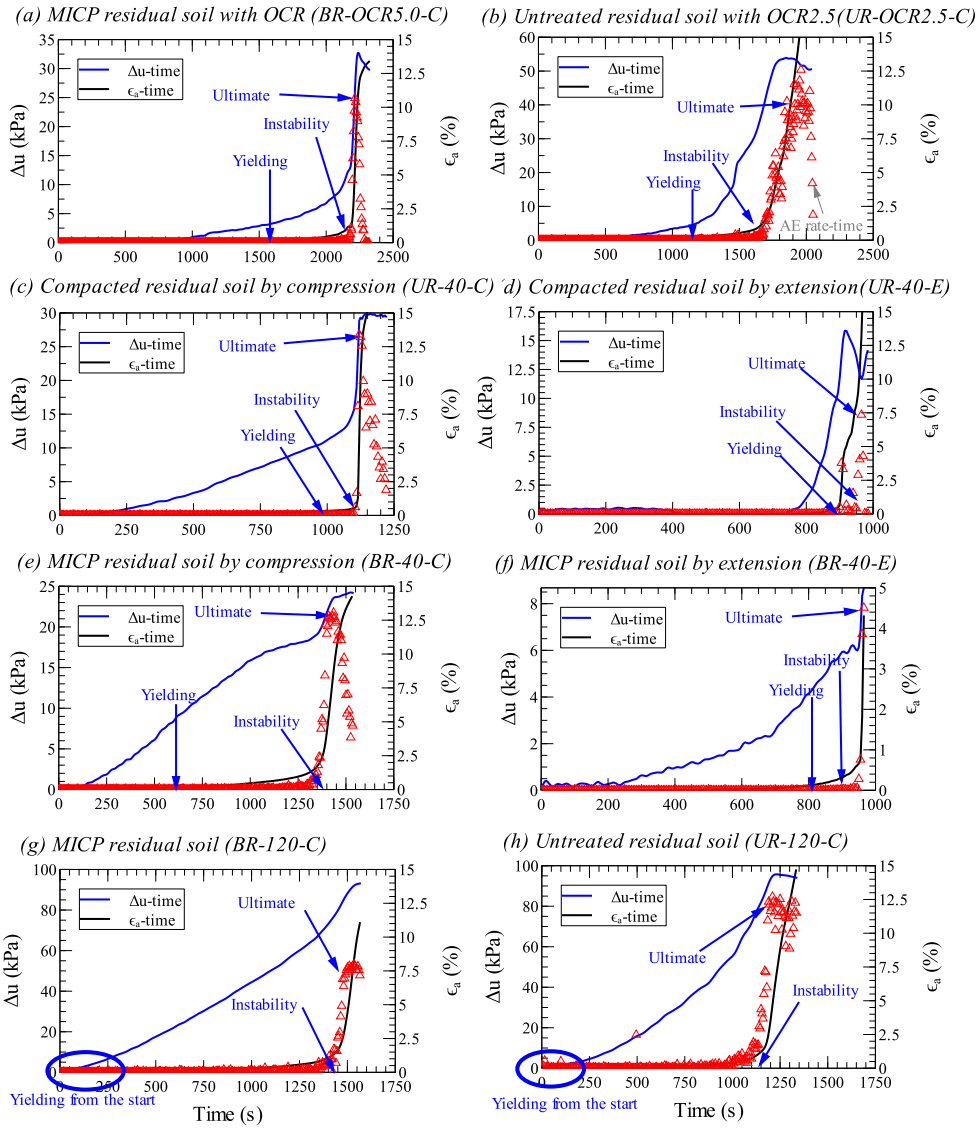

Figure 5.24: Correlation between mechanical and AE responses of tested residual soils at global strain range: (a) BR-OCR5.0-C; (b) UR-OCR2.5-C; (c) UR-40-C; (d) UR-40-E; (e) BR-40-C; (f) BR-40-E; (g) BR-120-C; (h) UR-120-C

The ultimate point was not able to be determined from the sands since the AE rate was still increasing (referred to Figure 5.25) and strain hardening effect was dominant. As different from the failure of (MICP) residual soils, the increasing AE rate in sands could be practically explained by the insignificant radial deformation on the verge of bulging failure. Beyond the instability phase, the excess pore-water pressures of all tested sands were continuously reducing. This observation implied that the instability point separated the soil behaviour of being compressible from dilatant behaviour (positive dilatancy).

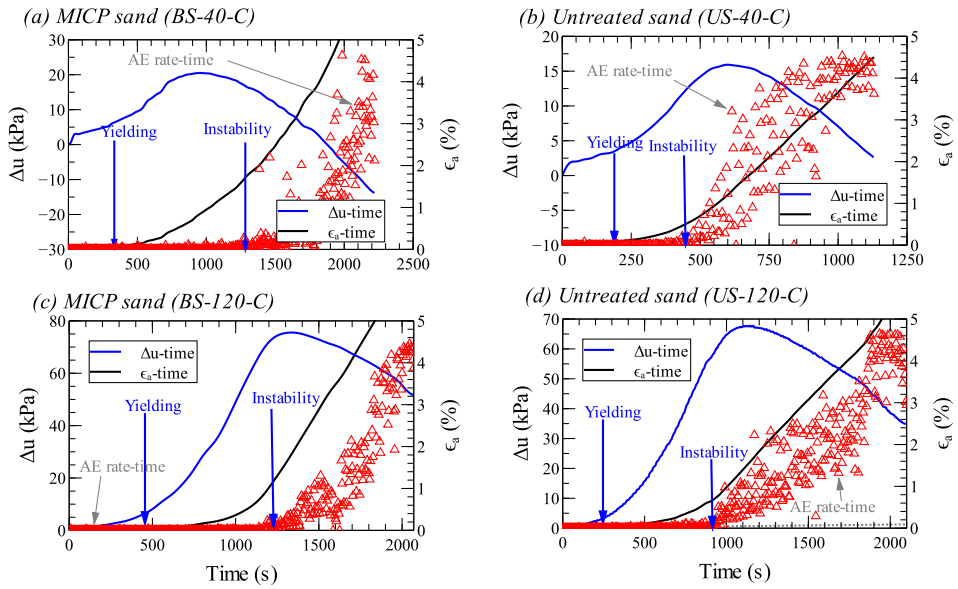

Figure 5.25: Correlation between mechanical and AE responses of tested sands at global strain range: (a) BS-40-C; (b) US-40-C; (c) BS-120-C; (d) US-120-C

5.3.3 Scrutiny of AE Points in *p'-q* Stress Space

In the preceding sections, progressive changes (namely, yielding, instability, and ultimate points) of deformation behaviours for tested residual soils and

sands were discovered through AE measurements. The yield point, which distinguished the soil elastic-plastic deformation behaviour, was able to be determined reliably by the suggested method of AE interpretation. Beyond the yield point, the behaviours of (MICP) residual soils were found to be divided by instability (grains mobilization phase) and ultimate points (failure state) distinctively. For (MICP) sands, the soils would only experience the instability state as the sand specimens were dictated by strain hardening mechanism and continuous increase of AE rate.

In this section, the determined AE points were scrutinized alongside the corresponding stress trajectory within *p'-q* stress space. It follows that the behavioural changes among tested soils (i.e. specimens adopted in Chapter 4) and (MICP) over-consolidated residual soils can be examined and compared with some reported findings, under the influence of consolidation pressure. For instance, the effect of bio-mediation on stress-deformation behaviour for MICP-treated residual soil can be contrasted to the untreated counterpart, in which only initial compaction effect could preserve. Importantly, the yield and instability points as obtained from all studied residual soils and sands were critically assessed in the *p'-q* stress space.

5.3.3.1 Progression of AE Points along Effective Stress Paths

Untreated and MICP-treated Residual Soils

The determined AE points of untreated and MICP-treated residual soils were summarized in Figure 5.26 (a) - (b), respectively. The effective stress paths of

respective residual soils were also shown in order to study the stress-deformation changes.

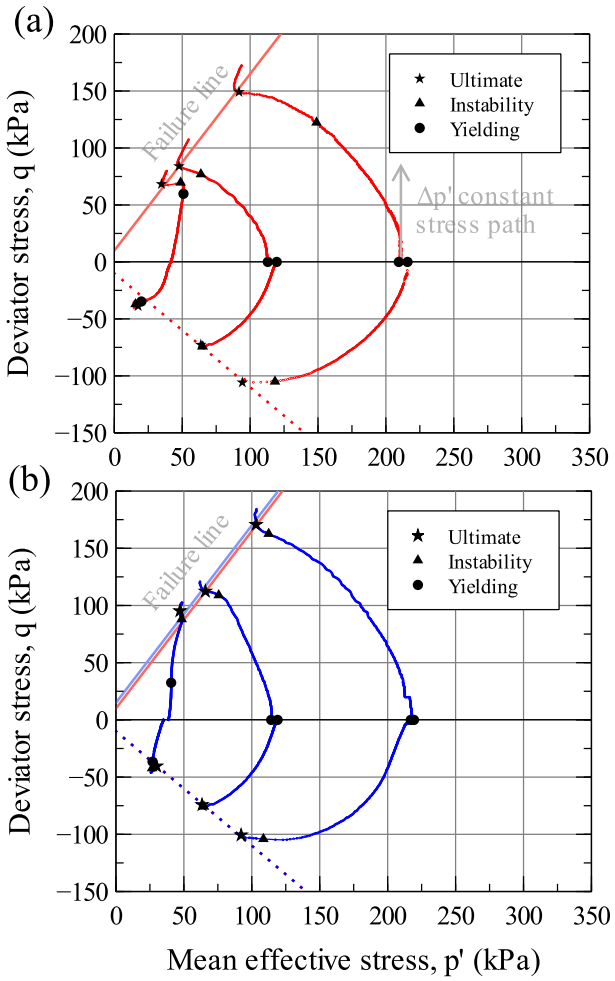

Figure 5.26: Effective stress paths and AE changes for tested residual soils: (a) untreated; (b) MICP-treated

Throughout the process of straining, the untreated and MICP-treated residual soils would transform from stable to unstable phase (i.e. from yielding to instability) before reaching the ultimate failure state. It is obvious that the (MICP-treated) residual soil and sand were characterized by different stress-deformation behaviours. The highly-consolidated residual soils (e.g. those consolidated to 120 kPa and 220 kPa) appeared to behave in similar fashion as

the typical loose sand (Chu et al., 2015) and normally-consolidated clay; the highly-consolidated soils would deform plastically by tracing down to the left of critical state line (i.e. towards the negative dilatancy direction with respect to the constant *p'* path in Figure 5.26 (a)).

A greater difference in peak shear strength (between BR-40-C and BR-40-E) was found in the effective stress path as the MICP-treated residual soil was inherent with anisotropic structure. All state points in the UR-40-C and UR-40-E specimens appeared to be very close to one another. At much higher consolidation pressures (i.e. 120 kPa and 220 kPa), the three state points could be distinguished easily. The present finding showed good agreements with the undrained triaxial testing on sand (Ishihara et al., 1975) by showing an early yielding before reaching instability (also called phase of transformation). Similarly, Lade (1992) reported that the yield point stayed closely with the instability point. The instability points as obtained in present experiment also did not occur at the maximum point of the effective stress paths as noticed in some studies (Lade, 1992; Lade, 1993; Chu et al., 2015). This was probably due to the fact that loose sands were tested in their studies.

Besides that, failure line was produced by fitting the ultimate state points for the soil specimens being consolidated to stress levels of 120 kPa and 220 kPa, respectively. After soil bio-mediation, the effective cohesion parameter was increased marginally from 4.8 kPa to 7.2 kPa, while the frictional angle remained unchanged at about 38°. This finding implied that no significant alterations in the properties of soil grains/ clogs, such as shape and

roughness. These results showed good agreements with the findings as reported by Feng and Montoya (2015) who studied the shear strength behaviour of lightly-cemented sand.

Untreated and MICP-treated Sands

Figure 5.27 shows the progressive AE points of untreated and MICP-treated sands along their respective stress paths.

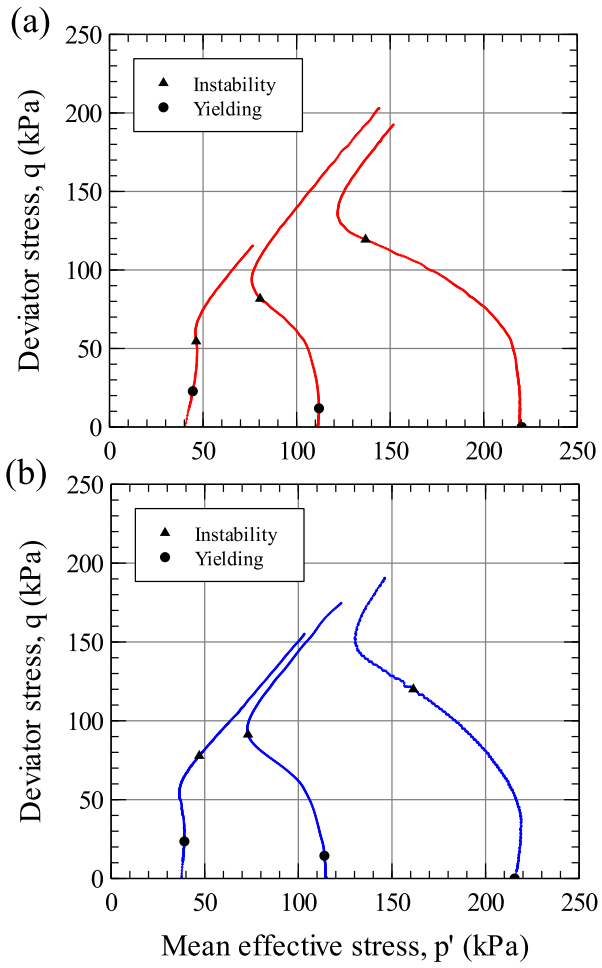

Figure 5.27: Effective stress paths and AE changes for tested sands: (a) untreated; (b) MICP-treated

Figure 5.27 highlights that the untreated and MICP-treated sands behaved like a dense sand, i.e. characterized with an apparent strain hardening until reaching a constant stress ratio asymptote (Chu et al., 2015). In such case, the ultimate point as to the critical state could not be obtained. It can be observed that the sands deformed elastically before they were yielded to transform into unstable phase. Dense sand would either exhibited apparent elasticity or strain hardening towards a constant stress ratio. Under a perfectly elastic and undrained situation, the increase of pore-water pressure equals the incremental mean effective pressure (external total stress is resisted by pore water). As such, the effective stress path would be vertically straight and there is zero change in the mean effective pressure (i.e. $\Delta p' \approx 0$).

Untreated and MICP-treated Over-consolidated Residual Soils

The effective stress paths for the untreated and MICP-treated over-consolidated residual soils are shown in Figure 5.28 (a) – (b), respectively.

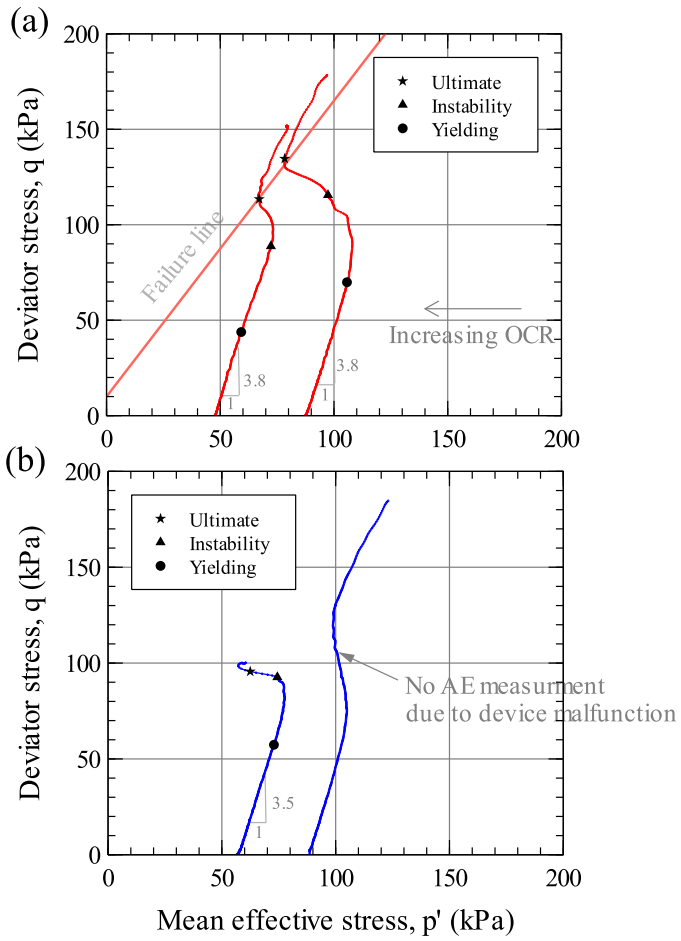

Figure 5.28: Effective stress paths and state changes for over-consolidated residual soils: (a) untreated; (b) MICP-treated

It is apparent from Figure 5.28 (a) that all the OC residual soil specimens exhibited strain hardening from the very beginning. The OC residual soils also manifested significantly greater elasticity than the other tested residual soils with different types of soil structures (e.g. compacted and MICP-treated). It is noticed that the yielding resistance of UR-OCR2.5-C specimen (q = 69.9 kPa) was much greater than that of UR-OCR5.0-C specimen (q = 43.8 kPa). Both untreated OC soils showed a similar gradient of incremental stress and strain changes (i.e. magnitude of gradients ≈ 3.8) along the effective stress path of yielding. It is also found that the gradient of stress change (i.e. magnitude of slope ≈ 3.5) of MICP-treated OC soil was very close

to those of the untreated OC soils. The outcome of comparison confirmed that the bio-mediated structure was substituted by the effect of over-consolidation.

When the deviator stress was continuously increased beyond the yield point, the UR-OCR2.5-C specimen apparently exhibited softening and gradually resembled the behaviour of a normally consolidated soil. The heavily OC residual soils could still retain their structural behaviour throughout the majority of undrained shearing (through yielding and instability phases). Moreover, the ultimate states were found to be compatible to the ultimate state envelope for the untreated residual soils (as already shown in Figure 5.26 (a)).

Through AE measurement, the progressive changes in soil deformation behaviour could be determined across different types of soils (residual soil, sand and bio-cemented soils). In line with a sound engineering design, AE monitoring can be implemented to detect the internal stability of soil skeleton and progression of deformation behaviour for in-situ ground.

5.3.3.2 Yield Loci of Residual Soils and Sands

Figure 5.29 compares the experimental yield points/ loci of tested residual soils and some previously reported yield points, which were reported on natural soil and soil consolidated under similar condition. The tested residual soil specimens included UR-OCR5.0-C, BR-OCR5.0-C, UR-OCR2.5-C, UR-CIUC, UR-CIUE, BR-CIUC, and BR-CIUE series of soils. It should be noted

that (MICP) residual soil specimens being consolidated to 80 kPa were additionally included in plotting yield loci to furnish a more comprehensive assessment on the yielding resistance of residual soils.

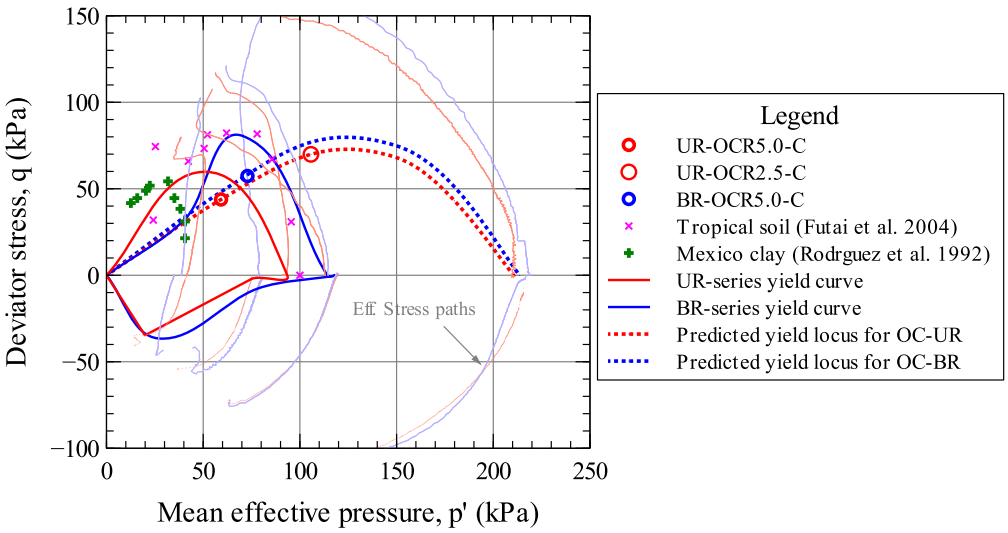

Figure 5.29: Yield locus for untreated and MICP-treated residual soils

The experimental yield loci of (MICP) residual soils were obtained by adjoining the experimental data points through Bézier curve (one kind of curve smoothening method), in which zero intercept was assumed. Particularly, the yield locus of OC residual soils were predicted by adjoining the front part (up to 120 kPa) of experimental data points from the untreated OC residual soils in conjunction with an anticipated isotropic parabola (Tanimoto and Tanaka, 1986) near the tailing end of the yield locus. The yield locus of MICP-treated OC residual soil was then predicted by multiplying a factor on the obtained loci of untreated OC soils to fit the only one available experimental data point from the BR-OCR5.0-C specimen. It should be noted that the present yield loci were only shown in dotted curves highlighting that

all predicted curves are not yet certain and further experimental data points have to be participated to form a more coherent results.

A soft Mexico clay (Rodrigues et al., 1992) and a tropical soil (Futai et al., 2004) were used to compare with the yielding results of (MICP) residual soils. These reported studies tested undisturbed soil specimens which were sampled from the superficial layer of soil deposit. Through the comparison, it can be realized from Figure 5.29 (a) that the MICP-treated residual soil had a much greater yielding resistance and coverage compared with the untreated residual soil. The yield loci of untreated residual soils apparently showed an apex at consolidation stress of 40 kPa. Also, the MICP-treated residual soil was prone to be anisotropic as manifested by the inclination of apex line (i.e. linear line adjoining the peak yields from the CIUC and CIUE tests). Therefore, it is essential to carry out additional tests within the prescribed consolidation pressure range to validate the above anticipation. Furthermore, the yield loci of OC residual soils were apparently greater and wider compared with those of untreated residual soils. The above findings confirmed that higher shearing resistance can be obtained in the overconsolidated and MICP-treated residual soil structures as attributed to the unloading-reloading compression and bio-mediation processes, respectively.

As depicted in Figure 5.30, the configurations of yield loci for both untreated and MICP-treated sands were quite similar to each other. The yielding resistances of MICP-treated sands were marginally greater than those of untreated sands. This finding was arguably linked to the uniform

distribution of weak calcite bonds within the dense sand specimens. It is also obvious that the dry-tamped and bio-mediated sands showed much lower yielding resistances as compared to the one observed in residual soils (as seen in Figure 5.29). This finding suggested that greater elasticity of soils can be obtained by compacting to a well-graded soil (comprising nearly 32 % of fines and some plasticity) or creating a stress-induced OC soil structure.

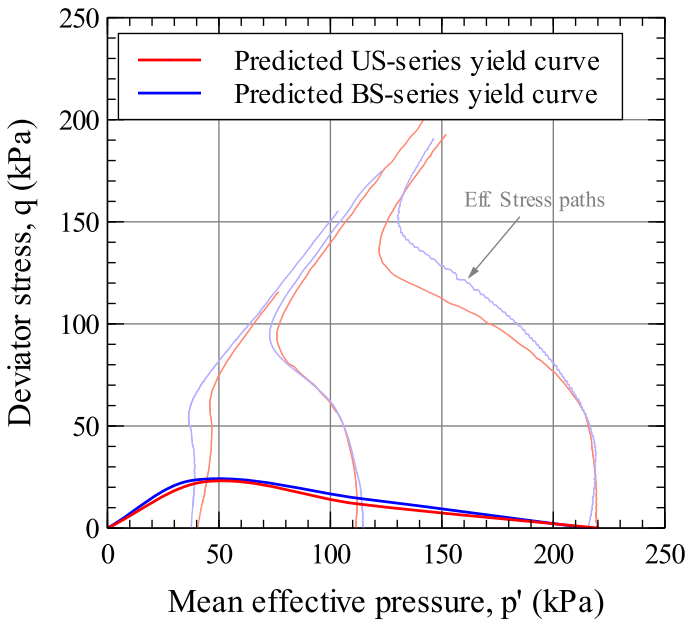

Figure 5.30: Yield locus for untreated and MICP-treated sands

-

5.3.3.3 AE Mobilization Changes in Stress Space

Figure 5.31 compares the progression of post-yielding AE mobilization in the stress space among all tested soil specimens, which constituted different types of structural formations. It is intended to compare the deviator stress levels required to mobilize the respective soil structural resistance and the rates of shear stress increase (i.e. *p'-q* ratio).

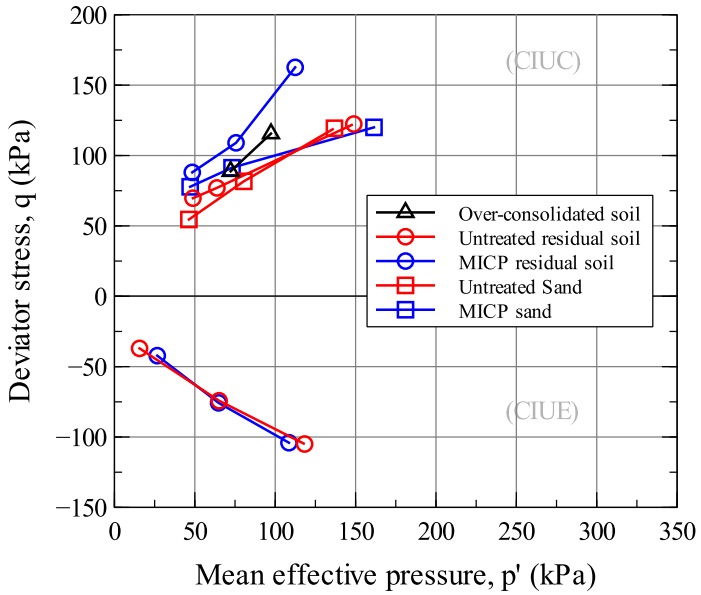

Figure 5.31: Comparison of instability points of soils with different structural formations

It is found that the instability points of MICP residual soils mobilized at a similar rate as compared to the untreated residual soil under triaxial extension condition. As compared to the untreated residual soils (formed with compacted structure), higher stress level was required to trigger the instability in MICP-treated residual soils. The gradient of shear stress increase for the MICP-treated residual soils was steepest among all types of soils. For the MICP-treated residual soil, the shear stress at the state of instability increased to the highest level when reaching consolidation pressure of 220 kPa. This could probably be justified by the greatest net calcite content (i.e. 2.7 %) being measured for the particular treated specimen (i.e. BR-220-C).

The over-consolidation effect was also profound since the rate of shear stress increase for OC residual soils was close to the one of bio-mediated residual soil. On the other side, a sign of structural degradation can be

observed in the MICP-treated sand that the gradient of shear stress increase instantaneously decreased after the MICP-treated sand was consolidated to 220 kPa. This observation was probably related to the unexpected high level of AE counts detected during the isotropic consolidation test as discussed in Section 5.2.

5.4 Influence of Bio-mediation effect on Soils as Investigated by Acoustic Emission

This section examines the behavioural differences of untreated and MICP-treated soils through mechanical and AE responses. The mechanical parameters, such as deviator stress and excess pore-water pressure, were fundamentally interpreted with respect to the axial strain parameter. Therefore, the progressive structural changes (namely, yielding, instability, and ultimate states) can be traced in the stress-strain, AE rate-strain, and excess pore-water pressure-strain relationships.

5.4.1 Behavioural Differences between Untreated and MICP-treated Residual Soils

5.4.1.1 Comparison of Deformation Behaviours between Untreated and MICP-treated Over-Consolidated Residual Soils

Figure 5.32 shows the relationships of stress-strain and AE counts rate-strain for the untreated and MICP-treated OC residual soils. It should be noted that

the AE measurement for BR-OCR2.5-C specimen was not obtained due to the malfunction of instrumentation device.

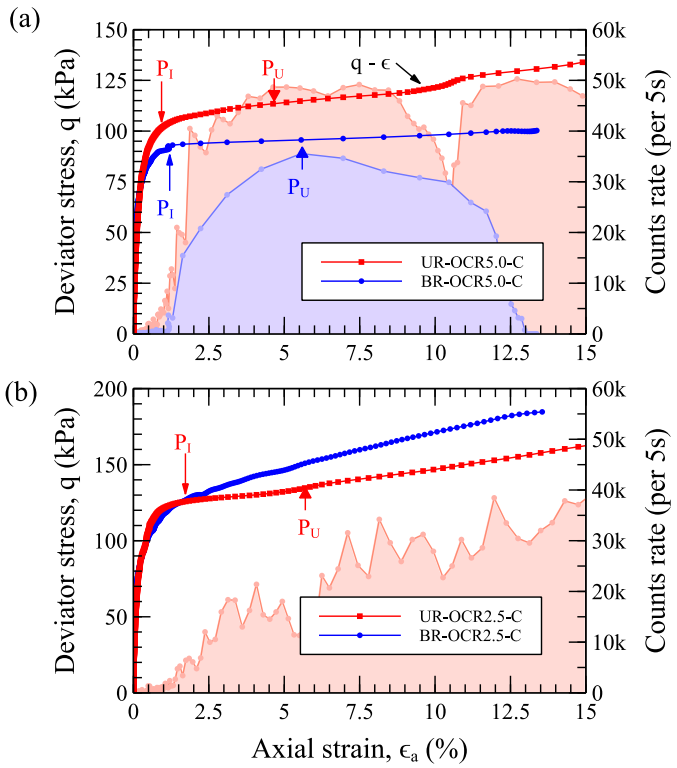

Figure 5.32: Mechanical-AE responses at full strain range for: (a) heavily over-consolidated; (b) lightly over-consolidated

It was observed that the shearing resistance at a larger strain range (> 1.0 %) of BR-OCR5.0-C was much lower than its untreated counterpart. This was due to lower density obtained for MICP-treated residual specimen compared with the untreated specimen at the end of isotropic consolidation stage. For instance, the final void ratio of MICP-treated specimen was 0.583 whereas the final void ratio for untreated specimen was only 0.571.

The structural resistance of OC residual soils, which were arguably relied upon the force chains and interactive contact between soil grains, would be dismantled when the applied stress was sufficient to mobilize the contacted soil grains and destruction of grains contacting network. These phenomena would occur once the soil had been yielded (as depicted in Figure 5.33) or transformed into an unstable state (reached instability point in Figure 5.32). The mobilization of soil particles could similarly be represented by the simplified soil interaction model as previously mentioned in Figure 4.7 of Chapter 4.

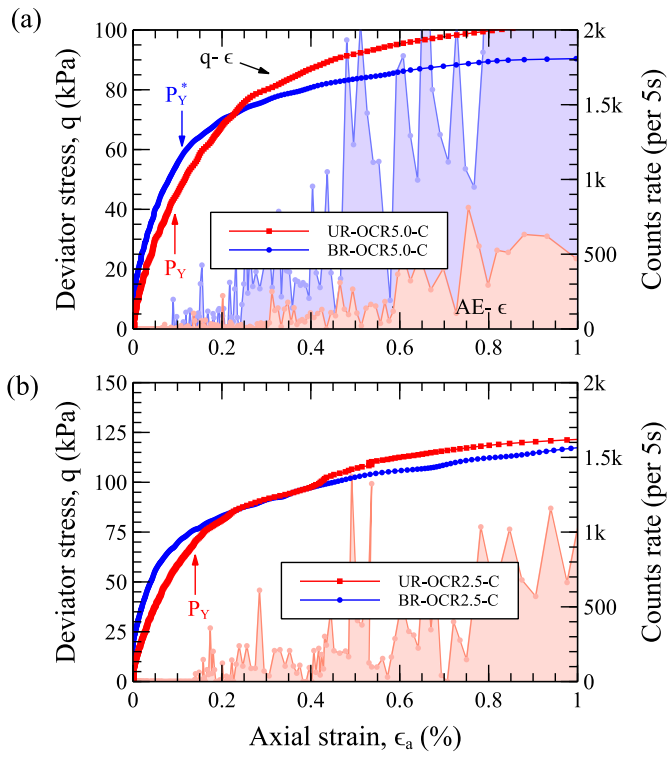

Figure 5.33: Yielding responses for: (a) heavily over-consolidated; (b) lightly over-consolidated

From the Figure 5.33, no early AE spike was detected for all untreated OC residual soils (UR-OCR5.0-C and UR-OCR2.5-C) before the yielding. The initial shearing resistances of MICP-treated OC residual soils appeared to be greater than the untreated residual soils. It was also observed that the yielding resistance of BR-OCR5.0-C was 57.38 kPa (in terms of deviator stress, q) and much greater than the untreated soil (q = 43.81 kPa), despite the shearing resistance at larger strain range (> 1.0 %) was overall greater in UR-OCR5.0-C (as found in Figure 5.32). This finding can perhaps be explained by the fact that the load-bearing resistant was greater in the MICP OC residual soil since a lower axial strain was measured in the isotropic unloading stage (referred to Section 4.3.1.4 in Chapter 4). It follows that the above-mentioned BR-OCR5.0-C specimen possessed higher yield resistance when it was lightly stressed.

Strangely, some earlier AE signals were detected prior to the yield point for the MICP OCR residual soil (i.e. BR-OCR5.0-C). This observation showed that a mild degree of calcite cementation would still be preserved in the bio-treated OC specimen even though it had been subjected to over-consolidation loading process. The dissipation of acoustic energy could be corresponded to the initial fracturing of calcite cementation. Unlike the fragmentation of a solid particles/ rock, in which high acoustic frequency (>100 kHz) was emitted, the present calcite cementation was so weak that its fracturing frequency was measurably low (<20 kHz).

Figure 5.34 shows the excess pore-water pressure responses of OC residual soils, namely UR-OCR5.0-C and BR-OCR5.0-C. The instability point (P_I) was found to be in proximity of the curvature change point of stress-strain responses and this point was corresponding to the major mobilization of soil grains. The increase of pore-water pressure for MICP-treated residual soil was lower in the lightly OC soil (i.e. OCR of 2.5) but greater when it was heavily OC residual soil (i.e. OCR of 5.0), in reference to the respective untreated counterparts. However, it is acknowledged that a more detailed investigation should be persuaded by conducting additional sets of over-consolidated soils. For instance, the reason of having lower magnitude in ultimate AE counts rate for the BR-OCR5.0-C specimen compared with UR-OCR5.0-C is still not understood.

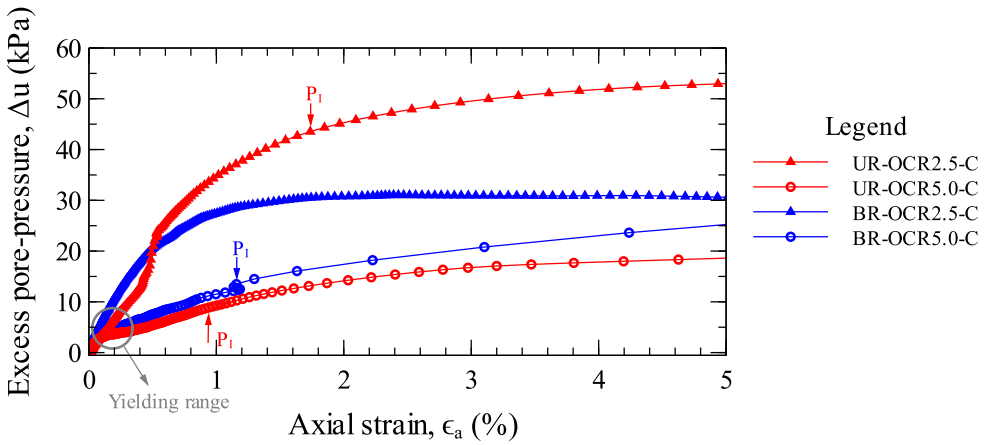

Figure 5.34: Excess pore-water pressure responses for untreated and MICP-treated over-consolidated residual soils

5.4.1.2 Comparison of Deformation Behaviours between Untreated and MICP-treated CIUC Residual Soils

Figures 5.35 (a) – (c) depict the stress-AE-strain responses for the untreated and MICP-treated residual soils under triaxial compression condition, from low to high consolidation stresses (i.e. 40 kPa, 120 kPa, and 220 kPa). The prescribed state points (i.e. instability and ultimate points) were marked to trace the soil structural progression in soils.

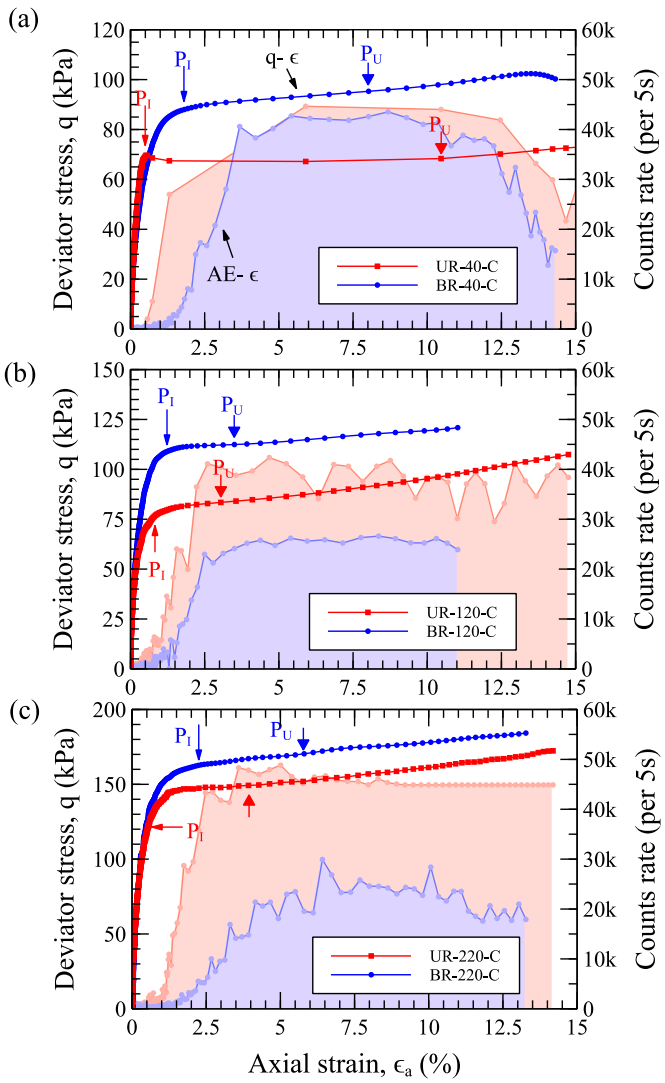

Figure 5.35: Mechanical-AE responses for CIUC-series untreated and MICP-treated residual soils at full strain range under different consolidation pressures: (a) 40 kPa; (b) 120 kPa; (c) 220 kPa

Generally, the instantaneous AE counts rate was comparable to the pattern of stress-strain curve, i.e. an initial rise and followed by a steady stress change. Lin et al. (2020) also observed that the mechanical responses of a silica sand were corresponded to the AE rate change throughout the shearing process. Interestingly, the ultimate levels of AE counts rate for MICP-treated residual soils (particularly BR-120-C and BR-220-C) were lower than those of untreated residual soils. This is probably linked to the calcite densification effect, in which the movement of soil particles were spatially restricted by the precipitated calcites in the pore spaces.

It can also be observed from Figure 5.35 that major grains mobilization (instability state) for the MICP-treated residual soils occurred at a much higher deviator stress level and strain amplitude, as compared to the untreated residual soils. This can be reasoned by the spotted calcite densification effect, which contributed to the increased load-bearing resistance and ultimate shearing strength. This is perhaps analogous to the mechanism of matrix-supporting system in bio-cemented sand as reported by Lin et al. (2016). The instability state for (MICP) residual soils were likely to be triggered by different kinds of mobility mechanisms, such as slippage of soil particles, reorientation of particles into the pore space (i.e. well-graded residual soil arrangement), collision between two particles, rolling of solid particles, and progressive fragmentation of grains/ calcite clusters. Figure 5.36 illustrates the above-mentioned bio-mediated soil structure in which the residual soil particles were idealized as spheres in order to facilitate the explanation. However, it should be kept in mind that the actual soil arrangement constituted

a well-graded soil distribution covering a variety of particle sizes and shapes. Since the present experiment focused on dislocation movement of soil particles and the resonant frequency of AE sensor was only 32 kHz, the high-frequency content (>100 kHz) of AE response as triggered by particle fragmentation (Lin et al., 2020) could not be taken into account. Even though a very sensitive (with wide range of measuring frequencies) AE sensor is used, it is still practically tough to distinguish soil movements (e.g. particles slippage, collision of particles, and grain fragmentation) based on the frequency contents of AE signals on account of the fact that the properties and physical configuration of each soil grain is different. The AE response of a soil body (e.g. triaxial specimen) might not be truthfully obtained by simply examining the AE response of a single particle.

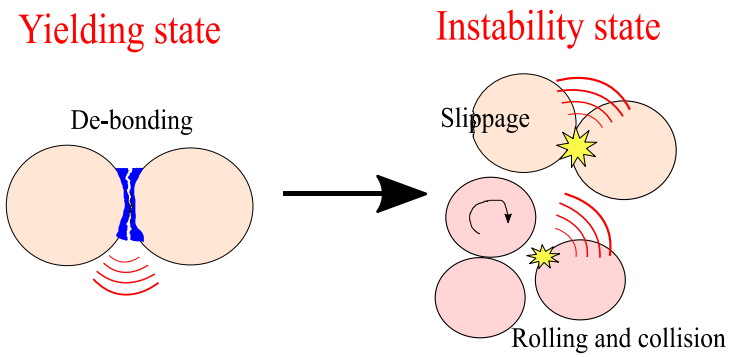

Figure 5.36: Idealized mobilization of MICP-treated residual soil grains under yielding and instability states

When the soil specimens were sheared to the ultimate state (P_U), the AE counts rate gradually became steady. The BR-40-C specimen somewhat showed greater magnitude of AE rate (i.e. 42591 counts per 5 s) as compared to the other MICP-treated residual soils (i.e. 23143 – 29923 counts per 5s) owing to the lowest confining pressure (i.e. 40 kPa) being applied among all

other MICP-treated residual soils. This finding was somehow in contrast to the BR-OCR5.0-C specimen (as depicted in Figure 5.32 (a)) inasmuch as the loading-unloading process, although both specimens were eventually consolidated to a similar pressure level (≈ 40 kPa).

At a much smaller strain range, as depicted in Figure 5.37, the yielding responses of untreated and MICP-treated residual soils can be examined closely.

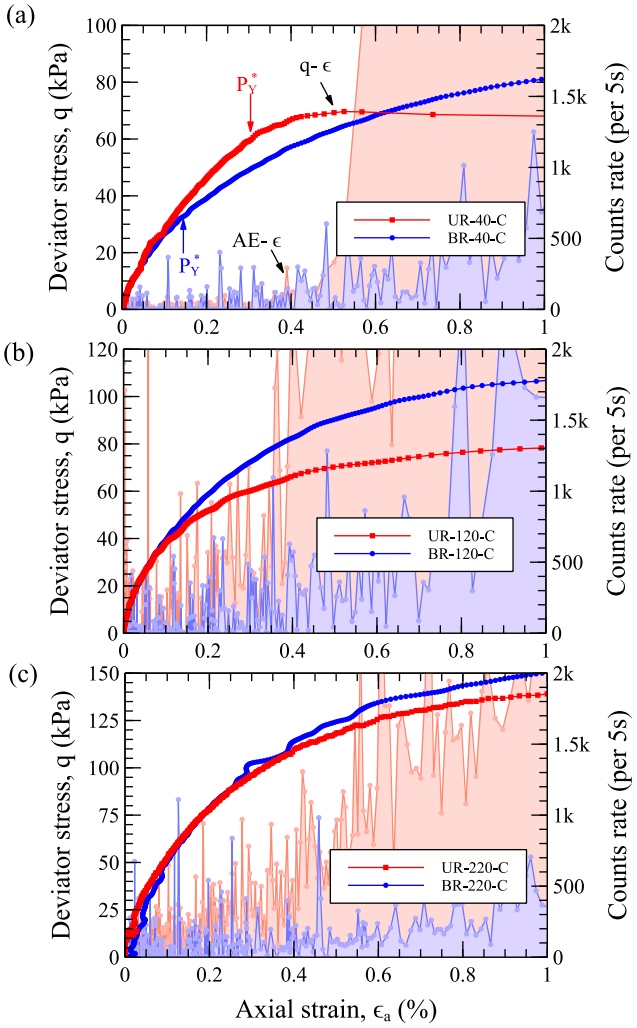

Figure 5.37: Yielding responses for CIUC-series untreated and MICP-treated residual soils under different consolidation pressures: (a) 40 kPa; (b) 120 kPa; (c) 220 kPa

Figure 5.37 (a) shows that the effect of initial compacted structure was more dominant than the MICP-treated structure at an effective consolidation pressure level of 40 kPa. The yielding resistance for UR-40-C specimen (i.e. q = 59.78 kPa) was much greater than that of BR-40-C specimen (i.e. q = 32.49 kPa). Some early spikes of AE signal, whose AE magnitude was below 500 counts per 5 s, were also detected before the yielding of BR-40-C specimen. This implied the fragmentation of weaker calcite cementation that was similarly observed in the MICP-treated OC residual soil. Calcite bonding would be completely destroyed upon the yielding state. At isotropic consolidation stress of 120 kPa and 220 kPa, both untreated and MICP-treated residual soils yielded from the start of undrained shearing.

From the above findings, it is noticed that untreated residual soil specimen possesses distinctive yield point when they were subjected to over-consolidation process or when the initial compaction effect was still preserved. Noticeable extent of early AE counts could be detected when the soil was subjected to bio-mediation effect or the soil was consolidated to a larger stress level (≥120 kPa). Figure 5.38 shows the excess pore-water pressure measurements for untreated and MICP-treated residual soils under triaxial compression condition.

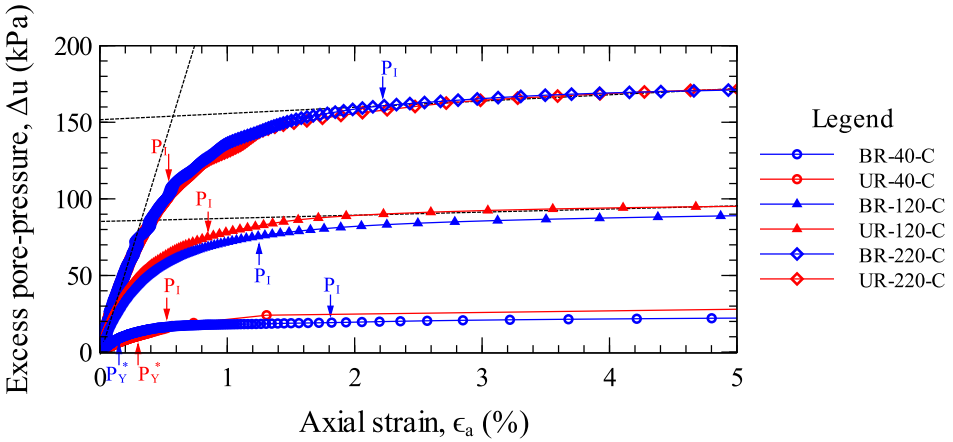

Figure 5.38: Excess pore-water pressure responses for untreated and MICP-treated residual soils under triaxial compression condition

For the normally consolidated soils, the pore-water pressure increased with the applied consolidation stress. All the tested soils showed a consistent trend, namely the inherent structure was diminished upon first yielding, contraction of soil skeleton accompanied by significant generation of pore-water pressure, and followed by the remobilization of soil grains (i.e. P_I state). As compared to the untreated residual soils tested at a same consolidation pressure level, MICP-treated residual soils tended to prolong the duration between incipient points of significant pore-water pressure (i.e. the curvature change point along the pore-water pressure curve) and remobilization of soil grains; manifesting greater deviator stress and strain amplitude. This is attributed to the greater shearing resistance and effect of calcite densification in the MICP-treated residual soil. The calcite clogging effect formed a less permeable soil matrix (Ivanov and Chu, 2012; Ng et al. 2014) in which the pore water would have less tendency to dissipate and therefore less particle movements were mobilized (Canakci et al. 2015). For this reason, the magnitudes of excess pore-water pressure for the MICP-treated residual soils

(except from soils being consolidated to 220 kPa) were found to be lower than the untreated residual soils. For example, the ultimate excess pore-water pressure levels for UR-120-C and BR-120-C specimen were 91.3 kPa and 85.9 kPa, respectively. At consolidation stress of 40 kPa, the untreated residual soil showed an ultimate excess pore-water pressure level of 27.0 kPa, which was much higher than that of MICP-treated (i.e. 20.41 kPa).

5.4.1.3 Comparison of Deformation Behaviours between Untreated and MICP-treated CIUE Residual Soils

Figure 5.39 shows the stress-AE-strain responses for the tested CIUE residual soil specimens. Considering the CIUE soil specimens deformed more abruptly than the CIUC specimens, the ultimate state point was herein chosen at the instant when the AE counts rate was on the verge of decreasing.

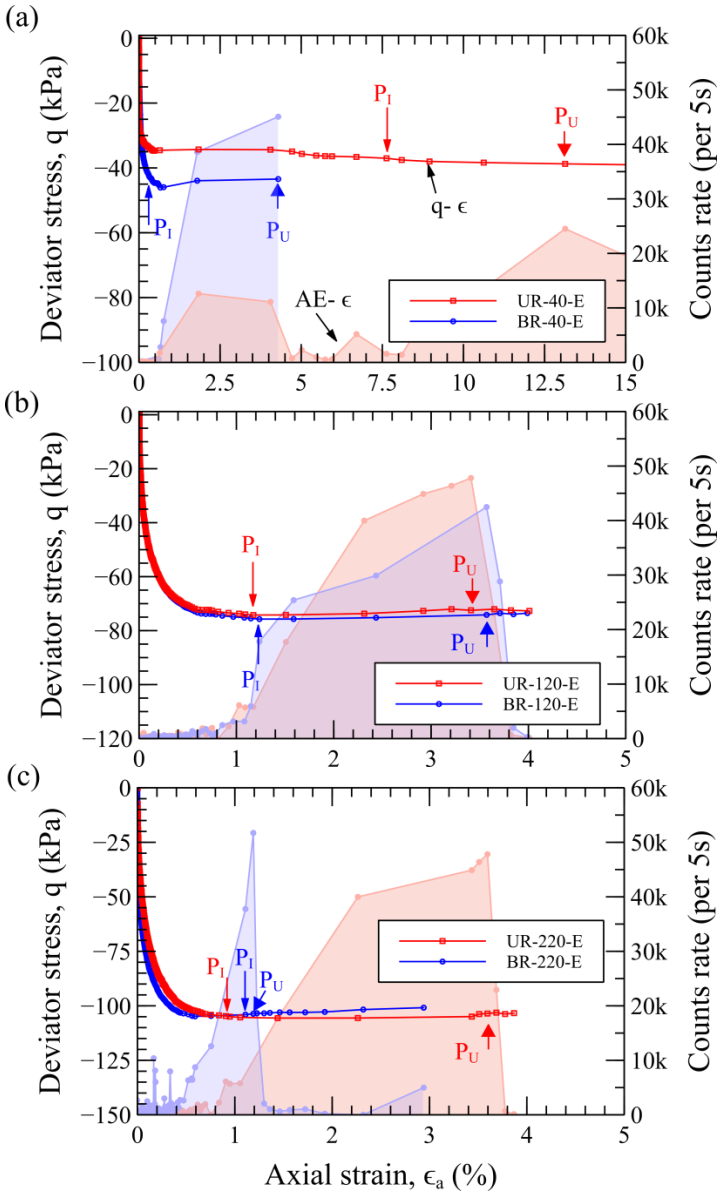

Figure 5.39: Mechanical-AE responses for CIUE-series untreated and MICP-treated residual soils at full strain range under different consolidation pressures: (a) 40 kPa; (b) 120 kPa; (c) 220 kPa

The BR-40-E somewhat exhibited strain-softening behaviour in conjunction with an abrupt rise in AE counts rate. This behaviour was similar to the strain-localized failure of extension tested specimen as reported by Lade and Tsai (1985). They claimed that localized failure would lead to a lower shear strength and induce dilatant behaviour. Beyond the consolidation pressure of 40 kPa, both untreated and MICP-treated residual soils resembled

to each other in terms of similar degree of ultimate shear strength and excess pore-water pressure responses (as evidenced in Figure 5.40). It was observed that the BR-40-E specimen exhibited dilation behaviour and coupled with a decrease in pore-water pressure (maximum excess pore-water pressure of nearly -6 kPa), whereas the remaining soil specimens showed continuous increase in excess pore-water pressure. The highest excess pore-water pressure from CIUE-series tests was found to be 90.82 kPa and significantly lower than that from CIUC-series soils (i.e. 168.5 kPa), resulting from the different nature of loading mechanism. The upward movement in CIUE test would tend to induce a less contractive behaviour in the soil.

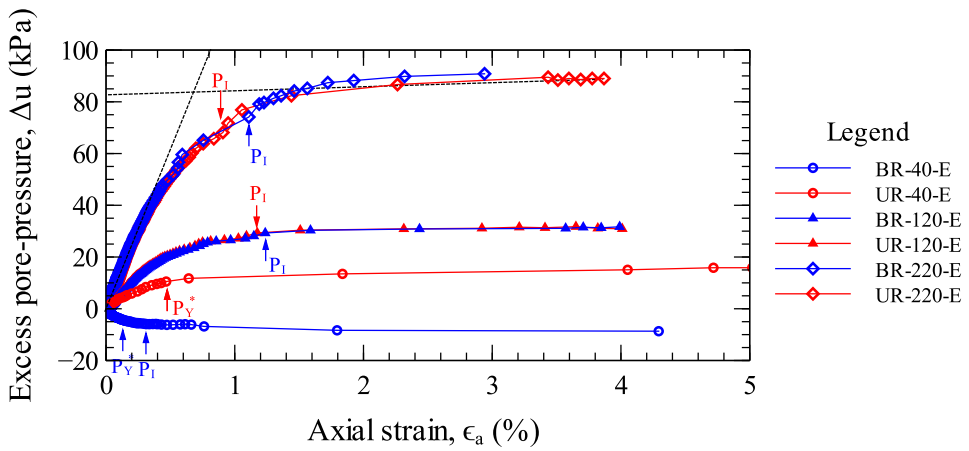

Figure 5.40: Excess pore-water pressure responses for untreated and MICP-treated sands under triaxial extension condition

Figure 5.41 (a) shows that the BR-40-E specimen possessed a higher yielding resistance at a lower axial strain range (<1.0 %), as compared to its untreated counterpart. Specifically, the (triaxial extension) yielding resistance of BR-40-E specimen was 36.53 kPa while the UR-40-E was 34.72 kPa. Once the (MICP) soil specimens were isotropically consolidated to 120 kPa and 220 kPa, they were yielded from the beginning of shearing stage. Surprisingly, the

shearing strength for the BR-220-C at a smaller strain range (<1.0 %) was still found to be greater than that of the BR-220-E since the anticipated anisotropic structure did not favour the increase in extension resistance (as illustrated in Figure 4.4 of Chapter 4).

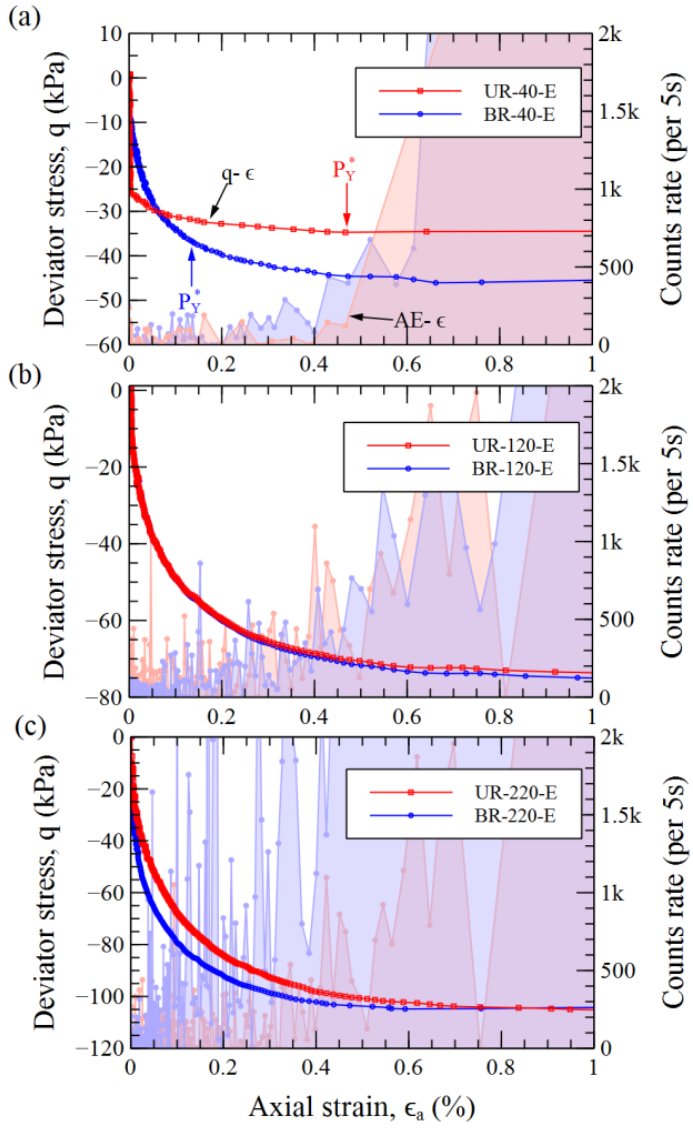

Figure 5.41: Yielding responses for CIUE-series untreated and MICP-treated residual soils under different consolidation pressures: (a) 40 kPa; (b) 120 kPa; (c) 220 kPa

5.4.2 Behavioural Differences between Untreated and MICP-treated Sands

Figure 5.42 clearly shows that the (MICP-treated) sands behaved differently from the (MICP-treated) residual soil. It is possible to differentiate the behaviour of MICP-treated sand from the untreated sand through AE measurement. The less tendency of calcite densification for MICP-treated sands as discussed in Chapter 4 was further verified in the present AE responses between BS-120-C and BS-220-C, in which the magnitudes of AE counts rate were not lower than those of untreated soils. However, it is still unclear on why BS-120-C specimen possessed lower ultimate shearing resistance when it had a much lower level of AE counts rate. Interestingly, it was observed for the BS-220-C specimen that the fracturing calcite crystals would cause a much weaker structure (based on the higher magnitude of AE counts rate) after the calcite cementation had been completely demolished (i.e. yielded).

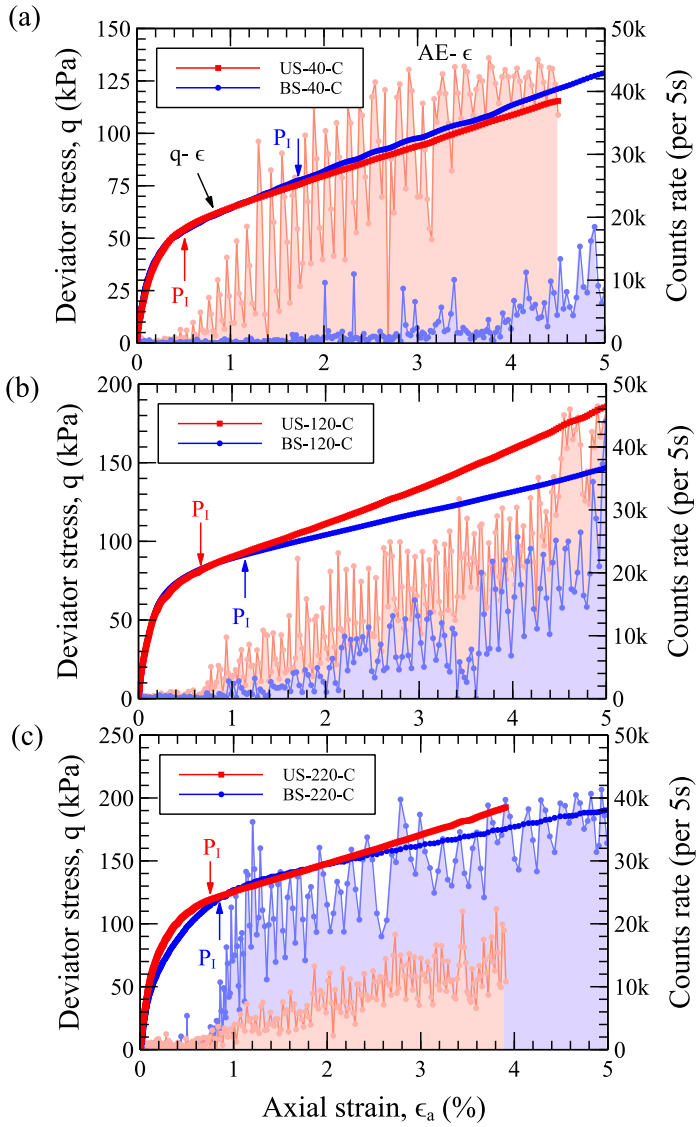

Figure 5.42: Mechanical-AE responses for untreated and MICP-treated sands at full strain range under different consolidation pressures: (a) 40 kPa; (b) 120 kPa; (c) 220 kPa

Unlike the (MICP-treated) residual soil, both untreated and treated sands manifested strain hardening and continuous increase of AE counts rate throughout the undrained shearing stage. This observation suggested that the mechanism behind strain-hardening phenomenon was in line with the increasing AE counts rate. As such, only two state points (i.e. first yielding and instability points) were determined for the tested sands and the ultimate

state point was unattainable. The instability points for the MICP-treated sands were found to be of greater magnitude than the untreated sands; the differences in deviator stress become less significant with the increase of isotropic consolidation pressure.

When the soil reached an instability condition, it is conceivable that the movement of soil grains would be dominated by plastic slippage over adjacent surfaces of particles and incipient dislocation at the contacted point of interlocking. The observed zig-zag AE responses (Figure 5.42) confirmed that mobilization of sand grains relied on the localized slippage within a densely-packed structure (i.e. D_r = 82 %), in which the sand grains were difficult to be relocated by occupying the voids like residual soil. After the applied stress was sufficiently high to trigger the localized slippage of particles, sand structure would immediately transform into a temporary meta-stable condition (as manifested by the sudden decrease of emission rate in the zig-zag AE response) prior to the consecutive remobilization of particles. The above microstructural interaction within bio-cemented sand can be simplified into an illustrative diagram as shown in Figure 5.43 below. For dense specimen made of rounded sands, Smith and Dixon (2019) also observed that the AE counts rate would experience peak-trough fluctuation after dilation. In fact, the described phenomenon was found to be sensitive to the rate of straining.

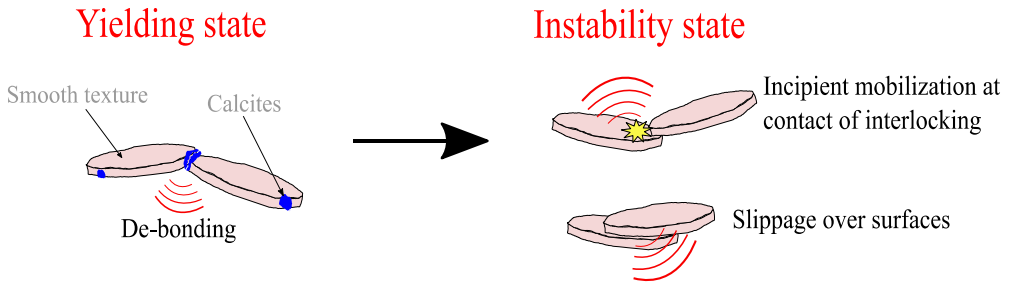

Figure 5.43: Idealized mobilization of weakly-cemented sand grains under yielding and instability states

The yielding resistances for the BS-40-C (q=23.54 kPa) and BS-120-C (q=14.41 kPa) specimens were found to be marginally greater than those of untreated sands (q=22.80 kPa for US-40-C; q=11.88 kPa for US-120-C), as shown in Figure 5.44 (a) - (b). The increase of yield resistance was largely caused by the weak calcite bonding as observed inside the MICP-treated sand structure. After the soil specimen had been consolidated to 220 kPa, both untreated and MICP-treated sands yielded from the commencement of undrained compression due to calcite de-bonding. The shearing resistance of BS-220-C specimen was overall lower than that of US-220-C specimen from small (Figure 5.44) to large strain range (Figure 5.42), in view of the MICP stress-strain curve progressed below the untreated curve.

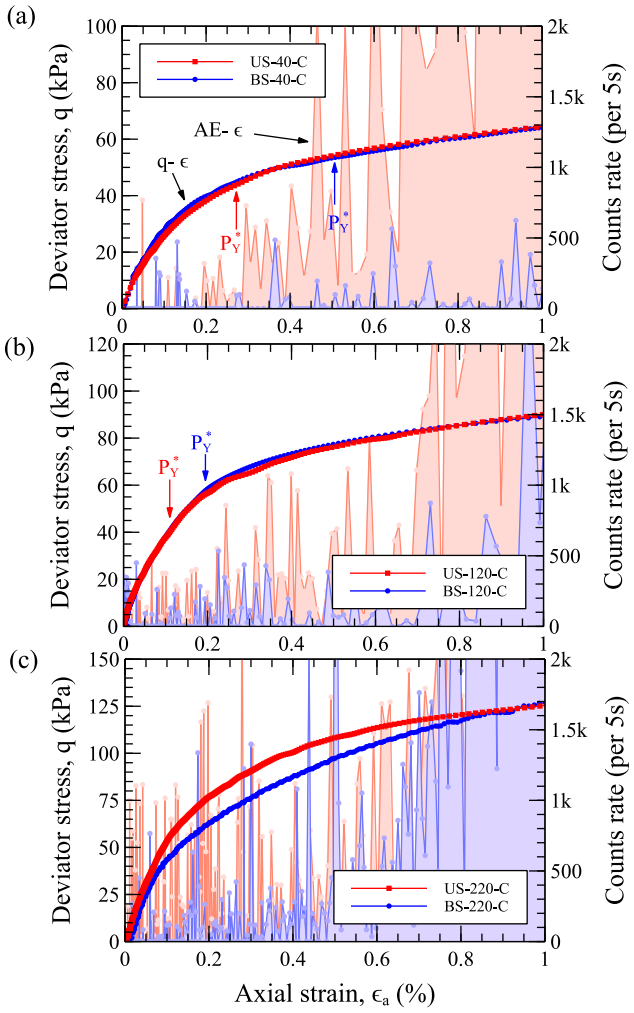

Figure 5.44: Yielding responses for untreated and MICP-treated sands under different consolidation pressures: (a) 40 kPa; (b) 120 kPa; (c) 220 kPa

As depicted in Figure 5.45, sand dilation was realized as the excess pore-water pressure was gradually reduced after reaching the instability point (particularly for soils consolidated to 40 kPa and 120 kPa). At a small strain range (≤ 1%), BS-40-C and BS-120-C had higher yielding resistances despite of having higher generations of pore-water pressure. At consolidation pressure of 220 kPa, the untreated sand somewhat showed a higher shearing resistance than the MICP-treated sand, owing to the formation of weak structure as mentioned in Figure 5.44. Within the large strain range (>3 %), all the tested

sands consistently showed that a higher shearing resistance corresponded to a lower change in excess pore-water pressure.

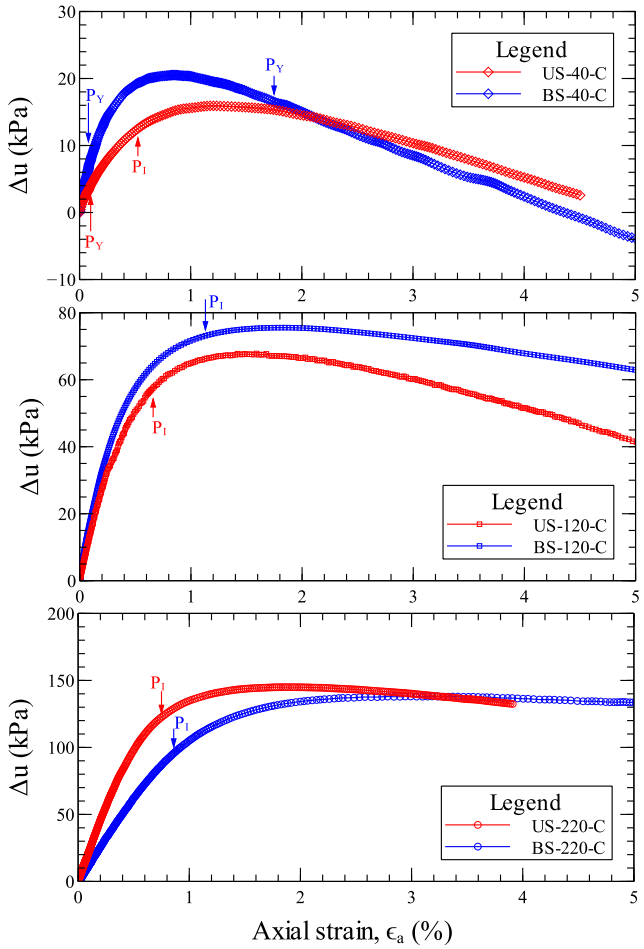

Figure 5.45: Excess pore-water pressure responses for untreated and MICP-treated sands

5.5 Concluding Remarks

Several conclusive statements can be drawn from the discussion in this chapter:

Isotropic consolidation behaviours

- The void ratio changes of the tested soils could be correlated to the change in cumulative AE counts. After the de-bonding, calcite densification played an important role to provide clogging and stiffness to the soils. These were evidenced by the increased isotropic yield pressure and reduced compressibility through AE and deformations interpretations. There were also signs of calcite fragmentation in the MICP-treated sands, which exhibited deformation characteristics very much like the untreated sands.
- Under normal consolidation state, the compression index increased with the AE incremental rate. The MICP-treated residual soil showed lower compressibility and AE incremental rate, as compared to the untreated residual soil. This was attributed to the effect of calcite densification in the MICP-treated residual soils.

Changes of AE points for residual soils and sands in Undrained Shearing

- All (MICP) residual soils underwent three distinctive AE changes: yielding, instability, and ultimate states. Upon yielding, inter-particles resistance and calcite bonding (for MICP-treated soils) were destroyed. The soils exhibited plastic deformation by dissipating energy in form

of Acoustic Emission (AE). Next, the soil experienced an instability state in which tremendous mobilizations of soil grains were triggered. The ultimate state was linked to the eventual failure of soil specimen after the AE rate became steady (CIUC) or ready to decrease abruptly (CIUE).

- The untreated and MICP-treated sands exhibited strain hardening and underwent two distinctive AE changes, namely yielding and instability points. Beyond the instability point, sand specimen being consolidated to 40 kPa and 120 kPa would manifest dilatant behaviour in view of the reduction in pore-water pressure.

Undrained shearing behaviours of (MICP) OCR residual soils

- Untreated OC residual soils showed no early sign of AE before yielding. Effect of OCR would provide distinctive structural resistance, which relied upon the force chains and interactive contact between solid grains. Over-consolidated soils can facilitate a more resistant structure as compared to the lightly-cemented residual soil structure.
- Although the original OC soils had a greater ultimate shearing resistance, yielding resistance could still be observed in the MICP-treated OC residual soil when it was lightly stressed.
- The structural resistance of OC residual soil was relied upon the force chains and interactive contact between solid grains. It would be dismantled when the applied stress was sufficient to mobilize the contacted soil grains and destruction of grains contacting network.

Undrained shearing behaviours of (MICP) residual soils

- The MICP-treated residual soil had a greater magnitude and extent of yielding resistance as compared with the untreated residual soil.
- Effect of calcite densification was dominant in providing greater ultimate shearing resistance. Significant grains mobilization (instability state) for the bio-mediated residual soils occurred at a much higher deviator stress level and strain amplitude. It could be related to the slippage of soil particles, reorientation of particles into the pore space (i.e. well-graded residual soil arrangement), collision between two particles, rolling of solid particles, and progressive fragmentation of grains/ calcite clusters.
- Compaction effect was still preserved in the residual soil when the residual soil specimen was consolidated to 40 kPa only. Both untreated and MICP-treated residual soils started to yield from the beginning when the soils were consolidated to higher pressure levels, namely 120 kPa and 220 kPa.
- As compared to the CIUC soils, the behaviour of soils under triaxial extension (CIUE) condition appeared to be more abrupt by failing at lower strain amplitude and exhibited strain-softening at consolidation pressure of 40 kPa. The yielding and ultimate shearing resistance for the MICP-treated soil at 40 kPa were higher than those of untreated soil. Beyond isotropic stress level of 40 kPa, the shearing behaviours of both the treated and untreated residual soils were resembled to each other.

Undrained shearing behaviours of (MICP) sands

- Comparing to the untreated sands, a slight improvement on yielding resistance was also realized in the MICP-treated sands, probably attributed to the weak calcite bonding within the sand.
- The untreated and MICP-treated sands manifested strain hardening and continuous increase of AE counts rate throughout the undrained shearing. Therefore, only yielding and instability states were determined for interpretation of progressive changes in deformation behaviour.
- When the soil reached an instability condition, it is conceivable that the movement of soil grains would be dominated by plastic slippage over adjacent surfaces of particles and incipient dislocation at the contacted point of interlocking.

CHAPTER 6

CONCLUSIONS

6.1 Summary

To date, no experimental study has yet been done in comparing the mechanical behaviours of MICP-treated residual soil and sand (as a benchmarked MICP material). Although the mechanical behaviour and microscopic formation (namely, fabric anisotropy) of MICP-treated sand have been studied intensively (DeJong et al., 2010; Montoya, 2012; Lin et al., 2016; Jiang et al., 2016; Cui et al., 2017), limited extent has been contributed to the residual soil (Lee et al., 2013; Sharma and Ramkrishnan, 2016; Chiet et al., 2016). Therefore, the mechanical and Acoustic Emission (AE) behaviours of MICP-treated tropical residual soil were investigated in comparison with the MICP-treated sand in the present research. The effect of bio-mediation and isotropic consolidation pressure towards the stress-deformation behaviours of soils were also investigated in detail. The behaviours of untreated and MICP-treated specimens were tested using a monotonic (i.e. static loading) triaxial apparatus which was instrumented with global stress-strain, pore-water pressure, and AE measurements. Specifically, a series of saturated triaxial soil specimens were first subjected to isotropic consolidation prior to the undrained shearing tests. The obtained mechanical responses were scrutinized in parallel

with the AE monitoring so as to examine the progressive changes in deformation behaviours of soils.

6.2 Concluding Statements

Three conclusions can be drawn from the present experimental study to address the three objectives set forth in the Chapter 1:

i. To study the effects of MICP on structural formations of soils.

The deformation behaviour of MICP residual soil was inherently anisotropic whereas the MICP sand was isotropic owing to their different structural formations.

MICP-treated residual soil

The MICP-treated residual soil was inherent with structural anisotropy in which calcite cementation was preferably formed at the sides of the soil grains. This anisotropic structure resulted in the bio-mediated residual soil tending to deform along the vertical direction of a specimen under isotropic compression (as evidenced in the correlation between radial and axial strains). This finding was further justified by a less profound bio-mediation effect in the triaxial extension test since the laterally-formed calcite cementation would not contribute much tensile strength along the vertical direction. During the isotropic unloading, the MICP-treated residual soils (namely, soils subjected to OCR = 5) tended to deform in the

lateral direction owing to the preceding effect of isotropic compression and relaxation on the bio-mediated residual soil structure.

Bio-mediation effect also markedly increased the calcite bonding and densification, based on the results of isotropic yield stress (increased by nearly 21 kPa in average) and compressibility (i.e. the average compression index decreased by 0.082). This improvement was comparable to those of artificially cemented soils (Rotta et al., 2003; Malandraki and Toll, 2001; Rios and Baudet, 2014) and attributed to the increase in inter-particles resistance (De Jong et al., 2010; Cui et al., 2017). The studied residual soil constituted a well-graded soil arrangement and favoured the calcite precipitations, but at the expense of having a less uniform and heterogeneous MICP soil structure.

MICP-treated sand

MICP-treated sand constituted an isotropic and stiffer soil structure compared with the MICP-treated residual soil. The isotropic structure was attributed to the tamping effect on the lightly-cemented sand, which constituted a structure with uniform calcite distribution. Anisotropic structure would be induced by free depositing the sand into a mould, but soil fabric would be diminished and transformed into isotropic arrangement after tamping process (Oda, 1972). It is confirmed that the isotropic yield stress of MICP-treated sand was improved by only 3.8 kPa and the compression index was slightly decreased by 0.003. Weak calcite bonding existed in the treated sand specimen as a result of light

cementation (average calcite content ≈ 3.73 %) precipitated within the dense structure (i.e. $D_r \approx 82$ %).

ii. To investigate the influence of consolidation stress on mechanical behaviours of MICP-treated soils in undrained shearing.

There was improvement in the shear strength of MICP residual soil from low to high consolidation stress, but the undrained shear strength for lightly-treated sand was not improved.

MICP-treated residual soil

When the applied consolidation pressure was increased to 120 kPa, the MICP-treated soils would become normally consolidated by tracing down to the left side of effective stress paths and exhibited plastic deformations (i.e. the soil yielded at the start of shearing). As compared to the CIUC-series soils, the effect of bio-mediation was not profound in the CIUE-series residual soil owing to the induced anisotropic structure in the MICP-treated residual soil. The stress-strain relationships of MICP-treated residual soils showed that the increase in ultimate compressive strength (i.e. 26.96 kPa) was much greater than that of triaxial extension test (i.e. 4.69 kPa), under a same consolidation pressure of 40 kPa. The ultimate shear strength of MICP-treated residual soil was arguably contributed by the effect of calcite densification (DeJong et al., 2010) in which calcite clusters occupied the pore spaces and furnished bearing resistance.

MICP-treated sand

Both untreated and MICP-treated sands progressed to an asymptote of constant shear stress ratio under different levels of consolidation pressure. As similar to the behaviour of typical dense sand (Chu et al., 2015), the MICP-treated sands exhibited strain hardening and dilatancy throughout the undrained compression. However, the strength of MICP-treated sand was not significantly improved as compared to the untreated counterpart. The insignificant improvement in undrained shearing resistance was caused by the bio-mediation effect being concealed as a result of the light cementation (net calcite content ≈ 3.8 %) in dense sand (D_r ≈ 82 %). The elastic stress-deformation behaviour (i.e. yielding resistance) was completely diminished when the sands were consolidated to 220 kPa.

iii. To examine the progressive changes in deformation behaviours of MICP-treated soils through mechanical and Acoustic Emission measurements.

Both MICP residual soil and sand experienced calcite de-bonding (isotropic yielding) and grains movement (major deformation) during isotropic consolidation stage. Under undrained shearing, the MICP residual soils manifested three state change points (i.e. yielding, instability, and ultimate failure states) whereas the MICP sand only showed two change points (i.e. yielding and instability states) owing to their different deformation behaviours.

Consolidation stage

During the isotropic consolidation test, the deformation (i.e. volumetric and axial strains) of tested soils would increase with the applied consolidation stress. When the isotropic consolidation pressure reached the isotropic yield stress (i.e. major structural degradation), calcite de-bonding would be triggered whereupon the load-bearing resistance would dominantly be substituted by the calcite filling (densification) effect. Progressing to a greater consolidation pressure, the calcite clusters in the pore space would experience progressive fracturing as evidenced from the observations of mechanical and AE.

Undrained shearing stage

MICP-treated residual soil

All MICP-treated residual soils first experienced yielding, in which the inter-particles resistance and calcite bonding (for MICP-treated soils) were dismantled. Prior to the yielding, fragmentation of calcites occurred and accompanied by dissipated acoustic energy. Next, the soil experienced an instability state in which tremendous dislocation of soil particles were triggered. Finally, the residual soil would reach the ultimate failure state as manifested by a steady or reduced-rate of AE change.

Under undrained compression, the yielding resistance (in terms of deviator stress) of MICP-treated residual soil was gradually diminishing as the applied isotropic consolidation pressure was increased from 40 kPa to 220 kPa. Calcite bonding in the bio-mediated residual soil structure could

not resist a consolidation pressure as high as 120 kPa, since the highest isotropic yield stress was only 102.8 kPa. It is also concluded that the yielding resistance of MICP-treated residual soil (i.e. 80.42 kPa) was much higher than that of untreated-treated residual soil (i.e. 59.78 kPa). With the increase of consolidation stress, the instability states were shown to be locating close to the failure state in conjunction with significant generation of pore-water pressure. A much higher shear stress was required to trigger the instability state in the MICP-treated residual soil as compared to other types of soils. Meanwhile, the difference between ultimate shear strength of MICP-treated and untreated soils would become lower (i.e. from 28.36 kPa to 21.61 kPa) owing to the continuous fragmentation of calcite clusters in the pores (decreasing effect in calcite densification).

Coincidentally, the MICP-treated residual soil in CIUE-series test would become normally consolidated when the isotropic consolidation pressure exceeded 40 kPa. The MICP residual soils would transform from dilatant to normal consolidation behaviour in light of the strain-softening effect and decreasing excess pore-water pressure.

MICP-treated sand

MICP-treated sands would first experience yielding upon the breakage of calcite bonding that adjoining the sub-angular sand particles. As the shear stress was increased monotonically, the sand would reach an instability point at which movement of soil grains would be dominated by plastic slippage over adjacent surfaces of particles and incipient dislocation at the

contacted point of interlocking. This would instantaneously result in a temporary metastable structure of dense sand. Beyond the instability point, the initial compressible behaviour of (MICP) sand was transformed into dilatant behaviour.

The yielding resistance of MICP-treated sand remained almost unchanged (ranging from 23.54 kPa to 14.41 kPa) as the consolidation pressure was increased from 40 kPa to 120 kPa, since the inter-particles resistance (average isotropic yield stress of 136 kPa) had not been fully mobilized. The MICP sand started to yield from the commencement of undrained shearing when the consolidation pressure was increased to 220 kPa. Beyond 40 kPa, the bio-mediation effect on shearing responses in larger-strain range (>1.0 %) was substituted by the dilatancy effect in dense sand. For MICP-treated sand, the shearing resistance at instability state was greater than the untreated sand from 40 kPa to 120 kPa of consolidation pressure, but reduced after being consolidated to 220 kPa.

6.3 Research Recommendations

I. It is suggested to carry out the local strain, precise membrane penetration calibration, and anisotropic small-strain stiffness measurements for the triaxial soil specimens in order to further validate the present experimental findings.

II. It is suggested to use a very sensitive AE transducer and high sampling rate data acquisition system in order to measure the fragmentation of solid grains (e.g. soil and calcite) which is normally triggered at very high frequency content.

III. To equip AE and anisotropic small-strain elastic measurements (e.g. bender element, local strain measurement, etc.) onto the triaxial soil specimen in order to identify the locality of yielding precisely and validate the soil anisotropy.

IV. To carry out more triaxial experiments for specimens which are consolidated to pressures in the range of 40 kPa ~120 kPa (with closer step of consolidation pressure, for example at an increment of every 10 kPa) in order to determine precise yielding loci for both untreated and bio-treated soils. To carry out additional tests for heavily over-consolidated MICP soils (i.e. OCR ≥ 5.0) in order to form a more complete understanding. Multiple AE sensors are also useful as it is well reported that heavily-cemented (dense) sands were usually characterized with an obvious shear band, which is visibly seen in a sheared soil specimen.

V. It is suggested to conduct more mechanical-AE tests for the lightly and heavily treated (say, net calcite content of about 10 %) residual soil under different percentage of fines and wide consolidation stress level.

VI. To equip strain-rate controlled loading system in the triaxial experiment in order to investigate the deformation and shearing responses more accurately. It is also beneficial to examine the secondary compression (creep deformation) behaviour of MICP soils using the loading system.

VII. To investigate the self-healing effect in the bio-mediated soils, in which the stressed specimens would probably able to regain some degree of structural integrity and stiffness upon retreatment by reinjecting nutrient and chemical reagent.

REFERENCES

Aiban, S.A. and Aurifullah, V., 2007. Effect of gravel size, type, and mold size on the carrying capacity of calcareous fines-gravel mixes. *ASCE Journal of materials in civil engineering*, 19 (10), pp. 834-847.

Ali, F., 2012. Stabilization of Residual Soils Using Liquid Chemical. *Electronic Journal of Geotechnical Engineering*, 17, pp. 115-126.

Al Qabany, A. and Soga. K., 2013. Effect of Chemical Treatment Used in MICP on Engineering Properties of Cemented Soils. *Ge´otechnique* , 63 (4), pp. 331-339.

Ampadu, S.K. and Tatsuoka, F., 1993. Effect of setting method on the behaviour of clays in triaxial compression from saturation to undrained shear. *Soils and Foundations*, 33 (2), pp. 14-34.

Andrus, R.D. and Chung, R.M., 1995. *Ground improvement techniques for liquefaction remediation near existing lifelines*. National Institute of Standards and Technology.

Arthur, J.R.F. and Menzies, B.K., 1972. Inherent anisotropy in a sand. *Ge´otechnique*, 22 (1), pp. 115-128.

ASTM, 2011: D4767-11. *Standard Test Method for Consolidated Undrained Triaxial Compression Test for Cohesive Soils*. United States: ASTM.

Atkinson, J.H., 1975. Anisotropic Elastic Deformations in Laboratory Tests on Undisturbed London Clay. *Ge´otechnique*, 25 (2), pp. 357-374.

Atkinson, J.H. and Bransby, P.L., 1978. *The mechanics of soil: An introduction to critical state soil mechanics*, Berkshire: McGraw-Hill Book Company (UK) Limited.

Basha, E.A., Hashim, R., Mahmud, H.B. and Muntohar, A.S., 2005. Stabilization of residual soil with rice husk ash and cement. *Construction and Building Materials*, 19 (2005), pp. 448-453.

Becker, D.E., Crooks, J.H., Been, K., and Jefferies, M.G., 1987. Work as a criterion for determining in situ and yield stresses in clays. *Canadian Geotechnical Journal*., 24 (4), pp. 549-564.

Blight, G.E. and Leong, E.C., 2012. *Mechanics of Residual Soils*, 2nd ed. London: Taylor and Francis.

Bishop, A.W. and Henkel, D.J., 1962. *The measurement of soil properties in the triaxial test*. London: E. Arnold.

Bogado, G.O., Reinert, H.O. and Francisca, F.M., 2017. Geotechnical properties of residual soils from the North-east Argentina. *International Journal of Geotechnical Engineering*, 13 (2), pp. 112-121.

BSI, 1990. British Standard 1377: 1990 Methods of test for soils for civil engineering purposes. United Kingdom: BSI Group.

Canakci, H., Sidik, W. and Halil, I., 2015. Effect of bacterial calcium carbonate precipitation on compressibility and shear strength of organic soil. *Soils and Foundations*, 55 (5), pp. 1211:1221.

Chan, C.M. 2010. Bender Element Test in Soil Specimens: Identifying the Shear Wave Arrival Time. *EJGE*, 15 (2010), pp. 1263-1276.

Chen, K.B. and Kassim, K.A., 2015. *Microbial Induced Cementation on Tropical Residual Soil*. Universiti Teknologi Malaysia.

Cheng, L., Shahin, M.A. and Mujah, D., 2016. Influence of key environmental conditions on microbially induced cementation for soil stabilization. *Journal of Geotechnical and Geoenvironmental Engineering*, 143 (1):04016083, pp. 1-11.

Chiet, K.T.P., Kassim, K.A., Chen, K.B., Martula, U., Chong, S.Y. and Arefnia, A., 2016. Effect of reagents Concentration on biocementation of tropical residual soil. *Soft Soil Engineering International Conference 2015, IOP Conf. Series: Materials Science and Engineering*, 136 (2016) 012030, pp. 1-8.

Chou, C.W., Seagren, E.A., Aydilek, A.H. and Lai, M., 2011., Biocalcification of Sand through Ureolysis. *Journal of Geotechnical and Geoenvironmental engineering, ASCE*, 137 (12), pp. 1179-1189.

Chu, J., Wanatowski, D., Loke, W.L. and Leong, W.K., 2015. Pre-failure instability of sand under dilatancy rate controlled conditions. *Soils and Foundations*, 55 (2), pp. 414–424.

Clough, G.W., Sitar, N., Bachus, R.C. and Rad, N.S., 1981. Cemented sands under static loading. *Journal of Geotechnical Engineering Division*, 107, No. GT 6, pp. 799–817.

Cui, M.J., Zheng, J.J., Zhang, R.J., Lai, H.J. and Zhang, J., 2017. Influence of cementation level on the strength behaviour of bio-cemented sand. *Acta Geotechnica*, 12, pp. 971-986.

DeJong, J.T., Fritzges, M.B. and Nusslein, K., 2006. Microbially induced cementation to control sand response to undrained shear. *Journal of Geotechnical and Geoenvironmental engineering, ASCE*, 132 (11), pp. 1381-1392.

DeJong, J.T., Fritzges, M.B. and Nusslein, K. 2010., Bio-mediated soil improvement. *Ecological Engineering*, 36, pp. 197-210.

Deng, L., Yuan, H., Chen, J., Sun, Z., Fu, M., Zhou, Y., Yan, S., Zhang, Z. and Chen, T., 2019. Experimental investigation on progressive deformation of soil slope using acoustic emission monitoring. *Engineering Geology*, 261 (2019), 105295, pp. 1-16.

Diaz-Rodriguez, J.A. , Leroueil, S. and Aleman, J.D., 1992. Yielding of Mexico City clay and other natural clays. *Journal of Geotechnical Engineering Division, ASCE*, 118 (7), pp. 981-995.

Dixon, N. Hill, R. and Kavanagh, J., 2003. Acoustic emission monitoring of slope instability: Development of an active wave guide system. *Institution of Civil Engineers Geotechnical Engineering Journal*, 156 (2), pp. 83-95.

Dixon, N., Spriggs, M.P., Smith, A., Meldrum, P. and Haslam, E., 2015 Quantification of reactivated landslide behaviour using acoustic emission monitoring. *Landslides*, 12 (3), pp. 549–560.

Do, J., Montoya, B.M., Mohammed and Gabr, A., 2019. Debonding of microbially induced carbonate precipitation-stabilized sand by shearing and erosion. *Geomechanics and Engineering*, 17 (5), pp. 429-438.

El-Sohby, M.A., 1969. Deformation of sands under constant stress ratios. *Proceeding. 7th ICSMFE*, Mexico.

Feng, K. and Montoya, B.M., 2014., Behaviour of Bio-Mediated Soil in K_o Loading. *New Frontiers in Geotechnical Engineering*, GSP 243 © ASCE 2014.

Feng, K. and Montoya, B.M., 2015. Influence of confinement and cementation level on the behaviour of microbial induced calcite precipitation sands under monotonic drained loading. *Journal of Geotechnical and Geoenvironmental engineering, ASCE*, 142 (1), pp. 1-9.

Francisca, F.M. and Bogado, G.O., 2019. Weathering effect on the small strains elastic properties of a residual soil. *Geotechnical and Geological Engineering*, 37, pp. 4031–4041.

Foo, K.Y., 1983. The Palaeozoic sedimentary rocks of Peninsular Malaysia-stratigraphy and correlation. *Proceedings of the Workshop on Stratigraphic Correlation of Thailand and Malaysia*. Haad Yai, Thailand, pp. 1-19.

Fujita, Y., Ferris, F.G., Lawson, R.D., Colwell, F.S., Smith, R.W., 2000. Subscribed content calcium carbonate precipitation by ureolytic subsurface bacteria. *Geomicrobiol J*, 17 (4), pp. 305–318.

Futai, M.M., Almeida, M.S.S. and Lacerda, W.A., 2004. Yield, Strength, and Critical State Behavior of a Tropical Saturated Soil. *Journal of Geotechnical and Geoenvironment, ASCE*, 130 (11), pp. 1169-1179.

Ghasemi, P. and Montoya, M.M., 2020. Field Application of the Microbially Induced Calcium Carbonate Precipitation on a Coastal Sandy Slope. *Geo-Congress 2020*, GSP 320, Minneapolis, Minnesota, United States.

Gomez, M.G., Dworatzek, S.M., Martinez, B.C., deVlaming, L.A., DeJong, J.T., Hunt, C.E., Major, D.W., 2015. Field-scale bio-cementation tests to improve sands. *Proc ICE Ground Improvement*, 168 (3), pp. 206–216.

Guo, L.Q., Huang, Y.X. and Huang, J.B., 2012. Experimental Study on Anisotropy of Granite Residual Soil. *Advances Materials Research*, 518-523 (2012), pp. 4721-4725.

Gue, S.S. and Tan, Y.C., 2006. Landslides: Case histories, lessons learnt and mitigation measures. *Landslide, Sinkhole, Structure Failure: MYTH or SCIENCE?*

Hazen, A., 1911., Discussion of Dams on sand foundations. A. C. Koenig ed., *Transactions of the American Society of Civil Engineers*, 73 (3), pp. 199–203.

Hardin, B.O., 1985. Crushing of soil particles. *Journal of Geotechnical Engineering, ASCE*, 111 (10), pp. 1177–1192.

Hardy, H.R., Jr., 2003. *Acoustic Emission/Microseismic Activity: Volume 1: Principles, Techniques and Geotechnical Applications, Volume 1*, United States: CRC Press.

Hataf, N. and Baharifard, A., 2019. Reducing Soil Permeability Using Microbial Induced Carbonate Precipitation (MICP) Method: A Case Study of Shiraz Landfill Soil, *Geomicrobiology Journal*, DOI: 10.1080/01490451.2019.1678703.

Henry, T.P.K., Kassim, K.A., Umar, M., Zango, M.U., Muhammed, A.S. and Ahmad, K., 2019. Microbially induced carbonate precipitations to improve residual soil at various temperatures. *Bulletin of the Geological Society of Malaysia*, 67, pp. 75-81.

Holtz, R. and Kovacs, W., 1981. *Introduction of Geotechnical Engineering*, New Jersey: Prentice Hall.

Huat, B.B.K., Toll, D.G. and Prasad, A., 2004. *Handbook of Tropical Residual Soils Engineering*, 1st ed. London: Taylor and Francis Group plc.

Ishihara, K., Tatsuoka, F. and Yasuda, S., 1975. Undrained deformation and liquefaction of sand under cyclic stresses, *Soils and Foundations*, 1 (1), pp. 29-44.

Ishihara, K. and Okada, S., 1978. Yielding of overconsolidated sand and liquefaction model under cyclic stresses, *Soils and Foundations*, 18 (1), pp. 57-72.

ISO, 2004. International Standard 13322-1 Particle size analysis-Image analysis methods- Part 1: Static image analysis methods. Switzerland: ISO.

Ivanov, V. and Chu, J., 2008. Applications of microorganisms to geotechnical engineering for bioclogging and biocementation of soil in situ. *Reviews in Environmental Science and Bio/Technology* ,7, pp. 139-153.

Ivanov, V., Chu, J., Stabnikov, V. and Li, B., 2015. Strengthening of soft marine clay using bioencapsulation. *Marine Georesources Geotechnoly* 33 (4), pp. 320-324.

Jiang, N.J., Soga, K. and Kuo, M., 2016. Microbially Induced Carbonate Precipitation for Seepage-Induced Internal Erosion Control in Sand-Clay Mixtures. *Journal of Geotechnical and Geoenvironmental Engineering*. doi:10.17863/CAM.24.

JGS. 2000. *Test methods for minimum and maximum densities of sands*. In Soil testing standards. Japanese Geotechnical Society (JGS). pp. 136–138. [In Japanese]

Khin, S.T., Lee, S.R. and Kim, Y.S., 2009. Comparison between shear behaviours of over-consolidated Nakdong River sandy silt and silty sand. *Marine Georesources & Geotechnology*, 27 (3), pp. 217-229.

Kim, G., Kim, J. and Youn, H.J., 2018. Effect of temperature, PH, and reaction duration on microbially induced calcite precipitation. *Applied Science*, 8 (1277).

Koerner, R. and Lord Jr, A.E., 1972 Acoustic emissions in medium plasticity clayey silt. *Proc. ASCE J. Soil Mech. and Found. Div*. 98, pp. 161- 165.

Koerner, R., McCabe, W. and Lord Jr, A.E., 1981. Acoustic emission behavior and monitoring of soils. In: *Acoustic Emissions in Geotechnical Engineering Practice, ASTM STP750*, pp. 93-141.

Kumruzzamanl, M.D. and Yin, J.H., 2011. Stress-strain Behaviour of Completely Decomposed Granite in both Triaxial and Plane Strain Conditions. *Malaysian Journal of Civil Engineering*, 23 (1), pp. 33-62.

Ladd, C.C., Foott, R., Ishihara, K., Schlosser, F. and Poulos, H.G., 1977. Stress-deformation and strength characteristics. *Proc. 9th Int. Conf. Soil Mech.*, Tokyo, 2, pp. 421-494.

Lade, P.V., and Tsai, J., 1985. Effects of localization in triaxial tests on clay. Proceedings of the 11th *ICSMFE*, San Francisco, 12-16 August 1985.

Lade, P.V., 1992. Static instability and liquefaction of lose fine sandy slopes. *Journal of Geotechnical Engineering ASCE*, 118 (1), pp. 51–72.

Lade, P.V., 1993. Initiation of static instability in the submarine Nerlerkberm. *Canadian Geotechnical Journal*, 30, pp. 895–904.

Lade, P.V., Trads, N., 2014. The role of Cementation in the Behaviour of Cemented Soils. *Geotechnical Research*, 1 (4), pp. 111-132.

Lee, M.L., Ng, W.S. and Tanaka, Y., 2013. Stress-deformation and compressibility responses of bio-mediated residual soils. *Ecological Engineering*, 60 (1), pp. 142-149.

Leong, E.C., Cahyadi, J. and Rahardjo, H., 2009. Measuring shear and compression wave velocities of soil using bender-extender elements. *Canadian Geotechnical Journal*, 46 (7), pp. 792-812.

Li, B., Zeng, X. and Yu, H., 2011. Effects of fabric anisotropy on seismic response of strip foundations. *Georisk 2011: Risk Assessment and Management, ASCE*, Reston, VA, GSP224.

Li, B., Chu, J. and Whittle, A., 2016. Biotreatment of Fine-grained Soil through the Bioencapsulation Method. *Geo-Chicago* 2016.

Liew. S.S., 2004. Slope failures in tropical residual soils. In: *Handbook of Tropical Residual Soils Engineering*. Taylor & Francis, pp. 128-179.

Lim, J.X., Chong, S.Y., Tanaka, Y. and Lee, M.L., 2019. CI and CK_o Triaxial tests for tropical residual soil in Malaysia. *1st Malaysian Geotechnical Society (MGS) and Geotechnical Society of Singapore (GeoSS) Conference 2019*, Petaling Jaya, Malaysia, 24-26 June 2019.

Lim, J.X., Chong, S.Y., Tanaka, Y., Ong, Y.H. and Lee, M.L., 2020. Influence of Consolidation Pressure on Stress-Deformation Responses of Biomediated Residual Soil in Malaysia. *International Journal of Geotechnical Engineering*, DOI: 10.1080/19386362.2020.1836113.

Lin, H., Suleiman, M.T., Brown, D.G. and Kavazanjian Jr, E., 2016. Mechanical behavior of sands treated by microbially induced carbonate precipitation. *Journal of Geotechnical and Geoenviornmental Engineering*, 142 (2): 04015066, pp. 1-13.

Lin, W.L., Liu, A., Mao, W.W. and Koseki, J., 2020. Acoustic emission characteristics of a dry sandy soil subjected to drained triaxial compression. *Acta Geotechnica*, 15, pp. 2493–2506. https://doi.org/10.1007/s11440-020-00932-w.

Mahawish, A., Bouazza, A. and Gates, W.P., 2018. Factors affecting the bio-cementing process of coarse sand. *Proceedings of the Institution of Civil Engineers – Ground Improvement*, https://doi.org/10.1680/jgrim.17.00039.

Malandraki1, V. and Toll, D.G., 2001. Triaxial tests on weakly bonded soil with changes in stress path. *Journal of geotechnical and geoenvironmental engineering*, 127 (3), pp. 282-291.

Mao, W.and Towhata, I., 2015. Monitoring of single-particle fragmentation process under static loading using acoustic emission. *Applied Acoustics*, 94, pp.39–45. https://doi.org/10.1016/j.apacoust.2015.02.007.

Mao, W., Yang, Y., Lin, W., Aoyama, S. and Towhata, I., 2018. High frequency acoustic emissions observed during model pile penetration in sand and implications for particle breakage behavior. *International Jounral of Geomechanics*. 18 (11), 04018143.

Mayne, P.W., 1999. Site Characterization Aspects of Piedmont Residual Soils in Eastern U.S. *Proceedings, 14th International Conference on Soil Mechanics and Geotechnical Engineering*, 4, pp. 2191-2195.

Meng, G,H. and Chu, J., 2011. Shear Strength Properties of a Residual Soil in. *Soils and Foundations*, 51 (4), pp. 565-573.

Montoya, B.R., 2012. *Bio-mediated Soil Improvement and the Effect of Cementation on the behaviour Improvement and Performance of Sand*. University of California Davis, PhD thesis.

Montoya, B.M., Feng, K. and Shanahan, C., 2013. Bio-mediated soil improvement utilized to strengthen coastal deposits. *Proceedings of the 18th International Conference on Soil Mechanics and Geotechnical Engineering*, pp. 2565-2568.

Mujah, D., Shahin, M.A. and Cheng, L., 2017. State-of-the-art review of biocementation by microbially induced calcite precipitation (MICP) for soil stabilization. *Geomicrobiology Journal*, 34 (6), pp. 524-37. https://doi.org/10. 1080/01490451.2016.1225866.

Naderi-Boldaji, M., Bahrami, M., Keller, T. and Or. D., 2017. Characteristics of Acoustic Emissions from Soil Subjected to Confined Uniaxial Compression. *Vadose zone journal*, 16 (7), pp. 1-12.

Nishimura, S., Minh, N.A. and Jardine, R.J., 2007. Shear strength anisotropy of natural London clay. *Ge´otechnique,* 57 (1), pp. 49-62.

Ng, W.S., 2013. *Improvements in Engineering Properties of Tropical Residual Soil by Microbial-Induced Calcite Precipitation*. Universiti Tunku Abdul Rahman, Master Thesis.

Ng, W.S., Lee, M.L., Tan, C.K. and Hii, S.L., 2013. Improvements in engineering properties of soils through microbial-induced calcite precipitation. *KSCE journal of Civil Engineering,*17 (4), pp. 718-728.

Ng, W.S., Lee, M.L., Tan, C.K. and Hii, S.L., 2014. Factors Affecting Improvement in Engineering Properties of Residual Soil through Microbial-Induced Calcite Precipitation. *Journal of Geotechnical and Geoenvironmental engineering, ASCE,* 140 (5), pp. 1222-1233.

Oda, M., 1972. Initial Fabrics and their relations to the mechanical properties of granular materials. *Soils and Foundations,* 12 (1), pp. 17-36.

Ooi, T,A., 1982. Malaysian soils and associated problems. *Geotechnical Engineering Course (Chapter 2)*, University Malaya, Kuala Lumpur.

Pitts, J. and Kannan, R., 1986. Residual soil development on sedimentary rocks of the Jurong Formation in Singapore. *GEOSEA V Proceedings*, Geological Society of Malaysia, Bulletin 19, 1, pp. 453-468.

Rahardjo, H., Aung, K.K., Leong, E.C. and Rezaur, R.B., 2004. Characteristics of residual soils in Singapore as formed by weathering. *Engineering Geology*, 73 (2004), pp. 157-169.

Rebata-Landa, V., 2007. *Microbial activity in sediments: effects on soil behaviour*. Gerogia Institution of Technology, PhD thesis.

Rotta, G.V., Consoli, N.C., Prietto, P.D.M., Coop, M.R. and Graham, J., 2003. Isotropic yielding in an artificially cemented soil cured under stress. *Ge´otechnique*, 53 (5), pp. 493–501.

Salih, A,G. and Kassim, K.A., 2012. Effective Shear Strength Parameters of Remoulded Residual Soil. *EJGE*, 17 (2012), pp. 243-253.

Sara Rios., Anto´nio Viana da Fonseca. and Be´atrice Anne Baudet., 2014. On the shearing behaviour of an artificially cemented soil. *Acta Geotechnica,* 9, pp. 215–226.

Sharma, A. and Ramkrishnan, R., 2016. Study on effect of Microbial Induced Calcite Precipitates on Strength of fine-grained soils. *Perspective in Science* (2016) 8, pp. 198-202.

Shipton, B. and Coop, M.R., 2012. On the compression behaviour of reconstituted soils. *Soils and Foundations*, 52 (4), pp. 668–681.

Sasaki, T. and Kuwano, R., 2016. Undrained cyclic triaxial testing on sand with non-plastic fines content cemented with microbially induced CaCO3. *Soils and Foundations* 56 (3), pp. 485-495.

Smith, A. and Dixon, N., 2019. Acoustic emission behaviour of dense sands. Géotechnique, 69 (12), pp. 1107-1122.

Taiebat, M. and Dafalias, Y.F., 2010. Simple Yield Surface Expressions Appropriate for Soil Plasticity, *International Journal of Geomechanics*, 10 (4), pp. 161-169.

Taha, M.R., Hossain, M.K. Chik, Z. and Nayan, K.A., 1998. Geotechnical Behaviour of a Malaysian Residual Granite Soil. *Pertanika Jurnul Science & Technol*ogy, 7 (2), pp. 151-169.

Tan, B.K., 2004. Slope failures in tropical residual soils. In: *Handbook of Tropical Residual Soils Engineering*. London: Taylor & Francis, pp. 418-431.

Tanimoto, K., Nakamura, J. and Fudo, R., 1978. Application of acoustic emission in in-situ test. In: *Proceedings of the 10th International Conference on Soil Mechanics and Foundation Engineering*. Rotterdam: Balkema A.A., pp. 573-576.

Tanimoto, K. and Nakamura, J., 1982. Study of acoustic emission in soils under triaxial shear, *Journal of JSSMFE*, 22 (3), pp. 137-144 (in Japanese).

Tanimoto, K. and Tanaka, Y., 1985. A method of determining yield locus of sandy soil, *Proceedings of the 11th International Conference of Soil Mechanics & Foundation Engineering*, 2, pp. 1069-1072.

Tanimoto, K. and Tanaka, Y., 1986. Yielding of soils as determined by acoustic emission. *Soils and Foundations*, 26 (3), pp. 69-86.

Tanaka, Y., 1999. On factors affecting liquefaction strength of fill materials for reclamation works. *Tsuchi –to Kiso, Ser*. No. 497, Vol. 47 (6), pp. 33-36. (in Japanese)

Tanaka, Y. and Lee, M.L., 2016. Laboratory study on dynamic properties of compacted residual soils in Malaysia. *Geotechnical Engineering Journal of the SEAGS & AGSSEA*, 47 (4), pp. 89-96.

Tanaka, Y. and Shirakawa, K., 1995. Changes of yield stress of sand during undrained cyclic loading, *International Conferences on Recent Advances in Geotechnical Earthquake Engineering and Soil Dynamics*. 20.

Taylor, D.W., 1948. *Fundamentals of soil mechanics*, New York: Wiley.

Terzaghi, K. and Peck, R., 1996. *Soil mechanics in engineering practice*. 3rd ed, United States: John Wiley & Sons.

Terzis, D. and L. Laloui., 2018. 3-D micro-architecture and mechanical response of soil cemented via microbial-induced calcite precipitation. *Scientific Reports*, 8, 1416 (2018).

Terzis, D. and Laloui, L., 2019. A decade of progress and turning points in the understanding of bio-improved soils: A review. *Geomechanics for Energy and the Environment*, 19 (2019) 100116.

Townsend, F.C., 1985. Geotechnical Characteristics of Residual Soils. *Journal of Geotechnical Engineering, ASCE*, 111 (1), pp. 77-94.

Umar, M., Kassim, K.A. and Chiet, K.T.P., 2015. Temperature effects on the strength properties of microbially stabilized residual soil. *Jurnal Teknologi (Science and Engineering)*, 78: 7-3, pp. 101-104.

Van Paassen, L.A., Daza, C.M., Staal, M., Sorokin, D.Y., Van der Zon, W., and Van Loosdrecht, M.C.M., 2010. Potential soil reinforcement by biological denitrification. *Ecological Engineering*, 36 (2), pp. 168-175.

Van Paassen, L.A., 2011. Bio-mediated ground improvement: From laboratory experiment to pilot applications. *Geo-Frontiers 2011© ASCE*, pp. 4099-4108.

Vaughan, P.R. Maccarini, M. and Mokhtar S.M., 1988. Indexing the engineering properties of residual soil. *Quaterly Journal of Engineering Geology*, London. 21 (1), pp. 69-84.

Velasco, E., 2013. *Scanning Electron Microscope (SEM) as a means to determine dispersibility*. Iowa State University, Msc thesis.

Viana da Fonseca, A., 2003. Characterising and deriving engineering properties of a saprolitic soil from granite in Porto. In *Characterisation and Engineering Properties of Natural Soils*. Swets & Zeitlinger, Lisse, pp. 1341-1378.

Wang, C.E. and Borden, R.H., 1996. Deformation characteristics of Piedmont residual soils. *Journal of Geotechnical Engineering, ASCE*, 122 (10), pp. 822-830.

Wang, Z., Zhang, N., Cai, G., Jin, Y., Ding, N. and Shen, D., 2017. Review of ground improvement using microbial induced carbonate precipitation (MICP). *Marine Georesources and Geotechnology*, 35 (8), pp. 1135–1146.

Xiao, P., Liu, H., Stuedlein, A.W., Evans, T.M. and Xiao, Y., 2019a. Effect of Relative Density and Bio-cementation on the Cyclic Response of Calcareous Sand. *Canadian Geotechnical Journal*, 56 (12), pp. 1849-1862.

Xiao, Y., Stuedlein, A.W., Ran, J., Evans, T.M., Cheng, L., Liu, H., Van Paassen, L.A. and Chu, J. ,2019b. Effect of Particle Shape on the Strength and Stiffness of Biocemented Glass Beads. *Journal of Geotechnical & Geoenvironmental Engineering*, 145 (11), 06019016, pp. 1-13.

Xiao, Y., Chen, H., Stuedlein, A.W., Evans, T.M., Chu, J., Cheng, L., Jiang, N., Lin, H., Liu, H. and Aboel-Naga, H.M., 2020. Restraint of Particle Breakage by Biotreatment Method. *Journal of Geotechnical & Geoenvironmental Engineering*,146 (11) 04020123, pp. 1-12.

Zamani, A. and Montoya, B.M., 2015. Undrained Behavior of Silty Soil Improved with Microbial Induced Cementation. *6th International Conference on Earthquake Geotechnical Engineering*.

Zamani, A. and Montoya, B.M., 2018. Undrained Monotonic Shear Response of MICP-Treated Silty Sands. *Journal of Geotechnical and Geoenvironmental Engineering*, 144 (6), pp.1-12.

Zamani, A. and Montoya, B.M., 2019. Undrained cyclic response of silty sands improved by microbial induced calcium carbonate precipitation. *Soil Dynamics and Earthquake Engineering*, 120 (2019), pp. 436-448.

Zhang, X.W., Kong, L.W., Yin, S. and Chen, C., 2017. Engineering geology of basaltic residual soil in Leiqiong southern China. *Engineering Geology*, 220, pp. 196-207.

APPENDICES

APPENDIX A: Preparation of nutrient agar

The agar solution was prepared by mixing 14 g of nutrient broth powder (agar-type) into 500 ml of distilled water. The nutrient agar mixture was sterilized in an autoclave machine at a temperature of 50 °C. After two hours, the agar solution was slowly poured into agar plates filling two-third of plate height and allowed to cool down for few hours. It is important that the preparation process was carried out inside a laminar flow machine in order to avoid the contamination from ambient environment.

```
# This script is used to mediate of mechanical data (e.g. stress, strain, and pore-water pressure) by digital filtering.

import numpy as np                      # Import Numpy library.
import matplotlib.pyplot as plt         # Import plotting module from library.
from scipy import signal                # Import signal processing module.

# Import the data file (in csv format) into python platform.
>>> data = np.loadtxt('1.csv', delimiter=',', skiprows=0, max_rows=None, usecols=0)

>>>N = len(data)                        # Defining length of data.
>>>fs = 0.4                            # Input sampling frequency.
>>>T = N/fs                            # Defining sampling frequency.
>>>x = np.linspace(0.0, T, N)          # Array adjustment of time axis.
>>>fc = 0.04                           # Input a cut-off frequency of the filter.
>>>w = fc / (fs / 2)                   # Normalize the frequency.
>>>b, a = signal.butter(5, w, 'low')   # Carry out Butterworth filtering.
>>>output = signal.filtfilt(b, a, data)
>>>plt.figure(1)                       # Plot the raw data and FFT.
>>>plt.plot(x,data,'b-')               # To set original data plot in blue line.
>>>plt.plot(x,output,'r')              # To set original data plot in red line.
>>>plt.show

# Save the processed data into a file (csv format) in a specified folder.
>>>saved=np.savetxt("output.csv", output, delimiter=",")
>>>print("done")                       # Show the output.
```

APPENDIX C: Threshold counting for AE data

```
import numpy as np                          # Import Numpy library.
from scipy.signal import find_peaks # Import the peaks detection module.
import matplotlib.pyplot as plt          # Input plotting module from library.

# Import the data file (in csv format) into python platform.
>>>data = np.loadtxt('1.csv', delimiter=',', skiprows=9, max_rows=None,
usecols=0)

>>>T = 0.02                              # Input a noise threshold level.
>>>t = abs(data)                      # Transform all raw data into absolute sense.
>>>t1 = data*0 + T                  # Transform threshold into an array.
>>>N = len(data)                     # Defining length of data.
>>>fs = 176400                       # Input sampling frequency of AE data.
>>>T1 = N/fs                          # Duration of AE record.
>>>x = np.linspace(0.0, T1, N) # Array adjustment of time axis.

#Detect the peaks of transient waveform above the prescribed noise level.
>>>peaks, _= find_peaks(t, height=T)

#Threshold counting on the identified peak data points.
>>>counter = np.count_nonzero(peaks)

# Plot the original AE wave and the detected spikes.
>>>plt.figure(1)
>>>plt.grid()
>>>plt.plot(x,data,'b-')   # Plot waveform of raw AE data in blue line.
>>>plt.plot(x,t1,'r-')        # Plot the noise threshold  in red line.
>>>plt.plot(x[peaks], t[peaks], "x") # Plot detected AE points on the graph.
>>>plt.show
>>>print(counter)            # Show the output.
```

```
# This script allows automation in threshold counting for a great number of
data files (which store the AE data), depending the performance of a pc and
the operating system being used. Based on the author's experience, Linux
system can perform more efficient than the other OS when Python is used.

import numpy as np                    # Import Numpy library.
from scipy.signal import find_peaks # Import the peaks detection module.

# creates an empty data variable, called "data_dict".
>>>data_dict = {}

# set the noise threshold level.
>>>T = 50

# concatenates number of files and defined data variable. In this case, the
Python file was in the same directory as the raw data files (i.e. an arbitrary
folder in Desktop).

>>>for i in range(4):

data_dict[i]= np.loadtxt('{0}.csv'.format(i),delimiter=',',skiprows=9,
max_rows=None, usecols=0)

# Transform all raw data into absolute sense.
>>>t = abs(data_dict[i])

#Detect the peaks of transient waveform above the prescribed noise level.
>>>peaks, _= find_peaks(t, height=T)

#Threshold counting on the identified peak data points.
>>>counter = np.count_nonzero(peaks)

>>>print(counter) # Show the output.
```

APPENDIX E: Relationships between cumulative strains and consolidation stress for untreated and MICP-treated residual soils under isotropic consolidation

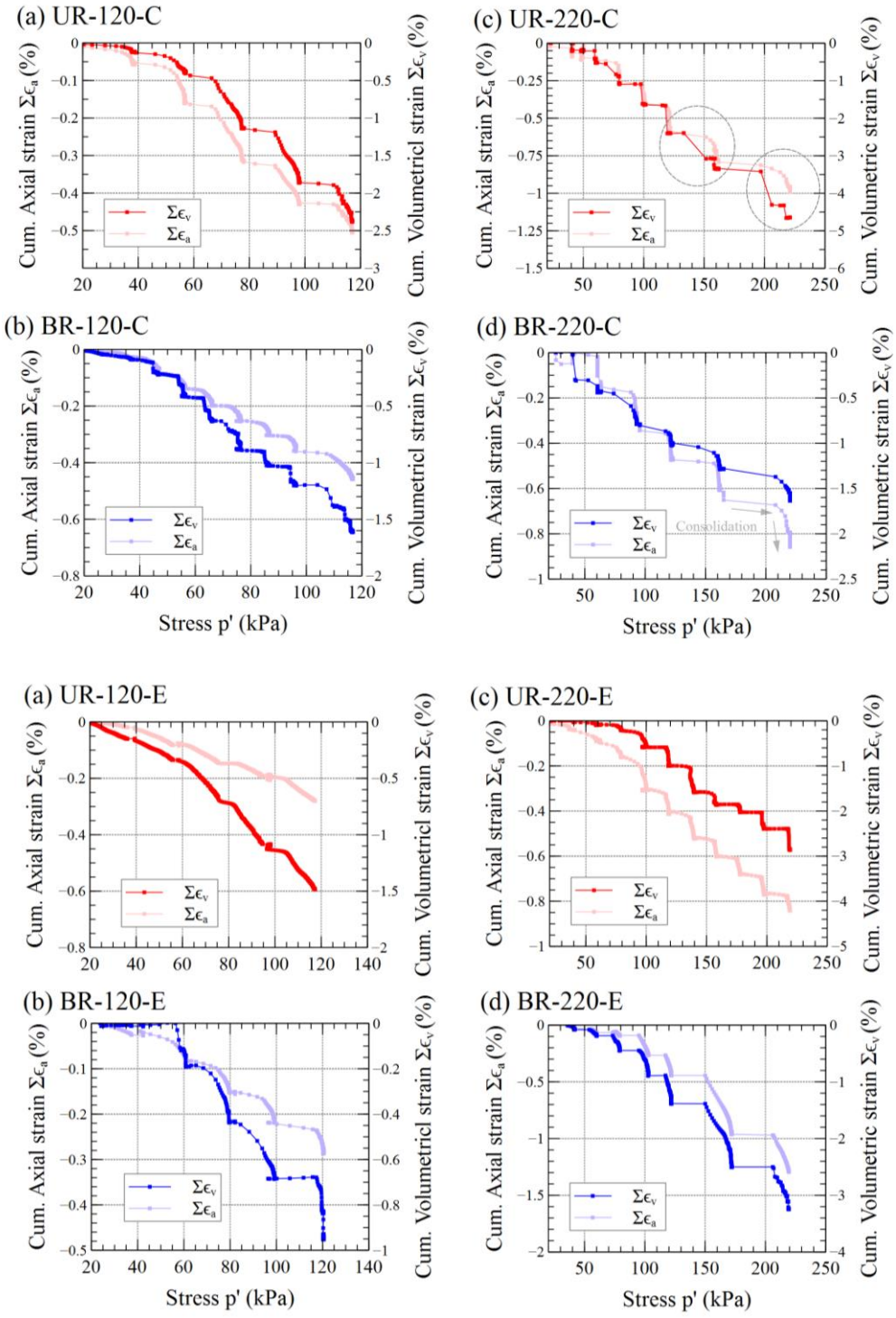

APPENDIX F: Comparisons of strain-log stress for all tested residual soils: (a) volumetric strain; (b) axial strain

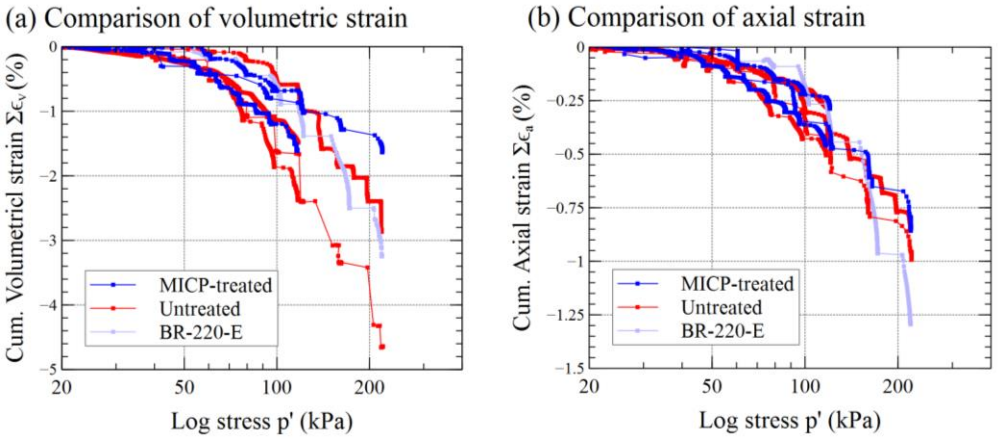

APPENDIX G: Relationships between cumulative strains and consolidation stress for untreated and MICP-treated sands under isotropic consolidation

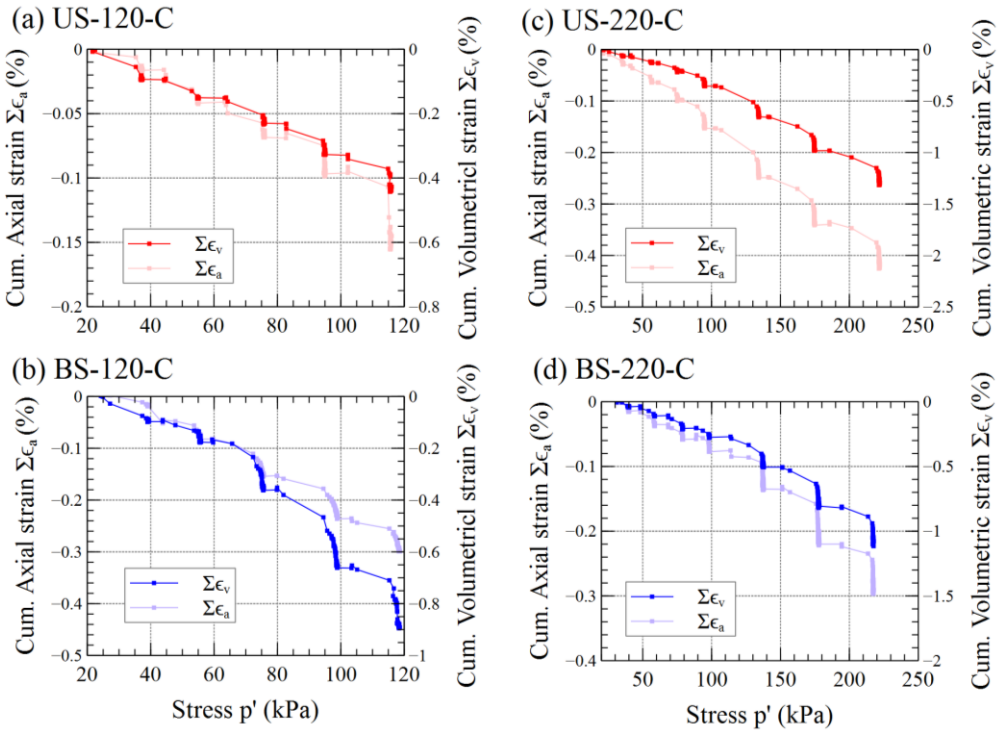

APPENDIX H: Comparisons of strain-log stress for all tested sands: (a) volumetric strain; (b) axial strain

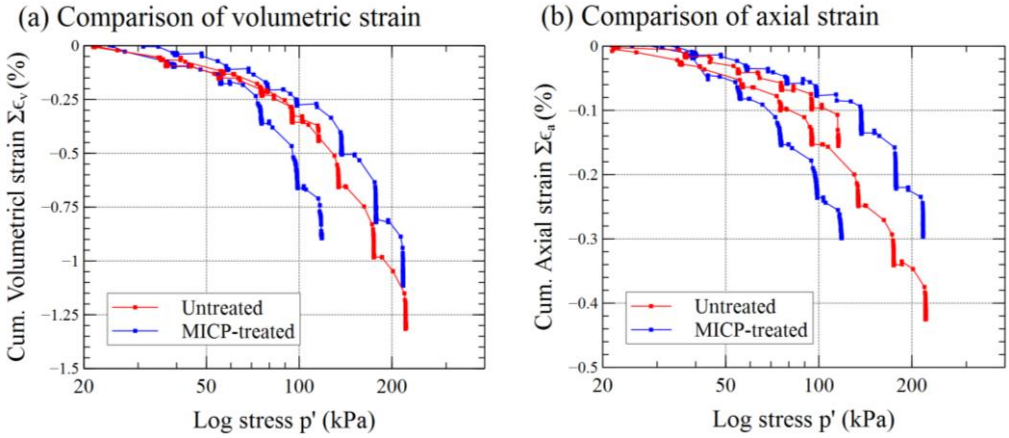

APPENDIX I: Mechanical-AE behaviour of Untreated and MICP-treated residual soils consolidated to 80 kPa in undrained compression (CIUC) in full-strain range

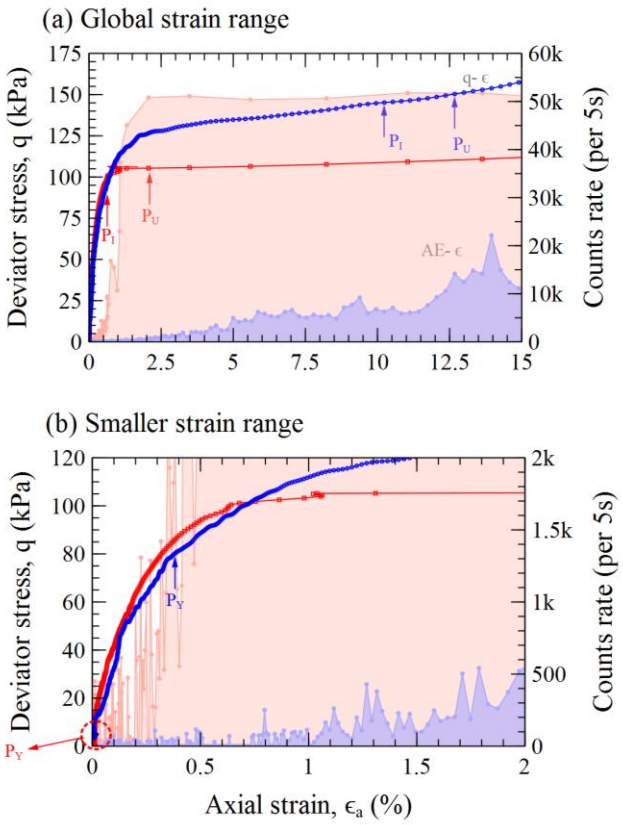

Notes: This particular set of data showed that the MICP-treated residual soil had stronger resistances (e.g. yielding, instability, and ultimate) and further tests shall be persuaded for sands to solidify the present findings.

APPENDIX J: Mechanical-AE behaviour of Untreated and MICP-treated residual soils consolidated to 80 kPa in undrained extension (CIUE) in smaller-strain range

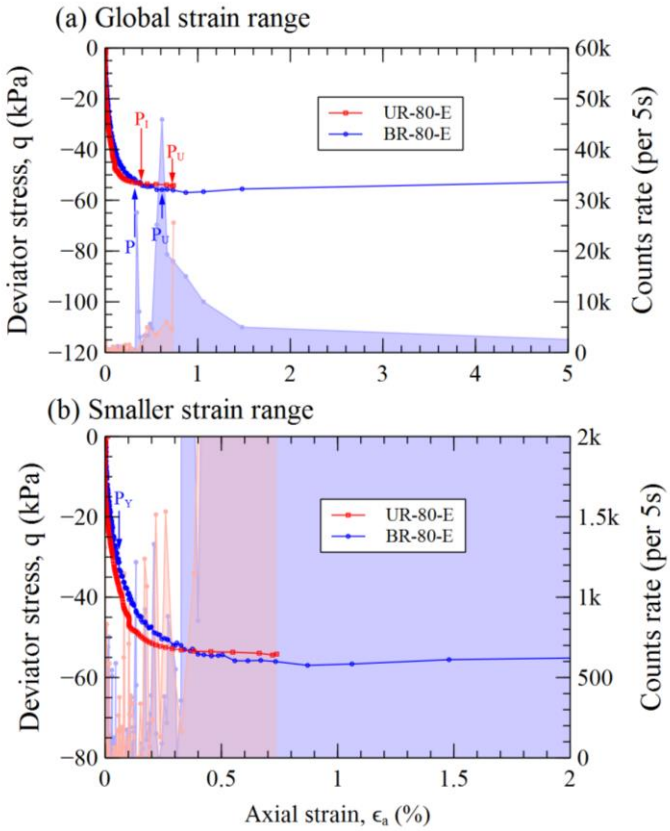

APPENDIX K: Correlation between AE counts rate and strain rate among tested residual soils and sand

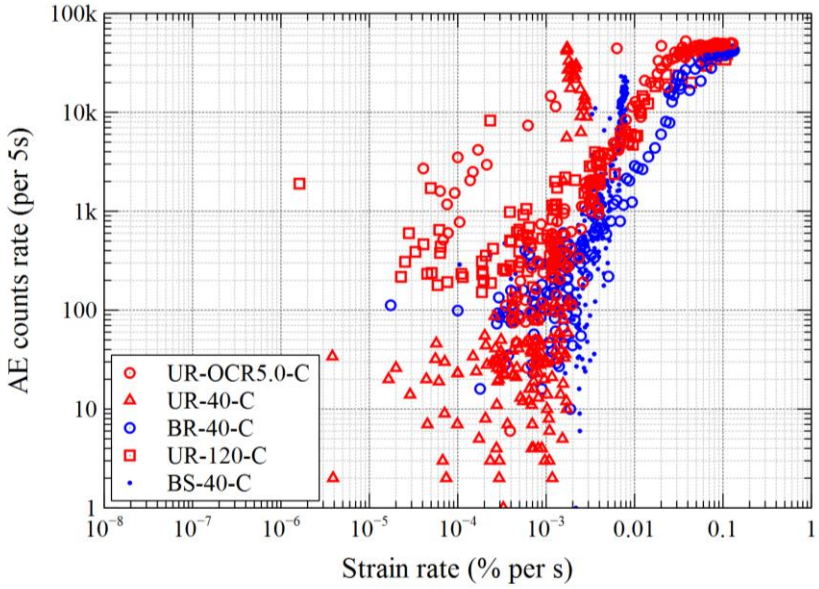

Note:

Strain rate = incremental strain divided by time interval (i.e. $\Delta\epsilon$ / Δt), % per s

APPENDIX L: Determination of yielding for BR-80-C and UR-80-C specimens

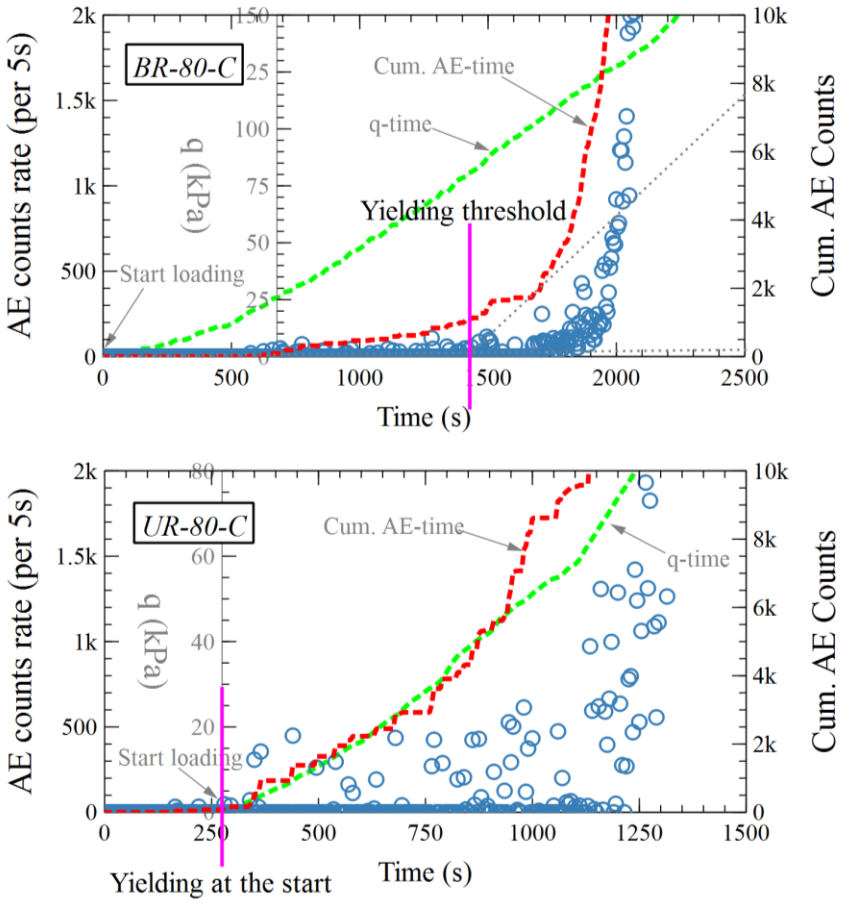

The yielding of BR-80-C was quite obvious, whereas the untreated specimen started to yield from the beginning.

APPENDIX M: Determination of yielding for UR-80-E and BE-80-E specimens

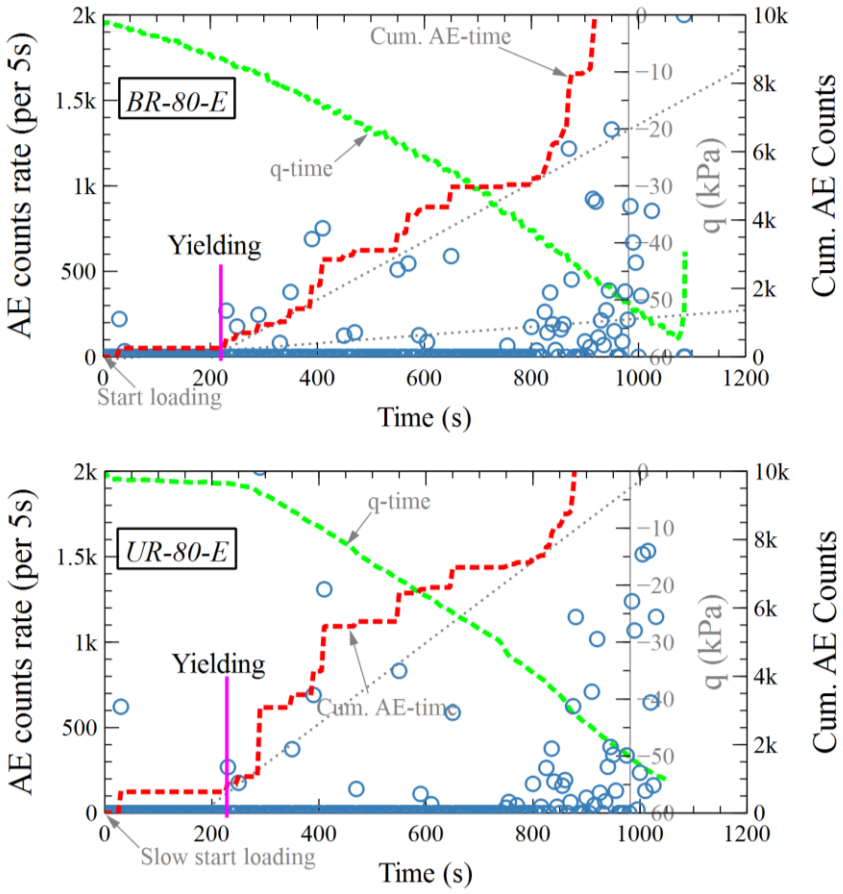

In the BR-80-E, the first rising slope of cumulative AE was corresponded to the yielding. The UR-80-E specimen started to yield at the beginning of undrained shearing (according to the deviator stress and AE rate changes).

APPENDIX N: Relationship of Secant modulus ratio and axial strain amplitude among tested residual soils

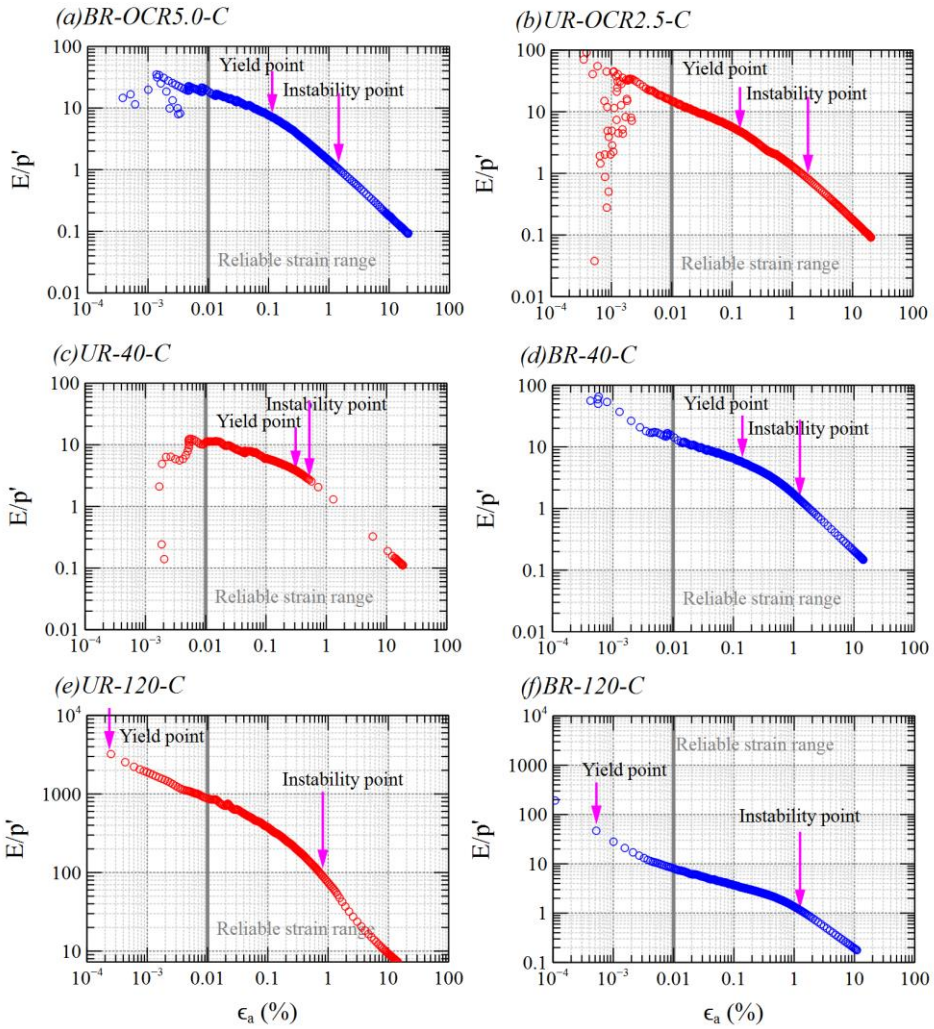

Note:

E = Secant Modulus (i.e. q/ϵ_a), kPa

p’ = Mean Effective Pressure, kPa

E/p’ = Secant Modulus Ratio

APPENDIX O: Relationship of Secant modulus ratio and axial strain amplitude for sands

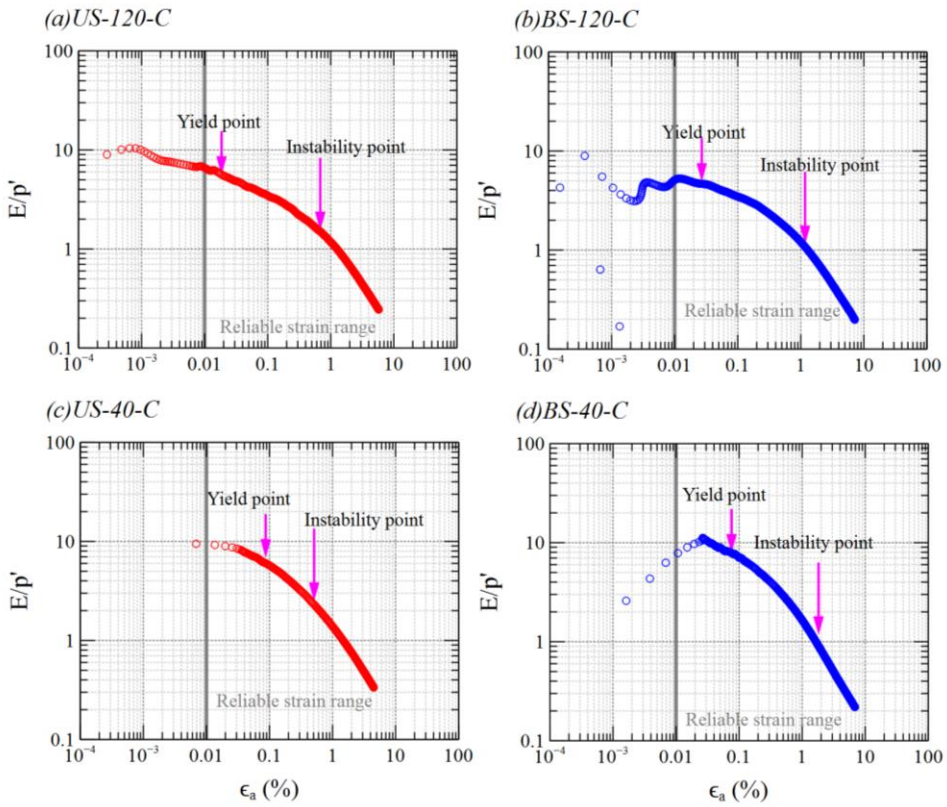

LIST OF PUBLICATIONS

Lim, J.X., Chong, S.Y., Tanaka, Y., Ong, Y.H. and Lee, M.L., 2018. Anisotropically Consolidated Undrained Compression Test on Residual Soil. *ICCEE, E3S Web of Conferences*, 65, 06006.

Lim, J.X., Chong, S.Y., Tanaka, Y. and Lee, M.L., 2019. CI and CKo Triaxial tests for tropical residual soil in Malaysia. *1st Malaysian Geotechnical Society (MGS) and Geotechnical Society of Singapore (GeoSS) Conference 2019*, Petaling Jaya, Malaysia, 24-26 June 2019.

Lim, J.X., Chong, S.Y., Tanaka, Y. and Ong, Y.H., 2020. Acoustic emission behaviour of tropical residual soil, *International journal of recent technology and engineering (IJRTE)*, 2277-3878 8 (5), pp. 1646-1655.

Lim, J.X., Chong, S.Y., Tanaka, Y., Ong, Y.H. and Lee, M.L., 2020. Influence of Consolidation Pressure on Stress-Deformation Responses of Biomediated Residual Soil in Malaysia. *International Journal of Geotechnical Engineering*, DOI: 10.1080/19386362.2020.1836113.

Tanaka, Y., Lim, J.X., Chong, S.Y., Ong, Y.H. and Lee, M.L., 2022. Effects of bio-mediation on deformation and yielding responses of residual soil as studied by Acoustic Emission. *20th International Conference on Soil Mechanics and Geotechnical Engineering*, Sydney, Australia (upcoming conference).